

PIEZOELECTRIC ANISOTROPY AND FREE ENERGY INSTABILITY IN CLASSIC PEROVSKITES

THÈSE N° 3514 (2006)

PRÉSENTÉE LE 12 MAI 2006

À LA FACULTÉ SCIENCES ET TECHNIQUES DE L'INGÉNIEUR
Laboratoire de céramique
SECTION DE SCIENCE ET GÉNIE DES MATÉRIAUX

ÉCOLE POLYTECHNIQUE FÉDÉRALE DE LAUSANNE

POUR L'OBTENTION DU GRADE DE DOCTEUR ÈS SCIENCES

PAR

Marko BUDIMIR

ingénieur physicien, Université de Zagreb, Croatie
et de nationalité croate

acceptée sur proposition du jury:

Prof. H. J. Mathieu, président du jury
Prof. N. Setter, Dr D. Damjanovic, directeurs de thèse
Prof. E. Cross, rapporteur
Prof. P. Stadelmann, rapporteur
Prof. J. Trodahl, rapporteur



ÉCOLE POLYTECHNIQUE
FÉDÉRALE DE LAUSANNE

Lausanne, EPFL

2006

Abstract

Several members of the perovskite family are investigated:

- the temperature dependence of dielectric, elastic, piezoelectric and coupling coefficients of KNbO_3 in its orthorhombic ferroelectric phase is determined experimentally;
- the values of dielectric stiffness coefficients at constant stress, α , are estimated for the 6th order Landau-Ginzburg-Devonshire phenomenological description of KNbO_3 ;
- the origins of the enhanced piezoelectric responses along non polar directions in perovskites are investigated by studying phenomenologically the temperature evolution of the piezoelectric anisotropy in a material with a sequence of ferroelectric-ferroelectric phase transitions (BaTiO_3) and in a material with only one ferroelectric phase (PbTiO_3);
- the influence of external bias fields on piezoelectric response and its anisotropy in ferroelectric perovskites is discussed phenomenologically by studying tetragonal BaTiO_3 , PbTiO_3 and $\text{Pb}(\text{Zr},\text{Ti})\text{O}_3$ under electric bias field applied anti-parallel to the spontaneous polarization and uniaxial compressive bias stress along the polarization direction;
- a discussion about a common underlying thermodynamic process able to generally describe the enhancement of the piezoelectric response and its anisotropy is given by investigating the Gibbs free energy flattening in tetragonal BaTiO_3 , PbTiO_3 and $\text{Pb}(\text{Zr},\text{Ti})\text{O}_3$ upon changes of temperature, bias fields and composition.

The main conclusions resulting from this work are:

- a comparison of the results of electromechanical properties measurements on KNbO_3 obtained in this work, the ones found in the literature, and estimates using LGD phenomenology from this work gives discrepancies that suggest that published measurements should be redone;
- in the absence of bias fields, the intrinsic origin of the enhanced piezoelectric responses in perovskites is the anticipation of a phase transition, no matter what is the cause of that transition (temperature, composition); in the presence of sufficiently high bias fields, an enhanced piezoelectric response along non-polar direction can be predicted in some materials (PbTiO_3 under high uniaxial compressive stress along the polar direction);

- the influence of the external bias fields on electromechanical properties of perovskites may generally be of significant importance: if the electric fields applied anti-parallel to the spontaneous polarization or the uniaxial compressive bias stresses applied along the polarization axis are high enough, the perovskite system can be strongly dielectrically softened (metastable state), increasing the values of dielectric permittivities and piezoelectric coefficients; in the vicinity of a coercive field or a phase transition these electromechanical coefficients can increase by several orders of magnitude;
- the flattening of the Gibbs free energy profile of each of examined perovskite systems, regardless of whether this flattening is caused by temperature or composition variation, or by applying compressive pressure or antiparallel electric field bias, leads to enhancements of dielectric susceptibilities and of the piezoelectric response; the anisotropy of the free energy flattening is the origin of the anisotropic enhancement of the piezoelectric response, which can occur either by polarization rotation or by polarization contraction.

Key words: piezoelectricity, ferroelectricity, phase transitions, single crystals, anisotropy, perovskites

Resumé

Plusieurs membres de la famille des perovskites sont étudiés :

- L'influence de la température sur les coefficients diélectriques, élastiques, piézo-électriques et sur le couplage electromécanique du KNbO_3 dans sa phase ferroelectrique orthorhombique est déterminée;
- les valeurs des coefficients de rigidité diélectriques à contrainte constante, α , sont estimées pour la description phénoménologique de Landau-Ginzburg-Devonshire du 6^e ordre de KNbO_3 ;
- les origines des réponses piézoélectriques augmentées le long des directions non polaires des perovskites sont étudiées phenomenologiquement; pour cela, l'évolution de l'anisotropie piézoélectrique en temperature dans un matériau avec une série des transitions de phase ferroelectrique-ferroelectrique (BaTiO_3) et dans un matériau avec seulement une phase ferroelectrique (PbTiO_3) est étudiée;
- l'influence des champs statique externes sur la réponse piézoélectrique et sur son anisotropie est discutée phenomenologiquement en étudiant les BaTiO_3 , PbTiO_3 et $\text{Pb}(\text{Zr}, \text{Ti})\text{O}_3$ tétragonaux sous champ électrique appliqué anti-parallèlement à la polarisation spontanée et à contrainte en pression uniaxial appliquée en direction de polarisation;
- une discussion au sujet d'un processus thermodynamique fondamental commun pour décrire généralement l'augmentation de la réponse piézoélectrique et de son anisotropie est donnée en étudiant l'aplatissement du profil de l'énergie libre de Gibbs dans les BaTiO_3 , PbTiO_3 et $\text{Pb}(\text{Zr}, \text{Ti})\text{O}_3$ tétragonaux sur des changements de la température, des champs externes et de la composition.

Les conclusions principales obtenues dans ce travail sont:

- une comparaison des résultats des mesures des propriétés electromécaniques du KNbO_3 obtenu pendant ce travail, ceux trouvés dans la littérature, et les évaluations utilisant la phénoménologie de LGD obtenus pendant ce travail, donne des anomalies qui suggèrent que des mesures publiées devraient être refaites;
- en l'absence des champs externes, l'origine intrinsèque des réponses piézoélectriques augmentées des perovskites est l'anticipation d'une transition de phase, quelque soit la cause de cette transition (la température, composition); en présence des champs externes, une réponse piézoélectrique augmentée le long de la direction

non polaire peut être prévue pour quelques matériaux sous un champ suffisamment élevée (PbTiO_3 sous une contrainte en compression uniaxiale élevée le long de la direction polaire);

- l'influence des champs externes sur les propriétés électromécaniques des perovskites peut généralement être d'une importance significative: si les champs électriques appliqués anti-parallèlement à la polarisation spontanée ou les contraintes en compression uniaxiales appliquées le long de l'axe de polarisation sont assez élevés, les perovskites peuvent être fortement diélectriquement adoucies (état métastable), augmentant les valeurs des constantes diélectriques et des coefficients piézoélectriques; dans la proximité d'une zone coercitive ou d'une transition de phase ces coefficients électromécaniques peuvent augmenter de plusieurs ordres de grandeur;

- l'aplatissement du profil d'énergie libre de Gibbs de chacun des systèmes de perovskites examiné, indépendamment de ce qui a provoqué cet aplatissement (variation de la température, variation de la composition, application d'une contrainte en compression ou d'un champ électrique antiparallèle) mène aux augmentations des susceptibilités diélectriques et de la réponse piézoélectrique; l'anisotropie de l'aplatissement de l'énergie libre est l'origine de l'augmentation de l'anisotropie de la réponse piézoélectrique, qui peut se produire par rotation ou par contraction de polarisation.

Acknowledgments

The completion of this PhD thesis has been a team effort.

First of all, I am greatly indebted to Prof. Nava Setter for giving me the opportunity to work in the Ceramics Laboratory, and for assuring me fantastic working conditions. If only I could be guaranteed the same conditions in all my future jobs.

I am extremely grateful to Dr. Dragan Damjanović who has been my thesis supervisor over the last 4 years, but, more than that, someone to share discussions about many areas of science, a great guide to the differences between Croatian and Swiss life styles, and a friendly face and a perfect consultant when things at work have gone wrong. Hvala Dragane, dužnik sam ti veliki.

I would further like to thank my thesis jury, Prof. H. J. Mathieu, Prof. L. E. Cross, Prof P. Stadelmann and Prof. J. Trodahl for their critical reading of my report and for some great comments and ideas for future work.

The "Croatian connection" and their logistic and moral support must also be mentioned. I am grateful to Prof. László Forró and Prof. Davor Pavuna from EPFL, Dr. Ana Smontara from the Institute of Physics, Zagreb, and Dr. Ante Bilušić from the Faculty of Natural Sciences and Mathematics, Split, for all their help.

I owe a special thank to my mate Dr. Matthew Davis who immensely improved my English language skills and with whom scientific discussions were excellent.

I would also like to thank Lino Olivetta and Jacques Castano, who helped me resolve certain technical problems with experiments, Evelyn Hollenstein and Dr. Brahim Belgacem for the critical reading of some parts of my thesis and, than, to all other members of the LC for a nice and friendly atmosphere during this period.

For everything else, not mentioned above but deeply patterned into this work, I thank my Iva.

Finally, I would like to acknowledge financial support from the Swiss National Science Foundation.

Contents

1	Introduction	1
2	Basic concepts and definitions	7
2.1	Spontaneous polarization. Ferroelectricity	7
2.2	Pyroelectric effect	10
2.3	Piezoelectric effect	10
2.4	Electrostrictive effect	12
2.5	Symmetry considerations	12
2.6	Thermodynamic considerations	13
2.6.1	Phenomenological Landau-Ginzburg theory	15
3	Literature	19
3.1	Electromechanical properties of single crystal potassium niobate	19
3.2	Phenomenological modeling on perovskites. Polarization rotation. Ultra-high electromechanical properties	27
4	Experimental techniques	33
4.1	Five-terminal setup for low capacity measurements	33
4.2	Domain structure and ferroelectric poling procedure of single crystal KNbO_3	35
4.2.1	Domain structure	35
4.2.2	Surface layer. Polishing. Impurities	36
4.2.3	Poling	36
4.3	Sawyer - Tower bridge	38
4.4	Pyroelectric measurements setup	38
4.5	Resonant technique	38
4.5.1	Experimental setup for simultaneous measurements of electromechanical properties	40
4.6	Some experimental constraints	42

5	Experimental results	43
5.1	Measured electromechanical properties	46
5.1.1	Spontaneous polarization values and ferroelectric hysteresis loops	47
5.1.2	Pyroelectric properties	49
5.1.3	Dielectric properties	50
5.1.4	Mechanical properties	51
5.1.5	Piezoelectric properties	52
5.1.6	Coupling coefficients	52
5.2	A discussion about Landau-Ginzburg-Devonshire theory of KNbO_3 . . .	55
5.2.1	Calculation of the LGD coefficients	55
5.2.2	Calculation of temperature and direction dependences of dielectric and piezoelectric constants, and spontaneous polarization in KN .	64
5.3	Conclusions	70
6	Piezoelectric anisotropy - phase transition relations in perovskites	71
6.1	Piezoelectric anisotropy as a function of temperature - intrinsic effects . .	73
6.2	Monodomain versus polydomain piezoelectric response of a relaxor ferro- electric single crystal along nonpolar directions	88
6.3	Conclusions	93
7	Enhancement of the piezoelectric response in perovskites by external bias fields	97
7.1	Electric bias field	98
7.2	Mechanical bias stress	102
7.2.1	Dependence of polarization, dielectric susceptibility and piezoelec- tric coefficients on uniaxial stress	103
7.2.2	Flattening of the elastic Gibbs free energy profile by compressive stress	109
7.3	Extension of the dielectric tunability range in ferroelectric materials by electric bias field antiparallel to polarization	115
7.4	Conclusions	118
8	Piezoelectric response and free energy instability in classic perovskites	121
8.1	Calculations and discussion	122
8.2	Conclusions	130
9	Conclusions and perspectives	133

A Transformations of coordinate systems. Diagonalization of matrices and eigenvalues	139
B Direction dependence of transverse and shear coefficients of barium titanate	143

Chapter 1

Introduction

One of the most important facts about ferroelectric perovskites is the enormous technological importance of their electromechanical properties. These materials are used today in a great variety of applications, from atomic force microscopy (AFM), through medical ultrasound probes and health-monitoring techniques in civil engineering, to ultrasound underwater applications such as sonars in submarines. A sonar, built from thin quartz crystals, for military purposes, was actually the first application of a piezoelectric material (*Paul Langevine* and his group, France, 1917). Nowadays, the diversity of products and the number of companies in the piezoelectric industry are impressive.

Apart from its attractiveness from the industrial point of view, the family of ferroelectric perovskites displays a large diversity in its physical properties, which makes these materials attractive for fundamental research. On one hand, different representatives of the family exhibit a multitude of physical phenomena, such as pyroelectricity, piezoelectricity, ferroelectricity (in general, perovskites can also show superconductivity), while, on the other hand, perovskite structure is relatively simple and, thus, attractive for studies, especially theoretical ones.

The general stoichiometric formula of the perovskite structure is



where A is a monovalent, divalent or trivalent metal, and B is a pentavalent, tetravalent or trivalent element, respectively. A typical perovskite structure (tetragonal $BaTiO_3$) is shown in Fig. 1.1. The family spans from simpler classic perovskites (for example $BaTiO_3$, $KNbO_3$, $PbTiO_3$) that represent a possibility for the fundamental theoretical investigations, to much more complex relaxor ferroelectric solid solutions (for example $(1-x)Pb(Zn_{1/2}Nb_{2/3})O_3-xPbTiO_3$, and $(1-x)Pb(Mg_{1/2}Nb_{2/3})O_3-PbTiO_3$, also known as PZN-PT and PMN-PT, respectively), with very high piezoelectric coefficients and hence with a great present and future in divers applications.

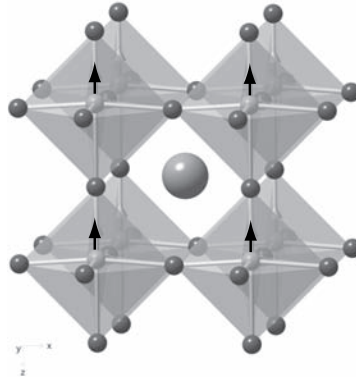


Figure 1.1: The tetragonal barium titanate ($BaTiO_3$) perovskite structure. Translucent octahedra reveal off-centered titanium atoms and the resulting ferroelectric dipoles are indicated by arrows.

The piezoelectric materials exist in single crystal and ceramic form, and as thin films. At present, most of the applications use piezoelectric ceramics. However, the applications of the single crystals are becoming more and more important - one can predict confidently that certain piezoelectric applications that use ceramics today have a single crystalline future.

The perovskites of the particular interest for this work are:

potassium niobate ($KNbO_3$) - firstly, the electromechanical properties data set of this material can be found in several papers (see *Chapter 3* for a review), and the most striking feature about these results is their inconsistency and incompleteness; secondly, the coefficients set of the commonly used phenomenological theory (*Landau-Ginzburg-Devonshire*) for describing the electromechanical properties of perovskite systems is incomplete for $KNbO_3$; so, the challenges with this material are to refine the measured data set, and to improve the phenomenological description of this material properties;

barium titanate ($BaTiO_3$) and lead titanate ($PbTiO_3$) - these two best known members of the perovskite family have already been thoroughly investigated experimentally, both in single crystal and ceramic form, and the phenomenological models describing their electromechanical behavior have been optimized - this state of affairs makes these two materials an excellent choice for a discussion of very important issue of *piezoelectric anisotropy in perovskites*;

lead based perovskites (PZT, PMN-PT, PZN-PT) - these perovskites are mostly not in the mainstream of this work, so not much attention will be given to them

- nevertheless, they will excellently serve as important comparative examples in some discussions.

Firstly, it can be easily illustrated where does the interest for potassium niobate come from. Potassium niobate single crystal (the abbreviation *KN* will be used throughout this report) is already known as an outstanding nonlinear optic material. But, it also has advantages for use in ultrasound medical applications. These are: a low dielectric constant, *the highest reported thickness mode coupling coefficient*¹ and a high longitudinal sound propagation velocity. It is then straightforward to see that KN represents an exceptional non-lead based (i.e. environmental friendly) candidate for high frequency single element transducers.

However, there are certain problems with this material. Ferroelectricity of KNbO_3 was first observed 55 years ago, and, to date, a large number of studies has been reported, but, considering the period passed since the discovery of its ferroelectricity (piezoelectricity), only some reports can be found in the literature on KNbO_3 crystals piezoelectric properties, with very discrepant results presented in them. There are two common reasons for this: the difficulty of growing of KNbO_3 crystals with sufficient electrical resistance and the difficulty in the poling treatment, i.e. the reconstruction of the preferred domain configuration.

Yet, the experimental investigation of the properties of KN is not the main subject of interest in this thesis work. Although of the obvious practical importance, these experiments are at the same time a step towards a discussion about a very important issue in the piezoelectric perovskites world - a question of *origins of piezoelectric anisotropy in classic perovskites*.

After the recent discovery of the *very large piezoelectric effect* in complex relaxor – ferroelectric single crystals PZN-PT and PMN-PT [118, 89], and the fact that the largest piezoelectric response and coupling coefficients *are not along the polar axes* of these materials, the interest in classical ferroelectric materials, such as barium titanate [7, 44, 46, 119, 155, 165] and potassium niobate [109], was renewed. One of the new and very interesting results of the revived investigations was that one could expect the en-

¹The electromechanical coupling coefficient is considered as the key parameter for transducer design. It is the parameter that measures the strength of piezoelectric interaction. High coupling factor corresponds to a transducer with improved axial resolution, broader bandwidth and higher sensitivity. Additionally, the ultrasonic imaging at frequencies from 20 to 100MHz provides a high spatial resolution tool for dermatological, ophthalmological, articular, and intravascular applications, or imaging during minimally invasive surgery (i.e. the high frequency ultrasound imaging is crucial in areas where resolution is critical but penetration requirements are small [98]). Since KN has an excellent value of the thickness mode (which is a high frequency mode) coupling coefficient, it is greatly promising for this kind of applications.

hanced longitudinal piezoelectric response along a direction that does not correspond to the polarization axes *in many perovskite ferroelectrics* [118, 119, 155]. The magnitude of this effect is by far the largest in lead-based materials [118, 147], but nevertheless, simpler systems, like BaTiO₃ and KNbO₃, which show *the same effect*, are also of interest because *the problems with mesoscopic structure of relaxor-ferroelectric solid solutions are avoided* [99]. However, it is still not clear whether the enhancement of the piezoelectric response in the complex solid solutions and in the simple perovskite ferroelectrics has the same origin.

Having in mind all the facts mentioned above, the research activities for this thesis work, thus, head in several directions:

1. experimental determination of temperature dependence of piezoelectric, dielectric and elastic material parameters in single crystal KNbO₃ will be attempted; such a study can be made only over a limited temperature range (orthorhombic ferroelectric phase), where single domain state can be assured – with these measurements the determination of missing coefficients of the Devonshire function and the refinement of existing coefficients will be tried;
2. the question of the intrinsic origins (temperature and composition related) of the piezoelectric anisotropy will be investigated in classical perovskites by combining the framework of phenomenological Landau-Ginzburg-Devonshire theory [31, 32], experimental data published in literature and experimental results obtained in this work; the task has a great importance because of the possibility to correlate between temperature effects on anisotropy in simple single crystal perovskites and the composition effects in the complex solid solutions of relaxor – ferroelectrics; this may give an opportunity to get a global picture (i.e. a general model) for behavior of the piezoelectric properties of all perovskite structures;
3. the influence of external bias electric fields and mechanical stresses on the piezoelectric response and its anisotropy in classical ferroelectric perovskites will be investigated phenomenologically - it turns out that, for some bias fields configurations, large changes in electromechanical properties of these materials can be expected;
4. the question *”Is there a common thermodynamic description behind the electromechanical properties enhancement and their anisotropy in all perovskite ferroelectrics?”* will be discussed in detail - and, hopefully, answered.

Structure of the report

The report is divided into 9 chapters.

Chapter 2 gives a short review of the theoretical background behind the work. Its purpose is to facilitate the reading to non-experts and to give the report a certain autonomy. In *Chapter 3* a review of key publications on which this thesis work relies is presented. The chapter is divided into two sections - a section reviewing the literature concerning the experimental and theoretical results of structural and electromechanical properties of potassium niobate in single crystal form, and a section on the phenomenological Landau - Ginzburg - Devonshire theory modeling of perovskite ferroelectrics electromechanical behavior and topics essentially related to studying the problem of piezoelectric anisotropy origins in classic perovskites.

Chapter 4 presents experimental techniques used to obtain the electromechanical properties values of KN.

In *Chapter 5* the temperature dependence of electromechanical coefficients is measured, and coefficients for a phenomenological description of potassium niobate are estimated. Using the phenomenological Landau-Ginzburg-Devonshire theory and classic ferroelectric perovskites, the intrinsic origins of the enhanced response along non-polar axes are investigated and discussed in *Chapter 6*.

In *Chapter 7* different classic perovskite systems under different configurations of electric and mechanic bias fields are discussed.

In *Chapter 8* the question of the origin of the piezoelectric properties enhancement in perovskite ferroelectrics is approached by analyzing the Gibbs free energy of tetragonal BaTiO_3 , PbTiO_3 and $\text{Pb}(\text{Zr,Ti})\text{O}_3$ in the framework of the Landau-Ginzburg-Devonshire theory.

General conclusions and perspectives are given in *Chapter 9*.

Chapter 2

Basic concepts and definitions

A short review of the theoretical background is given. Its purpose is to facilitate the reading to non-experts and to give a certain autonomy to this report.

2.1 Spontaneous polarization. Ferroelectricity

All dielectrics can be polarized by application of an electric field. Nevertheless, under certain conditions, some dielectrics also possess a *spontaneous polarization* or electric moment per unit volume.

A crystal is defined as *ferroelectric* when it has at least two orientation states of spontaneous polarization in the absence of an external electric field and can be shifted from one to another of these states by an electric field. Any two of the orientation states are enantiomorphous and differ only in dielectric polarization vector at null electric field.

This definition is oversimplified - whether or not a real material is ferroelectric depends on experimental limitations - crystal perfection, electrical conductivity, temperature and pressure are all factors which affect the reversibility of the polarization.

Ferroelectric domains. The spontaneous polarization in a ferroelectric material is usually not uniformly aligned throughout the whole material along the same direction. The regions in the material with uniformly oriented spontaneous polarization are called *ferroelectric domains* and the region separating two domains is called a *domain wall*. Ferroelectric domains form to minimize the electrostatic energy of depolarizing fields and the elastic energy associated with mechanical constraints to which the ferroelectric

material is subjected as it is cooled through paraelectric - ferroelectric or ferroelectric - ferroelectric phase transition.

Types of domain walls that can occur in a ferroelectric crystal depend on the symmetry of both non-ferroelectric and ferroelectric phases of the crystal. The criteria which may be used to derive possible types of domain walls in a ferroelectric material were derived by *Fousek* and *Janovec* [43]. The domain walls are usually labeled by the angle between the spontaneous polarization vectors in the domains that these walls separate. For example, 90° -walls are the ones that separate regions with mutually perpendicular polarization (although the angle between polarization directions on each side of a 90° domain wall is slightly smaller than 90° [134]).

The existence of ferroelectric domains in the material can contribute enormously to material's overall electromechanic performances. Small displacements of all types of domain walls will affect the polarization of the material whereas the movement of non- 180° walls will, in addition to the polarization change, directly contribute to the piezoelectric effect [26]. Movement of domain walls at weak to moderate fields is one of the most important so-called extrinsic (non-lattice) contributions to the dielectric, elastic and piezoelectric properties of ferroelectric materials [168, 167, 25, 56] and may be comparable to the intrinsic effect of the lattice [29, 12].

It is interesting to mention that ferroelectric domain walls are much thinner than domain walls in ferromagnetic materials. Observations with transmission electron microscopy show that domain walls thickness in ferroelectric films is of the order of $1 - 10nm$ [97, 134].

Ferroelectric hysteresis loop and polarization switching. The most important characteristic of ferroelectric materials is its *spontaneous polarization reversal* (or switching) by an electric field. One consequence of the domain-wall switching in ferroelectric materials is the occurrence of the *ferroelectric hysteresis loop*. The hysteresis loop can be observed experimentally by using a Sawyer-Tower circuit (see *Chapter 4*).

To discuss a hysteretic behavior more thoroughly, let us take a look at Fig. 2.1. This figure represents a behavior of a ferroelectric material under an applied electric field. At small values of the field, the polarization increases linearly with the field amplitude. In this region, the field is too weak to switch domains with the unfavorable direction of polarization. As the field is increased the polarization of domains with an unfavorable direction of polarization starts switching to the field direction, rapidly increasing the measured charge density. The polarization response in this region is strongly nonlinear. Once all the domains are aligned, the polarization again changes linearly (*the saturation region*). If the field strength now starts decreasing, some domains will back-switch but

at zero field the polarization is nonzero. This value of the polarization at zero field is called *the remnant polarization*, P_R . To reach the zero polarization state, the field must be reversed. Further increase of the field in the negative direction will cause a new alignment of dipoles and saturation. To complete the cycle, the field strength is then reduced to zero and reversed to the positive direction. The value of the electric field at which the polarization is zero is called *the coercive field*, E_C . The spontaneous polarization P_S is usually taken to be the value of the intercept of the polarization axis with the extrapolated linear segment of the saturation part of the hysteresis loop. It should be mentioned that the coercive field E_C that is determined from the intercept of the hysteresis loop with the field axis is not an absolute threshold field [15]. If a low electric field is applied over a (very) long time period, the polarization will eventually switch.

An ideal hysteresis loop is symmetrical so that $+E_C = -E_C$, and $+P_R = -P_R$. The

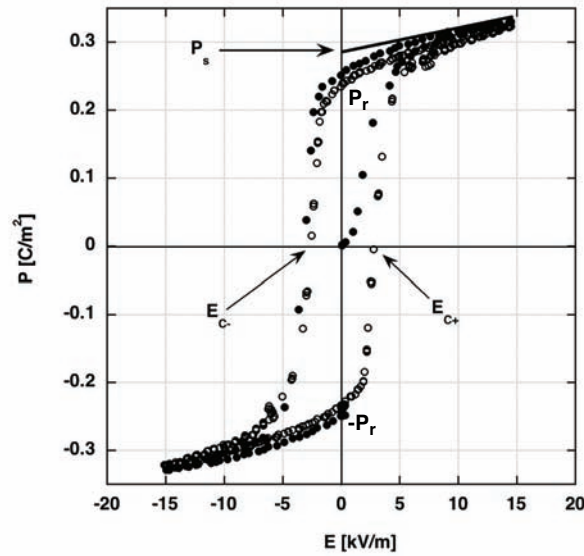


Figure 2.1: An example of the ferroelectric hysteresis loop (measured on a sample of a rhombohedral PMN-PT poled along the $[001]$ direction, courtesy of M. Davis). In this case (values measured along a non-polar direction) the value of the polarization at zero electric field is the remnant polarization, $P_R^{[001]}$, the value of the electric field at which the polarization is zero is the coercive field, $E_C^{[001]}$, and the spontaneous polarization, $P_S^{[001]}$, is usually taken to be the value of the intercept of the polarization axis with the extrapolated linear segment of the saturation part of the hysteresis loop. To get the values along the spontaneous polarization direction, one should multiply these values by $\sqrt{3}$.

coercive field, spontaneous and remnant polarization and shape of the loop may be affected by many factors - the thickness of the tested sample, the presence of charged

defects, mechanical stresses, preparation conditions, thermal treatment, surface state.

2.2 Pyroelectric effect

The ancient discovery of pyroelectricity¹ can probably be attributed to a fact that high electric fields can develop across insulating pyroelectrics subjected to relatively small temperature changes. For instance, a crystal with a typical pyroelectric coefficient of $10^{-8}Ccm^{-2}K^{-1}$ and a dielectric constant of 50 develops a field of $50kV/cm^{-1}$ - sufficient to break down air - with just a $25^\circ C$ temperature change.

The pyroelectric coefficient is thus defined as the change of the vector of spontaneous polarization with temperature T

$$p_i = \frac{\partial P_{s,i}}{\partial T} \quad (2.1)$$

Equation (2.1) may be also written in the form

$$D_i = \Delta P_{s,i} = p_i \Delta T, \quad (2.2)$$

where D_i is the surface charge density induced in the material by the temperature change ΔT .

The charge due to the spontaneous polarization is usually masked by charges from the surrounding part of the material, and it is experimentally easier to observe *changes* in the spontaneous polarization rather than the spontaneous polarization value itself.

2.3 Piezoelectric effect

Electric field and polarization. The linear relation between the electric field E_i applied to the dielectric and the induced polarization P_i

$$P_i = \chi_{ij} E_j \quad (2.3)$$

defines the dielectric susceptibility χ_{ij} of the material, a second rank tensor. Summation over the repeated indices is implied.

The relation (2.3) is only approximate - the polarization P_i generally depends on higher order terms of the field E_j . Similarly, in a general case the dielectric susceptibility χ_{ij} is a function of the electric field.

The polarization is thus related to the electric field, *and* to the dielectric displacement, by the equation

$$P_i = D_i - \varepsilon_0 E_i = \varepsilon_{ij} E_j - \varepsilon_0 E_i. \quad (2.4)$$

¹In writings of Theophrastus in 314 BC.

Stress and strain. Stress and strain describe the elastic properties of a homogenous, deformable, continuous solid in thermodynamic equilibrium. The stress, X_{ij} , is defined as the force per unit area and it is a second rank tensor. Components of the stress perpendicular to the surface are called the normal and those parallel to the surface upon which they act are called *the shear* components. The tensile stresses are defined as positive and the compressive stresses as negative. By this definition, the stress can be represented by a symmetrical tensor, and it can be shown that this is true even if the stress is not homogeneous [116].

A relative deformation of a body caused by stress is called the strain. The strain, x_{ij} , is a dimensionless, symmetrical, second rank tensor.

In the first approximation, a linear relation between the stress and strain is

$$x_{ij} = s_{ijkl}X_{kl}. \quad (2.5)$$

This is *Hook's law*. s_{ijkl} is the *elastic compliance* of the material, a fourth rank tensor. The inverse relation

$$X_{ij} = c_{ijkl}x_{kl}. \quad (2.6)$$

defines the *elastic stiffness* coefficients, also a fourth rank tensor. Obviously, $c_{ijkl}^{-1} = s_{ijkl}$. Due to the symmetry of the stress and strain there are a maximum of 36 independent components of the c_{ijkl} and s_{ijkl} tensors and this number is further reduced due to the *Maxwell relations*² (see *Section 2.6*), and due to the symmetry of the material.

Piezoelectric effect. Piezoelectric materials can be polarized, in addition to an electric field, also by a mechanical stress. The linear relation between the stress, X_{ik} , applied to a piezoelectric material, and the resulting charge density, D_i , is called the *direct piezoelectric effect* and may be written as

$$D_i = d_{ijk}X_{jk}, \quad (2.7)$$

where d_{ijk} is a third-rank tensor of piezoelectric coefficients. On the other hand, these materials change their dimensions (they contract or expand) when an electric field E_k is applied to them. The *converse piezoelectric effect* describes the strain that is developed in a piezoelectric material when the electric field is applied

$$x_{ij} = d_{kij}E_k = d_{ijk}^t E_k, \quad (2.8)$$

where t denotes the transposed matrix. The piezoelectric coefficients d for the direct and converse piezoelectric effect are thermodynamically identical (see *Section 2.5*), i.e.

²36→21 independent coefficients

$d_{direct} = d_{converse}$. It is common to call a piezoelectric coefficient in the direction of applied field *the longitudinal coefficient*, and that in the direction perpendicular to the field *the transversal coefficient*. Other piezoelectric coefficients are called *shear coefficients*. The piezoelectric effect was discovered in 1880 by *Pierre* and *Jacques Curie*. They predicted the occurrence of the electric charge on a surface of the crystal subjected to a compressive stress, if the structure possessed a certain symmetry. Later, they experimentally proved their prediction.

2.4 Electrostrictive effect

Electrostriction is a property of all dielectrics, regardless of their symmetry. It produces a relatively small mechanical deformation under an applied electric field. Reversal of the electric field does not reverse the direction of the deformation - it is an example of nonlinear coupling between elastic and electric fields. If an electric field E_i is applied on a material, the electrostrictive strain x_{ij} is defined by

$$x_{ij} = M_{ijkl}E_kE_l, \quad (2.9)$$

where M_{ijkl} are components of the fourth-rank tensor and are called *the electrostrictive coefficients*. The electrostrictive effect can also be expressed in terms of the vector of the induced polarization

$$x_{ij} = Q_{ijkl}P_kP_l, \quad (2.10)$$

where Q_{ijkl} and M_{ijkl} are related by

$$M_{ijmn} = \chi_{km}\chi_{ln}Q_{ijkl}. \quad (2.11)$$

In ferroelectric materials the polarization at strong fields is a nonlinear function of the electric field so that (2.9) and (2.10) cannot be both valid. The equation (2.10) is a more consistent way to describe the electrostrictive effect in dielectrically nonlinear materials.

2.5 Symmetry considerations

The fundamental postulate of crystal physics, known as *Neumann's Principle*, displays how the symmetry of a crystal is related to the symmetry of its physical properties:

"The symmetry elements of any physical property of a crystal must include the symmetry elements of the point group of the crystal."

The point group of a crystal is the group of macroscopic symmetry elements that its

structure possesses. It is the basis for the division of crystals into 32 crystal classes.

This principle does not state the equality of the symmetry elements of a physical property with the elements of the point group - the physical properties often possess more symmetry than the point group.

Of the 32 crystal classes, 21 are non-centrosymmetric, and of these, 20 exhibit direct piezoelectricity the remaining one being the cubic class 432. Ten of these are polar and exhibit pyroelectricity. If this dipole can be reversed by the application of an electric field, the material is ferroelectric as well.

Since the spontaneous polarization can occur in materials which possess an unique polar axis, all pyroelectric materials are piezoelectric, but only some piezoelectric materials (those whose symmetry belongs to polar groups) are pyroelectric (Fig. 2.2).

The symmetry requirements may significantly reduce the number of nonzero and independent elements of a property tensor. For example, the number of the independent elements in the piezoelectric tensor, Eqs. (2.7) and (2.8), is reduced from 27 to 18 because the strain and stress are symmetrical properties, and the piezoelectric tensor is symmetrical with respect to the same indices, $d_{ijk} = d_{ikj}$. The number of independent elements of d_{ijk} may be further reduced by the symmetry of the material - for example $mm2$ symmetry allows 5 independent nonzero tensor elements, while $3m$ symmetry allows only 4 of them [116].

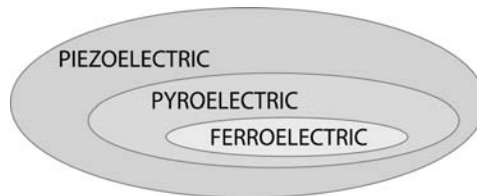


Figure 2.2: All ferroelectric materials are pyroelectric and all pyroelectric materials are piezoelectric.

2.6 Thermodynamic considerations

According to the first and the second law of thermodynamics, the reversible change dU in the internal energy U of an elastic dielectric subjected to a small change of the strain dx , electric displacement dD , and entropy dS is given by

$$dU = TdS + X_{ij}dx_{ij} + E_idD_i, \quad (2.12)$$

where T is the temperature of the material. If one investigates systems under isothermal conditions, and uses electric field and stress as independent variables, it is useful to change the set of independent variables from (S, x, D) to (T, X, E) . To change the independent variables from the original set to the other, a *Legendre transformation* [121, 13] of U has to be performed, by adding the expression $-TS - Xx - ED$ to U . The resulting free energy function

$$G = U - TS - X_{ij}x_{ij} - E_i D_i \quad (2.13)$$

is known as the *Gibbs free energy*. Any natural process occurs *if and only if* the associated change in G of the process is *negative*. Likewise, a system reaches an equilibrium when the associated change in G is *zero*.

The differential of G gives, together with (2.12),

$$dG = -SdT - x_{ij}dX_{ij} - D_i dE_i. \quad (2.14)$$

From this equation one obtains

$$S = -\left(\frac{\partial G}{\partial T}\right)_{X,E} \quad x_{ij} = -\left(\frac{\partial G}{\partial X_{ij}}\right)_{T,E} \quad D_i = -\left(\frac{\partial G}{\partial E_i}\right)_{T,X}, \quad (2.15)$$

where the subscripts indicate variables kept constant. The total differential of S , X , and D can be written as

$$dS = -\left(\frac{\partial S}{\partial T}\right)_{X,E} dT + \left(\frac{\partial S}{\partial X_{ij}}\right)_{T,E} dX_{ij} + \left(\frac{\partial S}{\partial E_i}\right)_{T,X} dE_i, \quad (2.16)$$

$$dx_{ij} = -\left(\frac{\partial x_{ij}}{\partial T}\right)_{X,E} dT + \left(\frac{\partial x_{ij}}{\partial X_{kl}}\right)_{T,E} dX_{kl} + \left(\frac{\partial x_{ij}}{\partial E_k}\right)_{T,X} dE_k, \quad (2.17)$$

$$dD_i = -\left(\frac{\partial D_i}{\partial T}\right)_{X,E} dT + \left(\frac{\partial D_i}{\partial X_{jk}}\right)_{T,E} dX_{jk} + \left(\frac{\partial D_i}{\partial E_j}\right)_{T,X} dE_j. \quad (2.18)$$

Each of the partial derivatives in these equations identifies a physical effect [116]. The order in which the derivatives are taken is irrelevant, and it follows that, for example

$$d_{ijk}^{T,X} = \left(\frac{\partial x_{ij}}{\partial E_k}\right)_{T,X} = -\left(\frac{\partial^2 G}{\partial E_k \partial X_{ij}}\right) = -\left(\frac{\partial^2 G}{\partial X_{ij} \partial E_k}\right) = \left(\frac{\partial D_k}{\partial X_{ij}}\right)_{T,E} = d_{kij}^{T,E} \quad (2.19)$$

This equation demonstrates *the thermodynamic equivalence of the direct and converse piezoelectric effect*. Using other thermodynamic potentials which can be formed by taking Legendre transformations of the internal energy, it is possible to write a total of 27 relations, such as this one, which are known as *Maxwell relations*.

It is common to express the equations (2.15) - (2.17) in integrated forms, taking dE and dX as small deviations from the zero initial stress and field

$$\Delta S = \frac{c^{X,E}}{T} \Delta T + \alpha_{ij}^{T,E} X_{ij} + p_i^{T,X} E_i, \quad (2.20)$$

$$x_{ij} = \alpha_{ij}^{X,E} X_{ij} \Delta T + s_{ijkl}^{T,E} X_{kl} + d_{ijkl}^{T,X} E_k, \quad (2.21)$$

$$D_i = p_i^{X,E} \Delta T + d_{ijk}^{T,E} X_{jk} + \varepsilon_{ij}^{T,X} E_j. \quad (2.22)$$

All these relations, (2.15) - (2.22), include *only the linear effects*. In the case of strong fields or strongly nonlinear material such as ferroelectric, these relations must be extended to include higher-order terms.

For isothermal processes, equations (2.21) and (2.22), written in the matrix notation, reduce to

$$x_m = s_{m,n}^{T,E} X_n + d_{im}^{T,X} E_i \quad (2.23)$$

$$D_i = d_{im}^{T,E} X_m + \varepsilon_{i,j}^{T,X} E_j. \quad (2.24)$$

These two are known as *the piezoelectric constitutive equations*.

It is important to mention and discuss the dielectric permittivity measured on a clamped (conditions of the zero strain) and free sample. It is trivial to calculate that the constitutive equations give (the tensor indices are omitted for simplicity) $X = -eE = -(d/s^E)E$, and, after inserting this stress into the expression for the dielectric displacement, $D = (\varepsilon^X - d^2/s^E)E = \varepsilon^x E$. The coefficient

$$\varepsilon^x = \varepsilon^X (1 - d^2/s^E \varepsilon^X) = \varepsilon^X (1 - k^2) \quad (2.25)$$

is called *the clamped (zero strain) dielectric constant*. The expression

$$k^2 = d^2/s^E \varepsilon^X \quad (2.26)$$

is known as *the electromechanical coupling coefficient*. In some ferroelectrics k may be as large as 0.9 [118] leading to up to 80% difference between the free and clamped dielectric constant. It can be shown, in a similar way, that the elastic compliance s^D , measured under open-circuit conditions (zero or constant D), and s^E measured under short-circuit conditions (zero or constant E), are related by

$$s^D = s^E (1 - d^2/s^E \varepsilon^X) = s^E (1 - k^2). \quad (2.27)$$

These two examples illustrate the importance of controlling experimental boundary conditions when measuring properties of piezoelectric materials³.

2.6.1 Phenomenological Landau-Ginzburg theory

Ginzburg and *Landau* constructed a completely general theory of continuous symmetry - breaking phase transitions which involves a Taylor series expansion of the Gibbs free

³Also discussed in *Chapter 4*.

energy in terms of the order parameter. One can, for instance, find discussions of this subject in books of *L. D. Landau* and *E. M. Lifshitz* [94], *L. E. Reichl* [121] or *Yu. B. Rumer* and *M. Sh. Ryvkin* [128].

It is assumed in this theory that the order parameter is a tensor η and, then, the general form of the free energy in the region of the phase transition is discussed as a function of η . The free energy must be such that it will be minimized for $\eta = 0$ above the transition and $\eta \neq 0$ below the transition. Furthermore, the free energy is a *scalar function of the order parameter*. Thus, if the order parameter is a vector (an order 1 tensor), the free energy can only depend on scalar products of the order parameter. In general, near the phase transition, the free energy Taylor series is

$$G(T, \eta) = G_0(T) + \alpha_1(T)\eta^2 + \alpha_{11}(T)\eta^4 + \dots \quad (2.28)$$

No first-order or third-order terms will appear because a scalar cannot be constructed from them.

The form of $\alpha_1(T)$ is chosen so that, at the critical temperature and above it, the free energy will only be minimized for $\eta = 0$, and below the critical temperature it will be minimized for $\eta \neq 0$. In general, the free energy will be in its minimum if $(\partial G/\partial \eta)_T = 0$ and $(\partial^2 G/\partial \eta^2)_T > 0$. If one chooses $\alpha_1(T) > 0$ for $T > T_C$ and $\alpha_1(T) < 0$ for $T < T_C$, where T_C is a phase transition temperature, the above condition is satisfied - $G(T, \eta)$ will have its minimum value for $T > T_C$ if $\eta = 0$, while for $T < T_C$ one can have $\eta \neq 0$ and have an energy minimum. Since the free energy must vary continuously through the transition point, at $T = T_C$ one must have $\alpha_1(T_C) = 0$. All these information can be combined if $\alpha_1(T)$ is written in the form

$$\alpha_1(T) = \alpha_0(T - T_C), \quad (2.29)$$

where α_0 can be some function of T .

In order to have a global stability of a thermodynamic system, one must have

$$\alpha_{11}(T) > 0. \quad (2.30)$$

This ensures that, if η increases to very large values, the free energy will increase, and not decrease.

The Ginzburg-Landau theory applies to all continuous symmetry-breaking transitions, although the form of the expansion varies considerably for different physical systems.

Most ferroelectric materials undergo a structural phase transition from a high-temperature non-ferroelectric (or paraelectric) phase into a low-temperature ferroelectric phase. The paraelectric phase may be piezoelectric or non-piezoelectric and is rarely polar [97]. The symmetry of the ferroelectric phase is always lower than the symmetry of the paraelectric phase. The temperature of the phase transition is called the Curie point, T_C . Above

the Curie point the dielectric permittivity falls off with temperature according to the *Curie-Weiss law*

$$\varepsilon = \varepsilon_0 + \frac{C}{T - T_0} \approx \frac{C}{T - T_0} \quad (2.31)$$

where ε_0 is the permittivity of vacuum, C is the *Curie constant*, $T_0 (T_0 \leq T_C)$ is the *Curie-Weiss temperature*. Thus, the coefficient $\alpha_1(T)$ reflects the Curie-Weiss behavior. Transition into a ferroelectric state may be of the first or second order⁴. In general, the order of the phase transition is defined by the discontinuity in the partial derivatives of the Gibbs free energy of the ferroelectric at the phase transition temperature. Thus, for an n th-order phase transition, the n th-order derivative of G is a discontinuous function at the transition temperature [106].

For the ferroelectrics of interest in this work, *the ferroelectric polarization* (P) can be chosen as the order parameter, and thus the Gibbs free energy can appropriately be written as

$$\begin{aligned} \Delta G = & G_0(T) + \alpha_1[P_1^2 + P_2^2 + P_3^2] + \alpha_{11}[P_1^4 + P_2^4 + P_3^4] + \alpha_{111}[P_1^6 + P_2^6 + P_3^6] \\ & + \alpha_{12}[P_1^2 P_2^2 + P_2^2 P_3^2 + P_3^2 P_1^2] \\ & + \alpha_{112}[P_1^4(P_2^2 + P_3^2) + P_2^4(P_1^2 + P_3^2) + P_3^4(P_1^2 + P_2^2)] \\ & + \alpha_{123}P_1^2 P_2^2 P_3^2 - \frac{1}{2}s_{11}[X_1^2 + X_2^2 + X_3^2] - s_{12}[X_1 X_2 + X_2 X_3 + X_3 X_1] \\ & - \frac{1}{2}s_{44}[X_4^2 + X_5^2 + X_6^2] - Q_{11}[X_1 P_1^2 + X_2 P_2^2 + X_3 P_3^2] \\ & - Q_{12}[X_1(P_2^2 + P_3^2) + X_2(P_1^2 + P_3^2) + X_3(P_1^2 + P_2^2)] \\ & - Q_{44}[X_4 P_2 P_3 + X_5 P_1 P_3 + X_6 P_1 P_2] \\ & + \dots \end{aligned} \quad (2.32)$$

⁴Most of the discussion about perovskite ferroelectrics centers around two end-member models for the transitions. At one extreme, the soft-mode [11, 57], displacive model assumes that a transverse optical phonon frequency softens and vanishes at the phase transition. This model can most easily be used to treat a material such as PbTiO_3 which has only one ferroelectric phase transition. At the other extreme, the order-disorder eight site model [139, 18, 20, 92, 37] assumes that in the cubic phase, the atoms are randomly displaced in local minima along the eight cube diagonal, $[111]_c$, directions. In the orthorhombic phase the displacements average over two cube diagonals giving an average $[110]_c$ displacement, and in the ground state rhombohedral phase the displacements are ordered along only one cube diagonal. Experimental evidence shows that far away from the transitions the displacive model is appropriate, but as the transitions are approached the order-disorder character predominates [107]. This is obvious if one, for example, studies BaTiO_3 by infrared spectroscopy; the soft-mode frequency of barium titanate does not vanish at cubic \rightarrow tetragonal transition in BaTiO_3 , for example, but rather the soft mode splits into a hard mode and two other modes; these latter modes continue to soften with decreasing temperature. At the tetragonal \rightarrow orthorhombic transition one of these two models hardens and the other continues to soften until the orthorhombic \rightarrow rhombohedral transition.

where α_i , α_{ij} , and α_{ijk} are ferroelectric dielectric stiffness coefficients at constant stress, s_{ij} elastic compliances at constant polarization, and Q_{ij} the coefficients of electrostrictive coupling between the ferroelectric polarization and stress.

Early theoretical investigations of phase transitions in perovskites in the framework of this model were concentrated on BaTiO_3 , which goes through a sequence of phases upon cooling: cubic, tetragonal, orthorhombic and rhombohedral. *Devonshire* [31, 32] explained the behavior of this material within the Landau-Ginzburg-Devonshire framework by expanding the Gibbs free energy of BaTiO_3 up to the sixth order in terms of the ferroelectric order parameter - the polarization. On the other hand, *relaxor ferroelectrics* or *relaxors* [22], such as $\text{Pb}(\text{Mg}_{1/3}\text{Nb}_{2/3})\text{O}_3$, characterized by a chemical heterogeneity on nanometer scale, display a diffuse and a broad maximum in the dielectric permittivity and a strong frequency dispersion of the permittivity below the temperature of the maximum permittivity [26]. Above the temperature of the maximum permittivity, relaxors do not obey the Curie-Weiss behavior.

It has been shown recently [131] that, in the case of perovskites, the Gibbs free energy has to be expanded up to the twelfth-order terms to describe completely the phase diagram induced by the ferroelectric order parameter.

Chapter 3

Literature

A review of key publications on which this thesis work relies is presented. The chapter is divided into two sections - a section reviewing the literature concerning the experimental and theoretical results of structural and electromechanical properties of potassium niobate in single crystal form, and a section on the phenomenological Landau - Ginzburg - Devonshire theory modeling of perovskite ferroelectrics electromechanical behavior and topics essentially related to studying the problem of piezoelectric anisotropy origins in classic perovskites.

The most useful textbooks for this work, considering the basic subjects of crystal physics, dielectric, ferroelectric and piezoelectric properties of perovskites and related materials were those of *J. F. Nye* [116], of *T. Mitsui, I. Tatsuzaki* and *E. Nakamura* [1], of *B. Jaffe, W. R. Cook* and *H. Jaffe* [79], of *F. Jona, G. Shirane* [81], and of *M. E. Lines* and *A. M. Glass* [97].

For the phenomenological theories descriptions, very useful were textbooks of *L. E. Reichl* [121], and of *L. D. Landau* and *E. M. Lifshitz* [94].

3.1 Electromechanical properties of single crystal potassium niobate

Potassium niobate in single crystal form has become only recently a material of interest for piezoelectric applications. Since its discovery, this material has mostly drawn attention as an excellent material for optical applications, and most investigations on its properties were directed by that fact.

An evidence of ferroelectricity in this material (and in NaNbO_3) was shown for the first

time in 1951 by *Matthias and Remeika* [100]. In that work the authors also presented photographs of dielectric hysteresis loops and values of saturation polarization taken at various points in the tetragonal phase temperature range (Fig. 3.1). Three years

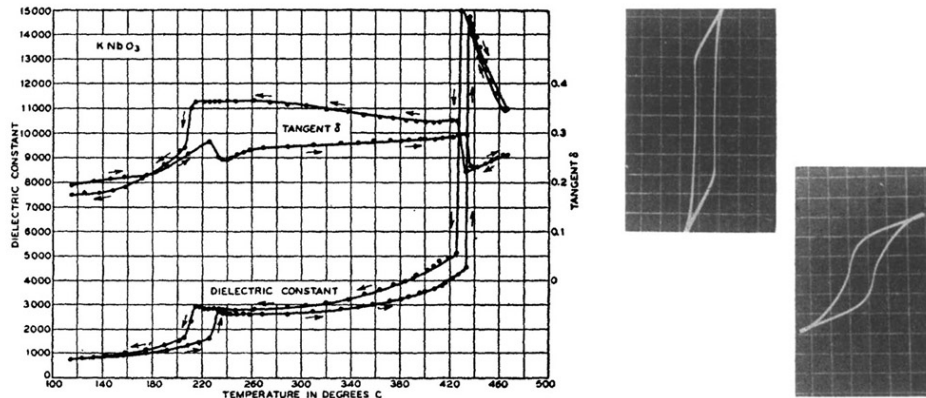


Figure 3.1: The first reported measurements of dielectric constant, loss tangent curves and hysteresis loops for single crystals of KNbO_3 , by *Matthias and Remeika* in 1951 [100].

later, *Shirane et al.* showed [132] that ferroelectric KNbO_3 undergoes another phase transition at -10°C upon cooling, in addition to two phase transitions previously reported at 435°C (paraelectric cubic \rightarrow ferroelectric tetragonal) and 225°C (ferroelectric tetragonal \rightarrow ferroelectric orthorhombic). At this, the lowest, phase transition temperature, KNbO_3 changes its orthorhombic structure to a rhombohedral one.

Spontaneous polarization. Pyroelectric coefficient. Surface layer properties and influence of impurities. Measurements of the spontaneous polarization values in KN have been quite a difficult problem for a long time because it has not usually been easy to grow crystals with a quality high enough to obtain good and reproducible results. Nevertheless, *Triebwasser* [144] reported in 1955 a spontaneous polarization value in the tetragonal ferroelectric phase. He measured a value of $P_s = 26\mu\text{C}/\text{cm}^2$ at the orthorhombic-tetragonal transition (with an uncertainty of 10%) from ferroelectric hysteresis measurements; the author also published, in 1956, the obtained ferroelectric hysteresis curves in the tetragonal ferroelectric phase of KN [143]. *Günter* measured in 1977 [55] $P_s = 41 \pm 2\mu\text{C}/\text{cm}^2$ in a single domain orthorhombic KNbO_3 by Camlibel pulse method [16]. The author reported in the same paper measurements of the temperature dependence of the KN pyroelectric coefficient and calculated the temperature dependence of the spontaneous polarization by using the Devonshire phenomenological model [31, 32], Fig. 3.3. Measurements of the spontaneous polarization were also done by *Hewat* in 1973 [65], *Kleemann et al.* in 1984 [87], and *Szot et al.* in 1996 [136], Table

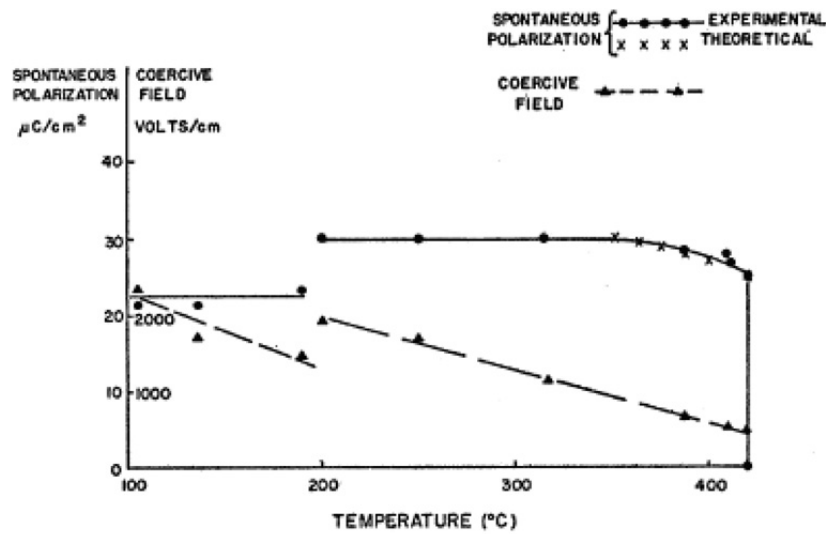


Figure 3.2: Spontaneous polarization and coercive field for KNbO_3 single crystal in the tetragonal and orthorhombic phase. Taken from Ref. [143].

3.1.

The spontaneous polarization has also been calculated theoretically by several authors - *Kam* and *Henkel* [84] have reported a good agreement of calculated value with measurements by *Günther*, and *R. Resta et al.* calculated [124] the spontaneous polarization value in KNbO_3 of $P_s = 35 \mu\text{C}/\text{cm}^2$ using the Bloch functions of the tetragonal crystal, Table 3.1.

That the influence of the surface layer properties and impurities on the bulk electromechanical properties is very important has been shown in many papers. For example, *Szot et al.* have shown [135] by electron spectroscopy investigations, that defects at various concentrations were inherently present on surfaces of KNbO_3 crystals, and that those defects were important for most classical measurements on this material. The same author has shown [136] that the surface layer of KN was very heterogeneous and that the anomalous increase of the spontaneous polarization at low frequencies, as well reported in this paper, was almost completely determined by the heterogeneous surface.

Domain structure. Poling. The domain structure of KN has a very important influence on its electromechanical properties, and the importance of this influence is still under discussion. For example: on one hand, *Topolov* has shown, theoretically [142], a strong role of domain-orientation effects on the longitudinal piezoelectric coefficient of polydomain KNbO_3 , while, on the other, *Nakamura et al.* have demonstrated that

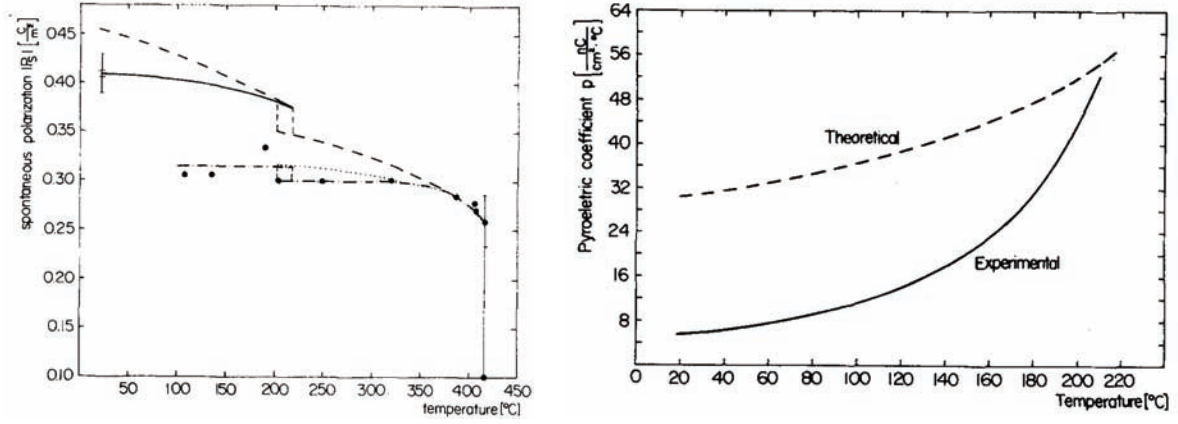


Figure 3.3: Spontaneous polarization of orthorhombic and tetragonal KNbO_3 as a function of temperature, solid lines and dots, and theoretical calculations in the framework of Devonshire free energy expansion, dashed lines, (left); temperature dependence of the pyroelectric coefficient p for orthorhombic KNbO_3 (relative errors $\pm 20\%$) and calculated theoretical value of p . Taken from Ref. [55].

Spontaneous polarization values of single domain KN, $P_s[\mu\text{Ccm}^{-2}]$		
	tetragonal phase	orthorhombic phase
<i>Triebwasser</i> [143]	26* (270°C)	-
<i>Hewat</i> [65]	30±2* (270°C); 33±2+ (270°C)	32±3* (20°C); 36±2+ (20°C)
<i>Kam and Henkel</i> [84]	39.6+ (270°C)	-
<i>Resta et al.</i> [124]	35+ (270°C)	-
<i>Günther</i> [55]	-	42±2*
<i>Szot et al.</i> [136]	31*	-
<i>Kim and Yoon</i> [86]	-	42* (RT)
<i>Fontana et al.</i> [40]	37.1+	42.9+
<i>Kleemann et al.</i> [87]	37.3* (227°C)	43.3* (27°C)
* - measured; + - calculated;		

Table 3.1: Literature review of single domain KN spontaneous polarization measurements and theoretical calculations.

the $(001)_{pc}$ cut crystal poled along the $\langle 001 \rangle_{pc}$ direction has a polar multidomain structure and that the material exhibits almost the same piezoelectric properties as those of single-domain crystals [110].

In 1973, *Wiesendanger* studied [159], by optical methods and etching techniques, the domain configurations in large KN samples grown by a top seeded flux growth technique - he presented an experimental evidence for existence of a new type of ferroelectric domain wall, so called the S-wall. Miller indices of such walls are irrational and depend on spontaneous strain tensor coefficients. The author as well described in that paper a procedure of preparation of large single domain crystals.

Further, *Lian et al.* investigated [96] the behavior of domain walls in KN with temperature variation from room temperature to 300°C by a heating visualisation system. They have observed that domain walls show active behavior only in a small temperature range from the phase transition temperature of 225°C , the range about 10°C in the orthorhombic phase and 15°C in the tetragonal phase.

It could have been easily concluded, both from the literature and from our own experience, that an optimized poling method of KN samples has been crucial for the electromechanical properties measurements. There are several reports of poling procedures descriptions in the literature. There is a paper by *Wada et al.* [154] in which the authors have found that the optimum procedure for poling of KN was a new 2-step poling method (Fig. 3.4), and, already mentioned, the paper from *Wiesendanger* [159].

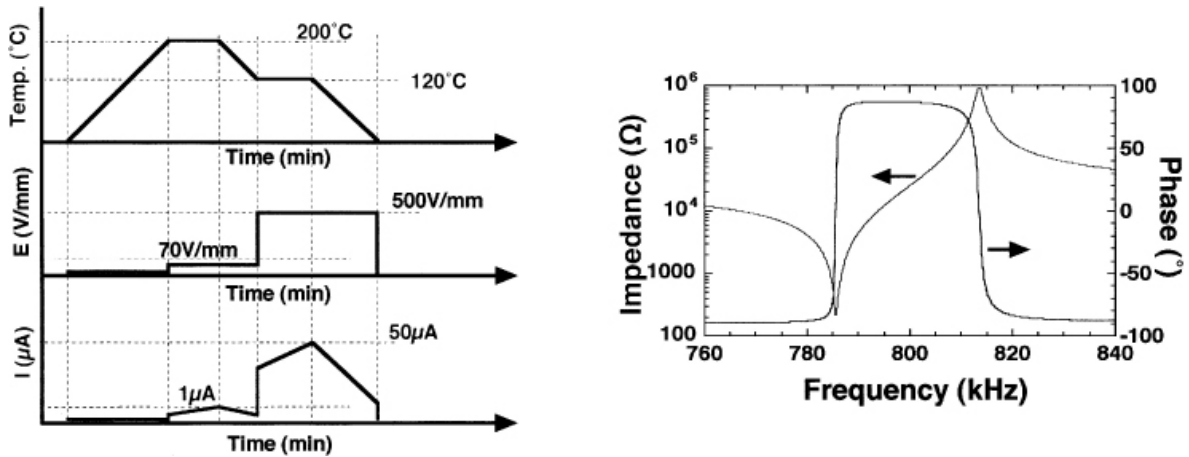


Figure 3.4: Schematic poling program using a 2-step poling method for $[110]_c$ oriented KNbO_3 crystals (left); frequency dependence of $|Z|$ and θ measured at 25° for $[110]_c$ oriented KNbO_3 crystals poled using the optimum conditions (right). Taken from Ref. [154].

There are also KN poling methods reported in papers by *Fukuda et al.* [45], *Kalinichev et al.* [83], *J. H. Kim and Yoon* [86] (they also measured the spontaneous polarization

value in that paper), and *Hirohashi et al.* [66]. In addition, *Hirohashi et al.* [67] have reported the investigation of the controllability of specific domain structures in KN by electric poling to several different orientations at room temperature¹. All these poling methods are gathered in Table 3.2.

Poling procedures for KN	
<i>Wiesendanger</i> , 1973 [159]	application of an electric fields in silicone oil at 200°C
<i>Fukuda et al.</i> , 1974 [45]	application of a DC electric field of $2kV/cm$ at about 190° along the polar axis
<i>Kalinichev et al.</i> , 1993 [83]	application of a DC electric field of $500V/cm$ in silicone oil at 198° along the polar axis
<i>Wada et al.</i> , 2001 [154]	two-step poling method with an etching of samples in $HNO_3:HCl$ mixture, to reduce microcracks of defects near the crystal structure, and with polishing
<i>Kim and Yoon</i> , 2002 [86]	application of a DC electric field of $400 - 600V/mm$ along the polar axis
<i>Hirohashi et al.</i> , 2003 [66]	application of a DC electric field of $200V/m$ along the polar axis at 215°C and then annealing for 120 hours at 195°C

Table 3.2: Literature review of different poling methods of KN.

Dielectric, elastic and piezoelectric properties. Landau-Ginzburg-Devonshire coefficients of $KNbO_3$. The electromechanical properties of KN have been investigated by several authors. As mentioned, after the work of *Matthias* and *Remeika* [100], *Triebwasser* was the first to report both the results of measured [143] dielectric constants and spontaneous polarization values on single crystal $KNbO_3$. He also found, from these values, the coefficients of the first three terms of the free energy expressed as a power series in the polarization - a comparison with Devonshire's phenomenological treatment showed a reasonable agreement with predicted values for dielectric constant and spontaneous polarization. Further, *Phatak et al.* determined, in 1972, all nine elastic constants of orthorhombic potassium niobate at room temperature from a diffractometric study of 006, 040 and 600 diffuse reflections [120]. Two years after this work, dielectric, piezoelectric and elastic constants were measured in single domain

¹By applying electric field to the direction corresponding to the differential direction between the original and intended spontaneous polarization directions 60°-, 90°-, and 180°-domain pairs were successfully fabricated under control in $KNbO_3$, while uncharged 120°-domain pairs are difficult to generate.

orthorhombic KNbO_3 by *Wiesendanger* [160], and temperature dependence dielectric constant of orthorhombic KNbO_3 single domain crystal was measured by *Fukuda et al.* [45]. In 1977, *Günter* publishes [54] room temperature values of piezoelectric coefficients

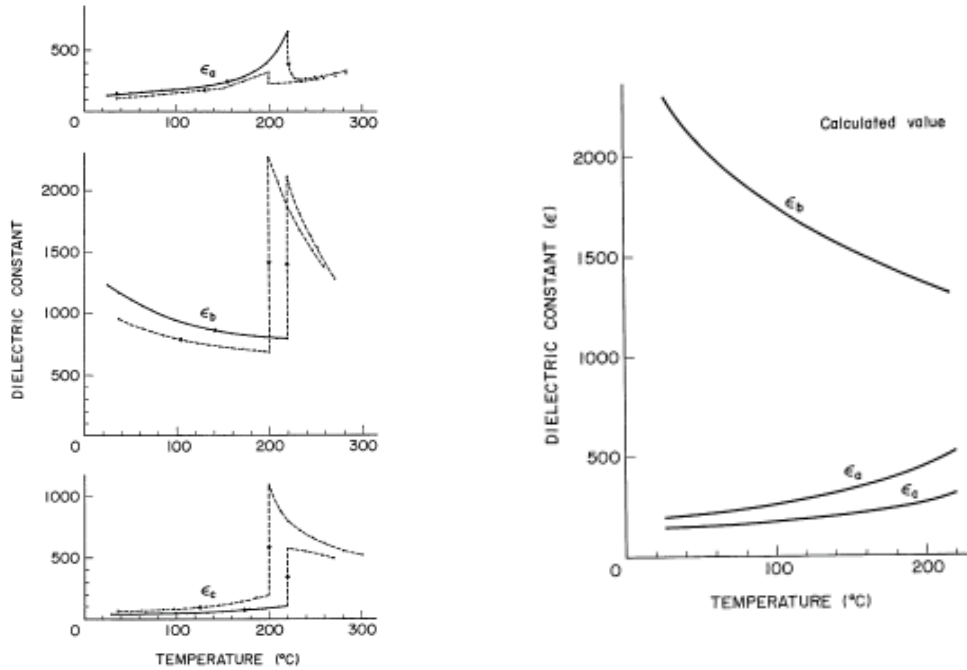


Figure 3.5: Relative dielectric permittivity of orthorhombic single domain KNbO_3 and tetragonal multidomain crystal versus temperature (left); the same constants for the orthorhombic phase calculated in the framework of the Landau-Ginzburg-Devonshire phenomenological theory. Taken from Ref. [45].

of single domain KN, together with the electrostrictive constants calculated from piezoelectric coefficients in the polar phase. The author as well showed in that paper the temperature dependence of the single domain KN longitudinal piezoelectric coefficient, d_{33} , throughout the orthorhombic ferroelectric phase (Fig. 3.6). In 1993, *Kalinichev et al.* [83] used Brillouin light scattering to obtain elastic and piezoelectric constants for single domain orthorhombic KN at room temperature and pressure, and *Zgonik et al.* determined the elastic, piezoelectric, dielectric, elasto-optic, and electro-optic tensors by numerically evaluating the measurements published before their work and using the additional measurements done by them [166]. Finally, in 2001, *Wada et al.* investigated [154] the piezoelectric properties of the material as a function of crystallographic orientations. This review is systematized in Table 3.3.

From the applications point of view, one of the most potential problems of KN is the high dielectric loss and its frequency dependence. The importance of this problem is

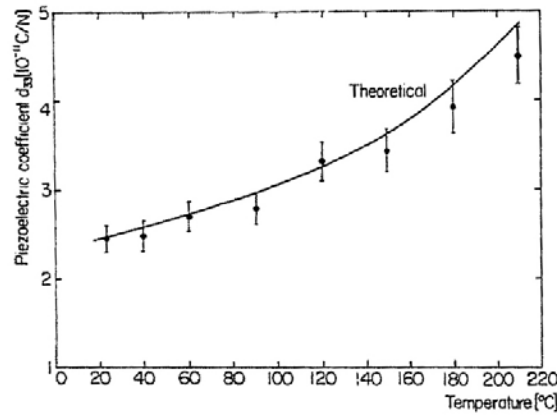


Figure 3.6: Temperature dependence of the piezoelectric coefficient d_{33} in orthorhombic single domain KNbO_3 from room temperature to temperatures near the orthorhombic-tetragonal phase transition, together with a theoretical fit. Taken from Ref. [54].

nically illustrated in the paper of *Kari et al.* [85]. There, the authors have investigated KN as an ultrasonic transducer material, and a comparison of the capacitance and dielectric loss for KNbO_3 and another single crystal, LiNbO_3 , was made. The results showed the relatively high losses for KNbO_3 at very low frequencies. These losses may be attributed to the relatively high porosity of the crystal². As the frequency increases, however, the loss reduces. Hence, for an optimally matched transducer the losses should not affect the overall performance.

Coupling coefficients. It has already been mentioned (*Chapter 1*) - the most attractive electromechanical property of KN is its high thickness mode coupling coefficient, which makes this material promising for designing the single element high frequency transducers.

In the paper of *K. Nakamura* [111] the orientation dependence of electromechanical coupling coefficients for bulk waves in KN was calculated for various types of vibration modes. It was found that the maximum coupling factor of the thickness-extensional mode and the thickness-shear mode, excited with a perpendicular field, k_t and k_s , respectively, were as high as 69% and 88% (larger than the largest reported before), for the rotated X - cut by an angle 49.5° about the Y-axis, and for the X-cut, respectively. These predictions were later experimentally confirmed in the work done by the same

²The crystal surface around the pores forms an easy path for the K^+ ions to drift under the measuring electrical field and hence gives rise to a dielectric loss and a space charge build up at the electrodes (*T. Ritter et al.* [125]).

	ε_{ij}	C_{ijkl}	d_{ijk}	Q_{ij}	LGD
<i>Matthias and Remeika</i> , 1951 [100]	+	-	-	-	-
<i>Triebwasser</i> , 1956 [143]	+	-	-	-	+
<i>Phatak et al.</i> , 1972 [120]	-	+	-	-	-
<i>Fukuda et al.</i> , 1974 [45]	+	-	-	-	-
<i>Wiesendanger</i> , 1974 [160]	+	+	+	-	-
<i>Günter</i> , 1977 [54]	-	+	-	+	-
<i>Kalinichev et al.</i> , 1993 [83]	-	+	+	-	-
<i>Zgonik et al.</i> , 1993 [166]	+	+	+	-	-
<i>Wada et al.</i> , 2001 [154]	+	-	+	-	-

Table 3.3: Publications review of measurements of single domain KN electromechanical properties.

author, together with *Tokiwa* and *Kawamura* [110].

3.2 Phenomenological modeling on perovskites. Polarization rotation. Ultrahigh electromechanical properties

The basic concepts of the phenomenological Landau-Ginzburg theory are given in *Chapter 2*, while useful textbooks about this subject are presented at the beginning of this chapter.

Evolution of the phenomenological theory for perovskite ferroelectrics. The theory of the dielectric and crystallographic properties of barium titanate was considered for the first time in 1949 by *Devonshire* [31]. By expanding the Gibbs free energy as a function of polarization and strain as order parameters, and making reasonable assumptions about the coefficients, he found possible to account for the various phase transitions in the crystal and to calculate the dielectric constants, crystal strains, internal energy, and self polarization as functions of temperature. One year later, the same author extended the theory [32], and obtained expressions for the piezoelectric constants, elastic coefficients for constant field and dielectric constant strain in terms of other physical constants of the material.

The refinement of the phenomenological theory of barium titanate was continued in 1966, when *Buessem et al.* [14] have used the Devonshire phenomenological thermody-

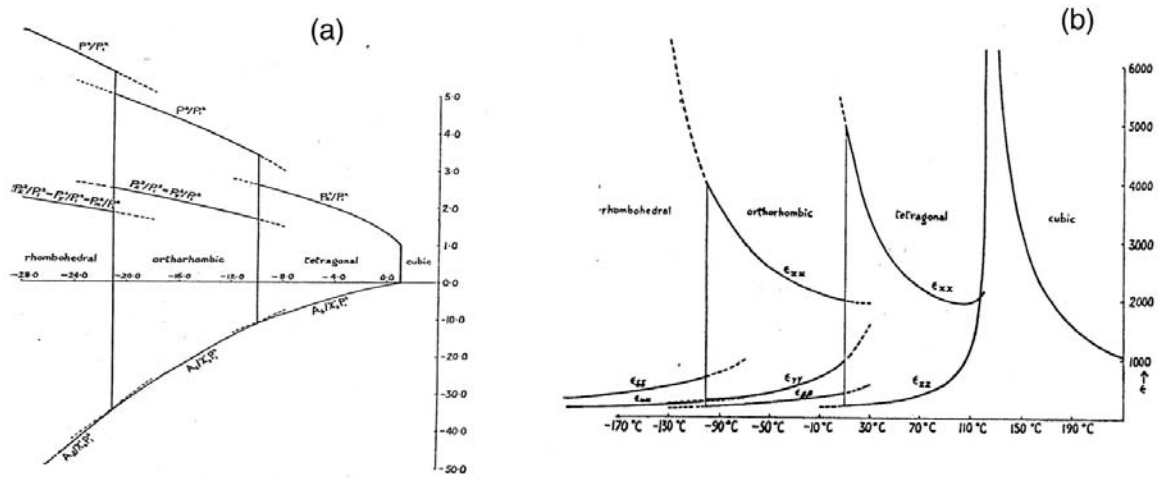


Figure 3.7: The first Landau-type phenomenology calculations for a perovskite: (a) Free energy and polarization of BaTiO_3 as a function of temperature. (b) Principal dielectric constants of the same material. Taken from the work by Devonshire, Ref. [31].

dynamic method and a simplified model to involve the stresses that are in the origin of the anomalously high permittivity in fine-grained ceramic barium titanate. In 1984, *Bell* and *Cross* modified [8] that theory further, by including the last symmetry permitted sixth order term $\alpha_{123}P_1^2P_2^2P_3^2$ (see Eq. (2.32)). Their function then predicted the correct high electric field behavior of the low temperature ferroelectric-ferroelectric phase changes in the single crystal and suggested a change of sign of the pyroelectric effect at high field levels in the induced tetragonal ferroelectric phase.

In 1987, *Haun et al.* developed [62] a phenomenological thermodynamic theory of an another perovskite family member - PbTiO_3 . They used a modified Devonshire form of the elastic Gibbs free energy and were able to predict the intrinsic single domain dielectric and piezoelectric properties of this material, not completely determined from experimental measurements. Further, in 2001, *Bell* [7] reviewed, the possible domain states of perovskite ferroelectrics under applied fields. He performed a phenomenological study of barium titanate to illustrate that review. The electric field-temperature phase diagrams, the polarization, and the lattice strain of barium titanate single crystals were obtained for applied fields up to $20\text{MV}/\text{m}$ and for temperatures from 1 to 450K . Some results from that work are shown in Fig 3.8.

In 2001, *Iniguez et al.* showed [76] that the typically assumed form of the potential, a sixth-order expansion in polarization around the paraelectric cubic phase, properly accounts for the behavior of the system, but they found a nontrivial temperature dependence for all the coefficients in the expansion, including the quadratic one, which is shown to behave nonlinearly. Their results also prove that the sixth-order terms in the

free-energy expansion (needed to account for the first-order character of the transitions and the occurrence of an orthorhombic phase) emerge from an interaction model that only includes terms up to the fourth order.

In 2002, *Sergienko et al.* showed [131] that an adequate Landau-type description of the ferroelectric Landau potential in highly piezoelectric mixture compounds PZT, PMN-PT and PZN-PT, is achieved by the use of a twelfth-order expansion of the Landau potential in terms of the phenomenological order parameter.

Recently (2005), a new phenomenological free energy description was constructed based

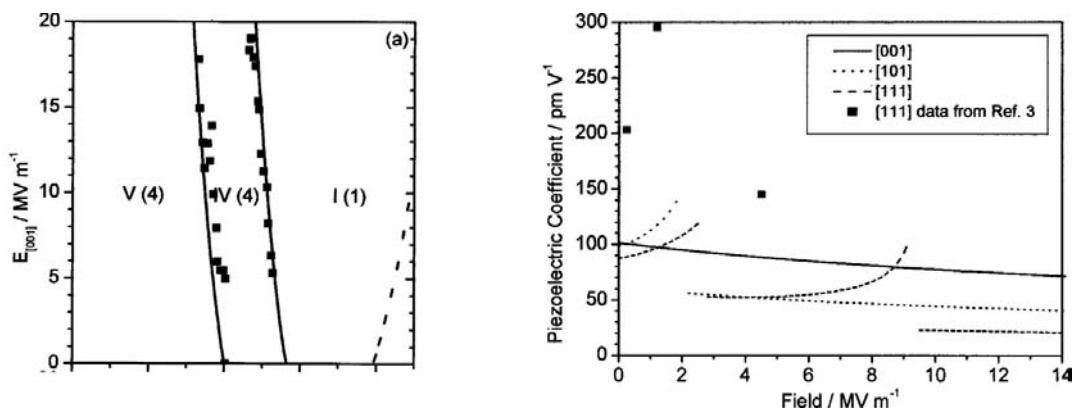


Figure 3.8: Phase diagram of barium titanate as a function of temperature and electric field applied parallel to $[001]_c$ direction, including the data points of Fesenko and Popov [38] (left); calculated piezoelectric coefficient as a function of electric field at 300K for fields parallel to $[001]_c$, $[001]_c$ and $[001]_c$ - measurements from literature compared with the calculated results (right). Calculations were not done for negative values of E . Taken from Ref. [7] (reference number in the right figure does not correspond to a reference in this thesis report).

on the properties of bulk BaTiO_3 single crystals by *Li et al.* [95] by using an eight-order polynomial of Landau-Ginzburg-Devonshire expansion. This new thermodynamic potential reproduced bulk properties, including the three possible ferroelectric transition temperatures, and their dependence on electric fields, as well as the dielectric and piezoelectric constants. The difference from the existing thermodynamic potential is that this model is applicable to predicting the ferroelectric phase transitions and properties of BaTiO_3 thin films under large compressive biaxial strains.

In 1997, *Du et al.* calculated phenomenologically [34] the crystal orientation dependence of piezoelectric properties for lead zirconate titanate (PZT) in the three dimensional space. The calculations were made for tetragonal PZT 40/60 (40% PZ and 60% PT) and rhombohedral PZT 60/40 compositions; later, in 1998 they calculated the values for the same properties of PZT near the morphotropic phase boundary [35], see Fig 3.9.

The origin of the appearance of the morphotropic phase boundary in the perovskite-

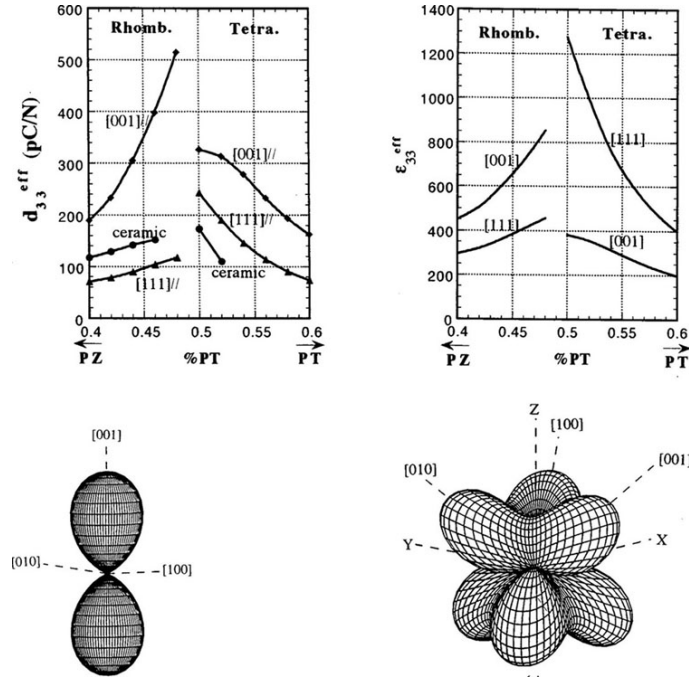


Figure 3.9: Effective piezoelectric constants d_{33} , and dielectric constants ϵ_{33}^{eff} of PZT with various compositions (upper row); Effective piezoelectric constants d_{33} of tetragonal PZT 48/52 (lower left) and rhombohedral PZT 52/48 (lower right). Taken from Ref [35].

type oxide solid solution systems and the increase in the dielectric susceptibilities in the vicinity of the boundary was theoretically clarified on the basis of a Landau-type free energy function by *Ishibashi and Iwata* [77] - the dielectric susceptibilities were concretely expressed in terms of the model parameters, and found to diverge at the morphotropic phase boundary within the present model. In 2001, *Iwata et al.* calculated [78] the angle dependence of the piezoelectric displacement along the driving electric field near the morphotropic phase boundary in the perovskite-type oxide family on the basis of the Landau-Devonshire type free energy function. In both phases the piezoelectric displacements are strongly enhanced near the morphotropic phase boundary.

Giant piezoelectric response. The very important papers in the science of piezoelectric materials are the ones in which the discovery of ultrahigh electromechanical properties of relaxor based ferroelectric single crystals are reported. These are the papers by *Kuwata et al.* [89] from 1982, and by *Park et al.* [118] from 1997. In the first paper the dielectric, piezoelectric and elastic properties of $0.91\text{Pb}(\text{Zn}_{1/3}\text{Nb}_{2/3})\text{O}_3\text{-}0.09\text{PbTiO}_3$ single crystals were investigated as functions of temperature and applied electric field -

in particular, the sample poled along the pseudo-cubic [001] axis revealed anomalously large piezoelectric and electromechanical coupling constants at room temperature in the rhombohedral phase ($d_{[001]} = 1500 \text{ pC/N}$, $k_{[001]} = 0.92$). The second paper presents the work on the piezoelectric properties of $(1-x)\text{Pb}(\text{Zn}_{1/2}\text{Nb}_{2/3})\text{O}_3$ - $x\text{PbTiO}_3$ and $(1-x)\text{Pb}(\text{Mg}_{1/2}\text{Nb}_{2/3})\text{O}_3$ - PbTiO_3 single crystals - piezoelectric coefficients $> 2500 \text{ pC/N}$, subsequent strain levels up to $> 0.6\%$ with minimal hysteresis and high electromechanical coupling $k > 90\%$ were observed.

These two papers increased the interest in novel piezoelectric materials, but also, revived

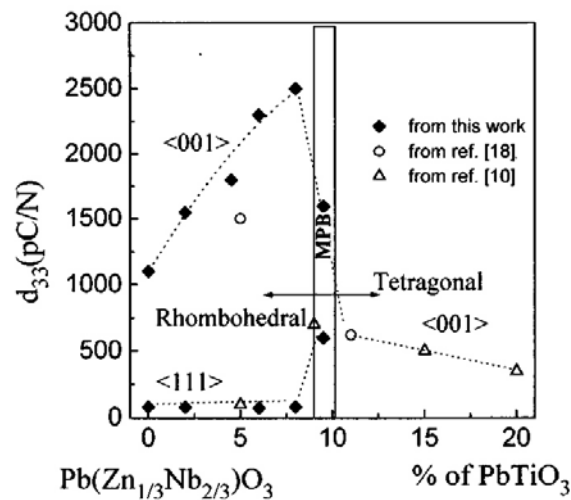


Figure 3.10: Piezoelectric coefficient d_{33} as a function of crystal composition and orientation. Taken from Ref. [118] (reference numbers in the figure do not correspond to references in this thesis report).

the investigations on classic perovskites, known and investigated for decades already.

Polarization rotation. *Fu* and *Cohen* have reported a first principle study of BaTiO_3 where they have shown that a large piezoelectric response could be driven by polarization rotation induced by an external electric field [44]. Furthermore, the polarization rotation origin of ultrahigh piezoelectricity in a relaxor ferroelectric PZN-PT was studied by *Noheda et al.* [114], and the origin of the high piezoelectric response in PZT was shown in the paper of *R. Guo et al.* [52].

Influence of the domain density on piezoelectric properties. In 1999, *Park et al* investigated [119] dielectric and piezoelectric properties of BaTiO_3 single crystals polarized along the $\langle 001 \rangle$ crystallographic axes as a function of temperature and dc bias.

Electromechanical coupling $k_{33} \approx 85\%$ and piezoelectric coefficients $d_{33} \approx 500\text{pC/N}$, better or comparable to those of lead based PZT, were found from $\langle 001 \rangle$ -oriented orthorhombic crystals at 0°C , as a result of crystallographic engineering. Later, in 2005, *Wada et al.* studied the influence of the domain size on the piezoelectric properties of tetragonal BaTiO_3 [156]. They found that the piezoelectric properties increased significantly with decreasing domain size (with increasing domain density).

Intrinsic vs measured coercive field. One can find, in *Chapter 6* of this report, a discussion about the importance of the difference of, phenomenologically predicted, intrinsic values of coercive electric fields and their experimental counterparts, that are always much smaller because of dynamic properties (nucleation) not included in the phenomenological theory. For that purpose, a paper by *Ducharme et al.* [36], published in 2001 is of a great importance. The authors measured for the first time the intrinsic coercive field in a ferroelectric material. It was in two-dimensional Langmuir-Blodgett polymer films as thin as 1nm . The reported coercive field was in good agreement with the theoretical intrinsic value, and exhibited the expected dependence on temperature and did not depend on thickness below 15nm .

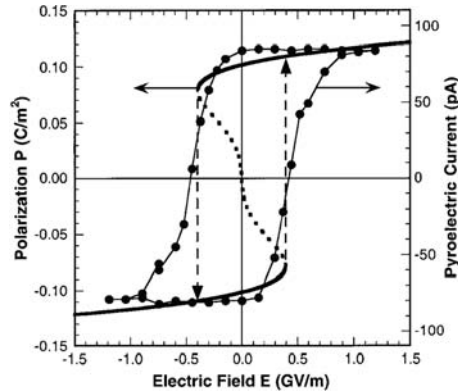


Figure 3.11: The theoretical polarization $P(E)$ at 25°C (thick-solid line) of $P(\text{VDF-TrFE } 70:30)$ calculated from the Landau-Ginzburg theory and the hysteresis in the pyroelectric response at 25°C (circles) in a 30-ML LB film of $P(\text{VDF-TrFE } 70:30)$. One can note that the thermodynamic and experimental coercive fields are almost equal. Taken from Ref. [36].

Chapter 4

Experimental techniques

All experimental techniques used to obtain the electromechanical properties values of KN are presented.

The experimental part of this work is to *refine the electromechanical properties set* of ferroelectrically monodomain potassium niobate in single crystal form, and to calculate the coefficients in the Landau-Ginzburg-Devonshire phenomenological theory by fitting the obtained experimental results. For these measurements, small resonator bars of KN were prepared (see *Chapter 5*).

4.1 Five-terminal setup for low capacity measurements

One of the first problems encountered during experiments was how to measure precisely the relative dielectric constant of the resonator bars, ϵ_{33} . The single domain KN value is very low (the relative permittivity $\epsilon_{33}^r \approx 45 - 55$). Thus, the resonator bars for measurements of d_{33} , which were prepared as capacitors with electrode surface $S \approx 1\text{mm}^2$ and a distance between them $d \approx 6\text{mm}$, have values of the capacity around $C_p = 80\text{fF}$ ($C_p = \epsilon\epsilon_0 S/d$) - a very good accuracy of capacity measurements of such samples can be a demanding task because the stray capacitance of the experimental setup can easily be commensurable with the sample capacitance. So, for these measurements, a special *5-terminal setup* was made [149].

To connect a sample to the measurement terminals of the auto balancing bridge instrument (*Impedance Analyser HP4192A*) that we used for the measurements, there are

several connection configurations to choose from. This auto balancing bridge instrument is equipped with four terminals (H_c , H_p , L_p and L_c) on its front panel. The possible ways to connect the sample to the terminals are described in Ref. [117]. Out of suggested connection schemes in this reference *the five-terminal (5T) configuration* is the most appropriate for our measurements of dielectric constants (i.e. capacities lower than $100fF$). In this configuration all of the outer conductors of the four coaxial cables are connected to the guard terminal, improving the low impedance measurements accuracy, Fig. 4.1. A 5T configuration sample holder, with the accuracy of about $\pm 1fF$, was

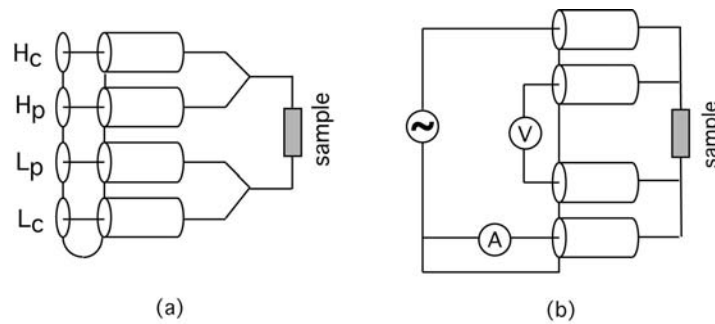


Figure 4.1: Five terminal setup for low capacity measurements: (a) connection diagram, (b) schematic diagram.

made in our laboratory (Fig. 4.2).

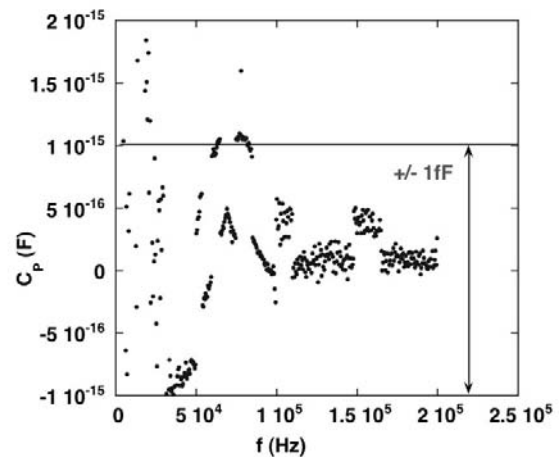


Figure 4.2: The sample holder, with the five terminal configuration, for low capacity measurements made in our laboratory (left); the stray capacity of the 5-terminal setup as a function of frequency - the accuracy of the configuration can be estimated to $\pm 1fF$ (right).

4.2 Domain structure and ferroelectric poling procedure of single crystal KNbO_3

Since we were aiming to perform experiments exclusively on *single domain KN* samples, it was clear that the control of a sample domain structure was one of key issues.

4.2.1 Domain structure

Potassium niobate has a pseudocubic structure which allows the presence of a variety of domain structures. Domain walls of 180° , 120° , 90° , which generally appear and distribute randomly, and 60° (Fig. 4.3), which are mostly distributed at the corners of the crystals [96], are commonly observed at room temperature in as-grown KN. The

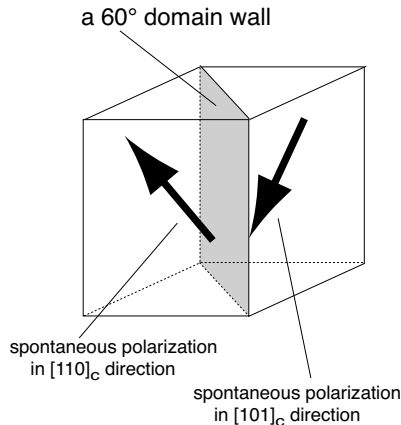


Figure 4.3: An example of a domain structure in KN. Since the material has the orthorhombic symmetry at room temperature, the appearance of 60° domains like the one here is possible.

structure of such poly-domains can be a serious obstacle for applications because it drastically influences the piezoelectric properties.

The domain walls are regarded as zero-net-strain planes, i.e. planar boundaries that satisfy conditions for complete internal stress relief [6]. There are two origins of ferroelectric domains: a) a change in the electrostatic forces owing to the spontaneous polarization [96], and b) internal defects and stresses help the nucleation of domain walls [42, 105, 104, 74, 72].

It is complicated to obtain and keep the single domain structure in KN samples throughout a broad temperature interval. The reason is that in this material the domain state tends to be easily changeable and is very sensitive to electric fields [101, 108, 66, 74], mechanical stresses [74, 75, 96, 70, 73], and an abrupt temperature change [66].

4.2.2 Surface layer. Polishing. Impurities

The importance of *the surface region* in materials of perovskite structure has been mentioned in the literature for about 50 years. However, the surface region has been traditionally considered to be homogeneous with different electrical and dielectric properties compared to the bulk of the crystals. It is found that the surface region of perovskite crystals shows a rather complicated chemical composition¹[135].

The influence of the surface layer on electromechanical properties of a KN sample thus turns out to be of great significance. It has been demonstrated for the case of the hysteresis loop of KNbO_3 that the anomalous increase of P_s at low frequencies is almost completely determined by the heterogeneous surface [136]. Another example of the sample surface influence on experimental results is a fact that in many classical experiments it can be found that the electric properties of KNbO_3 are affected by the atmosphere in which experiments are carried out [135].

To perform experiments that will give only the bulk properties, the polishing of sample surfaces is important. Polishing in our experiments has been used, but, since the KN samples are very fragile, its usage was minimized - the mechanical treatment of KN samples tends to introduce a slight curvature to the sample surfaces, especially near the edges [83], and it is also considered as a possible origin of creating ferroelectric domains [151, 152, 153]. For the polishing procedure diamond surfaces (1μ and 6μ grains size) and graphite paper (2400) were used.

On the other hand, it is worth mentioning that *impurities* in KN can also influence experimental results. It has been shown that impurities in an amount of 0.1 at.% may significantly change the dielectric properties of KNbO_3 [163], not to forget to emphasize the impurities as problematic domain wall pinning centers which make poling procedure and restoring of the single domain state in samples more difficult. Impurities and dislocations can induce domain nucleation even at low electric fields of the order of $100\text{V}/\text{cm}$, and this may lead to the nucleation of unwanted domains even in poled crystals [75]. Impurities have been found to give rise to anomalous hysteresis loops [71].

4.2.3 Poling

It is clear then, from preceding sections, that the starting point for the experimental study of KN to refine the material parameters set was the preparation of ferroelectrically single domain samples. In most materials electrical poling may be achieved by cooling

¹The existence of extended defects in the surface region, which serve as fast diffusion path for oxygen and A-type atoms, leads to a segregation of A or AO-complexes already at room temperature. With a rise in temperature, a continuous transition in the surface region between ABO_3 and $\text{AO}(\text{ABO}_3)_n$ is found.

a crystal from the paraelectric phase into the ferroelectric phase in an applied bias electric field parallel to the polar crystallographic axis under constant field conditions. The single-domain state is then thermodynamically stable in an unstressed crystal since depolarization fields are neutralized by charge flow in the external circuit. Short-circuiting the polar faces of a crystal during cooling could, in principle, be sufficient to produce the single-domain state, but in practice this is not the case because of temperature gradients, internal strains, and surface effects.

In the case of KNbO_3 , even though it has been known that poly-domains can be converted to single domain by a strong electric field [45], it is difficult to achieve good yield because KN crystals easily crack and new domains can be generated in KN crystals during such a poling process.

Most industrial research teams keep their KN poling procedures as a confidentiality, but one can nevertheless find several poling procedures proposed in the literature. By doing a literature research (see *Chapter 3*), one can find different attempts of poling, with different results of electromechanical properties obtained on single domain samples after the poling was done. In some papers the poling has not even been done, although it would be logical to do experiments on the single domain crystals [162], or sometimes it has just been mentioned that the poling at elevated temperature has been required if one wished to obtain a single domain crystal [103].

Since the domain structure of KN at room temperature is complicated, and these domains can easily be created in samples, the optimal poling procedure is the major tool for the high quality measurements. In our experiments, the two-step poling method proposed by *S. Wada et al.* [154] was the one most frequently used (see Table 3.2).

Verification of the domain structure

There are several common methods of determination whether a crystal is fully poled: a) the direct observation of domains by optical microscope, optical interferometer, or x-ray diffraction analysis [66], b) the measurements of the pyroelectric coefficient², c) the second harmonic generation.

There is an another simple method to verify and discuss the domain structure of a sample. It is the investigation of its dielectric permittivity. The presence of domains contributes to the increased polarizability of the sample (also, the dielectric permittivity is, generally, anisotropic) and thus the dielectric constant is different for a sample containing domains than the one fully poled.

The most frequent methods of domain structure verification in samples used in this work

²For the pyroelectric measurement it is necessary to know dP_i/dT for the poled material or else to assume that the maximum attainable dP_i/dT corresponds to the fully poled state.

were the dielectric and pyroelectric constants measurements and the optical microscopy.

4.3 Sawyer - Tower bridge

The Sawyer - Tower bridge has been the common method for characterizing ferroelectric devices due to its simplicity and cost. However, this method is susceptible to significant errors from parasitic elements and is limited by the accuracy to which the sense capacitor value is known.

The bridge uses a capacitive voltage divider comprising the test sample and a sensing capacitor (C_{sense}) supplied by the user (Fig. 4.4). The voltage generated across the sense capacitor is proportional to the charge stored in the sample.

This circuit is commonly used for investigating P_s switching, i.e. for obtaining ferroelectric hysteresis curves (See *Chapter 2*).

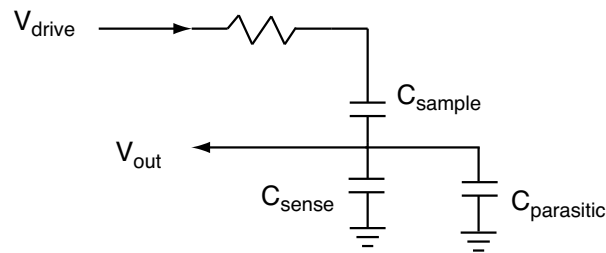


Figure 4.4: Schematic representation of Sawyer - Tower bridge for ferroelectric hysteresis loops measurements.

4.4 Pyroelectric measurements setup

The pyroelectric measurements have been performed by a dynamic method constructed in our lab [24]. It was possible to measure a temperature dependence of pyroelectric properties in the range $[200K - 300K]$.

4.5 Resonant technique

Among several techniques for investigation of the piezoelectric response (such are interferometry, atomic force microscopy, direct methods, measuring the displacement of the cantilever, ...) the resonant technique is one of the most efficient ones.

The basis of this technique lies in a fact that the mechanical response of a piezoelectric

body excited by an electric field is a function of *all electromechanical material parameters and its dimensions and density*. The magnitudes of excited vibrations depend on the frequency of this (alternating) electric field, because if this frequency is close to a natural mechanical resonance of the body, the elastic vibrations will be very large, and according to the piezoelectric constitutive equations³, so will the electrical impedance. Measuring of the frequency dependence of the sample electric impedance thus gives an indirect way to determine the material coefficients.

Theory of vibrating piezoelectric bodies is not simple - usually, one considers only linear cases, assuming additionally that the velocity of elastic effects in the material is much smaller than the velocity of electrical effects. Further, it is also sufficient for the most cases to assume that the body is in the homogeneous thermal equilibrium, that the material is a perfect insulator and that magnetic effects are negligible.

If one wants to determine the complete set of the material coefficients from the piezoelectrically induced mechanical resonance, it is sufficient to consider a few of the simplest geometries and vibration modes. For our measurements, piezoelectric vibrating bars were used⁴, to determine the transversal piezoelectric coefficients, d_{31} and d_{32} . It can be shown [68] that the admittance $Y = G(\omega) + iB(\omega)$ (the inverse of the impedance $Y^{-1} = Z = R(\omega) + iX(\omega)$) of such a geometry (convenient aspect ratios [2]) can be approximately written in the analytical form, for example

$$Y = i \frac{\omega w l}{t} \left(\varepsilon_{33}^X - \frac{d_{31}^2}{s_{11}^E} \right) + i \frac{2 w d_{31}^2}{\sqrt{\rho s_{11}^E s_{11}^E} t} \tan \frac{\omega l \sqrt{\rho s_{11}^E}}{2}. \quad (4.1)$$

From this equation material coefficients such as the dielectric constant along the polarization direction, ε_{33} , the elastic compliance s_{11} and the piezoelectric coefficient d_{31} can be calculated by fitting the expression to the experimentally obtained resonance curves such as ones shown in Fig. 4.5. Equivalent equations can be derived for s_{22} , d_{32} and s_{33} , d_{33} .

On the other hand, there are simplified equations for calculations of the material coefficients, according to the "IEEE Standard on piezoelectricity" [1]. For the transversal resonator bar, one can use

$$f_s = \frac{1}{2l} \frac{1}{\sqrt{\rho s_{11}^E}}, \quad (4.2)$$

to relate the material's conductance (G) resonant frequency with its density (ρ) and elastic compliance (s_{11}), then

$$\frac{k_{31}^2}{1 - k_{31}^2} = -\frac{\pi f_p}{2 f_s} \operatorname{ctg} \left(\frac{\pi f_p}{2 f_s} \right) \quad (4.3)$$

³These equations are discussed in *Chapter 2*.

⁴More details in *Chapter 5*.

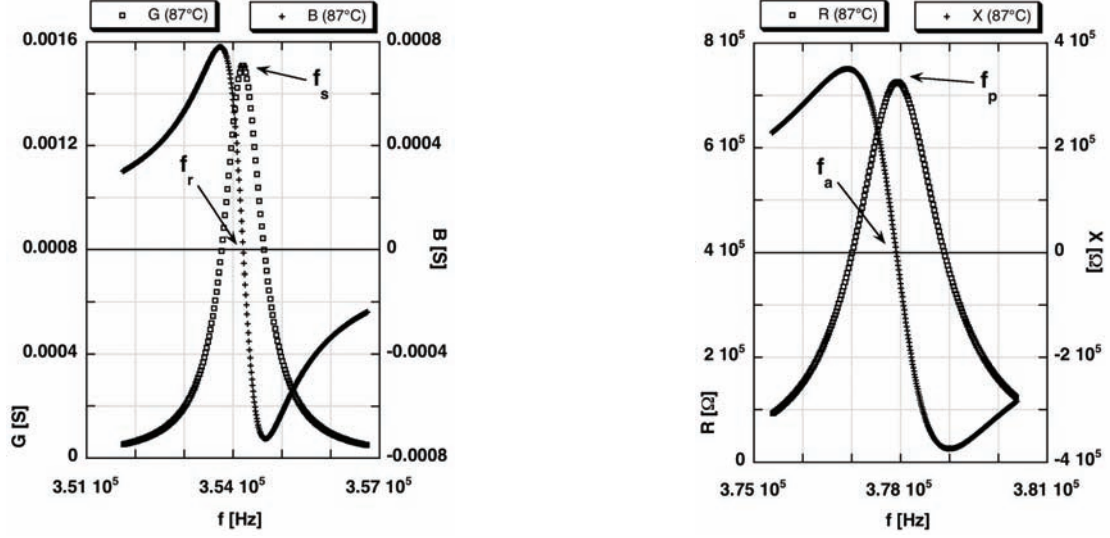


Figure 4.5: The frequency dependence of the impedance and admittance of the potassium niobate in the vicinity of the first natural resonance frequency of the sample.

to relate the electromechanical coupling coefficient k_{31} with the ratio of the resonance frequencies for the conductance and the resistance (R). Finally, the expression

$$k_{31} = \frac{d_{31}}{\sqrt{\varepsilon_{33}^T s_{11}^E}}. \quad (4.4)$$

relates the piezoelectric coefficient with the coupling coefficient, dielectric permittivity and the elastic compliance. Of course, the equations for elastic compliances, electromechanical coupling coefficients and piezoelectric coefficients in other crystallographic directions are equivalently derived.

It follows, then, that it is possible to measure the temperature dependence of the electromechanical coefficients by simultaneously measuring the temperature dependence of the resonant frequencies of the real parts of the impedance and admittance, f_s and f_p respectively, and the capacity of the sample (i.e. its dielectric constant).

4.5.1 Experimental setup for simultaneous measurements of electromechanical properties

The experimental setup used for simultaneous measurements of dielectric, mechanic and piezoelectric constants of KN was as following (Fig.4.6):

- samples surfaces perpendicular to the spontaneous polarization direction were electroded with gold, i.e. resonator bars were tested as capacitors;

- samples were attached by $30\mu\text{m}$ gold wires to a sample holder; the wires were glued on the center of the sample surface by silver paint, or by bicomponent Duralco 124 highly conductive epoxy, dissolved in the 4-Methyl-2-pentanone, which is usually used as a silver paint solvent; in the case where epoxy was used, the epoxy was not supposed to be dissolved, but the mixing of two components and drying of this mixture would last extremely long; the other side of golden wires were soldered to a sample holder; the samples were hanging freely, i.e. they were not clamped;
- the sample holder was put inside the Delta9023 Chamber in which the temperature of the samples was easily controlled with high precision (down to 0.1°) throughout the whole temperature range of the orthorhombic phase of KNbO_3 [from -60° to 230°]; the temperature was measured by a thermocouple;
- the electromechanical properties (resonance curves and dielectric constants) of the samples were measured by *HP4194A* impedance analyser; the measurements were automatized using *LABVIEW* software package.

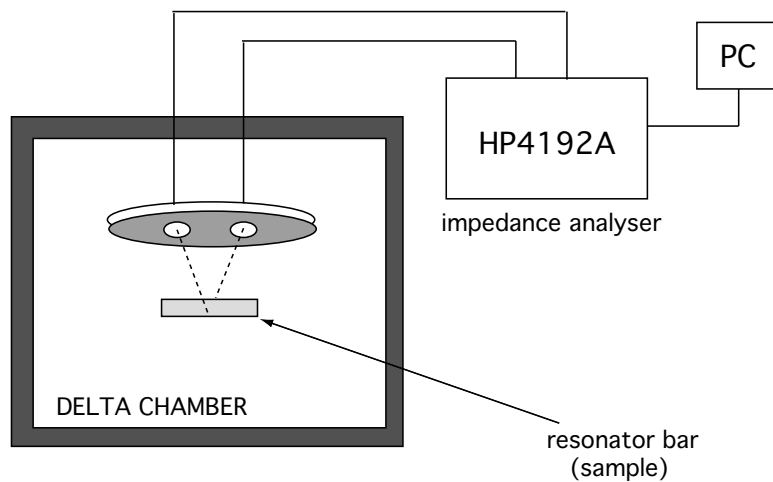


Figure 4.6: Scheme of the experimental setup used for the simultaneous electromechanical properties measurements of KN vibrators.

The easiest way to verify the performance quality of the setup was to measure the temperature dependence of the electromechanical properties of a piezoelectric material with a previously known data set. For that purpose, a sample from a family of langasite materials was used and reproducible results were obtained, with no noticeable influence

of the setup on the quality of results.

During measurements, heating and cooling rates were $0.5^\circ/min - 1.0^\circ/min$ (the same rate was also used in Ref. [149]), although it was reported that a cooling rate of about $5.0^\circ/min$ was not large enough to generate cracks in samples of KN [96].

4.6 Some experimental constraints

For ordinary dielectrics it is well known that measurements at constant stress ($X = const.$) may differ significantly from measurements at constant strain ($x = const.$) - there are elastic contributions to the various compliances. In ferroelectrics, additionally, important differences also exist between measurements at constant dielectric displacement ($D = const.$) and constant electric field ($E = const.$). In practice clamped measurements are normally made with a dynamic method at frequencies well above the fundamental mechanical resonance frequency, while unclamped measurements are made at low frequencies. Adequate clamping of a crystal by external means is normally difficult. Similarly, open-circuit ($D = const.$) and short-circuit ($E = const.$) measurements are performed above and below the dielectric relaxation frequency [69]. External short-circuiting of crystals is adequate for constant electric field measurements provided that any stresses or temperature changes of the crystal are uniform.

Chapter 5

Experimental results

Potassium niobate is a member of the perovskites family that has, because of the highest reported thickness mode coupling coefficient in the single crystal form and environmental friendly lead free composition, a promising future in various applications. At present, the set of electromechanical properties values at room temperature is complete, and the phenomenological description of KNbO_3 is incomplete. In this chapter, we will try to measure the temperature dependence of some electromechanical coefficients, and to obtain a phenomenological description of potassium niobate.

One can note that published reports cite significant deviations for the various phase transition temperatures in potassium niobate single crystals [39, 64, 51, 162]. At room temperature, KNbO_3 is *ferroelectric and belongs to the orthorhombic $mm2$ class* with cell parameters $a \approx 0.5697\text{nm}$, $b \approx 0.3971\text{nm}$, and $c \approx 0.5722\text{nm}$. As the temperature falls from the crystal growth temperature¹ ($\approx 1100\text{K}$), this material undergoes three phase transitions²: 1) paraelectric cubic \rightarrow ferroelectric tetragonal at $\approx 435^\circ\text{C}$, 2) ferroelectric tetragonal \rightarrow ferroelectric orthorhombic at $\approx 225^\circ\text{C}$, and 3) ferroelectric orthorhombic \rightarrow ferroelectric rhombohedral at approximately -10°C . This structural phase transformation sequence is schematically shown in Fig. 5.2, and it is completely analogous to that of barium titanate (only the transition temperatures are different,

¹Typical growing procedures of KN can be found in the literature [96, 138]. It is *now* possible to obtain high quality KN crystals with highly transparent, colorless, and crack free features (as shown in Fig. 5.1) - growing high quality KN single crystals has been a problem for a long period.

²The mechanisms of the phase transitions (i.e. their displacive or order-disorder character) in KN are still under the discussion. [33, 40, 41]. There is experimental evidence for both of these scenarios. It is quite possible, that real ferroelectric transitions involve a combination of these behaviors [40, 41].



Figure 5.1: A crystal of potassium niobate

being in BaTiO_3 393K, 278K and 183K, respectively).

According to its symmetry ($mm2$), the orthorhombic KNbO_3 has nine independent elastic, five piezoelectric, and three dielectric constants [116]. A review of these coefficients measurements is given in *Chapter 3*. Since the set of the experimentally obtained electromechanical coefficients is discrepant³, a refinement is attempted here, by measuring temperature dependences of some coefficients in the orthorhombic phase.

The KN crystals used for these measurements were grown by *Forschungsinstitut für*

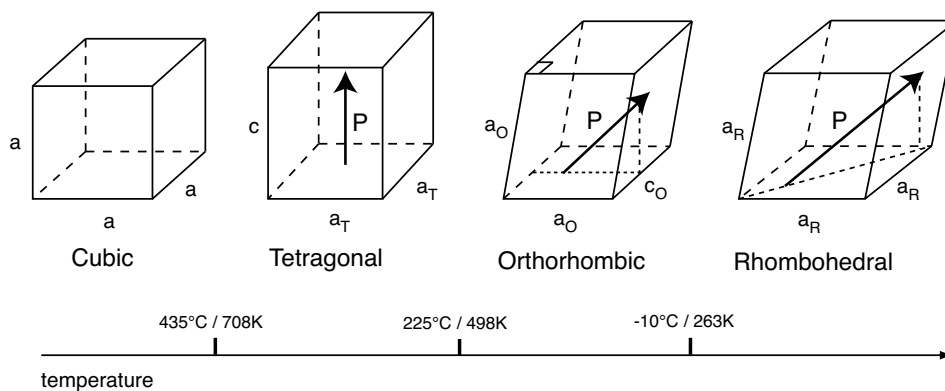


Figure 5.2: The phase transition sequence of potassium niobate upon cooling, according to the literature data.

*mineralische und metallische Werkstoffe - Edelsteine/Edelmetalle - GmbH*⁴ (FEE) from Germany. The samples were cut in forms of expedient resonator bars: along the a , b and c side of an orthorhombic single domain cuboid, having appropriate aspect ratios, to get 31–, 32– and 33– resonator bars, respectively (Fig. 5.3). With this set of samples,

³For example, the entire set of elastic constants of KN at room temperature was first calculated by Phatak et al. [120] from diffuse x-ray scattering data. Then, by using dielectric measurements, Wiesendanger later showed [160] that the values of Phatak et al. were in error.

⁴www.fee-io.de

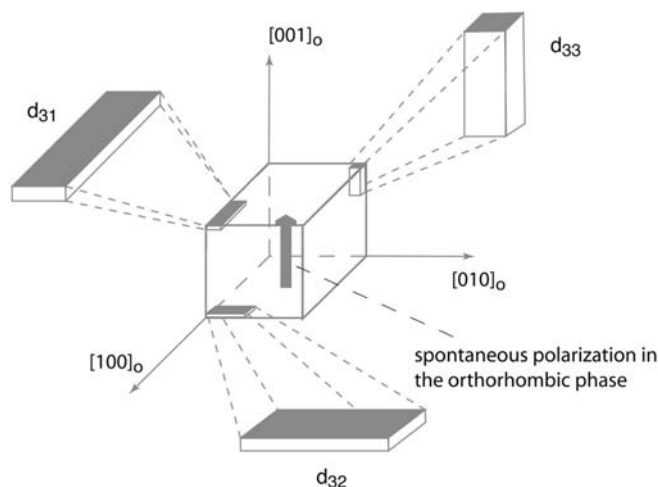


Figure 5.3: Schematic showing how the samples were cut from a poled single domain KN cuboid. The direction of the spontaneous polarization in the orthorhombic phase is along $[001]_o$ direction of the orthorhombic phase axes frame, and along $[110]_c$ direction in the cubic phase axes frame. Shaded surfaces denote sample sides that were electroded.

it was possible to measure the temperature dependence of d_{31} , d_{32} and d_{33} piezoelectric coefficients in the orthorhombic phase. The method used for measurements was a modified resonance method, described in *Chapter 4*.

The orientation of the resonator bars with respect to the orthorhombic unit cell principal directions was verified by Laue camera. The figures obtained have proven that the samples were cut very accurately. Typical Laue figures are shown in Fig. 5.4.

Since the aim of measurements was to determine *single domain properties* of KN, practi-

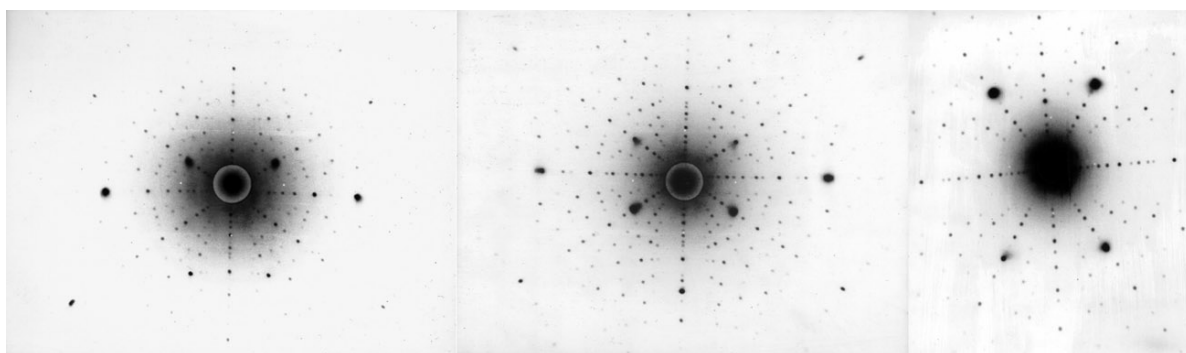


Figure 5.4: Typical Laue figures obtained for verification of the accuracy of sample cuts. Samples were cut along the principal axes of the orthorhombic system with high accuracy.

cally the most important experimental procedures were the poling procedure, to remove

residual domains, and the verification of the domain structure in samples. The domain state verification was done either by pyroelectric and dielectric measurements (no need to remove gold electrodes), either by polarization microscope (necessary to remove the electrodes mechanically, and, like that possibly creating domains, which makes this method rather unreliable). Typical figures obtained by polarization microscopy are shown in Fig. 5.5, for different domain structures in samples.

Experimental problems that can happen if a non-stoichiometric composition of the KN

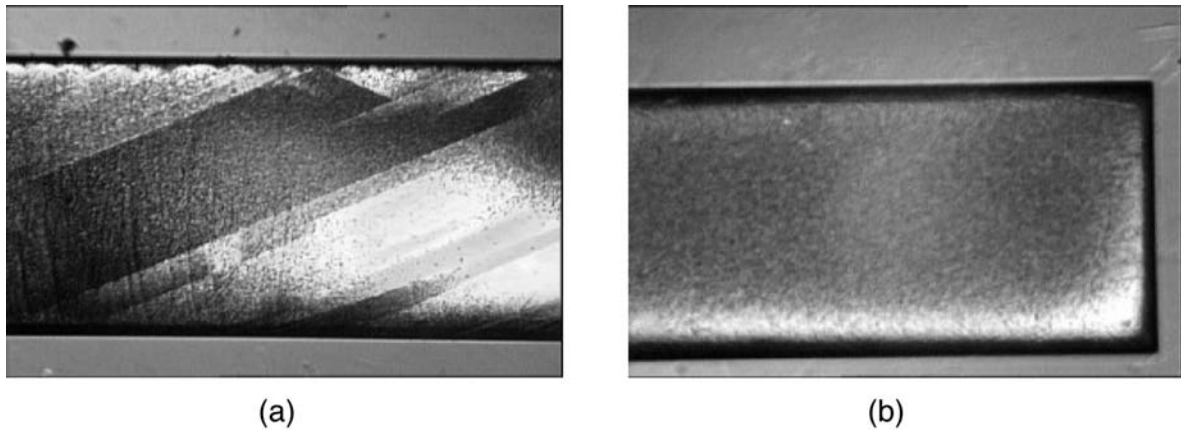


Figure 5.5: Polarization microscope images of (a) multidomain and (b) single domain KN sample.

sample surface layer appears are discussed in *Chapter 3* and *Chapter 4*. To remove the surface layer from some samples, etching in the mixture of HF and HNO₃ acids was done. The surfaces of the samples after etching became rough and non-transparent for the polarized light - therefore, the domain structure verification of the samples by optical methods became impossible. The surface of an etched KN sample is shown in Fig. 5.6. To make the sample transparent for optical microscopy, surface polishing should be done, but this procedure is highly unreliable because of the high probability of additional domains creation.

5.1 Measured electromechanical properties

Prior to all other electromechanical properties measurements, a behavior of the dielectric constant along the spontaneous polarization direction, ϵ_{33} , was investigated as a function of temperature - to verify the temperature extent of the orthorhombic phase of the samples. Upon heating, the ferroelectric orthorhombic \rightarrow ferroelectric tetragonal phase transition was observed at 220°C, while the transition from the orthorhombic to

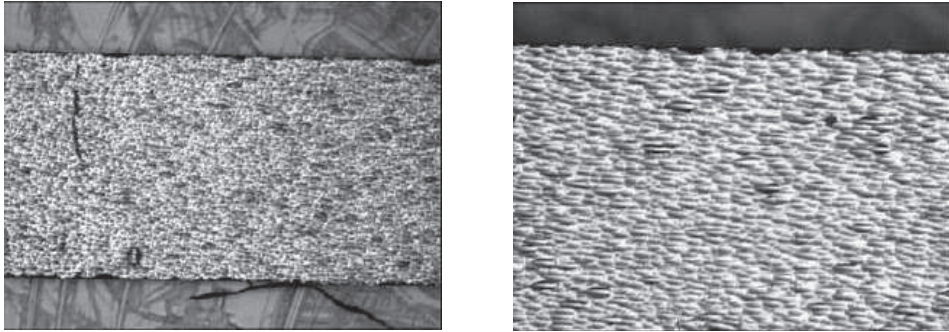


Figure 5.6: Surface of a KN sample after etching in a mixture of HF and HNO₃ acids. The surface layer that may cause experimental problems has been removed, but it is not possible any more to verify the domain structure by polarized light microscopy.

the ferroelectric rhombohedral phase occurred at -61°C on cooling⁵. To preserve the usefulness of the samples for multiple experiments (to have them as long as possible in the single domain state), measurements were never performed close to the phase transition temperatures, to avoid sizeable energetic instabilities in samples and a possibility of easy creation of domains. The temperature dependence of the dielectric constant of the test samples is shown in Fig. 5.7.

5.1.1 Spontaneous polarization values and ferroelectric hysteresis loops

If one wants to study, by phenomenological modeling, the behavior of electromechanical properties of a ferroelectric, the knowledge of the spontaneous polarization value, P_s , is of critical importance. It will be shown in many examples in this and further chapters that, in the framework of the phenomenological Landau-Ginzburg-Devonshire theory [31, 32], the dielectric properties can be represented as polynomial functions of the spontaneous polarization value, while piezoelectric coefficients are directly proportional the products of dielectric constants and the spontaneous polarization. Hence, having the experimental values of P_s is crucial.

In principle, there are two common methods for measuring the spontaneous polarization in a ferroelectric material: a) *Sawyer - Tower bridge* [129] - the most used procedure (described in *Chapter 4*), b) a special rectangular pulses technique (the so-called *Camlibel pulse method*) [55].

⁵Note that this temperature is 51°C lower than the usually reported temperature of the particular phase transition.

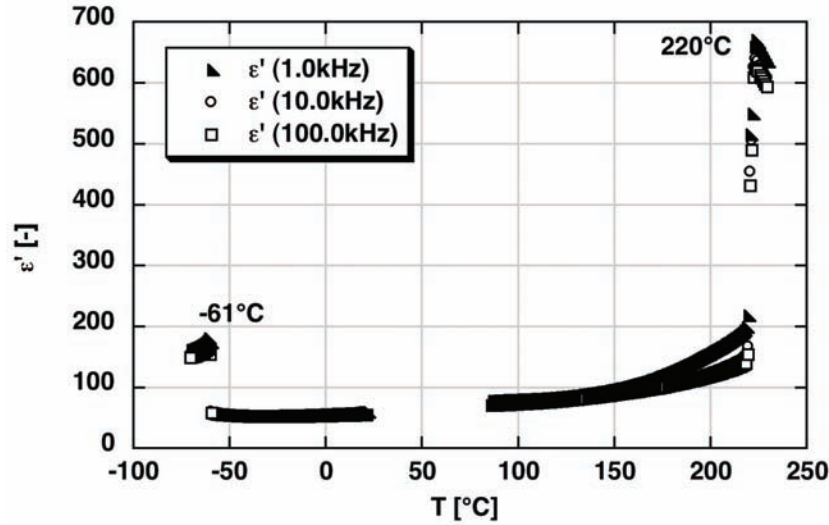


Figure 5.7: The relative dielectric permittivity of the orthorhombic potassium niobate as a function of temperature. The phase transition to tetragonal phase takes place upon heating above 220°C , while the one to the rhombohedral phase happens upon cooling below -61°C . Measurements were performed for different frequencies of the measuring field.

There were several previous attempts of measuring the spontaneous polarization in KN - for example, *Triebwasser* measured the spontaneous polarization values for several temperatures in the tetragonal and orthorhombic phase [143], *Hewat* measured values of P_s at 270°C (tetragonal phase) and at 20°C (orthorhombic phase) [65], while *Günther* measured the temperature dependence of the spontaneous polarization in the whole orthorhombic phase temperature interval [55]. These and all other references related to spontaneous polarization values of KN are systematized in *Chapter 3*, Table 3.1.

It is in general difficult to observe the proper ferroelectric hysteresis loops of KN, especially at low frequencies, where an anomaly of the hysteresis loop is reported⁶ [136]. This is seen in the fact that published results on the spontaneous polarization at room temperature in this material differ up to 40%. *Günther* [55] additionally reports inapplicability of the usual P-E hysteresis loops (Sawyer-Tower bridge) method in measuring the spontaneous polarization of KN, because of the very rapid change of loops from the ferroelectric type to the paraelectric type⁷, so he uses a pulse-field method. *Camlibel* [16] also points out to experimental difficulties in the determination of P_s from hysteresis loops.

The method available in our laboratory for measurements of the ferroelectric hysteresis

⁶Together with the explanation of an anomaly as a consequence of the existence of non-stoichiometric surface layer.

⁷Due to appearance of 90° domains

loops and, indirectly, the spontaneous polarization, was the Sawyer-Tower bridge. Typical hysteresis loops obtained on KN samples are shown in Fig. 5.8. The measurements were done by applying electric fields at frequency $f = 5kHz$ (limited by experimental setup), and the results shown reveal a high electric conductivity behavior of samples. This method is thus not reliable for obtaining the spontaneous polarization values.

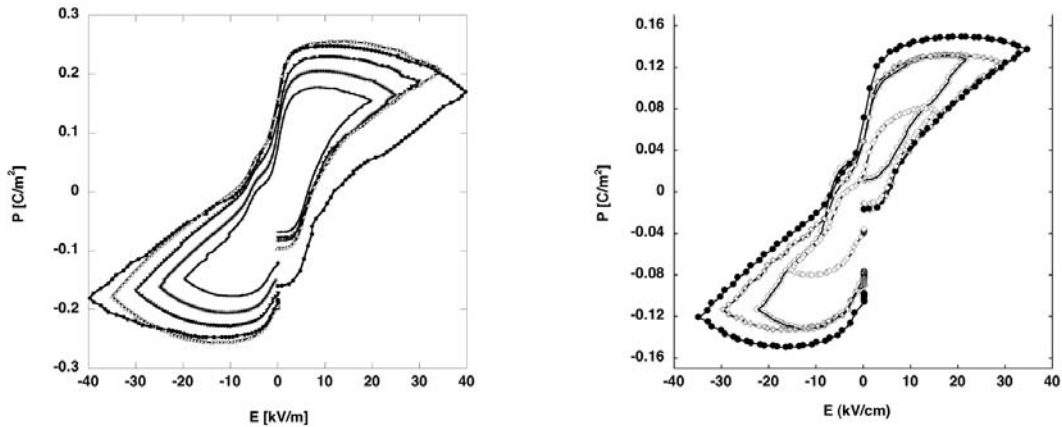


Figure 5.8: Typical results of measurements of the hysteresis loops on KN samples. The samples show electrical conductivity for electric fields applied at $f = 5kHz$.

5.1.2 Pyroelectric properties

Measurements of pyroelectric coefficient of a sample is an indirect way of obtaining some information on sample domain structure. Taking a step further, by doing measurements of the temperature dependence of the pyroelectric coefficient, one can reveal the temperature dependence of the spontaneous polarization, if its value for a certain temperature is known.

It is not difficult to show by calculations that the presence of domains in the sample decreases the value of the pyroelectric coefficient. Thus, if one compares pyroelectric coefficients of several samples cut from the same batch, the one with the highest pyroelectric coefficient will be the closest to the single domain state.

Up to our best knowledge, there is only one report on single domain KN pyroelectric coefficient measurements (*Günter* in 1977 [55]). In that work the value of the room temperature pyroelectric coefficient was $p \approx 75 \frac{\mu C}{m^2 K}$ and the author noted a relative experimental error of $\pm 20\%$.

In this thesis work, pyroelectric measurements on several samples were done. The typical results are shown in Fig. 5.9. By using optical methods, it was revealed that some samples were not single domain. Nevertheless, all samples gave higher average

room temperature values of pyroelectric coefficients than the one reported by *Günter*, showing the better quality of samples and a small influence of domains present.

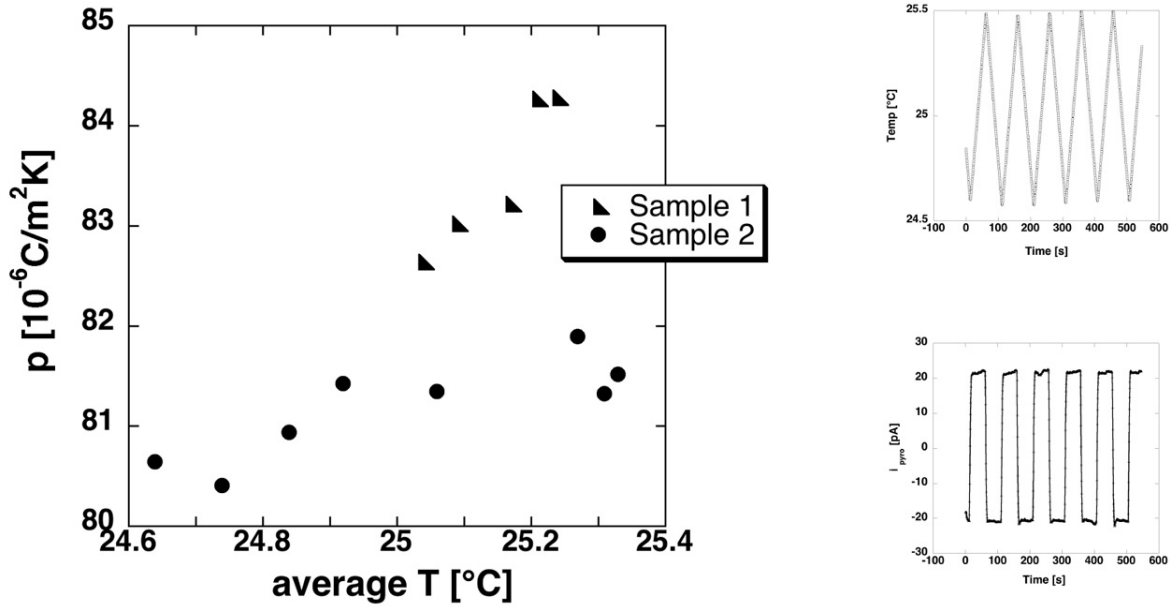


Figure 5.9: Typical results of pyroelectric coefficient measurements on KN samples at room temperature. Sample 2 appears to have more domains influencing the pyroelectric effect than Sample 1. Small graphs on right depict the time dependence of a sample temperature change (upper graph) and the electric current caused by that temperature change (lower graph).

5.1.3 Dielectric properties

While doing measurements of electromechanical properties of a piezoelectric material, one has to keep in mind that these materials generally display frequency dispersion in most electromechanical properties [157]. Considering an example of interest, KNbO_3 shows relatively high dielectric losses at very low frequencies⁸ [85]. On the other hand piezoelectrics also show nonlinear behavior of their properties with increasing of applied fields.

The frequency dependence of dielectric properties of KN samples was measured by *HP Impedance Analyser 4192A*. The measured frequency dependence of a KN sample capacity and its dielectric loss at room temperature is shown in Fig. 5.10, while the temperature dependence of ε_{33} is depicted in Fig. 5.11. The measurements of the tem-

⁸These losses may be attributed to the relatively high porosity of the crystal. The grain surface around the pores forms an easy path for the K^+ ions to drift under the measuring electrical field and hence gives rise to a dielectric loss [125].

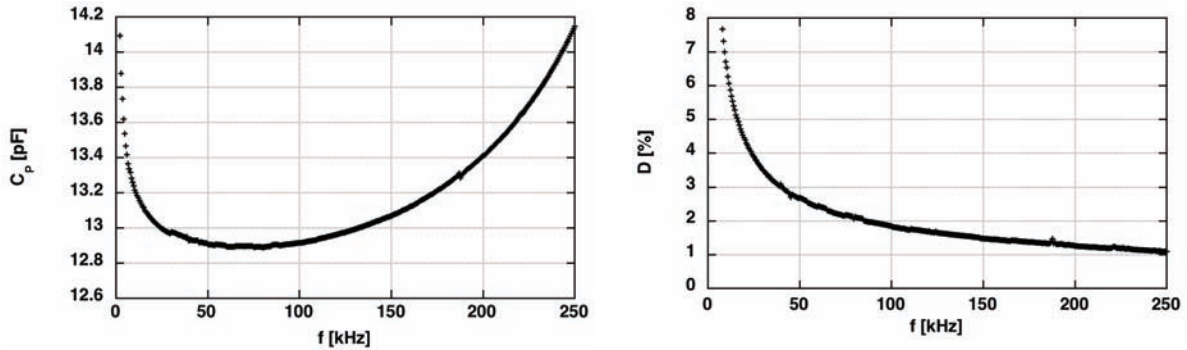


Figure 5.10: Capacity of a KN sample (left) and its dielectric loss (right) as functions of the measuring electric field frequency. High capacity at higher frequencies is due to approaching the natural resonance frequency of the sample. The applied measuring fields were very small.

perature dependence of ϵ_{33} were performed at frequencies far from the natural resonance frequency of the sample and at which samples had a low dielectric loss, and for very small measuring fields. The room temperature value of ϵ_{33} is compared to the literature results in Table 5.1.

It is interesting to note that the relatively low values of permittivity hint a poor performance of KNbO_3 in transducer arrays applications, but do suggest its application in single element transducer technology⁹ [85].

	Wada [153]	Zgonik [166]	this work	Wiesendanger [160]
ϵ_{11}	872.8	985	-	1000
ϵ_{22}	155.3	150	-	160
ϵ_{33}	43.6	44	45.1	55

Table 5.1: Measured free (no mechanical constraints) dielectric constants of single domain KN, compared to the values from the literature. One can note the large anisotropy in the constants.

5.1.4 Mechanical properties

Since the frequency dependence of the electric impedance of a piezoelectric material is in general a function of all electromechanical material constants¹⁰, measurements of

⁹In this case, the low dielectric constant translates into a smaller capacitance (and hence a higher impedance), which allows optimum impedance matching with the pulsing and receiving electronics while still maintaining a large aperture.

¹⁰Discussed in Section 4.5.

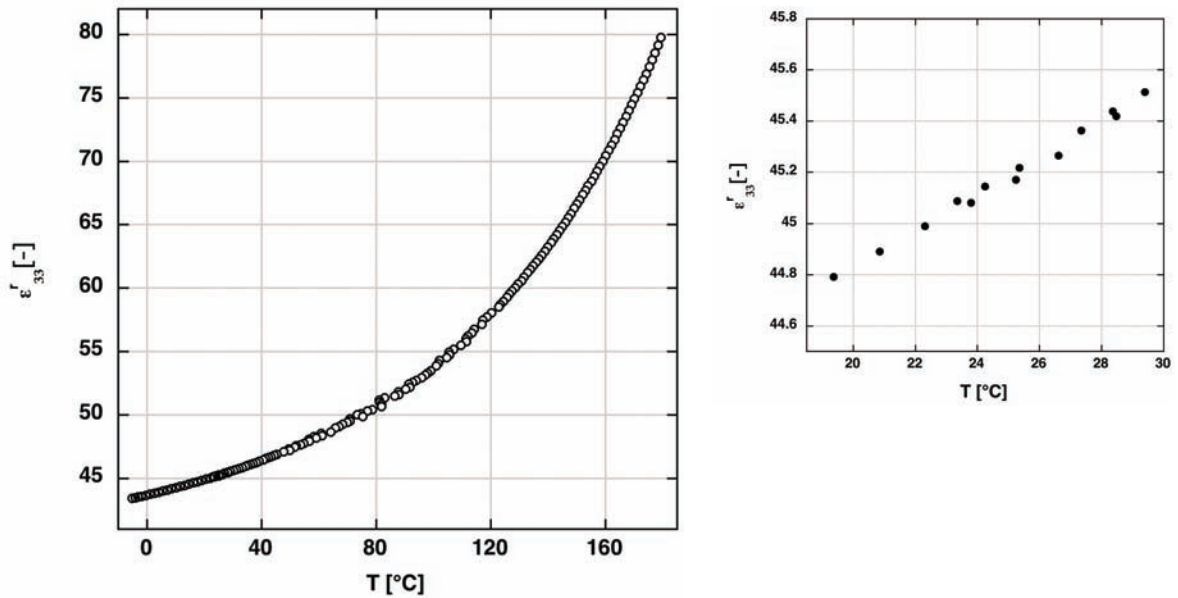


Figure 5.11: Dielectric permittivity of potassium niobate in the orthorhombic phase as a function of temperature. Smaller graph on the right shows the same function, but only in the vicinity of the room temperature.

temperature dependencies of the impedance indirectly give us the temperature dependencies of material electromechanical properties. The temperature dependence of elastic constants of KN samples were calculated from the experimentally obtained piezoelectric resonance curves, using Eq. (4.2). The temperature dependence of the elastic compliances s_{11} and s_{22} is given in Fig. 5.12, while their room temperature values are compared with the results found in the literature in Table 5.2.

5.1.5 Piezoelectric properties

The temperature dependence of the measured piezoelectric coefficients is shown in Fig. 5.13, while the room temperature values are compared with the literature values in Table 5.3. The temperature dependence of the d_{33} has already been measured by *Günter* [54].

5.1.6 Coupling coefficients

The temperature dependence of the coupling coefficients k_{31} and k_{32} are plotted in Fig 5.14. The room temperature values are extracted from the graphs and compared with

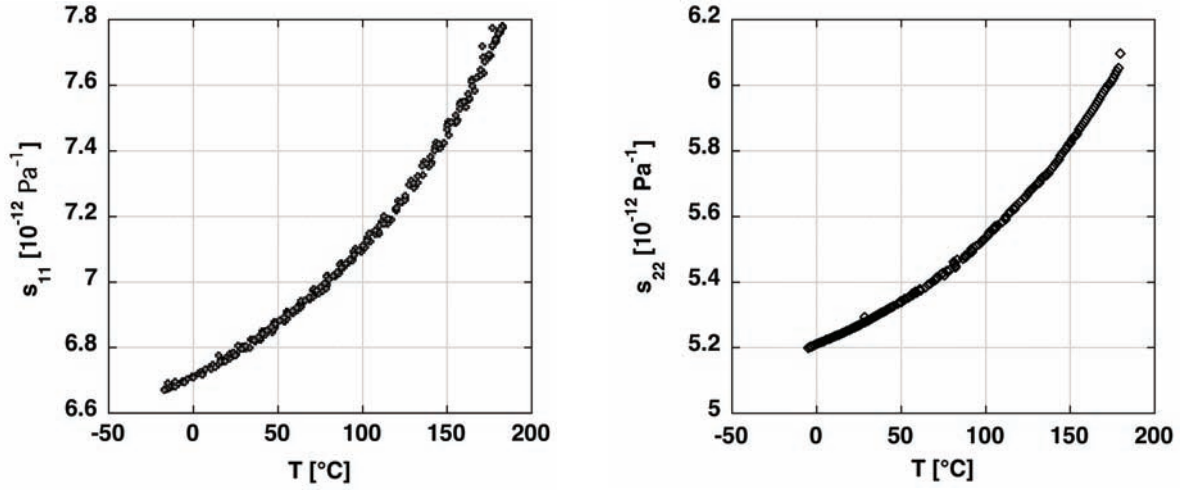


Figure 5.12: Elastic compliances s_{11} (left) and s_{22} (right) of KN samples in the orthorhombic phase as a function of temperature.

$s_{ij}^E [10^{-12} Pa^{-1}]$	Wada [152, 153]	this work	Zgonik [166]
s_{11}^E	5.41	6.78	5.41
s_{22}^E	5.12	5.27	5.06
s_{33}^E	6.44	-	7.0
s_{44}^E	38.9	-	40.0
s_{55}^E	12.5	-	13.5
s_{66}^E	-	-	-
s_{12}^E	-	-	-
s_{13}^E	-	-	-
s_{23}^E	-	-	-

Table 5.2: Measured elastic compliances in comparison with the corresponding literature data.

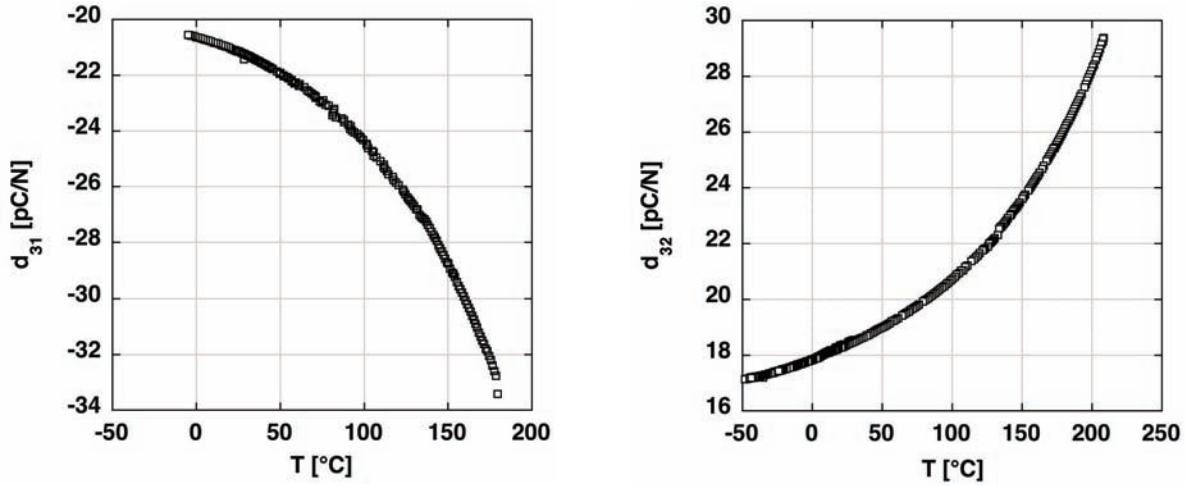


Figure 5.13: Transversal piezoelectric coefficients d_{31} (left) and d_{32} (right) of potassium niobate samples in the orthorhombic phase as functions of temperature.

(pC/N)	Wada et al. [153]	Zgonik [166]	Günther [54]	this work
d_{15}	135.8	156.0	159.0	-
d_{24}	204.0	206.0	215.0	-
d_{31}	-22.3	-19.5	-19.5	-21.2
d_{32}	18.5	9.8	9.8	18.4
d_{33}	29.6	29.3	24.5	-

Table 5.3: Experimentally obtained room temperature values of the piezoelectric coefficients, compared to previously published results. Note a much more pronounced discrepancy of the d_{31} coefficient than of d_{32} . Our experimental results are in a very good agreement with the results obtained by Wada et al.

the corresponding values found in the literature (Table 5.4).

	Zgonik [166]	Wada [152, 153]	this work
k_{15}	0.455	0.437	-
k_{24}	0.894	0.882	-
k_{31}	0.439	0.468	0.461
k_{32}	0.213	0.395	0.391
k_{33}	0.561	0.608	-

Table 5.4: Measured room temperature values of the coupling coefficients, compared with previously published results.

5.2 A discussion about Landau-Ginzburg-Devonshire theory of KNbO_3

5.2.1 Calculation of the LGD coefficients

To discuss the behavior of electromechanical properties of potassium niobate single crystals in the framework of Landau-Ginzburg-Devonshire phenomenological theory, one has to start with the Taylor expansion of the Gibbs free energy. This expansion has already been presented in *Chapter 2*, Eq. (2.32), but it will be rewritten here for practical reasons:

$$\begin{aligned}
\Delta G = & G_0(T) + \alpha_1[P_1^2 + P_2^2 + P_3^2] + \alpha_{11}[P_1^4 + P_2^4 + P_3^4] + \alpha_{111}[P_1^6 + P_2^6 + P_3^6] \\
& + \alpha_{12}[P_1^2 P_2^2 + P_2^2 P_3^2 + P_3^2 P_1^2] + \alpha_{112}[P_1^4(P_2^2 + P_3^2) + P_2^4(P_1^2 + P_3^2) + P_3^4(P_1^2 + P_2^2)] \\
& + \alpha_{123}P_1^2 P_2^2 P_3^2 - \frac{1}{2}S_{11}[X_1^2 + X_2^2 + X_3^2] - S_{12}[X_1 X_2 + X_2 X_3 + X_3 X_1] \\
& - \frac{1}{2}S_{44}[X_4^2 + X_5^2 + X_6^2] - Q_{11}[X_1 P_1^2 + X_2 P_2^2 + X_3 P_3^2] \\
& - Q_{12}[X_1(P_2^2 + P_3^2) + X_2(P_1^2 + P_3^2) + X_3(P_1^2 + P_2^2)] \\
& - Q_{44}[X_4 P_2 P_3 + X_5 P_1 P_3 + X_6 P_1 P_2] \\
& + \dots
\end{aligned} \tag{5.1}$$

If one now wants to determine the series expansion coefficients (α, S, Q) , one can do that by fitting the experimental results obtained for different phases of KNbO_3 .

In general, dielectric permittivity values can be calculated from (5.1) as

$$\frac{1}{\varepsilon_{ij}} = \frac{\partial^2 \Delta G}{\partial P_i \partial P_j}. \tag{5.2}$$

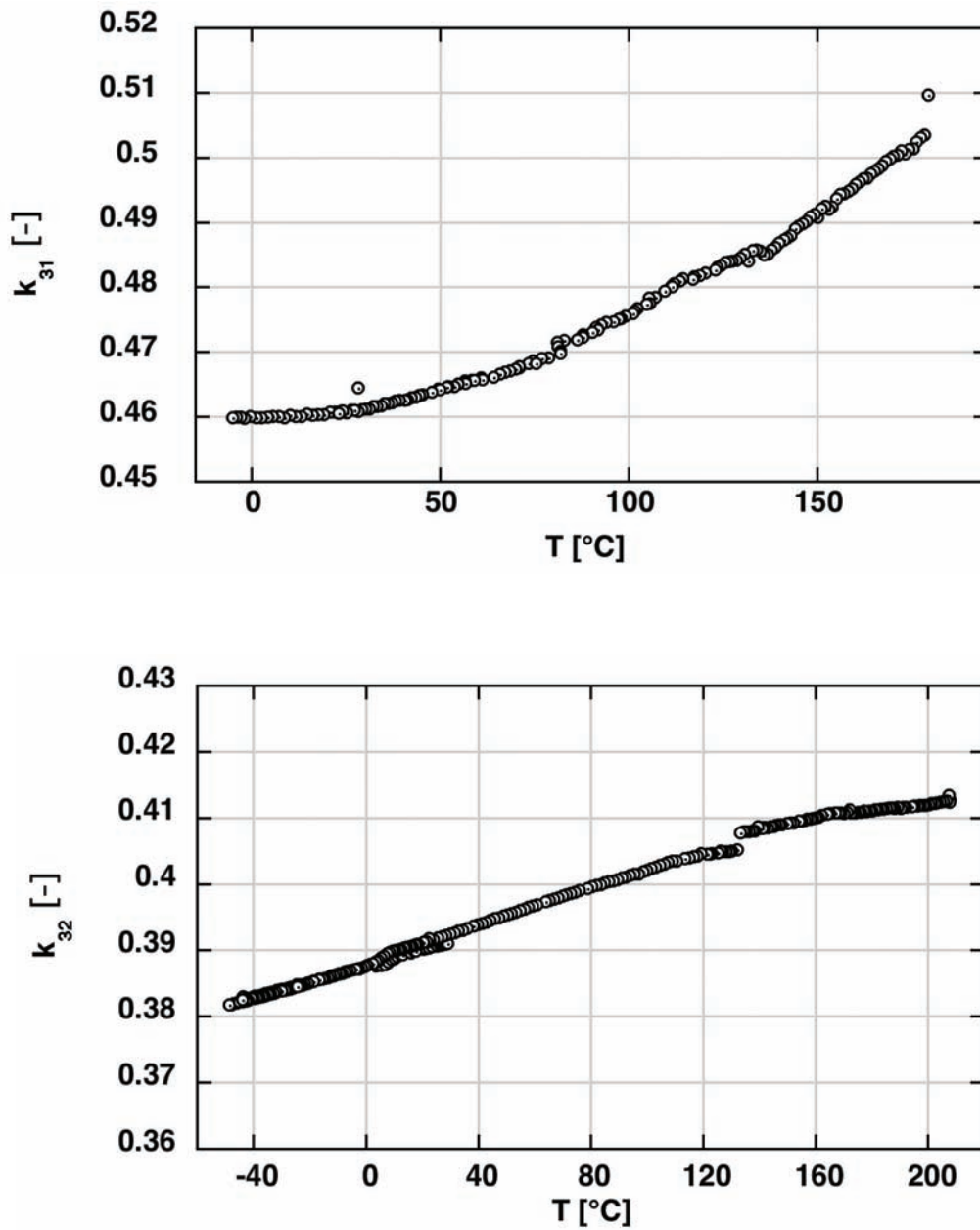


Figure 5.14: Coupling coefficients k_{31} and k_{32} of KN samples in the orthorhombic phase as functions of temperature.

In the paraelectric cubic phase ($P_1 = P_2 = P_3 = 0$), for a system without mechanical constraints ($X_i = 0$)¹¹, this equation will give

$$\frac{1}{\varepsilon_{ij}} = 2\alpha_1. \quad (5.3)$$

The paraelectric phase is macroscopically isotropic, and so is its dielectric constant. Since the dielectric permittivity of the paraelectric phase obeys *Curie-Weiss law*, the coefficient α_1 is thus obtained by fitting the measurements taken in the cubic paraelectric phase onto this law,

$$\varepsilon = \frac{C}{T - T_C} = \frac{1}{2\alpha_1}. \quad (5.4)$$

The measurements and fitting results are shown in Fig. 5.15.

The Curie constant then can be calculated to be $C = 2.293 \cdot 10^5 K$, the Curie temperature

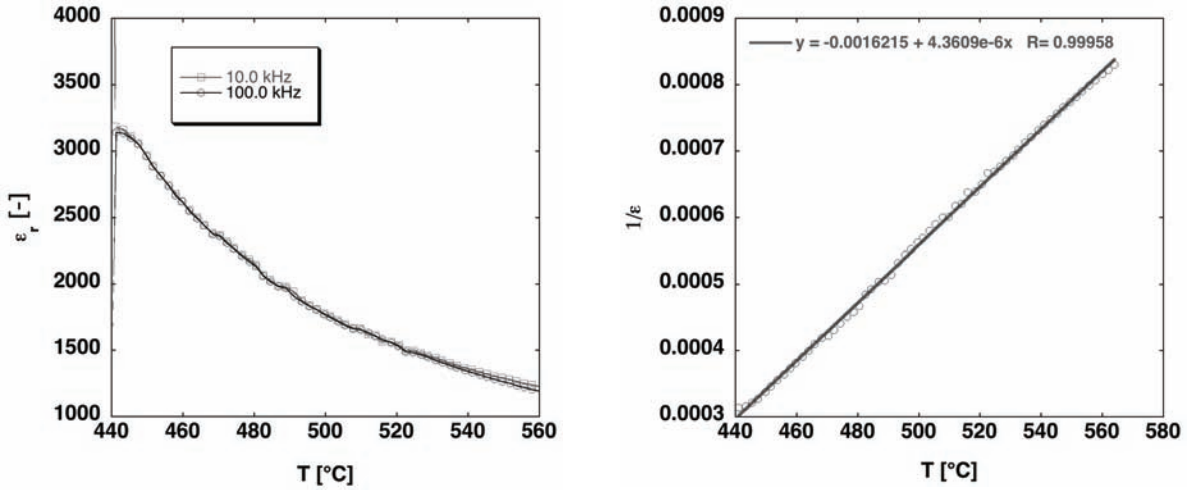


Figure 5.15: Temperature dependence of the dielectric constant of paraelectric cubic potassium niobate (left), and fitting of these measured values to Curie-Weiss law (right).

$T_C = 645K$, and value of α_1 to be

$$\alpha_1(T) = 2.462 \cdot 10^5 (T - 645) \frac{Vm}{C}. \quad (5.5)$$

When describing phenomenologically many perovskite systems (for example, $PbTiO_3$ [62], $PbZrO_3$ [58], PZT systems with different concentration ratios of the components [?, 59]), α_1 is considered to be the only coefficient depending on temperature. But this is not the case for *all* perovskites. An excellent example is *barium titanate*. In this material, some higher order terms are necessarily considered to be temperature dependent, if one

¹¹This condition is assumed throughout the whole chapter.

wants to obtain highly accurate agreement of the phenomenological description and measured results. Taking this into account, and the fact that potassium niobate has the same crystal structure and can undergo the same sequence of phase transitions as barium titanate, one can rise the question of number of the LGD coefficients for KN not depending on temperature as an important one.

If one now wants to make assumptions about the temperature dependence of higher order coefficients in the same manner as it has been done for the case of barium titanate, than one has that coefficients have to possess analytical forms as

$$\alpha_{11} = A_{11}(T - T_{11}) + B_{11}, \quad (5.6)$$

$$\alpha_{111} = A_{111}(T - T_{111}) + B_{111}, \quad (5.7)$$

$$\alpha_{12}, \alpha_{112}, \alpha_{123} \neq f(T). \quad (5.8)$$

In the tetragonal ferroelectric phase ($P_1 = 0$, $P_2 = 0$, $P_3 \neq 0$) the dielectric constants calculated from the Gibbs free energy will have the form

$$\frac{1}{\varepsilon_{11}} = \frac{\partial^2 \Delta G}{\partial P_1 \partial P_1} = \chi_{11} = 2(\alpha_1 + \alpha_{12}P_3^2 + \alpha_{112}P_3^4) = \frac{\partial^2 \Delta G}{\partial P_2 \partial P_2} = \chi_{22} = \frac{1}{\varepsilon_{22}}, \quad (5.9)$$

and

$$\frac{1}{\varepsilon_{33}} = \frac{\partial^2 \Delta G}{\partial P_3 \partial P_3} = \chi_{33} = 2(\alpha_1 + 6\alpha_{11}P_3^2 + 15\alpha_{111}P_3^4), \quad (5.10)$$

while the spontaneous polarization can be calculated using the condition of the thermodynamic stability of the system

$$\frac{\partial \Delta G}{\partial P_i} = E_i = 0, \quad (5.11)$$

giving

$$P_{t,s}^2 = -\frac{\alpha_{11}}{3\alpha_{111}} + \frac{\sqrt{\alpha_{11}^2 - 3\alpha_1\alpha_{111}}}{3\alpha_{111}}, \quad (5.12)$$

where t denotes the tetragonal ferroelectric phase.

For the orthorhombic phase the dielectric stiffnesses can be calculated to be

$$\begin{pmatrix} \chi_{11} & 0 & 0 \\ 0 & \chi_{22} & \chi_{23} \\ 0 & \chi_{32} & \chi_{33} \end{pmatrix}, \quad (5.13)$$

where

$$\chi_{11} = (4\alpha_{112} + 2\alpha_{123})P_3^4 + 4\alpha_{12}P_3^2 + 2\alpha_1, \quad (5.14)$$

$$\chi_{22} = \chi_{33} = (30\alpha_{111} + 14\alpha_{112})P_3^4 + (12\alpha_{11} + 2\alpha_{12})P_3^2 + 2\alpha_1, \quad (5.15)$$

$$\chi_{23} = \chi_{32} = 16\alpha_{112}P_3^4 + 4\alpha_{12}P_3^2. \quad (5.16)$$

and for the dielectric permittivities one has

$$\begin{pmatrix} \varepsilon_{11} & 0 & 0 \\ 0 & \varepsilon_{22} & \varepsilon_{23} \\ 0 & \varepsilon_{32} & \varepsilon_{33} \end{pmatrix}, \quad (5.17)$$

where

$$\varepsilon_{11} = \chi_{11}^{-1}, \quad (5.18)$$

$$\varepsilon_{22} = \varepsilon_{33} = \frac{\chi_{33}}{\chi_{33}^2 - \chi_{23}^2}, \quad (5.19)$$

$$\varepsilon_{23} = \varepsilon_{32} = \frac{-\chi_{23}}{\chi_{33}^2 - \chi_{23}^2}, \quad (5.20)$$

The spontaneous polarization can be calculated to be

$$P_{o,s}^2 = \frac{-2\alpha_{11} - \alpha_{12} + \sqrt{-4\alpha_1(3\alpha_{111} + 3\alpha_{112}) + (2\alpha_{11} + \alpha_{12})^2}}{2(3\alpha_{111} + 3\alpha_{112})}, \quad (5.21)$$

where o denotes the orthorhombic phase.

Since the dielectric constants for the orthorhombic phase are calculated here in the paraelectric cubic axis reference frame, and the experimental results reported in the literature and obtained from our measurements are in the orthorhombic crystallographic reference frame, one has to transform from one reference frame to the other¹². In the orthorhombic system the dielectric stiffness values along principal axes have the form

$$\begin{pmatrix} \chi_{11}^o & 0 & 0 \\ 0 & \chi_{22}^o & 0 \\ 0 & 0 & \chi_{33}^o \end{pmatrix}, \quad (5.22)$$

where

$$\chi_{11}^o = \chi_{11}, \quad (5.23)$$

$$\chi_{22}^o = \chi_{33} - \chi_{23} = (30\alpha_{111} - 2\alpha_{112})P_3^4 + (12\alpha_{11} - 2\alpha_{12})P_3^2 + 2\alpha_1, \quad (5.24)$$

$$\chi_{33}^o = \chi_{33} + \chi_{23} = (30\alpha_{111} + 30\alpha_{112})P_3^4 + (12\alpha_{11} + 6\alpha_{12})P_3^2 + 2\alpha_1. \quad (5.25)$$

Then, in the orthorhombic axes system, the nonzero dielectric constants can be written as

$$\varepsilon_{ii}^o = \frac{1}{\chi_{ii}^o}. \quad (5.26)$$

When fitting experimental results to a theoretical expression, it is always more advantageous to have simpler analytical expressions with as few as possible unknown coefficients.

¹²These transformations are discussed in *Chapter 6* and in *Appendix A*

It is clear then, by comparing the expressions for the tetragonal and orthorhombic phase presented here, that it is most preferable having the experimental results obtained in the tetragonal phase. However, for measurements of single domain properties in the tetragonal phase, it is necessary to master a method that will simultaneously pole a KN sample at elevated temperatures (the tetragonal phase of KNbO_3 occurs in the temperature range $225^\circ\text{C} - 435^\circ\text{C}$) and then measure the dielectric properties for different orientations in the sample, taking into account possible problems with elevated conductivity of the material at high temperatures. One can consider this as the reason why there is no, up to our best knowledge, published results on dielectric properties measurements on single domain KN crystals in the tetragonal phase. For this phase there are only measurements reported for the temperature dependence of the spontaneous polarization [55]. This is not enough to determine any of the LGD coefficients.

On the other hand, trying to measure the dielectric properties of the single domain samples in the tetragonal phase was impossible with the set of crystals in our possession because the crystals did not have proper cuts (they were cut for measurements of piezoelectric coefficients d_{31} , d_{32} and d_{33} and dielectric constant ϵ_{33} in the orthorhombic ferroelectric phase).

However, by gathering the results from the literature and the results of measurements shown in this chapter, it is possible to make a first step towards obtaining the LGD coefficients of single crystal KNbO_3 - an estimation of values of all the coefficients α in the 6th order description is feasible using measurements obtained in the orthorhombic phase.

For this estimation, it suffices:

- to combine the results of measurements of temperature dependence of dielectric constants done in our laboratory and by *Fukuda* [45], and the results of the temperature dependence of the spontaneous polarization in the orthorhombic phase by *Günter* [55];
- to make an assumption that higher order coefficients are temperature independent, because the fitting by taking the coefficient forms as in Eqs. (5.6) - (5.8) is very difficult without having the experimental data of dielectric constants in the tetragonal phase.

It can be seen from Eqs. (5.14) - (5.26) that the Landau-Ginzburg-Devonshire theory coefficients can be obtained by fitting the spontaneous polarization dependence of the dielectric constants. The calculation in this manner is not unusual - for example *Wiesendanger* used in his thesis report [158] and in Ref. [160] the spontaneous polarization values obtained by *Hewat* [64, 65] and Curie constant and Curie temperature from a

work by *Triebwasser* [143, 144] to fit his own experimental results to the LGD theory. From these measurements the spontaneous polarization dependences of the dielectric

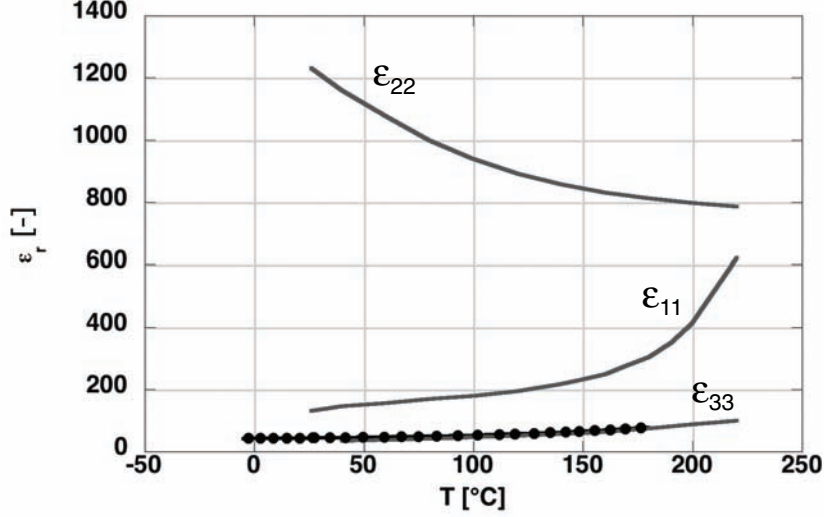


Figure 5.16: Temperature dependences of the dielectric constants in the orthorhombic phase of potassium niobate along the phase principal axes. Closed circles denote our measurements. The rest of the data (solid lines) taken from the Ref. [45].

constants can be derived. These dependences are shown in Figs. 5.18 - 5.20.

Now, the dependence of ε_{11}^o , shown in Fig. 5.19, is fitted using the Eqs. (5.14), (5.23), and (5.26), and the coefficients are obtained:

$$2\alpha_{112} + \alpha_{123} = 6.4076 \cdot 10^{10} \frac{Vm^9}{C^5} \quad (5.27)$$

and

$$\alpha_{12} = -4.0089 \cdot 10^9 \frac{Vm^5}{C^3} \quad (5.28)$$

Further, the dependence of ε_{22}^o , shown in Fig. 5.18, is fitted using the Eqs. (5.24), and (5.26), and the following relations are obtained:

$$6\alpha_{11} - \alpha_{12} = 7.8835 \cdot 10^8 \frac{Vm^5}{C^3}, \quad (5.29)$$

and

$$15\alpha_{111} - \alpha_{112} = -3.0405 \cdot 10^7 \frac{Vm^9}{C^5}. \quad (5.30)$$

Finally, the dependence of ε_{33}^o , shown in Fig. 5.20, is fitted using the Eqs. (5.25), and (5.26), and the following relations are obtained:

$$2\alpha_{11} + \alpha_{12} = -8.2098 \cdot 10^9 \frac{Vm^5}{C^3}, \quad (5.31)$$

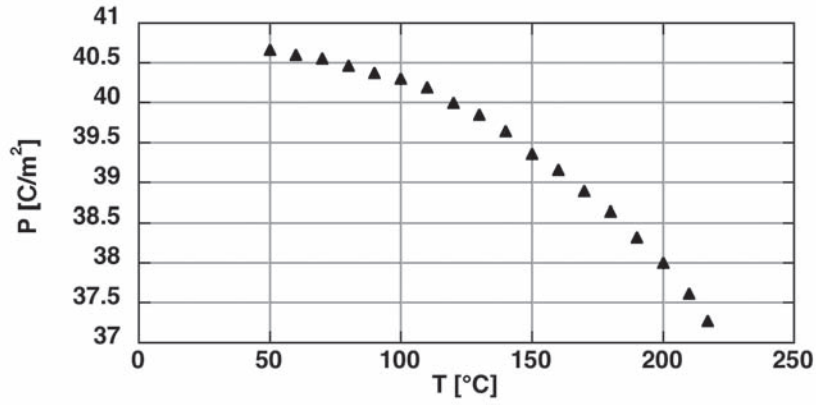


Figure 5.17: Temperature dependence of the spontaneous polarization in the orthorhombic phase of KN. Data extracted from the Ref. [55].

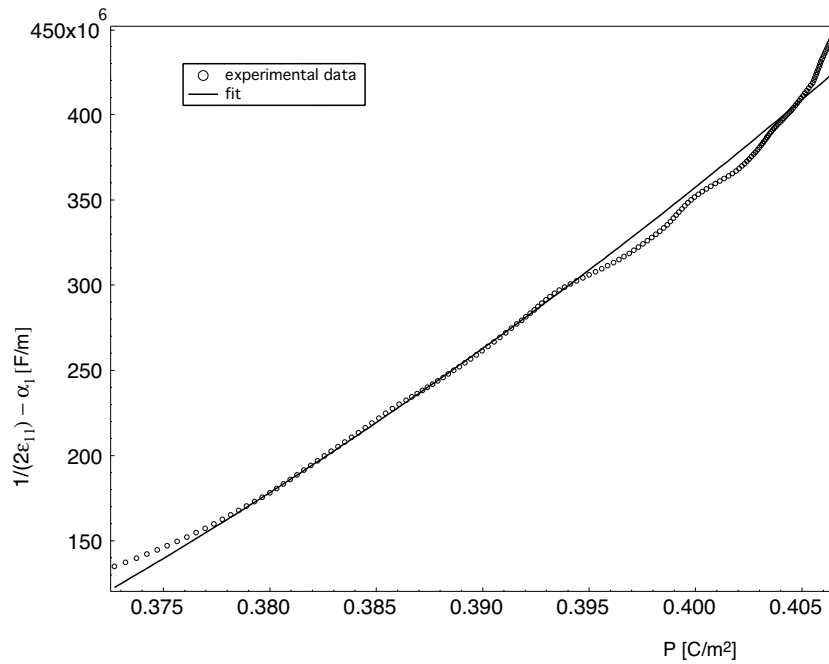


Figure 5.18: Spontaneous polarization dependence of the value $\frac{1}{2\epsilon_{11}} - \alpha_1(T)$ and the fitted curve. Fitting of these results by using Eqs. 5.14, 5.23 and 5.26 gives the values of α_{12} and $2\alpha_{112} + \alpha_{123}$.

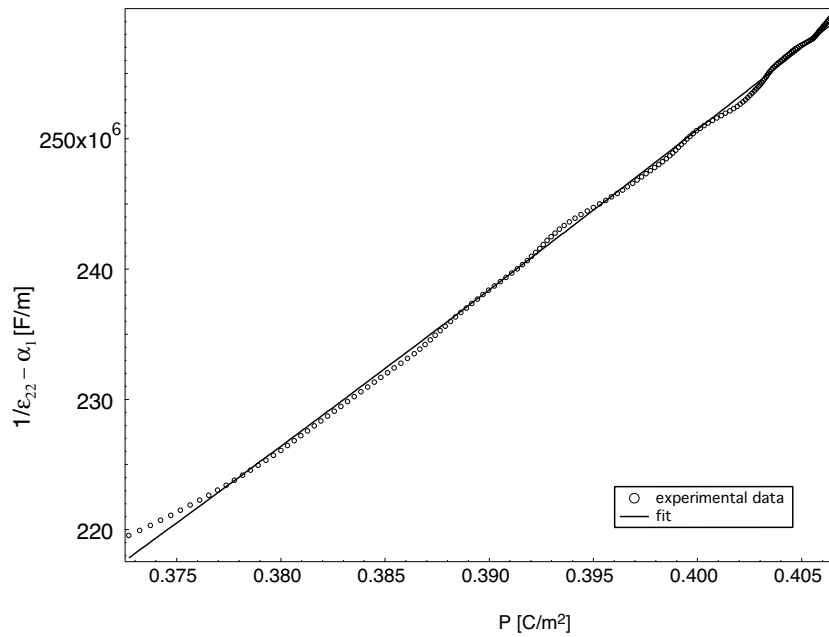


Figure 5.19: Spontaneous polarization dependence of the value $\frac{1}{\epsilon_{22}} - \alpha_1(T)$ and the fitted curve. Fitting of these results by using Eqs. 5.24 and 5.26 gives the values of $6\alpha_{11} - \alpha_{12}$ and $15\alpha_{111} - \alpha_{112}$.

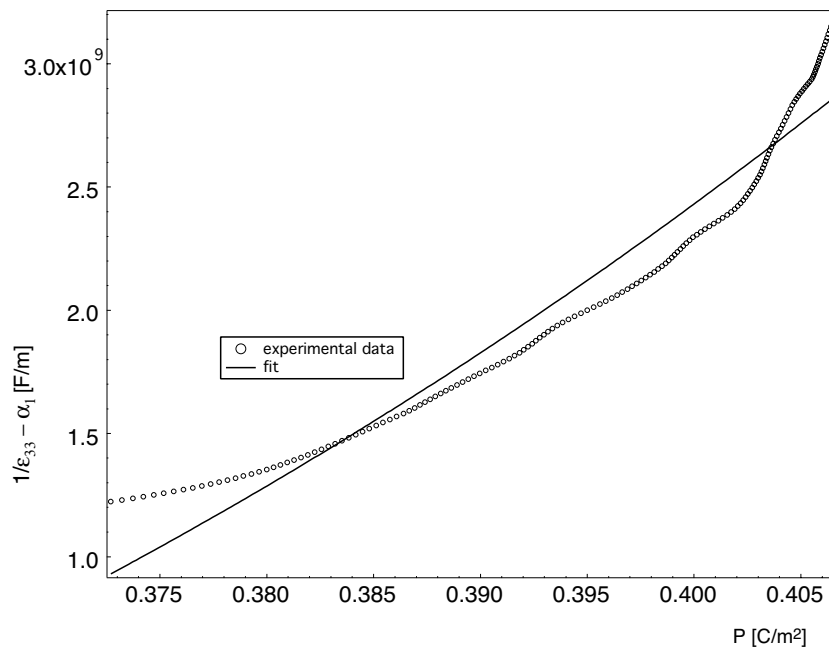


Figure 5.20: Spontaneous polarization dependence of the value $\frac{1}{\epsilon_{33}} - \alpha_1(T)$ and the fitted curve. Fitting of these results by using Eqs. 5.25 and 5.26 gives the values of $2\alpha_{11} + \alpha_{12}$ and $\alpha_{111} + \alpha_{112}$.

and

$$\alpha_{111} + \alpha_{112} = 1.3428 \cdot 10^{10} \frac{Vm^9}{C^5}. \quad (5.32)$$

Solving the equations system obtained by fitting the spontaneous polarization dependences of dielectric constants one can obtain (estimate) all the coefficients α of the 6th order LGD phenomenological theory. These coefficients are shown in Table 5.5.

α_1	$2.463 \cdot 10^5 (T - 645) \frac{Vm}{C}$
α_{11}	$-5.3676 \cdot 10^9 \frac{Vm^5}{C^3}$
α_{12}	$-4.0089 \cdot 10^9 \frac{Vm^5}{C^3}$
α_{111}	$8.3735 \cdot 10^8 \frac{Vm^9}{C^5}$
α_{112}	$1.2591 \cdot 10^{10} \frac{Vm^9}{C^5}$
α_{123}	$3.8895 \cdot 10^{10} \frac{Vm^9}{C^5}$

Table 5.5: Estimated values of dielectric stiffness coefficients at constant stress, α , for single domain single crystal potassium niobate.

5.2.2 Calculation of temperature and direction dependences of dielectric and piezoelectric constants, and spontaneous polarization in KN

Using the coefficients from Table 5.5, it is possible now to estimate theoretically the temperature dependences of the spontaneous polarization, dielectric constants, in all three ferroelectric phases of KN. The calculated values for the spontaneous polarization in the orthorhombic phase are shown in Fig. 5.21, together with the experimental values obtained by *Günter* [55], which helped us to estimate the coefficients α , while the calculated values of the spontaneous polarization for all three ferroelectric phases are shown in Fig. 5.22. Dielectric constants are calculated for the orthorhombic phase and compared to the experimental results obtained by *Fukuda* [45] and our experiments, Fig. 5.23, while values for all three ferroelectric phases are shown in Fig. 5.24.

Further, using the electrostrictive coefficients from the work of *Günther* [54], we estimated the temperature dependence of the piezoelectric coefficients. These calculated values are shown in Fig. 5.25 for the d_{15} , d_{24} and d_{33} in the orthorhombic phase, while in Fig. 5.26 one can find d_{31} and d_{32} together with our experimental results for the same coefficients.

In the orthorhombic phase (symmetry), one has that five piezoelectric coefficients can have non-zero values

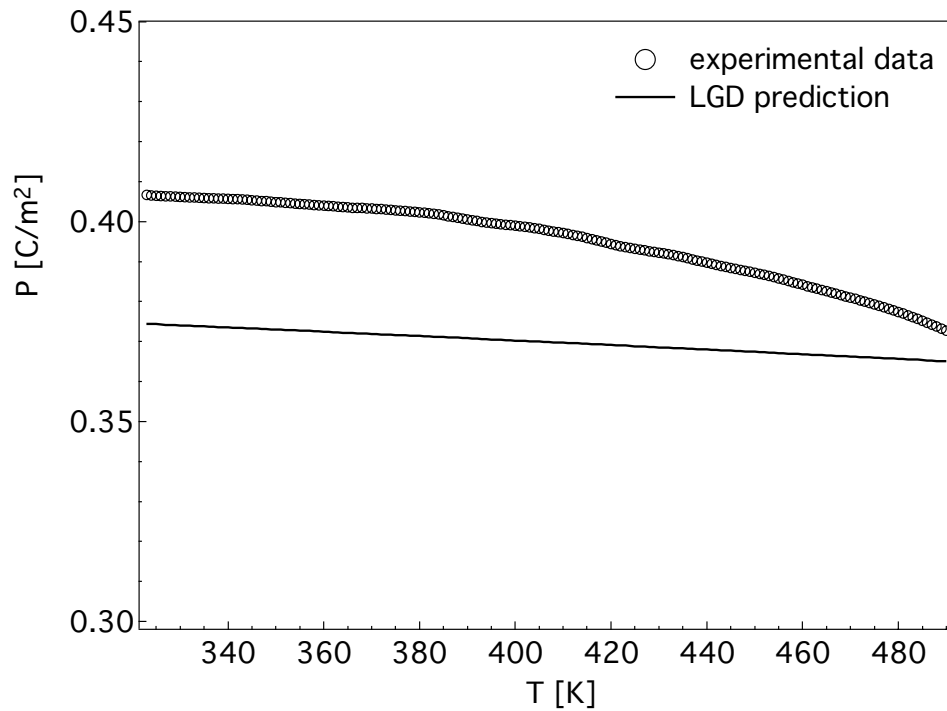


Figure 5.21: Temperature dependence of the spontaneous polarization of orthorhombic KN - LGD calculations compared to experimental data from Ref. [55] (see Fig. 3.3).

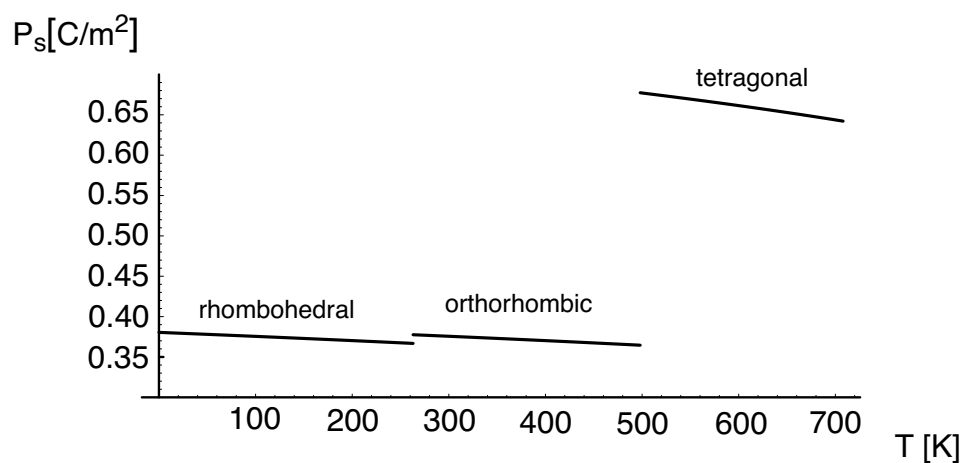


Figure 5.22: Temperature dependence of the spontaneous polarization of KN for all three ferroelectric phases - LGD calculations. Compare to Fig. 3.2.

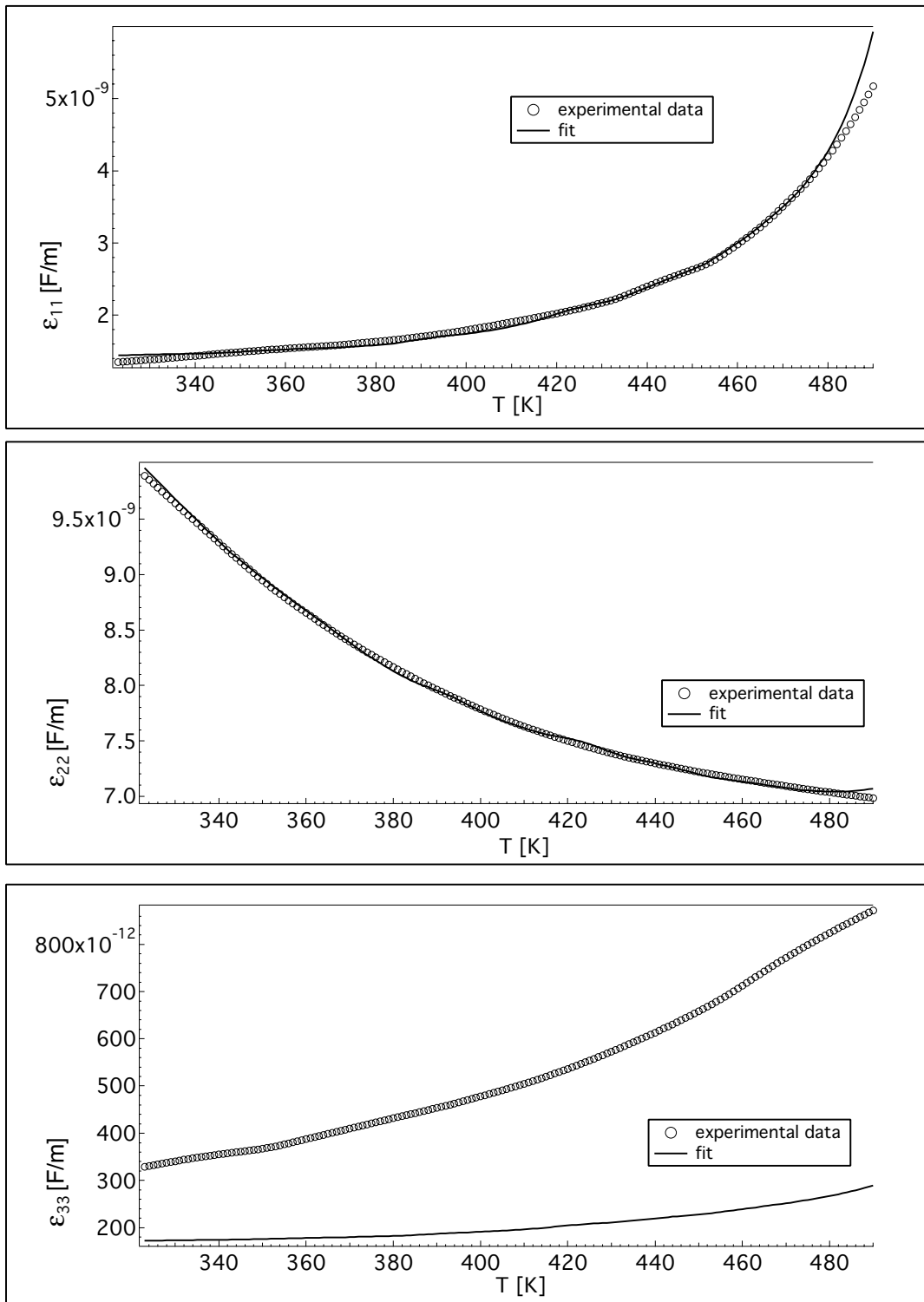


Figure 5.23: Temperature dependence of the dielectric constants of single domain orthorhombic KN - a LGD estimate compared to experimental values from Ref. [45] (see Fig. 3.5).

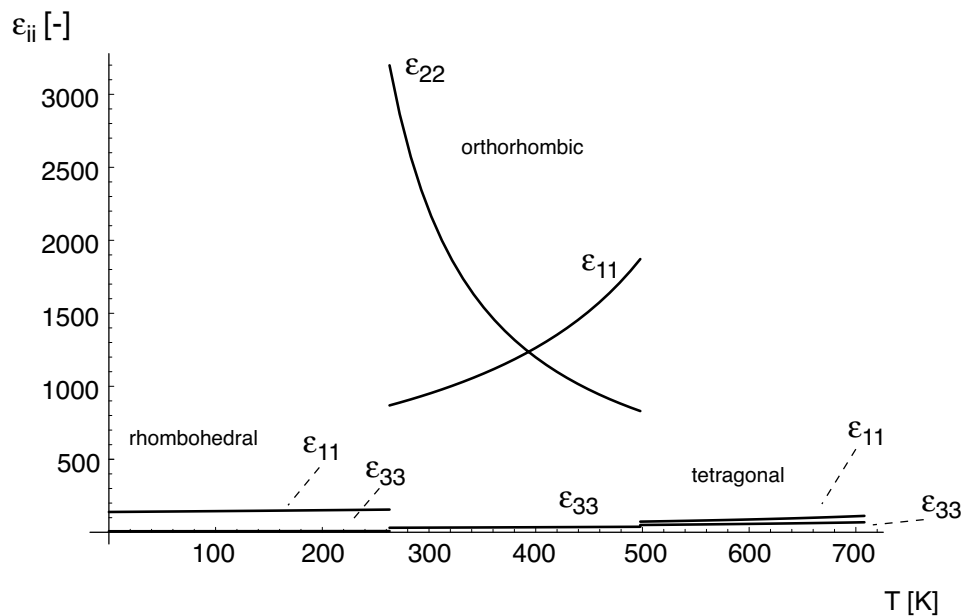


Figure 5.24: Temperature dependence of the dielectric constants of single domain KN for all three ferroelectric phases - LGD calculations.

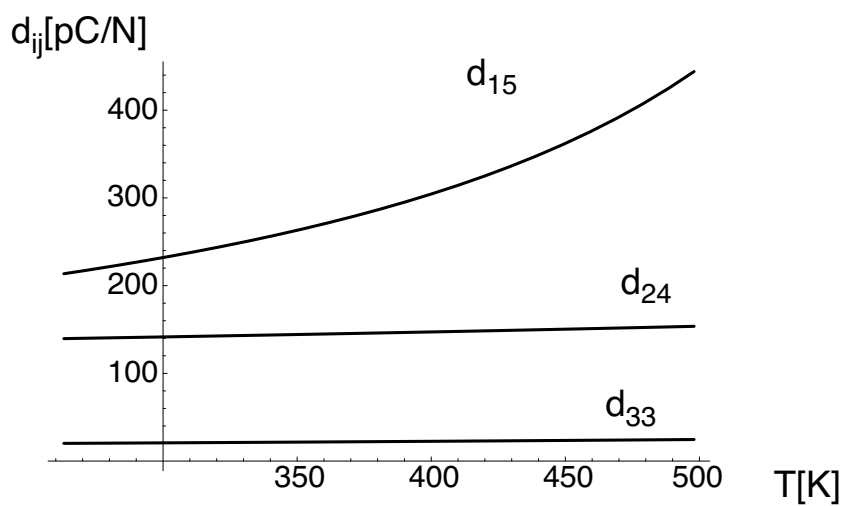


Figure 5.25: Temperature dependence of the piezoelectric constants of single domain orthorhombic KN - LGD calculations.

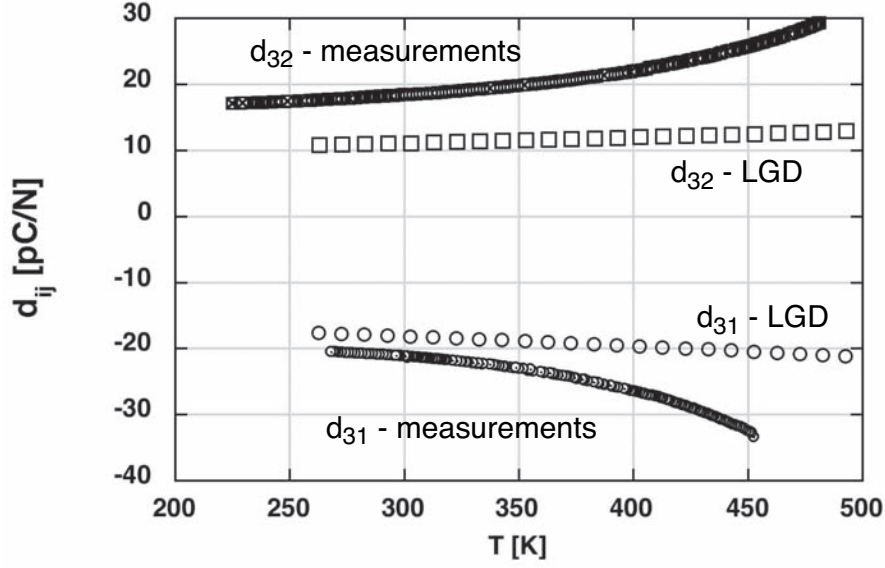


Figure 5.26: Temperature dependence of the transverse piezoelectric constants of single domain orthorhombic KN - LGD calculations compared to experimental results obtained in this work.

$$\begin{pmatrix} 0 & 0 & 0 & 0 & d_{15}^o & 0 \\ 0 & 0 & 0 & d_{24}^o & 0 & 0 \\ d_{31}^o & d_{32}^o & d_{32}^o & 0 & 0 & 0 \end{pmatrix}, \quad (5.33)$$

where

$$d_{15}^o = \sqrt{2}d_{15}^c; \quad (5.34)$$

$$d_{24}^o = \sqrt{2}(d_{33}^c - d_{32}^c); \quad (5.35)$$

$$d_{31}^o = \sqrt{2}d_{31}^c; \quad (5.36)$$

$$d_{32}^o = \frac{1}{\sqrt{2}}(d_{33}^c + d_{33}^c - d_{24}^c); \quad (5.37)$$

$$d_{33}^o = \frac{1}{\sqrt{2}}(d_{33}^c + d_{33}^c + d_{24}^c), \quad (5.38)$$

are the coefficients represented in the orthorhombic axes reference system, related to the corresponding coefficients in the cubic axes system, in which we calculated the coefficients α ,

$$d_{15}^c = \varepsilon_{11}Q_{44}P_3; \quad (5.39)$$

$$d_{24}^c = (\varepsilon_{32} + \varepsilon_{33})Q_{44}P_3; \quad (5.40)$$

$$d_{31}^c = 2(\varepsilon_{32} + \varepsilon_{33})Q_{12}P_3; \quad (5.41)$$

$$d_{32}^c = 2(Q_{11}\varepsilon_{32} + Q_{12}\varepsilon_{33})P_3; \quad (5.42)$$

$$d_{33}^c = 2(Q_{12}\varepsilon_{32} + Q_{11}\varepsilon_{33})P_3. \tag{5.43}$$

Finally, using the estimated and measured results of the dielectric and piezoelectric properties in the orthorhombic phase, we can calculate three dimensional representations of the dielectric and piezoelectric constants in a general direction for this phase. The angle dependence of the dielectric constant is shown in Fig. 5.27, while the same dependence, but for the related piezoelectric constant is shown in Fig. 5.28. One can note that the dielectric constant has a very anisotropic behavior with the temperature change, while piezoelectric response does not follow that anisotropy evolution in the same qualitative manner.

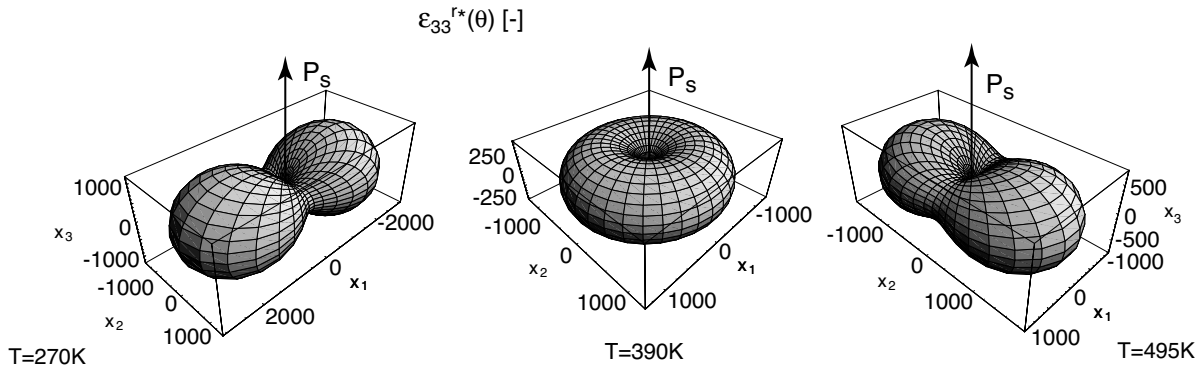


Figure 5.27: Temperature and direction dependence of the dielectric constant ε_{33}^* (see Appendix A) in the orthorhombic phase of KN - calculations.

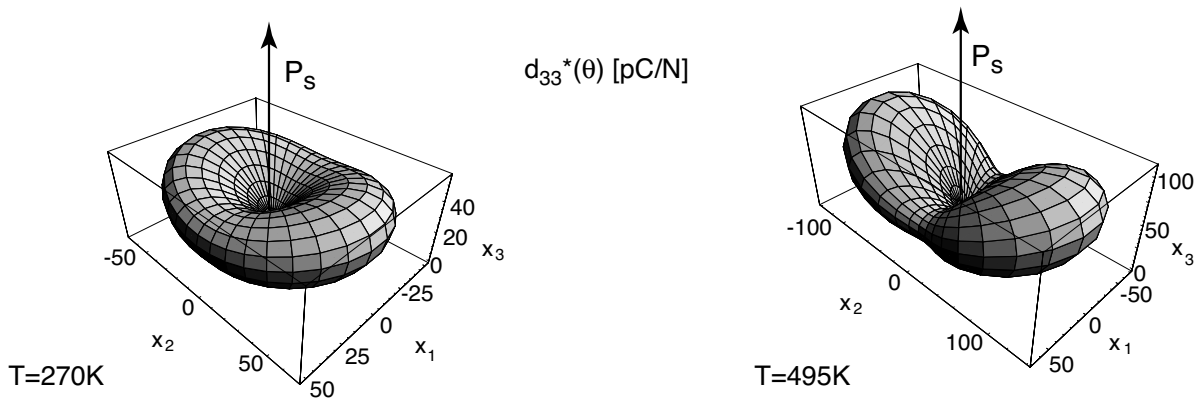


Figure 5.28: Temperature and direction dependence of the piezoelectric constant d_{33}^* , Eq. 6.10, in the orthorhombic phase of single domain KN - calculations.

5.3 Conclusions

Potassium niobate in single crystal form has a long experimental history. Despite that fact, the phenomenological description of its electromechanical properties has never been done as complete as for some other classic perovskites, such as BaTiO_3 , PbTiO_3 , or different compositions of PZT. There are several reasons: difficulties in growing high quality crystals and in obtaining and preserving ferroelectrically single domain state¹³, high phase transition temperature between orthorhombic and tetragonal ferroelectric phase, and problems with the increased material conductivity at high temperatures and low frequencies. These facts have made measurements of the temperature dependence of the spontaneous polarization and single domain dielectric properties at higher temperatures very difficult. Since the accurate obtaining of the LGD coefficients for KN requests experimental results of the single domain electromechanical properties in the tetragonal phase, these coefficients have never been published completely.

In this work measurements of the temperature dependence of some electromechanical properties of potassium niobate were performed. The number of the independent measured values was limited by the set of samples in our possession. Combining the results obtained by our measurements with the experimental results for the orthorhombic phase of KNbO_3 from the literature, it was possible to calculate the coefficients of the 6th order Gibbs free energy expansion for a free dielectric. The assumption while doing calculations was that no higher order coefficients have the temperature dependence. Up to our best knowledge, this is the *first time* that all coefficients α for the series expansion of the KN Gibbs free energy up to the 6th order have been calculated (estimated).

One can note that the calculated dielectric response of KN in a general direction is very anisotropic upon temperature change - it changes its maximal value direction by 90° if the material goes throughout the orthorhombic phase. However, our LGD coefficients estimate that the piezoelectric response in a general direction will not follow that anisotropy. The reason might be the large $\varepsilon_{11}/\varepsilon_{33}$ and Q_{44}/Q_{11} ratios that prevent a dominant contribution of d_{24}^o over d_{15}^o in a general direction piezoelectric response in the orthorhombic phase - one should come back to this question after reading *Chapter 6*.

The experimental results on KNbO_3 are fitted to LGD theory and all coefficients α for the series expansion of the Gibbs free energy up to the 6-th order have been calculated (estimated).

¹³Even recently (2003), there is a paper by *Wada et al.* [152] in which the authors state that their samples of potassium niobate had *almost* the single domain state after they performed the poling procedure.

Chapter 6

Piezoelectric anisotropy - phase transition relations in perovskites

The discovery of the exceptionally large piezoelectric response along directions that not coincide with polar directions in single crystals of lead-based relaxor-ferroelectric solid solutions has risen the question of origins of the enhanced response along non-polar axes, and the origins of the large piezoelectric coefficients in these materials. By using the phenomenological Landau-Ginzburg-Devonshire theory and classic ferroelectric perovskites, these origins are investigated and discussed.

The work presented here was initiated by the discovery of the unusually large piezoelectric response along *non - polar* directions in single crystals of lead-based relaxor-ferroelectric solid solutions [118]

- $(1 - x)Pb(Zn_{1/2}Nb_{2/3})O_3 - xPbTiO_3$ (PZN-PT), and
- $(1 - x)Pb(Mg_{1/2}Nb_{2/3})O_3 - PbTiO_3$ (PMN-PT)

with the piezoelectric and coupling coefficients $d_{33} > 2500pC/N$ and $k_{33} > 90\%$. Before this discovery, materials the most used in applications were piezoelectric ceramics such as soft PZT, exhibiting piezoelectric coefficients d_{33} as high as $750pC/N$ (but having a disadvantage of hysteretic behavior), low hysteresis hard piezoelectric ceramics (but with d_{33} values of only $\sim 200 - 300pC/N$), or electrostrictive ceramics with the maximum strain level limited by its dielectric breakdown strength and polarization saturation. On the other hand, the piezoelectric response which is an order of magnitude higher

piezoelectric response measured in PZN-PT and PMN-PT along a non - polar axis than along the polar axis was *opposite* of what was always observed in poled piezoelectric ceramics where the largest piezoelectric response is measured along the poling direction and thus macroscopic average polar axis [82]. The same behavior has subsequently been observed in simple perovskites BaTiO₃ and KNbO₃ [155, 110, 111].

This observation in the perovskite family of piezoelectric materials revived, generally, investigations in this field and thus has also renewed the interest in the piezoelectric properties of classical ferroelectric materials, through attempts to *explain the mechanisms* of the enhanced response along non-polar axes, and as well to indirectly explain the origins of the large piezoelectric coefficients in relaxor - ferroelectrics. Here, in this chapter, a phenomenological model treating this *piezoelectric anisotropy* is presented.

Although the magnitude of the piezoelectric effect is, with few exceptions [81], by far the largest in lead-based complex perovskites, classical ferroelectric systems, such as BaTiO₃ and KNbO₃, are also of interest for the following reasons:

- like complex PMN-PT and PZN-PT compositions, barium titanate and potassium niobate exhibit enhanced piezoelectric response along certain non-polar directions [155, 110, 111]; in the case of KNbO₃, as discussed in previous chapters, its large thickness coupling coefficient $k_t \approx 69\%$ along a nonpolar axis is of a practical interest [111];
- barium titanate and potassium niobate do not exhibit problems associated with the mesoscopic structure present in the relaxor-ferroelectric solid solutions [91];
- it has been seen that both BaTiO₃ and KNbO₃ exhibit a temperature induced sequence of phase transitions and that sequence is, in principle, similar to that in PMN-PT and PZN-PT crystals; however, in contrast to the complex solid solutions [148], all crystal phases in BaTiO₃ and KNbO₃ are well-defined [81, 97].

These compositions may thus be used as convenient modeling materials [44] and may give important clues on mechanisms of the enhanced piezoelectric response along non-polar directions in complex perovskites. One of the most interesting and *unexpected* results obtained from these recent investigations was that the enhanced piezoelectric response could be expected in *many* perovskite ferroelectrics along crystal axes that do not coincide with the direction of the spontaneous polarization, i.e. non-polar directions, for a given ferroelectric phase [118, 155, 110]. This result is *not trivial*, as will be shown in following sections of this chapter by considering examples of the orientation dependence of the longitudinal piezoelectric coefficient in tetragonal phases of two struc-

turally similar, but qualitatively different¹ [19], members of perovskite family PbTiO_3 and BaTiO_3 .

6.1 Piezoelectric anisotropy as a function of temperature - intrinsic effects

The goal of this section is to calculate the *orientation dependence* of the piezoelectric coefficients d_{ij}^* (the asterisk denotes the fact that the piezoelectric response is determined along an arbitrary crystallographic direction) in all ferroelectric phases of ferroelectrically single domain BaTiO_3 and PbTiO_3 single crystals as a function of temperature, and then to demonstrate how the *existence or absence of phase transitions* influences the piezoelectric anisotropy in these materials. The longitudinal piezoelectric coefficient d_{33}^* , will be considered in detail here, while the shear and transverse coefficients will be briefly presented and discussed in *Appendix B*.

Barium titanate is an excellent model material to investigate the most important issues of this problem. On cooling, it transforms from the cubic paraelectric phase (point group $m\bar{3}m$) into the ferroelectric tetragonal phase ($4mm$) at $393K$, to the ferroelectric orthorhombic phase ($mm2$) at $278K$ and to the ferroelectric rhombohedral phase ($3m$) at $183K$ [79], Fig. 6.1 Considering that the orthorhombic point group $mm2$ can be described as a special case of the monoclinic point group m [79], this sequence is similar to that observed in complex perovskite solid solutions [21, 90, 112]. BaTiO_3 is therefore a rich source for determination and discussion of the phase transition effects on the orientation dependence of the piezoelectric coefficients in perovskite materials. On the other hand, PbTiO_3 exhibits only tetragonal ferroelectric phase [62, 88] and is thus a convenient example of a material where ferroelectric - ferroelectric phase transitions do not affect the temperature dependence of the piezoelectric properties. So, it is important to have in mind that this discussion compares systems with and without a *sequence* of ferroelectric - ferroelectric phase transitions.

To calculate the temperature dependence of the coefficient d_{33}^* , it is necessary to know the full set of the piezoelectric coefficients measured along the principal crystal axis for each crystal phase. Unfortunately, the experimental values of these piezoelectric coeffi-

¹The differences in behavior between BaTiO_3 and PbTiO_3 stem from their different electronic structures - the Pb $6s$ and O $2p$ states are strongly hybridized in PbTiO_3 , whereas Ba is essentially fully ionic Ba^{2+} ion in BaTiO_3 . The $Ti-O$ hybridization is crucial to allow ferroelectricity in both materials, and $Pb-O$ hybridization changes the behavior of PbTiO_3 relative to BaTiO_3 in a way that it leads to a large Pb polarizability and stabilizes a large tetragonal c/a strain which stabilizes the tetragonal over the rhombohedral phase in PbTiO_3 .

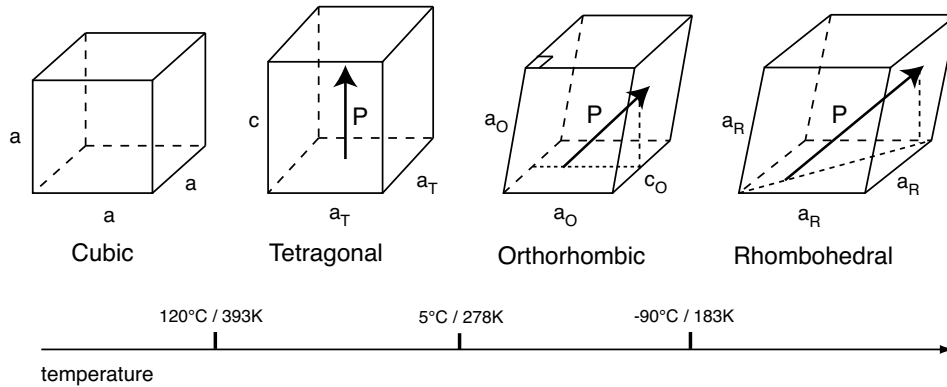


Figure 6.1: Phase transition sequence of barium titanate with decreasing temperature. The sequence is qualitatively the same as the one of potassium niobate, Fig. 5.2, only the transition temperatures are respectively much lower.

coefficients are not available for BaTiO_3 and PbTiO_3 (or any other perovskite) crystals over a sufficiently large temperature range. Here, these piezoelectric coefficients are determined in the framework of the phenomenological Landau–Ginzburg–Devonshire (LGD) theory [31, 32, 106].

The coefficients of the LGD function are well documented in the literature, both for barium titanate [7] and lead titanate [62]. They are usually determined with respect to the coordinate system of the prototypic cubic phase, while for this subject it is always more convenient to express piezoelectric coefficients with respect to the crystallographic coordinate system of each phase. Thus, we first calculate temperature dependence of all piezoelectric coefficients in the cubic system using LGD function, then find corresponding values in the crystallographic coordinate system, and then calculate coefficients along an arbitrary direction with respect to the crystallographic system. The orientation dependence of d_{33}^* will be expressed in terms of the Euler angles (ϕ, θ, ψ) that are defined in the following way [48]:

- the rotation is first made by angle ϕ around the z-axis, then
- around the new x-axis by angle θ , and finally
- by angle ψ around the new z-axis.

All rotations are in the positive direction (counterclockwise). This rotation procedure is visualized in Fig. 6.17.

The dielectric permittivity, polarization, and piezoelectric coefficients in the crystallographic coordinate system for each phase are denoted by ε_{ij}^p , P_{ij}^p and d_{ij}^p , respectively,

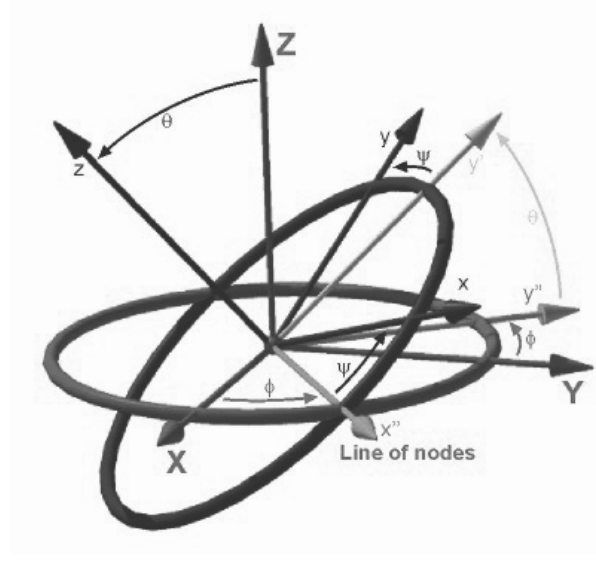


Figure 6.2: Euler angles

where $p = t, o, r$ stands for tetragonal, orthorhombic and rhombohedral phase. The variable d_{ij}^{p*} designates piezoelectric coefficients along an arbitrary direction in the crystallographic coordinate system of the phase p . The electrostrictive coefficients are denoted by Q_{ij} . The dielectric permittivity, ε_{ij}^p , is related to the *dielectric susceptibility* by the relation $\varepsilon_{ij} = \chi_{ij} + 1$, and in the case of ferroelectric materials, one can write $\varepsilon_{ij} \approx \chi_{ij}$, see Eq. (5.2). Finally, crystallographic directions are written as $\langle hkl \rangle_p$ and $[hkl]_p$ where index $p = c, t, o, r$; c stands for the prototypic cubic phase and remaining indices are defined as above.

Tetragonal phase

In the tetragonal phase the value of the longitudinal piezoelectric coefficient d_{33}^{t*} in the crystallographic coordinate system along *an arbitrary direction* can be expressed as²

$$d_{33}^{t*} = \cos\theta(d_{15}^t \sin^2\theta + d_{31}^t \sin^2\theta + d_{33}^t \cos^2\theta) \quad (6.1)$$

where angle θ describes a rotation away from the $[001]_t$ axis of the tetragonal cell. The temperature dependences of d_{ij}^t for BaTiO_3 and PbTiO_3 in the tetragonal phase are shown in Figs. 6.3 and 6.4. In both compositions the term containing the transverse coefficient is small comparing to the other two terms in Eq. (6.1), so that the temperature dependence of d_{33}^{t*} is dominated by the longitudinal coefficient d_{33}^t and by the shear

²Calculations of the piezoelectric and dielectric coefficients in arbitrary directions are shown in Appendix A.

coefficient d_{15}^t .

It can be seen from Figs. 6.3 and 6.4 that the d_{15}^t has the opposite temperature dependences for BaTiO₃ and PbTiO₃. This different temperature dependence of the shear coefficients is directly related to *the presence* of the tetragonal-orthorhombic phase transition in BaTiO₃ and its *absence* in PbTiO₃. In the tetragonal phase the shear piezoelectric coefficients are proportional to the dielectric permittivities ε_{11}^t and ε_{22}^t along $[100]_c$ and $[010]_c$ axes (i.e., along directions perpendicular to the direction of the spontaneous polarization P_3) [62, 31, 32, 59]

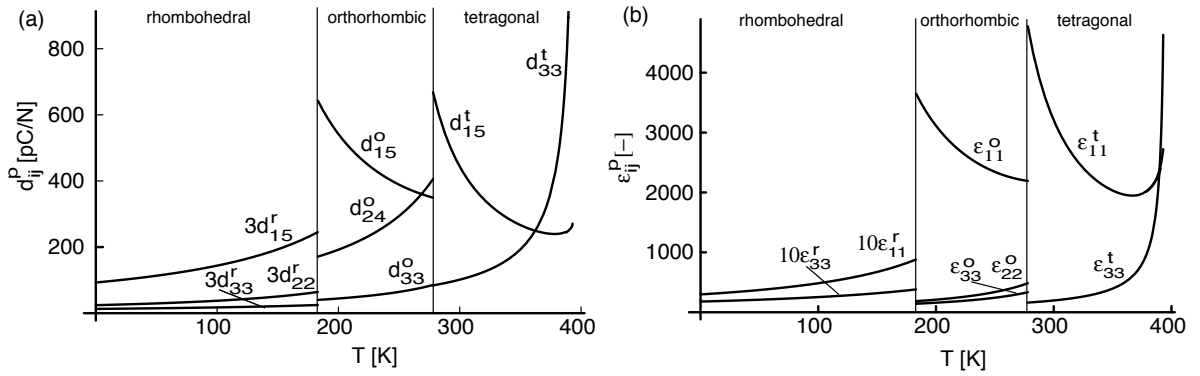


Figure 6.3: Calculated temperature dependence of (a) the longitudinal and shear piezoelectric coefficients, d_{ij}^p , and (b) the relative dielectric permittivities, ε_{ij}^p for BaTiO₃ in all three ferroelectric phases.

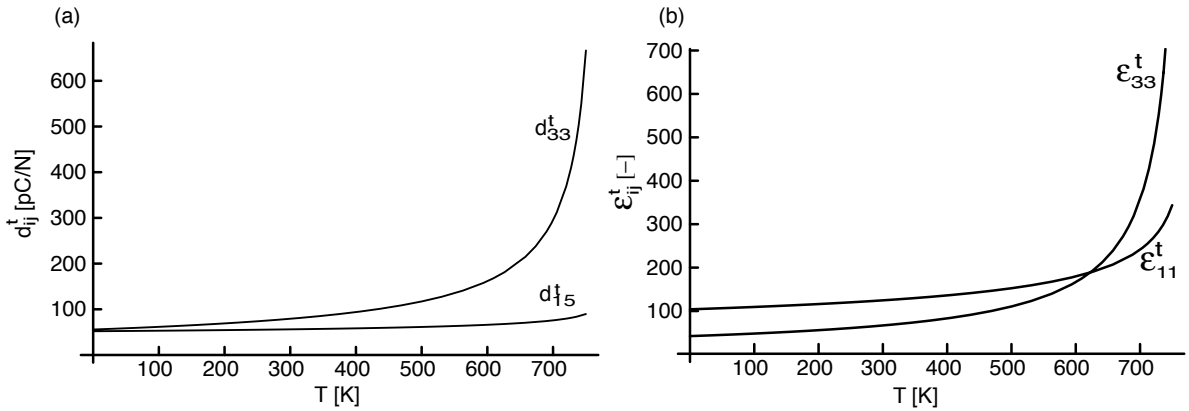


Figure 6.4: Calculated temperature dependence of (a) the longitudinal d_{33}^t and shear d_{15}^t piezoelectric coefficients and (b) the relative dielectric permittivities, ε_{ij}^t for PbTiO₃ in the tetragonal ferroelectric phases. The paraelectric - ferroelectric phase transition temperature is $T = 763\text{K}$.

$$d_{15}^t = d_{24}^t = \varepsilon_{11}^t Q_{44} P_3^t, \quad (6.2)$$

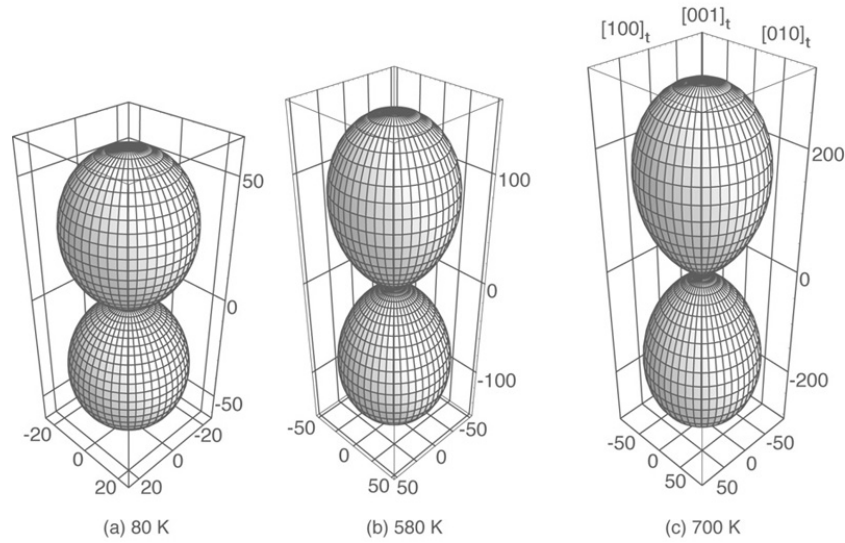


Figure 6.6: The orientation dependence of the d_{33}^{t*} coefficient of PbTiO_3 in the tetragonal ferroelectric phase (the only one) for three different temperatures. Note different scales as the temperature changes. The maximum d_{33}^{t*} occurs at $\theta_{max} = 0^\circ$ at all temperatures. The tetragonal cell axes $[hkl]_t$ are indicated in (c). The units of the numerical values marked on the axes are $[pC/N]$.

BaTiO_3 , deep in the tetragonal phase ($330K < T < 393K$), where d_{15}^t is relatively small with respect to d_{33}^t , the term containing d_{33}^t in Eq. (6.1) dominates. In this temperature range, the largest d_{33}^{t*} appears in both materials *along* the polar $[001]_t$ direction. As the temperature decreases towards the orthorhombic phase in barium titanate, this material will show a qualitative change of the d_{33}^{t*} . The shear term for BaTiO_3 , in Eq. (6.1), becomes dominant at temperatures sufficiently close to the orthorhombic phase, leading to a distortion of the d_{33}^{t*} surface - the maximum in d_{33}^{t*} develops along a direction *other* than $[001]_c$. For example, at $T = 279K$, the maximum $d_{33}^{t*} = 256pC/N$ is along direction determined by $\theta = 51.6^\circ$, while along the polar direction, $\theta = 0^\circ$, $d_{33}^{t*} = d_{33}^t = 84.7pC/N$. In PbTiO_3 , which does not exhibit an orthorhombic phase, the shear coefficient stays sufficiently small at all temperatures so that the d_{33}^{t*} surface *does not change qualitatively* with temperature; the direction of the maximum d_{33}^{t*} in PbTiO_3 remains along the axis of its spontaneous polarization at all temperatures, Fig. 6.6. Results for BaTiO_3 and PbTiO_3 are summarized in Fig. 6.7 which plots $d_{33}^{t*}(\theta)$ at selected temperatures.

One can understand intuitively why the shear coefficients in the tetragonal phase increase as the orthorhombic phase is approached on cooling by considering Fig. 6.8. A shear stress $\sigma_{13} \equiv \sigma_5$ (or $\sigma_{23} \equiv \sigma_4$) applied on a tetragonal $4mm$ material deforms the crystal and produces charges on (100) [or (010)] planes, i.e. *it rotates* the polarization

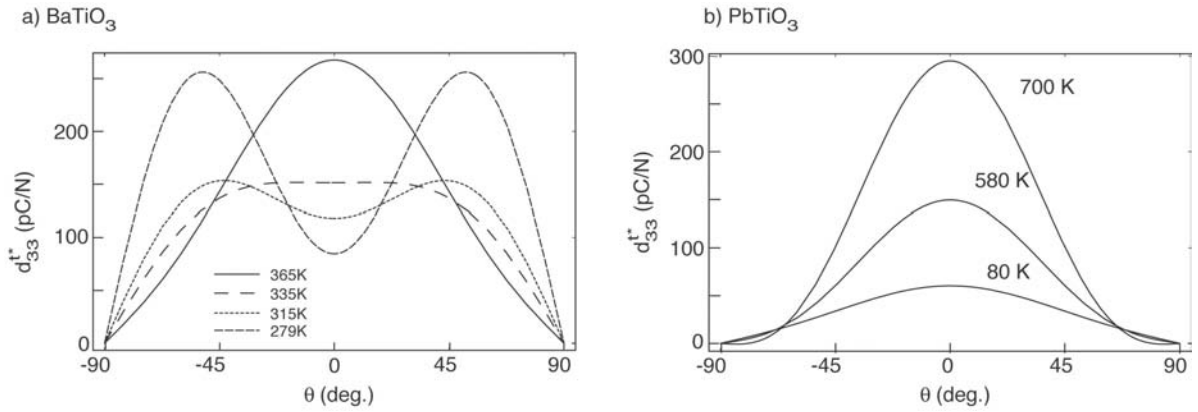


Figure 6.7: Orientation dependence of d_{33}^{t*} for (a) $BaTiO_3$ and (b) $PbTiO_3$ at selected temperatures.

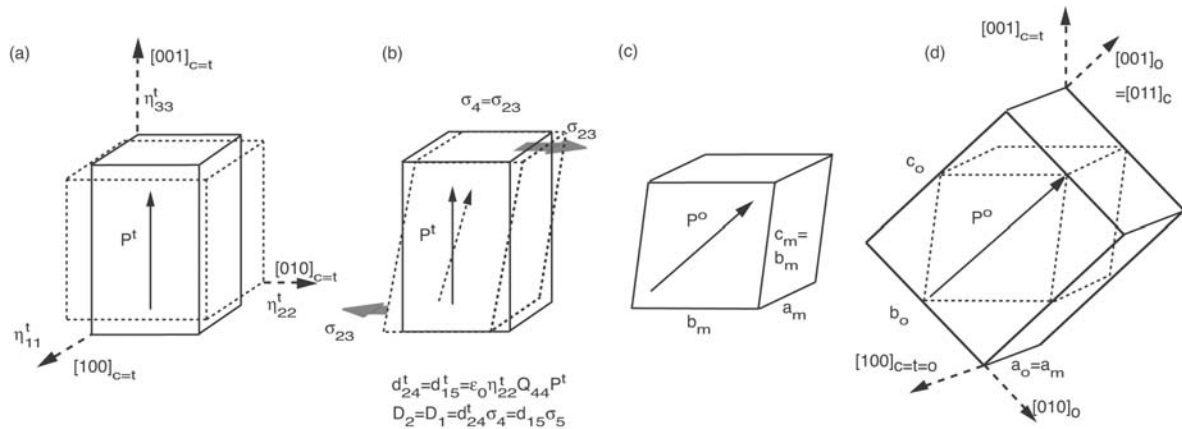


Figure 6.8: Effect of shear σ_{23} stress on the polarization rotation and crystal deformation in a tetragonal $4mm$ crystal and its relation to the orthorhombic distortion and polarization. (a) A tetragonal (solid lines) and a cubic (dotted lines) crystal; (b) The polarization rotation in the tetragonal unit cell under the shear stress. Deformation of the unit cell and polarization rotation are shown with dotted lines; (c) The pseudomonoclinic representation of the orthorhombic cell of $BaTiO_3$; (d) The orthorhombic cell (solid lines) and pseudomonoclinic cell (dotted lines). The crystallographic axes $[hkl]_p$ are indicated for each phase with dashed lines. Note that the choice of the a , b and c axes for the orthorhombic phase is arbitrary.

from $[001]_c$ polar axis toward $[100]_c$ (or $[010]_c$) axis. The polarization rotation is easier as the orthorhombic phase is approached because the material becomes increasingly dielectrically softer along $[010]_c$ and $[100]_c$ axes, anticipating the onset of the polarization along $[011]_c$ in the incipient orthorhombic phase, Fig. 6.3. This temperature behavior of the piezoelectric shear coefficient in the vicinity of a phase transition is analogous to the Curie-Weiss behavior of the permittivity in the cubic paraelectric phase, where crystal becomes dielectrically soft and permittivity increases as the ferroelectric phase is approached by decreasing the temperature. In fact, it is seen from Fig. 6.8 that the shear stress has *the same effect* on the tetragonal lattice deformation and change in polarization direction as the temperature-induced tetragonal \leftrightarrow orthorhombic phase transformation. On the other hand, at high temperatures, near the tetragonal \leftrightarrow cubic phase transition temperature, the piezoelectric properties are influenced by the incipient cubic phase that does not involve change in the polarization direction. In this region, the d_{33}^{t*} is dominated by the term containing d_{33}^t and the shear effect plays only a small role.

It is possible to derive a condition that piezoelectric coefficients must satisfy for a crystal to exhibit a maximum d_{33}^{t*} along a nonpolar direction [28]. In addition to Eq. (6.2), the piezoelectric coefficients d_{ij}^t can be written as

$$d_{33}^t = 2\varepsilon_{33}^t Q_{11} P_3^t, \quad (6.3)$$

$$d_{31}^t = 2\varepsilon_{33}^t Q_{12} P_3^t. \quad (6.4)$$

Equation (6.1) shows that the direction along which d_{33}^{t*} is the largest depends on d_{33}^t , d_{31}^t and d_{15}^t . The condition that these coefficients must satisfy in order that d_{33}^{t*} may have the maximum along a direction other than $[001]_c$ (i.e., $\theta_{max} \neq 0^\circ$) may be calculated by taking $\partial d_{33}^{t*}(\theta)/\partial\theta = 0$. One obtains:

$$\cos^2\theta_{max} = \frac{(d_{31}^t + d_{15}^t)}{3(d_{31}^t + d_{15}^t - d_{33}^t)} \quad (6.5)$$

For $\theta_{max} \neq 0^\circ$, it follows that

$$d_{15}^t + d_{31}^t > 3d_{33}^t/2. \quad (6.6)$$

Furthermore, since from Eqs. (6.2)-(6.4) one has that $d_{33}^t/d_{31}^t = Q_{11}/Q_{12}$, the above inequality may be rewritten as

$$d_{15}^t > d_{33}^t \left(\frac{3}{2} - \frac{Q_{12}}{Q_{11}} \right) \equiv d_{33}^t q. \quad (6.7)$$

This condition is *general* and valid for all perovskite crystals belonging to the point group $4mm$. Note that, by using Eqs.(6.3) and (6.4), this inequality can be expressed in

terms of permittivities ε_{11}^t and ε_{33}^t . Assuming that Q_{ij} are independent of temperature, q is constant. For the special case of BaTiO₃, one has

$$q = 1.9 \quad (6.8)$$

so that the d_{33}^* exhibits a maximum along a direction different from the polar axis ($\theta_{max} \neq 0^\circ$) whenever $d_{15}^t > 1.9d_{33}^t$. This result is supported by calculations of the dependence of the angle θ_{max} , at which d_{33}^* will have the maximum value, as a function of the d_{15}^t/d_{33}^t ratio (shown in Fig. 6.9). At temperatures below approximately 332K, where $d_{15}^t > 1.9d_{33}^t$, θ_{max} deviates from 0° . In this temperature region ($T \leq 332K$) the proximity of the orthorhombic phase transition temperature leads to a significant softening of the crystal along the pseudocubic $\langle 110 \rangle$ axes and to an increase in ε_{11}^t and, therefore, also to an increase in the shear d_{15}^t coefficient. Consequently, d_{15}^t/d_{33}^t ratio increases and reaches the critical value required to have $\theta_{max} \neq 0^\circ$.

Another condition which can be derived from Eq.(6.5) is that

$$\frac{1}{\sqrt{3}} < \cos\theta_{max} \leq 1, \quad (6.9)$$

i.e., $0 \leq \theta_{max} < 54.73^\circ$. Note that the case in which $\theta_{max} = 54.73^\circ$ (i.e., that $d_{33}^{t*}(\theta_{max})$ lies along the pseudocubic [111] axis) is possible only in the limit $d_{33}^t \rightarrow 0$. This condition is clearly seen in Fig. 6.9 where θ_{max} approaches 54.73° asymptotically. This analysis thus shows that in monodomain crystals belonging to the point group $4mm$, under zero external fields, the maximum d_{33}^{t*} *never* lies exactly along the pseudocubic [111] axis. This result is *in contrast* with the usual assumption that the highest response in tetragonal BaTiO₃ is along this direction [155]. In addition, the maximum d_{33}^{t*} as well as the angle at which maximum d_{33}^{t*} occurs, θ_{max} , are strongly temperature dependent. Implications of these results on PbTiO₃ are straightforward. In this material $q = 1.8$, but d_{15}^t is too small at all temperatures (see Fig. 6.4) and the condition in Eq. (6.7) is never fulfilled, in the absence of external bias fields (see *Chapter 8*). Ferroelectric PbTiO₃ thus exhibits the maximum d_{33}^{t*} *along the polar direction at all temperatures*.

Orthorhombic phase

In this phase, the temperature dependence of the piezoelectric coefficient d_{33}^* is more complex than in the tetragonal phase. Instead of two equal shear coefficients that exist in the tetragonal phase, $d_{15}^t = d_{24}^t$, that are related to the permittivities perpendicular to the spontaneous polarization axis, and that give the ∞m symmetry to the d_{33}^{t*} surface, the orthorhombic phase $mm2$ possesses two distinct shear coefficients, $d_{15}^o \neq d_{24}^o$. Their influence on the longitudinal piezoelectric coefficient is given by

$$d_{33}^{o*}(\theta, \phi) = \cos\theta[(d_{15}^o + d_{31}^o)\sin^2\theta\sin^2\phi + (d_{24}^o + d_{32}^o)\sin^2\theta\cos^2\phi + d_{33}^o\cos^2\theta]. \quad (6.10)$$

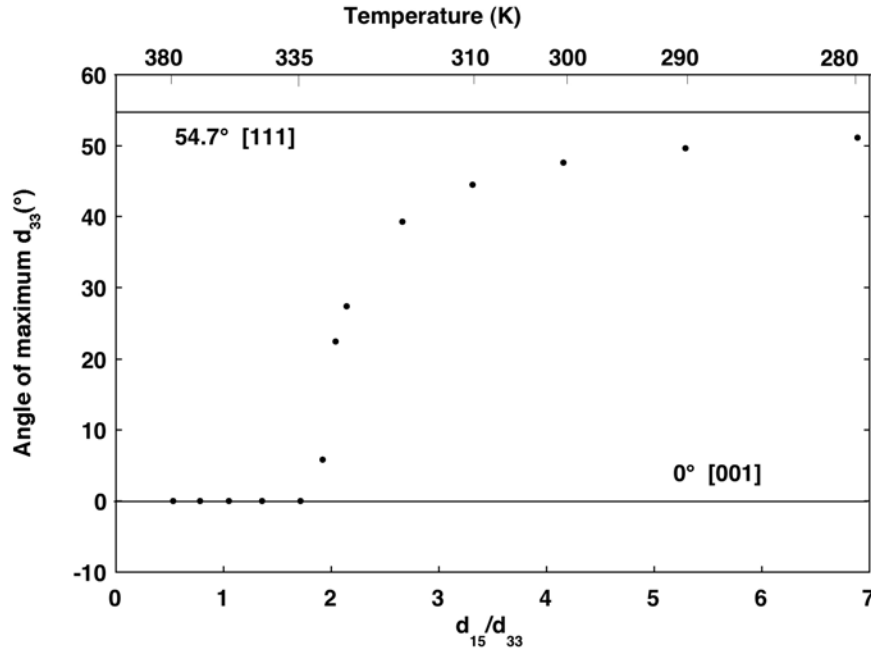


Figure 6.9: The angle θ_{max} indicating the direction along which the maximum d_{33}^* occurs as a function of the d_{15}^t/d_{33}^t ratio and temperature.

The calculated temperature dependencies of the d_{15}^o , d_{24}^o and d_{33}^o piezoelectric coefficients are shown in Fig. 6.3. One can see that the two shear coefficients have *qualitatively opposite* temperature dependences. Neglecting, for the sake of discussion only, comparatively small transverse coefficients, it can be seen that close to the orthorhombic \leftrightarrow tetragonal phase transition temperature, the coefficient d_{24}^o dominates the expression Eq. (6.10). On cooling, the d_{15}^o shear coefficient increases and becomes dominant near the temperature of the orthorhombic \leftrightarrow rhombohedral phase transition. The opposite influence of the two shear coefficients can be clearly observed in the three-dimensional plot of the d_{33}^{o*} , shown in Fig. 6.10. The direction of the maximum d_{33}^{o*} is rotated by 90° after the term containing d_{15}^o becomes the dominant term in expression (6.10). For example, at 193K , $d_{33max}^{o*} \approx 215.8\text{pC/N}$ and it lies along the direction defined by $\theta \approx 53^\circ$, $\phi \approx 90^\circ$, while at 273K $d_{33max}^{o*} \approx 176.5\text{pC/N}$ and it lies along the direction defined by $\theta \approx 49.9^\circ$ and $\phi = 0^\circ$. At approximately 250K , the d_{33}^{o*} surface is nearly symmetrical in the $[100]_o - [010]_o$ plane, indicating that terms containing $d_{15}^o + d_{31}^o$, and $d_{24}^o + d_{32}^o$ are comparable. For example, at 253K , $d_{33max}^{o*} \approx 141.3\text{pC/N}$ for $\theta \approx 49.6^\circ$ and $\phi = 0^\circ$ while for the same θ and $\phi = 90^\circ$, $d_{33max}^{o*} \approx 138.4\text{pC/N}$. As in the tetragonal phase, both the coefficient d_{33max}^{o*} and its direction are strongly temperature dependent. In order to gain a deeper insight of the origins of the temperature dependence of the

shear coefficients, one can analyze phenomenological expressions for these coefficients [59], expressed below in the crystallographic coordinate system

$$d_{15}^o = \varepsilon_{11}^o Q_{44} P_3^o, \quad (6.11)$$

$$d_{24}^o = 2\varepsilon_{22}^o (Q_{11} - Q_{12}) P_3^o. \quad (6.12)$$

It is seen from Fig. 6.3 that, during cooling from the orthorhombic↔tetragonal phase

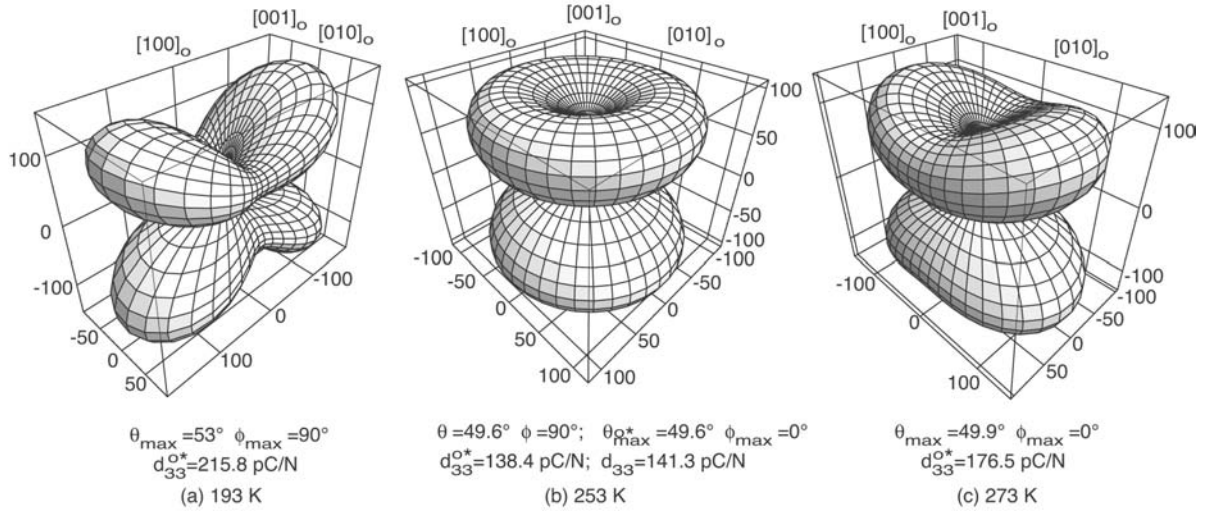


Figure 6.10: The orientation dependence of the d_{33}^{o*} coefficient of BaTiO_3 in the ferroelectric orthorhombic phase for three temperatures. Note different scales as the temperature changes. Angles θ_{\max} and ϕ_{\max} , at which maximum d_{33}^{o*} occurs, are indicated for each temperature. The $[hkl]_o$ axes of the orthorhombic cell are indicated in (c). The units of the numerical values marked on the axes are [pC/N].

transition temperature, the dielectric permittivity ε_{22}^o , and consequently d_{24}^o decrease, while the permittivity η_{11}^o , and accordingly d_{24}^o , increase, due to incipient transition into the rhombohedral phase.

As in the case of the tetragonal phase, one can intuitively understand the reasons for the temperature dependence of the shear piezoelectric coefficients by considering the sketches shown in Figs. 6.11 and 6.12. The $\sigma_4 \equiv \sigma_{23}$ shear stress rotates the polarization from the $[110]_c$ cubic ($[001]_o$ orthorhombic) axis towards the $[001]_c$ cubic/tetragonal axis, Fig. 6.11, and deforms the crystal in such a way that it becomes increasingly tetragonal-like. A very large shear σ_4 stress would have a similar effect on the crystal as the temperature induced orthorhombic↔tetragonal phase transformation. The electrical effect of the shear stress σ_4 is described by the shear piezoelectric coefficient d_{24} . It is thus reasonable to expect that d_{24} should increase when the crystal is heated in the

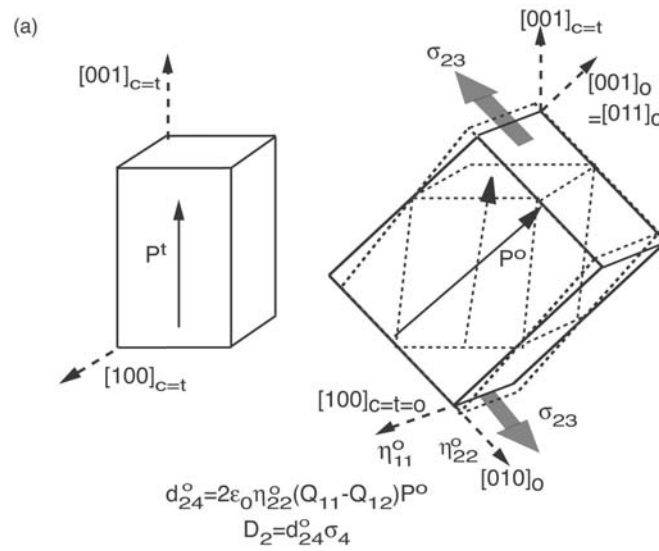


Figure 6.11: Effect of shear stresses on deformation and polarization rotation in an orthorhombic $mm2$ crystal and its relation to the distortion and polarization in neighboring tetragonal and rhombohedral phases. (a) Tetragonal and orthorhombic cells and corresponding polarizations are given by solid lines while the orthorhombic cell deformed by σ_{23} shear stress and polarization rotation are indicated by dotted lines.

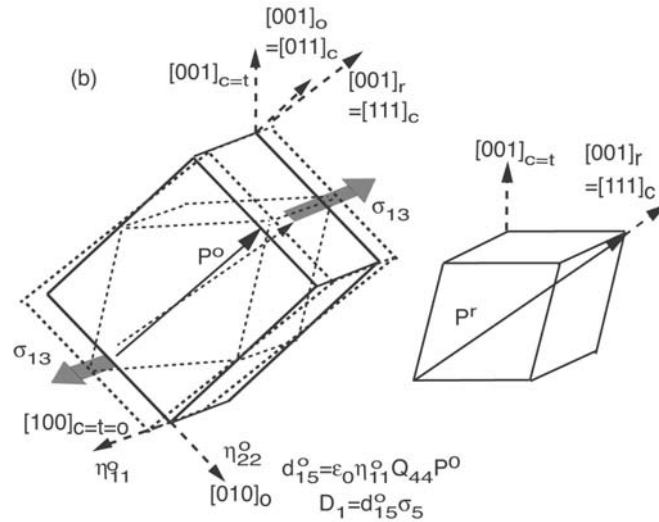


Figure 6.12: b) Orthorhombic and rhombohedral cells and corresponding polarizations are presented by solid lines while the orthorhombic cell deformed by σ_{13} shear stress and polarization rotation are given by dotted lines. Deformed pseudomonoclinic cell (dotted line) is shown within the orthorhombic cell (see Fig. 6). The crystallographic axes $[hkl]_p$ are indicated for each phase with dashed lines.

orthorhombic phase, anticipating the orthorhombic \leftrightarrow tetragonal phase transition. On the other hand, the $\sigma_5 \equiv \sigma_{13}$ shear stress rotates the polarization from the $[110]_c$ cubic ($[001]_o$ orthorhombic) axis towards $[111]_c$ cubic axis ($[001]_o$ rhombohedral axis) and deforms the lattice in such a way that it becomes rhombohedral-like, Fig.6.12. The σ_5 has a similar electro-mechanical effect on the crystal lattice as the temperature-induced orthorhombic \leftrightarrow rhombohedral phase transition. The electrical effect of the shear stress σ_5 is described by the shear piezoelectric coefficient d_{15}^o . As in the previous case, it is not surprising that d_{15}^o increases as the sample is cooled within orthorhombic region towards the rhombohedral phase. The competing effects of the d_{15}^o and d_{24}^o are clearly seen in Fig. 6.10 where three-dimensional surface of d_{33}^{o*} evolves with the temperature in a function of the proximity of the two crystal phases that surround the orthorhombic region.

Figure 6.13 summarizes the orientation dependence of the d_{33}^{o*} at selected temperatures. Note that d_{33}^{o*} exhibits its maximum at $\phi_{max} = 90^\circ$ for low temperatures and at $\phi_{max} = 0^\circ$ for high temperatures reflecting influences of the phase transitions into rhombohedral and tetragonal phases. In the intermediate temperature region, the orientation dependence of d_{33}^{o*} is similar to that in the tetragonal phase (compare Fig. 6.10b and Fig. 6.5b).

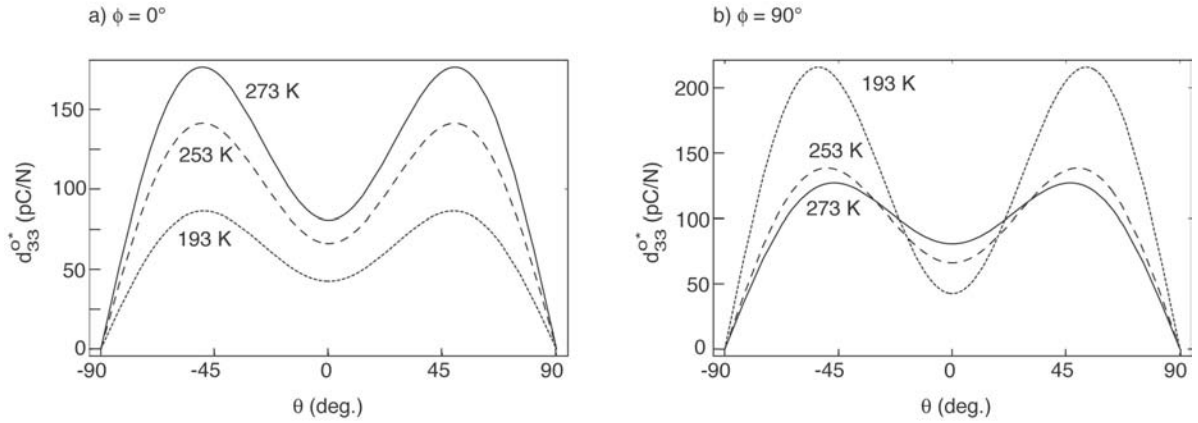


Figure 6.13: Orientation dependence of d_{33}^{o*} in $BaTiO_3$ at selected temperatures for $\phi_{max} = 0^\circ$ and $\phi_{max} = 90^\circ$. Note that at 253K d_{33}^{o*} has nearly the same value for both orientations.

Rhombohedral phase

Lastly, in the rhombohedral phase, d_{33}^{r*} is given by

$$d_{33}^{r*}(\theta, \phi) = d_{15}^r \cos\theta \sin^2\theta - d_{22}^r \sin^3\theta \cos 3\phi + d_{31}^r \sin^2\theta \cos\theta + d_{33}^r \cos^3\theta. \quad (6.13)$$

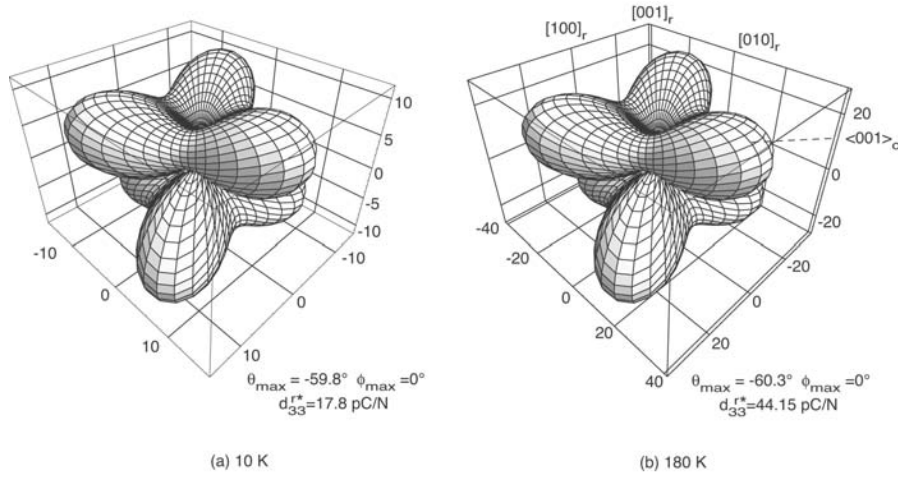


Figure 6.14: The orientation dependence of the d_{33}^{r*} coefficient of BaTiO_3 in the rhombohedral phase for two temperatures. Note different scales as the temperature changes. The maximum d_{33}^{r*} occurs at and $\theta_{\max} \approx 60^\circ$ and ϕ_{\max} and this direction changes little with the temperature. The $[hkl]_r$ axes of the rhombohedral cell are indicated in (c). The units of the numerical values marked on the axes are (pC/N).

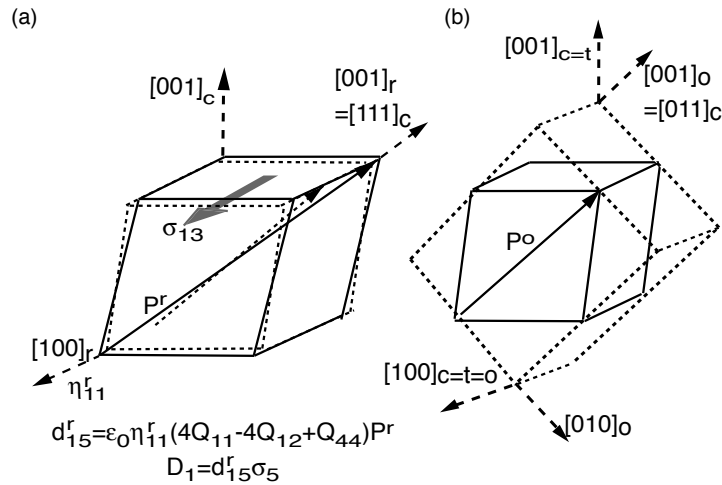


Figure 6.15: Effect of $\sigma_{13} = \sigma_5$ shear stress on deformation and polarization rotation of a rhombohedral $3m$ crystal and its relation to the distortion and polarization in the orthorhombic phase. (a) The rhombohedral cell and its polarization are presented by solid lines while the rhombohedral cell deformed by the σ_{13} shear stress and the rotated polarization are indicated by dotted lines; (b) The pseudomonoclinic cell and its polarization (solid lines) and orthorhombic cell (dotted lines). The crystallographic axes $[hkl]_p$ are indicated for each phase by dashed lines.

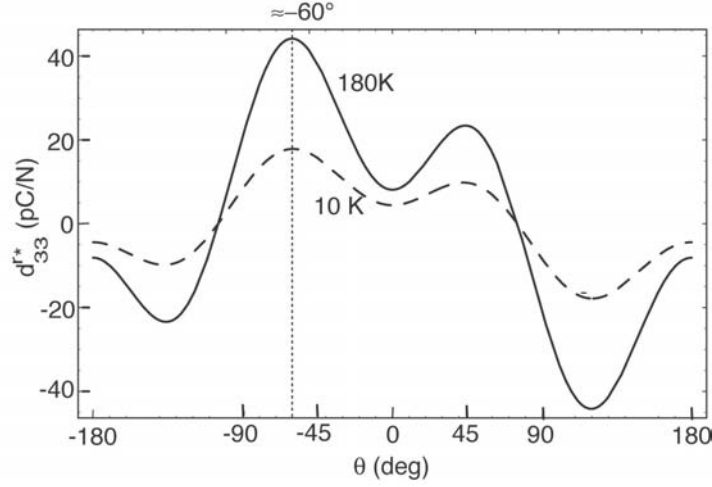


Figure 6.16: Orientation dependence of d_{33}^{r*} in BaTiO_3 at selected temperatures.

In contrast to the tetragonal and orthorhombic phases, the three – dimensional surface representation of d_{33}^{r*} does not qualitatively change with the temperature, Fig. 6.14. The d_{15}^r remains approximately two times larger than d_{33}^r throughout the temperature range of the rhombohedral phase, Fig. 6.3. The direction of the maximum value of d_{33}^{r*} changes with temperature inside a small interval of the Euler angle θ . At 180K the maximum $d_{33}^{r*} \approx 44.1 \text{ pC/N}$ lies along the direction defined by $\theta \approx -60.3^\circ$ and $\phi = 0^\circ$, while at 10K the maximum $d_{33}^{r*} \approx 17.8 \text{ pC/N}$ is at $\theta \approx -59.8^\circ$ and $\phi = 0^\circ$. It should be noted that these θ angles are higher than $\theta = -54.73^\circ$ which corresponds to the $[001]_c$ (or $[111]_r$) direction, often quoted in the literature as the angle along which the maximum d_{33}^{r*} lies. The rhombohedral phase is the most stable one as it does not transform to another lower-symmetry phase as the temperature is reduced towards 0K. There is no longer an increase of the dielectric susceptibility perpendicular to the direction of the spontaneous polarization with decreasing temperature, and no more corresponding increase of the shear coefficient, which is related to the susceptibility by:

$$d_{15}^r = \frac{1}{3}(4Q_{11} - 4Q_{12} + Q_{44})\varepsilon_{11}^r P_3^r. \quad (6.14)$$

The shape of the d_{33}^{r*} surface, determined by the rhombohedral \leftrightarrow orthorhombic phase transition, remains therefore unchanged as the crystal response gradually freezes during cooling towards 0K.

In analogy to the behavior of the shear piezoelectric coefficients in the tetragonal and orthorhombic phases, the coefficient d_{15}^r increases with temperature as the rhombohedral \leftrightarrow orthorhombic phase transition is approached on heating. As in the previous cases, this can be understood from Fig. 6.15. Under the action of the $\sigma_5 \equiv \sigma_{13}$ shear stress,

the rhombohedral cell deforms and its polarization rotates in such a way that the cell becomes orthorhombic-like. This electrical effect of the σ_5 shear stress is presented by the d_{15}^r coefficient, which increases with increasing temperature anticipating the transition into the orthorhombic phase. Finally, Fig. B.7 gives a summary of the d_{33}^{r*} orientation dependence at two temperatures. The angular dependence changes only quantitatively, in agreement with the absence of a low temperature phase with a lower symmetry.

6.2 Monodomain versus polydomain piezoelectric response of a relaxor ferroelectric single crystal along nonpolar directions

As a side effect of the work on investigating the origins of the piezoelectric anisotropy, analytical tools and way of reasoning from this chapter can be now used to discuss another problem of practical significance.

The domain configurations in the ferroelectric materials can strongly influence their properties³. Therefore, one of the most interesting questions related to applications is the control of the desirable domain configuration - so called *domain engineering*. There are several domain engineering techniques (an example is controlling of the pinning level of domain walls in ferroelectrics by introducing impurities - "hardening" and "softening" of ferroelectrics). Among these approaches, the one based on the crystallographic anisotropy of the ferroelectric single crystals is known as *engineered domain configuration*.

A discussion about the difference between the piezoelectric responses of a perovskite in the *monodomain* and in the *engineered domain configuration* is presented here. The material suitable for the discussion is a relaxor ferroelectric solid solution PMN-PT (rhombohedral $0.67\text{Pb}(\text{Mg}_{1/3}\text{Nb}_{2/3})\text{O}_3-0.33\text{PbTiO}_3$).

When a crystal is poled along a nonpolar direction the resulting crystal state is necessarily multidomain, as shown schematically in Fig. 6.17 for rhombohedral symmetry. The multidomain structure created by poling a crystal along a nonpolar direction is called an *engineered domain state* [118] and its role on the large piezoelectric response has been discussed by many authors [155, 119, 123, 169, 99]. *Park* and *Shrout* [118] determined that the optimal angle (i.e., the cut which gives the large piezoelectric response and smallest strain hysteresis) in rhombohedral compositions is inclined by 54.7° with respect to the polar axis of the rhombohedral crystallographic system, i.e. it lies

³A review of publications concerning this problem for a particular case of potassium niobate is given in *Chapter 3*.

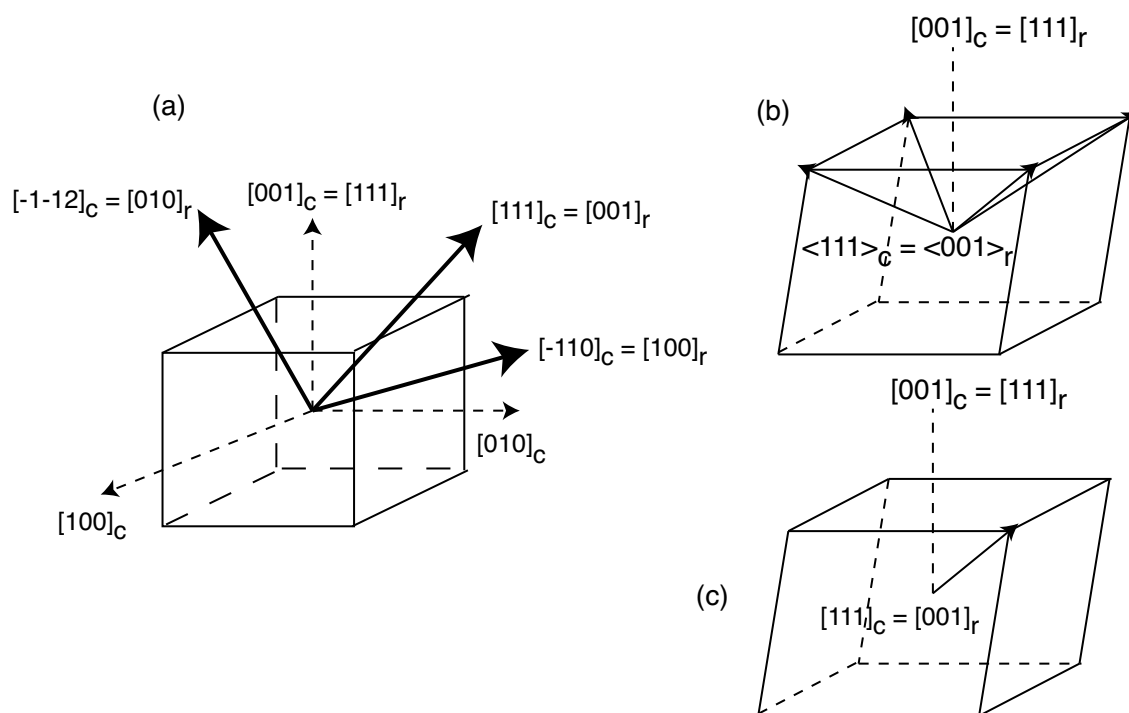


Figure 6.17: (a) Relation between coordinate systems of the crystals with rhombohedral (solid lines) and cubic (dashed lines) prototypic symmetries. Subscripts r and c denote directions with respect to the rhombohedral and cubic coordinate systems, respectively. (b) Multidomain rhombohedral crystal obtained by poling along the $[001]_c$ axis. The arrows show possible directions of the polarization vector in a fully poled crystal. The resulting domain structure is called the engineered domain configuration. (c) Monodomain rhombohedral crystal poled along the $[111]_c$ axis. Ideally, only one domain, whose direction is indicated by the arrow, should be present.

along the $\langle 001 \rangle_c$ axes of the prototypic cubic symmetry. Poling of the crystal along one of the $\langle 001 \rangle_c$ axes leads to the special domain configuration illustrated in Fig. 6.17. In addition to rhombohedral materials, an enhanced piezoelectric response along nonpolar directions has been observed in complex perovskites with monoclinic [123] symmetry and, albeit to a lesser extent, in the orthorhombic [119, 111] and tetragonal [155] phases of simple perovskites such as BaTiO_3 and KNbO_3 .

Wada et al. [152, 150], and *Nakamura et al.* [110] were the first to point out that in tetragonal BaTiO_3 and orthorhombic KNbO_3 , respectively, the special multidomain state is not necessary to obtain an enhanced piezoelectric response along a nonpolar direction. They obtained comparable enhancement of piezoelectric properties along the same nonpolar direction in monodomain crystals and in crystals with special “engineered” multidomain configurations. The enhanced piezoelectric effect in BaTiO_3 and KNbO_3 along a nonpolar direction is therefore due to crystal lattice properties, i.e. crystal anisotropy and large shear piezoelectric coefficients [110, 28] but not to a special domain configuration.

The domain state created by poling a crystal along a nonpolar direction can, in general, contribute to the piezoelectric response if an external electric field moves non-180° domain walls and if this displacement changes the shape of the crystal. Ideally, this should not be the case for the most commonly used “engineered” domain configuration, illustrated for a rhombohedral crystal in Fig. 6.17b. In the pseudocubic symmetry, the four $\langle 111 \rangle_c$ domain states are equivalent and application of a field along the cubic $[001]_c$ direction should not move the domain walls [155, 35, 34]. Experimental support for this conjecture is shown by the small piezoelectric strain hysteresis [110] and small nonlinearity [140] for rhombohedral crystals with this special domain structure. It is, however, possible that mechanisms other than domain walls displacement might contribute to the piezoelectric response in a crystal with “engineered domain structure”. For example, besides the presence of domain states that are not equivalent with respect to the driving field direction, the domain structure of a poled crystal may be accompanied by internal stresses [122] and electric fields, and poling field along a nonpolar direction may locally induce different crystal phases in the crystal [99], all of which could affect the piezoelectric properties.

To experimentally verify how much a polydomain or an “engineered domain state” contributes to the piezoelectric response it is necessary to compare piezoelectric properties along the same crystallographic direction of both poled monodomain and multidomain crystals, as was done by *Nakamura et al.* [110] for BaTiO_3 and KNbO_3 . Difficulties in obtaining monodomain crystals made, until recently, such comparison impossible for complex perovskites. Recently, *Renault et al.* [122] investigated multidomain and quasi-

monodomain 0.91PZN-0.09PT monoclinic crystals and suggested that the longitudinal piezoelectric coefficient of a crystal with such an “engineered domain state” is more than two times higher than that of a monodomain crystal measured along the same nonpolar direction. The authors suggested that the difference is due to internal shear strains associated with the multidomain state. If confirmed, this result would indicate an important difference in piezoelectric behavior between simple and complex perovskites. Elucidating the contribution of the multidomain or “engineered domain state” is thus of a crucial importance for understanding the origins of the giant piezoelectric properties in complex relaxor ferroelectrics.

Zhang et al. [169, 170] have recently published a complete set of materials coefficients for 0.67PMN-0.33PT crystals with a rhombohedral $3m$ structure. Using different techniques they derived all elastic, dielectric and piezoelectric coefficients of crystals with multidomain “engineered domain states” and of monodomain crystals with respect to the rhombohedral crystallographic coordinate system. In this section we use the data of *Zhang et al.* [170] to calculate the orientation dependence of the longitudinal and transverse piezoelectric coefficients of monodomain 0.67PMN-0.33PT crystals. The calculated values are then compared with experimentally-determined coefficients for multidomain crystals along a given direction. Results of these calculations give direct information on contribution of the multidomain state to the large piezoelectric effect in 0.67PMN-0.33PT crystals.

Fig. 6.17a shows the relationship between the coordinate axes of the prototypic cubic

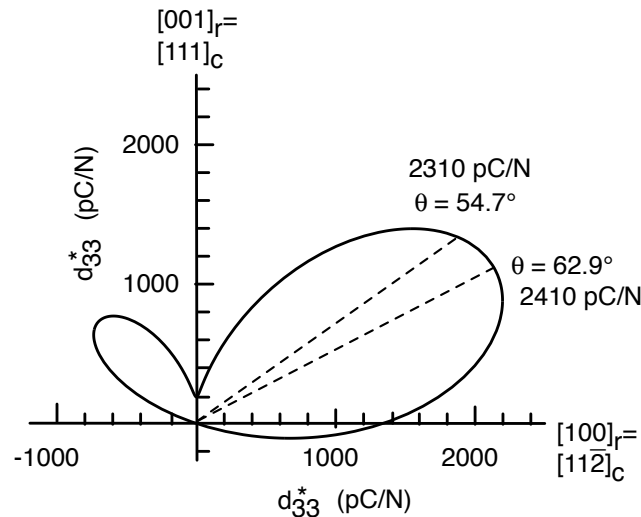


Figure 6.18: Orientation dependence of the d_{33}^* piezoelectric coefficient of a 0.67PMN-0.33PT single domain crystal in the plane determined by $[111]_c = [001]_r$ and $[100]_r = [11-2]_c$. Only a half of the plane is shown.

and rhombohedral coordinate systems, as defined by *Zhang et al* [169, 170]. $[hkk]_c$ and $[hkk]_r$ denote crystal directions with respect to the cubic and rhombohedral coordinate systems, respectively. Directions of polarization vectors in a multidomain crystal obtained by poling along the $[001]_c$ axis (the “engineered domain state”) are shown in Fig. 6.17b; the polarization vector in a monodomain crystal obtained by poling along the $[111]_c$ axis is shown in Fig. 6.17c. Values of the piezoelectric coefficients d_{ij}^* along an arbitrary direction in a monodomain crystal can be expressed in terms of the coefficients d_{ij} measured along principal crystallographic axes and Euler angles (ϕ, θ, ψ) [48]. For the d_{33}^* coefficient, one uses Eq. (6.13).

For d_{ij} we take the values determined by *Zhang et al*⁴ [170]. The expression for d_{31}^* depends on all three Euler angles and is not shown. Fig. 6.18 shows $d_{33}^*(\phi = 0^\circ, \theta)$ is obtained for $\theta \approx 62.9^\circ$ and its value is $\approx 2410pC/N$. At $\phi = 0^\circ$ and $\theta = 54.73^\circ$ (response measured along $[001]_c$) $d_{33}^* \approx 2310pC/N$. In a multidomain crystal with an engineered domain state, which is obtained by poling a crystal along the $[001]_c$ axis, the equivalent piezoelectric coefficient d_{33}^{*multi} measured along the same direction is between 2500 (Ref. [170]) and 2800pC/N [169]. These values are about 8% – 20% higher than those for a monodomain crystal. Thus, the contribution of the special engineered domain state amounts to at most 20% of the d_{33}^{*multi} value in a multidomain crystal. In other words, at least 80% of the piezoelectric response of a multidomain crystals poled along the $[001]_c$ axis originates from intrinsic lattice effects. A similar result is obtained for the transverse d_{31}^* coefficient. Its value in a monodomain crystal, $d_{31}^*(\phi = 0^\circ, \theta = 54.73^\circ, \psi) \approx -1150pC/N$, is only 13% lower than the experimentally determined value for a multidomain crystal [170], $d_{31}^{*multi} = -1300pC/N$, measured along the same direction. An exceptionally large value for the transverse coefficient, $d_{31}^* = -1922pC/N$, is predicted along several directions within the monodomain crystal, e.g., $\phi = 0^\circ, \theta = 130^\circ, \psi = 90^\circ$, and $\phi = 60^\circ, \theta = 50^\circ, \psi = 90^\circ$, as shown in Fig. 6.19.

It should be pointed out that the values of materials coefficients given by *Zhang et al* [169, 170] are partly directly measured and partly calculated from other experimental data using the constitutive equations. This introduces certain errors in the values of the coefficients. In addition, since the monodomain state of 0.67PMN-0.33PT is unstable, all measurements on monodomain crystals were made under the application of a dc bias field of about 2 kV/cm on the samples, whereas measurements on multidomain crystals were made on poled crystals under zero bias field. The effect of this bias field has not been taken into account in the present calculations. Additional source of discrepancy in values of piezoelectric coefficients may be small variations in crystal composition, quality

⁴ $d_{33} = 190pC/N, d_{31} = -90pC/N, d_{22} = 1340pC/N, d_{15} = 4100pC/N$

and orientation between the different crystals used by Zhang et al. for the coefficients determination.

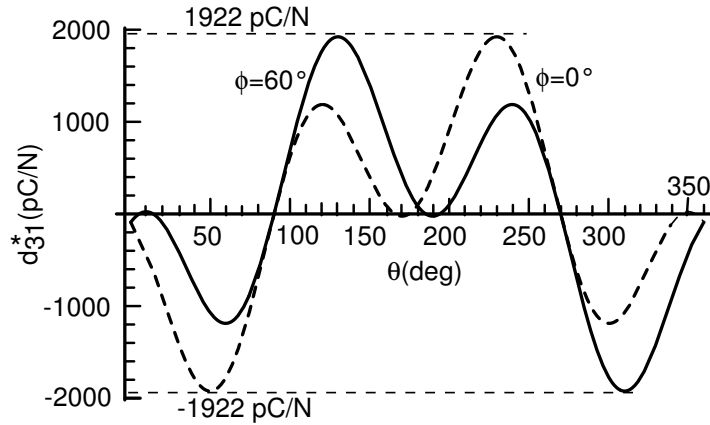


Figure 6.19: Orientation dependence of the d_{31}^* piezoelectric coefficient of a 0.67PMN-0.33PT monodomain crystal as a function of angle θ for different values of ϕ and $\psi = 90^\circ$.

6.3 Conclusions

The main results presented in this chapter deal with the effects of *temperature-induced phase transitions* on the *piezoelectric anisotropy* in perovskite materials. The LGD relations clearly show how *dielectric softening* of the material along directions perpendicular to the polarization axis, taking place in the vicinity of a phase transition, leads to *large shear piezoelectric coefficients* and, consequently, to *enhanced d_{33}^{D*}* along nonpolar directions. It is useful to note that the change of polarization direction, i.e. the dielectric softening, required for the d_{33}^{D*} to exhibit a maximum along a nonpolar direction, is an incipient process. One can use analogy with the Curie-Weiss law, where a ferroelectric material becomes dielectrically soft tens of degrees before the transition from the paraelectric to ferroelectric phase actually occurs.

The presented results can be generalized to include other processes involving a change in the polarization direction. For example, it has been observed experimentally [52, 140] that the largest longitudinal piezoelectric response in $\text{Pb}(\text{Zr},\text{Ti})\text{O}_3$ (PZT) compositions near the morphotropic phase boundary (MPB) occurs along non-polar directions. It is well known that composition variation of PZT in a vicinity of the MPB is accompanied by phase transitions [79, 115]. As shown in the literature [77], the dielectric susceptibility in a direction perpendicular to the direction of the spontaneous polarization diverges as a function of composition at the MPB. This divergence of the susceptibility leads to

large shear piezoelectric coefficients and consequently to the large d_{33}^{p*} along non-polar axes. Another example can be deduced from the results of first-principle calculations [10], which indicate that the application of a strong electric field on PZT may lead to exceptionally large shear piezoelectric coefficients in the vicinity of the field-induced phase transitions. Clearly, the field driven phase transitions and associated enhancement of the shear coefficients may have the similar effect on the piezoelectric anisotropy as composition and temperature variation.

In situations when the largest d_{33}^{p*} is observed along a nonpolar axis, two questions become interesting from the both practical and fundamental point of view.

1. The first is related to *the direction along which d_{33}^{p*} is maximal*. In the literature dealing with perovskite crystals, this direction is almost invariably assigned to $\langle 001 \rangle$ and $\langle 111 \rangle$ pseudocubic directions for, respectively, rhombohedral [118] and tetragonal [155] phases. The results obtained here clearly show that the direction of maximum d_{33}^{p*} is a strong function of temperature in orthorhombic and tetragonal phases and that this dependence is related to the proximity of a phase transition temperature. In the rhombohedral phase this direction deviates by several degrees from $\langle 001 \rangle$ pseudocubic axes both in simple and complex perovskites (present results and Ref. [170]). However, it must be mentioned that, from the practical point of view, the direction of the optimal piezoelectric response in a poled multidomain rhombohedral crystal appears to be along $\langle 001 \rangle$ pseudocubic axes. Besides exhibiting a large d_{33}^{p*} , this direction also possesses a stable domain wall configuration and a small strain-electric field hysteresis [118].
2. The second question is related to the fact that poling of a crystal along a nonpolar direction results in a multidomain state [118]. The question is then raised *whether the presence of the multidomain state contributes to the piezoelectric response*. Our results based on available experimental data, show that the values of d_{33}^* and d_{31}^* coefficients in $[001]_c$ oriented monodomain crystal are lower by $< 20\%$ and 13% , respectively, than the corresponding values in multidomain crystals oriented and poled along this same $[001]_c$ axis. This result demonstrates that, the multidomain configuration contributes relatively little to the piezoelectric response of 0.67PMN-0.33PT single crystals - it appears that the dominant contribution to the large piezoelectric response *in this composition* are intrinsic lattice effects (such as the large shear piezoelectric coefficients). In this respect, behavior of 0.67PMN-0.33PT crystals may be qualitatively similar to those of BaTiO₃ and KNbO₃, even though the size of the coefficients in the relaxor-ferroelectric is an order of magnitude higher, if the domain structure in classic perovskites is not very dense, in which case the piezoelectric response is greatly enhanced with this

dense domain structure, as shown by *Wada et al* [156]. However, the results from this chapter and recent studies [170, 110] seem to indicate that, *at least in some* complex relaxor-ferroelectrics compositions and in simple perovskites poled along special directions, giving a mechanically equivalent set of domain walls, the enhanced d_{33}^{p*} is dominated by the response of the single domain. However, when poling is made along a direction which does not lead to a mechanically equivalent set of domain walls, one may expect strong contribution to the from the domain wall displacement.

Briefly, it can be said that the existence of *a sequence* of phase transitions in ferroelectric perovskites implies the significant change in the direction of the maximal value of the longitudinal piezoelectric coefficient, no matter whether these phase transitions are induced by temperature, composition variation or by an electric field. The dielectric softening becomes pronounced as the phase transition temperature, composition or field are approached. In some examples of tetragonal materials, such as PbTiO_3 under the temperature change, this effect is absent and d_{33}^{p*} remains maximal along the polar axis over the whole ferroelectric region, because this material does not undergo a phase transition sequence. This behavior can be changed by application of electric fields and stresses.

This subject considering the piezoelectric anisotropy and enhancement of the piezoelectric response is extended further in *Chapter 8*, where the discussion is based on the treatment of the free energy.

It is shown in this chapter that the direction of the maximum longitudinal piezoelectric response is a strong function of temperature in orthorhombic and tetragonal ferroelectric phases of barium titanate, but not in the tetragonal phase of lead titanate, and that the temperature dependence of the anisotropy is related to the proximity of a phase transition temperature. It is also indicated and shown by calculations that at least in some complex relaxor ferroelectrics compositions and in simple perovskites poled along special directions giving mechanically equivalent set of domains, the enhanced longitudinal piezoelectric response is dominated by the response of the single domain.

Chapter 7

Enhancement of the piezoelectric response in perovskites by external bias fields

Having discussed the influence of intrinsic system parameters to the piezoelectric response and its anisotropy in the previous chapter, one can now make a step further by including external bias fields (electric and mechanic) as new parameters in the same problem. Here we discuss different classic perovskite systems for different configurations of electric and mechanic bias fields. Some special configurations reveal very interesting results, possibly with broad implications.

A discussion of influences of temperature and existence of ferroelectric phase transitions in perovskites on their piezoelectric properties has been presented in the previous chapter. The next step is a discussion about the question of possible influence of *bias fields* on piezoelectric properties and the piezoelectric anisotropy in perovskites. What happens with the electromechanical properties of a perovskite system if one applies a bias electric field, or a mechanical stress is discussed in detail by using the phenomenological approach and classic perovskites as examples.

7.1 Electric bias field

To discuss the influence of the bias electric field on electromechanical properties of perovskites, we start by considering the tetragonal phase of monodomain BaTiO₃ single crystal under an electric bias field applied either along the polar axis [001]_c or anti-parallel to it, i.e. along the [00 $\bar{1}$]_c direction. Although it is rather counterintuitive, it is this latter field orientation that leads to the most interesting results.

For the tetragonal phase the Gibbs free energy expanded up to the sixth power of polarization is given by

$$\Delta G = \alpha_1 P_3^2 + \alpha_{11} P_3^4 + \alpha_{111} P_3^6 - E_3 P_3, \quad (7.1)$$

where E_3 and P_3 are the applied electric bias field and the polarization along the [001]_c axis. If the field is applied along the [00 $\bar{1}$]_c direction, the value of E_3 is negative, by definition [4]. The stability condition, Eq. (5.11), defines the relation between the applied electric field and the overall polarization in the material,

$$E_3 = 2\alpha_1 P_3 + 4\alpha_{11} P_3^3 + 6\alpha_{111} P_3^5. \quad (7.2)$$

This equation can be used for implicit numerical calculation of the field dependence of polarization P_3 within the temperature and field range where the tetragonal phase is stable. The results for selected temperatures are shown in Fig.7.1 in form of familiar

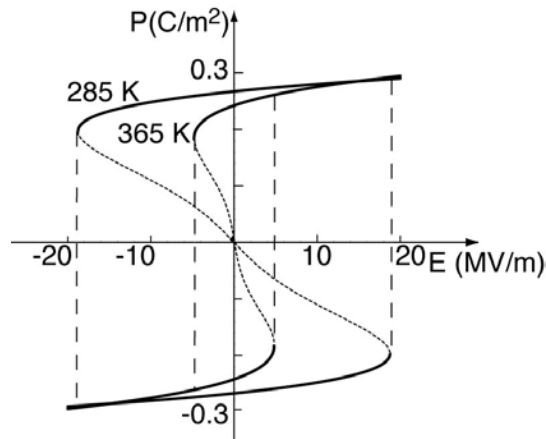


Figure 7.1: Dependence of polarization on electric field in BaTiO₃ at two temperatures. Vertical dashed lines indicate coercive field, while dashed curves indicate nonphysical solutions of thermodynamic $P(E_3)$ relation.

hysteresis loops. The values of temperature dependent coefficients α are taken from literature [7]. The polarization decreases with decreasing electric bias field until it switches

direction at coercive field. This thermodynamic coercive field increases with the lowering of the temperature.

The field dependence of the dielectric permittivity can be calculated numerically from $E_3(P_3)$ and Eqs. (5.9) and (5.10), and, the longitudinal, transverse, and shear piezoelectric coefficients in the crystallographic coordinate system are given, respectively, by

$$d_{33} = 2\varepsilon_{33}(E_3)Q_{11}P_3(E_3), \quad (7.3)$$

$$d_{31} = 2\varepsilon_{33}(E_3)Q_{12}P_3(E_3), \quad (7.4)$$

and

$$d_{15} = \varepsilon_{11}(E_3)Q_{44}P_3(E_3). \quad (7.5)$$

The analytical form of the longitudinal piezoelectric response along a general direction, $d_{33}^*(\theta)$, is given in Eq. (6.1), where the θ is the angle between the weak measuring field (not the bias field E_3) and polar axis $[001]_c$. The calculated orientation dependence of $d_{33}^*(\theta)$ is shown in Fig. 7.2 for different bias fields at $T = 285K$. This temperature

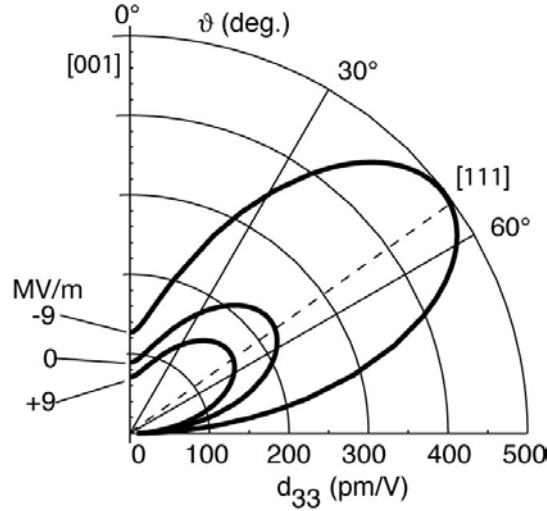


Figure 7.2: Orientation dependence of the longitudinal piezoelectric coefficient, $d_{33}^*(\theta)$, in $BaTiO_3$ at $285K$ and for three values of bias field E_3 . Note that from Eq. (6.1) $d_{33}^*(\theta) = d_{33}^*(-\theta)$.

is about $7K$ higher than the tetragonal \leftrightarrow orthorhombic phase transition temperature at zero bias field. The $d_{33}^*(\theta)$ exhibits its maximum value for all bias fields at approximately $\theta \approx 50^\circ$, i.e. close to $[111]_c$ axis. This agrees well with experimental data [118] for $E_3 = 0$. The value of $d_{33}^*(\theta_{max})$ depends strongly on the bias field. For $E_3 = 0$, $d_{33}^*(\theta_{max}) = 227pm/V$. While positive bias fields decrease $d_{33}^*(\theta_{max})$, calculations predict

that negative bias fields (anti-parallel to polarization) strongly *enhance* the piezoelectric coefficient. A field of $-9MV/m$ (applied along $[00\bar{1}]_c$) increases $d_{33}^*(\theta_{max})$ to $497pm/V$, which represents more than a five fold increases with respect to zero bias value along the polar axis ($d_{33}^*(\theta = 0^\circ) = d_{33} = 89pm/V$), and more than two fold increase with respect to the maximum value measured approximately along $[111]_c$ axis at $E_3 = 0$ [$d_{33}^*(\theta = 50^\circ) = 227pm/V$].

Interesting results are also observed at higher temperatures, closer to the tetragonal-cubic phase transition temperature that occurs at $393K$. At these temperatures the condition for having a maximum in $d_{33}^*(\theta_{max})$ along a non-polar direction is not fulfilled¹ [28] and the piezoelectric response exhibits maximum value along the polar axis. The positive bias field decreases the piezoelectric coefficient, similarly to what has been reported in ferroelectric thin films [23], while the negative field enhances the piezoelectric response, Fig. 7.3. At $E_3 = -4MV/m$ and at $365K$, the maximum $d_{33}^*(\theta = 0)$ is

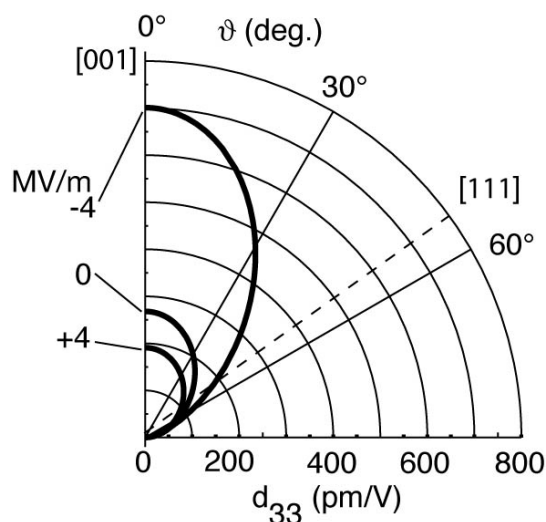


Figure 7.3: Orientation dependence of the longitudinal piezoelectric coefficient, $d_{33}^*(\theta)$, in $BaTiO_3$ at $365K$ and for three values of bias field E_3 . Note that from Eq. (6.1) $d_{33}^*(\theta) = d_{33}^*(-\theta)$.

$700pm/V$, compared to $268pm/V$ at $E_3 = 0$.

The above results can be understood by analyzing Eqs. (7.3)-(7.5) and the field dependences of susceptibilities and piezoelectric coefficients, shown in Fig. 7.4. Except at very high temperatures, the transverse coefficient d_{31} is small and can be ignored in the discussion for the sake of simplicity. Let us first consider behavior at temperatures close to the tetragonal-orthorhombic phase transition, depicted in Fig. 7.2. The negative bias

¹Discussed in Chapter 6

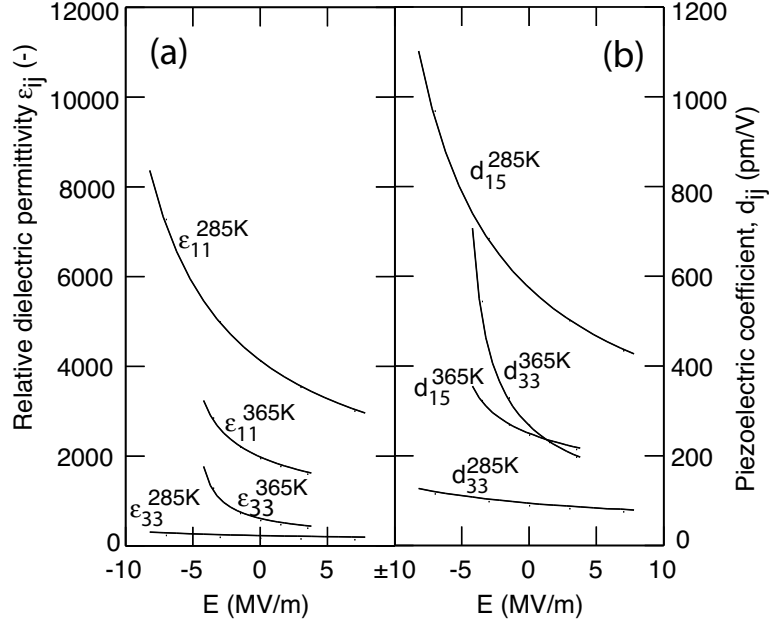


Figure 7.4: (a) Relative dielectric permittivities, ϵ_{11} and ϵ_{33} , and (b) piezoelectric coefficients, d_{33} and d_{15} , of BaTiO_3 as a function of electric bias field E_3 at $T = 285\text{K}$ and 365K .

fields strongly increase ϵ_{11} , Fig. 7.4a, and, consequently, lead to high d_{15} coefficient, see Fig. 7.4b and Eqs. (7.3)-(7.5). In agreement with Eqs.(7.3) and (7.4), a high d_{15} leads to a maximum of $d_{33}^*(\theta)$ along a nonpolar direction. Large ϵ_{11} implies an easier polarization rotation away from the polar axis, as predicted by the first principle calculations [44]. In contrast to earlier studies where strong bias fields were always applied along nonpolar directions, we now show that a weak-field polarization rotation may be facilitated by application of strong bias fields anti-parallel to polarization. Note that the proximity of the tetragonal \leftrightarrow orthorhombic phase transition temperature by itself leads to a maximum $d_{33}^*(\theta)$ close to the $[111]_c$ axis - however, we now show that this effect is *enhanced* considerably by anti-parallel bias fields.

At higher temperatures, towards tetragonal \leftrightarrow cubic phase transition, the maximum in $d_{33}^*(\theta)$ must appear along the polar axis, Eq. (6.7). At these temperatures ϵ_{11} and d_{15} are relatively small, and the effect of the weak measuring field applied along nonpolar directions is small. However, our calculations show, Fig. 7.4b, that $d_{33}^*(\theta = 0)$ increases with the negative bias field, the effect being entirely due to the dielectric softening of the crystal along the polar axis; this softening is reflected in the large ϵ_{33} at negative bias fields, Fig. 7.4a. Thus, a considerable enhancement of piezoelectric coefficients may be obtained by mechanisms that are *not related to the polarization rotation*.

Calculations show that the effect of the Curie temperature shift by the applied bias fields

on the value of $d_{33}^*(\theta)$ is relatively small (20%) compared to the field induced changes. It can be speculated that presented results are *a general characteristic* of perovskite materials that exhibit multiple phase transitions.

A comment on use of high values of negative bias fields in these calculations should be made. It is a known fact that experimental coercive fields needed to switch ferroelectric polarization are much smaller than the thermodynamic coercive fields predicted by the LGD theory [44]. The lower experimental coercive fields are due to the nucleation of domains with reversed polarization on crystal imperfections. However, recent experimental results [36] suggest that thin layers may exhibit much higher coercive fields than corresponding bulk samples, and in materials whose thickness is only a few crystal layers, the experimental and thermodynamic (intrinsic) coercive fields become equal. The results from this section, thus, not only indicate fundamental behavior of perfect perovskite crystals, but may be directly applicable to thin layers.

7.2 Mechanical bias stress

One can now replace the electric bias field from the previous section by a mechanical bias stress and make a qualitatively similar discussion about the piezoelectric response and its anisotropy in tetragonal perovskites under uniform bias stresses. The tetragonal BaTiO₃ and PbTiO₃ at uniaxial mechanical stresses applied along the polar axis will be used as examples.

The influence of the hydrostatic stress on dielectric properties of BaTiO₃ has been discussed in the past [10]. Here, on the other hand, the effect of *uniaxial stresses* applied along the polar [001]_c direction is investigated.

If one considers a *4mm* tetragonal ferroelectric crystal with the zero external electric field and with a stress applied along the polar axis, the elastic Gibbs free energy, expanded up to the sixth power of polarization, is given by

$$\Delta G = \alpha_1 P_3^2 + \alpha_{11} P_3^4 + \alpha_{111} P_3^6 - \frac{1}{2} s_{11}^D X_3^2 - Q_{11} X_3 P_3^2, \quad (7.6)$$

where X_3 and P_3 are the applied mechanical bias stress and the polarization along the polar axis, respectively. If the stress is compressive, the value of X_3 is negative, by definition [4]. For barium titanate, the coefficients α and electrostrictive constants Q are taken from literature [7], while the value of the elastic compliance s_{11}^D at constant polarization is taken as $9 \times 10^{-12} m^2/N$ at all temperatures within the tetragonal phase [130]. Coefficients for lead titanate are taken from Ref. [62], and $s_{11}^D = 8 \times 10^{-12} m^2/N$. As will be shown later, a sufficiently high compressive stress X_3 can switch the polarization P_3 by 90°. The result of switching is so called an *a-domain* of the tetragonal

phase, denoted here as T_{90° and characterized by $P_2 \neq 0$ or $P_1 \neq 0$ and $P_3 = 0$. In addition, barium titanate transforms into orthorhombic phase at $T = 278K$ by developing a polarization component along the $[010]_c$ axis, such that $P_2 = P_3 \neq 0$ and $P_1 = 0$. This phase is unstable in the temperature region of the tetragonal phase stability. To investigate the effect of the stress X_3 on the polarization switching by 90° , on the polarization rotation in the $(100)_c$ plane, and on the stability of the tetragonal phase of BaTiO_3 , especially near the orthorhombic-tetragonal phase transition temperature, we shall consider the following free energy function, assuming $P_2 \neq 0$ [50, 49, 31, 32, 60]

$$\begin{aligned} \Delta G = & \alpha_1(P_2^2 + P_3^2) + \alpha_{11}(P_2^4 + P_3^4) + \alpha_{12}P_2^2P_3^2 + \alpha_{111}(P_2^6 + P_3^6) + \\ & \alpha_{112}(P_2^4P_3^2 + P_2^2P_3^4) - \frac{1}{2}s_{11}^D X_3^2 - Q_{11}X_3P_3^2 - -Q_{12}X_3P_2^2. \end{aligned} \quad (7.7)$$

For the purposes of these calculations the following things have been ignored: (i) the rhombohedral phase ($P_1 = P_2 = P_3 \neq 0$) which in BaTiO_3 is stable below $183K$, (ii) the polarization rotation in the $(110)_c$ plane, as well as (iii) the switching of P_3 by 90° from $[001]_c$ to $[100]_c$ axis. Due to the symmetry of the tetragonal phase the latter is equivalent to the 90° switching from the $[001]_c$ to the $[010]_c$ axis, which is taken into account by Eq. (7.7).

7.2.1 Dependence of polarization, dielectric susceptibility and piezoelectric coefficients on uniaxial stress

The stress dependences of spontaneous polarization, dielectric susceptibility and piezoelectric coefficients for the tetragonal phase can be calculated from the condition for the elastic Gibbs free energy minimum, Eq. 5.11. The stress dependence of the spontaneous polarization, $P_3(X_3)$, is shown in Fig. 7.5 for BaTiO_3 and PbTiO_3 at selected temperatures. A tensile stress applied along the $[001]_c$ increases the tetragonality and the polarization of each material. For a compressive stress (i.e. $X_3 < 0$), the polarization P_3 decreases, and at some critical stress, which is a function of temperature, it drops to zero. This stress corresponds to the compressive stress necessary to switch the polarization by 90° , from $[001]_c$ to $[100]_c/[010]_c$ axis and is equivalent to the coercive electric field in the polarization-electric field hysteresis [78]. We shall return to this case in the next section. In this section we will discuss crystals properties only for stresses where $P_3 > 0$, and $P_2 = 0$.

The dielectric permittivity ε_{ij} in the tetragonal phase ($\varepsilon_{11} = \varepsilon_{22}, \varepsilon_{33}$) can be calculated from Eqs. (7.7) and (5.2). One obtains for the susceptibility perpendicular to the

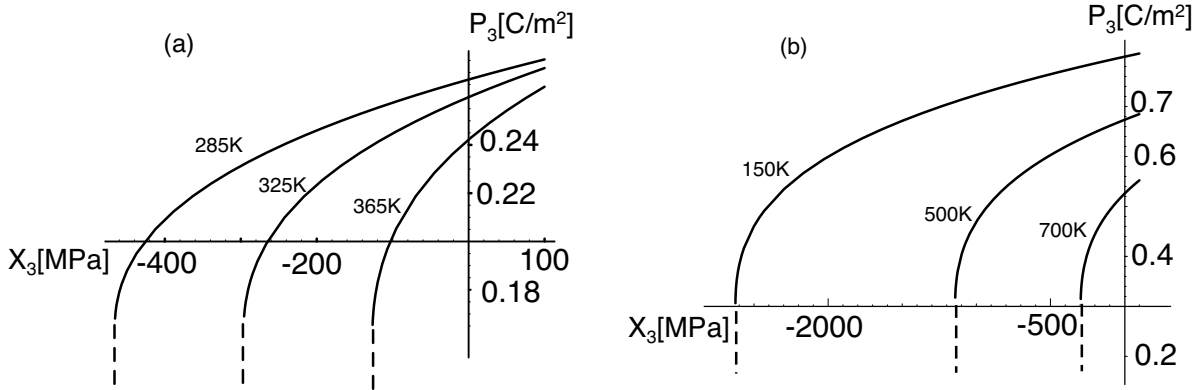


Figure 7.5: The stress dependence of polarization in the $[001]_c$ direction of the tetragonal (a) $BaTiO_3$ and (b) $PbTiO_3$ at several temperatures. For each temperature there is a critical value of the compressive stress (negative values) that causes the polarization switching for 90° .

spontaneous polarization

$$\varepsilon_{11} = [2\Lambda_1 + 2\alpha_{12}P_3^2(X_3) + 2\alpha_{112}P_3^4(X_3)]^{-1}, \quad (7.8)$$

where $\Lambda_1 = \alpha_1 - Q_{12}X_3$, and for the susceptibility along the polar direction

$$\varepsilon_{33} = [2\Lambda_3 + 12\alpha_{11}P_3^2(X_3) + 30\alpha_{111}P_3^4(X_3)]^{-1}, \quad (7.9)$$

where $\Lambda_3 = \alpha_1 - Q_{11}X_3$. The shear, transverse and longitudinal piezoelectric coefficients in the crystallographic coordinate system are given, respectively, as

$$d_{33} = 2\varepsilon_{33}(X_3)Q_{11}P_3(X_3), \quad (7.10)$$

$$d_{31} = 2\varepsilon_{33}(X_3)Q_{12}P_3(X_3), \quad (7.11)$$

and

$$d_{15} = \varepsilon_{22}(X_3)Q_{44}P_3(X_3). \quad (7.12)$$

The orientation dependence of the longitudinal piezoelectric coefficient $d_{33}^*(\theta)$ is expressed in Eq. (6.1), where θ is the angle between the polar axis and the measuring field (note: the measuring field is a weak field applied to measure the piezoelectric coefficient, not the bias field X_3). The calculated orientation dependence of $d_{33}^*(\theta)$ is shown in Figs. 7.6 and 7.7 for selected uniaxial stresses applied to the tetragonal $BaTiO_3$ and $PbTiO_3$ along the polar $[001]_c$ axis. For $BaTiO_3$, the calculations have been done for $T = 285K$ (Fig. 7.6a), close to the tetragonal \leftrightarrow orthorhombic phase transition temperature ($T = 273K$) and $T = 365K$ (Fig. 7.6b), closer to the tetragonal \leftrightarrow cubic phase transition temperature ($393K$). Calculations for $PbTiO_3$ have been done for $T = 700K$

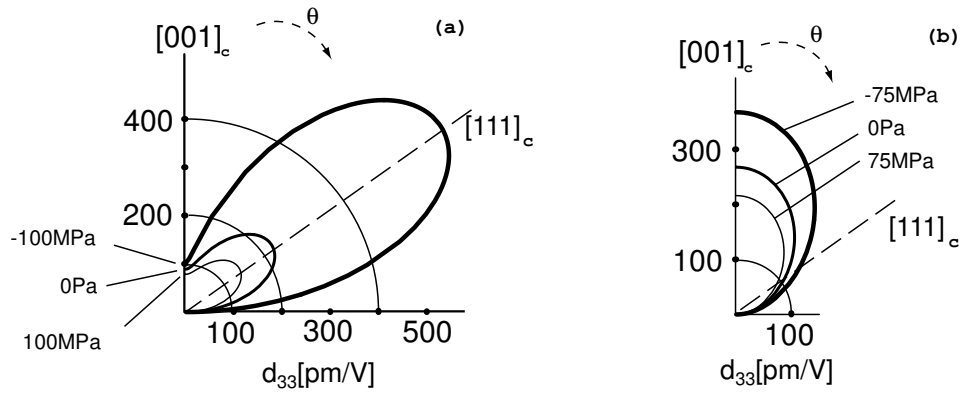


Figure 7.6: The orientation dependence of the longitudinal piezoelectric coefficient, $d_{33}^*(\theta)$, in BaTiO_3 at (a) 285K and (b) 365K for different values of bias stress X_3 . Note that from Eq. (6.1) $d_{33}^*(\theta) = d_{33}^*(-\theta)$.

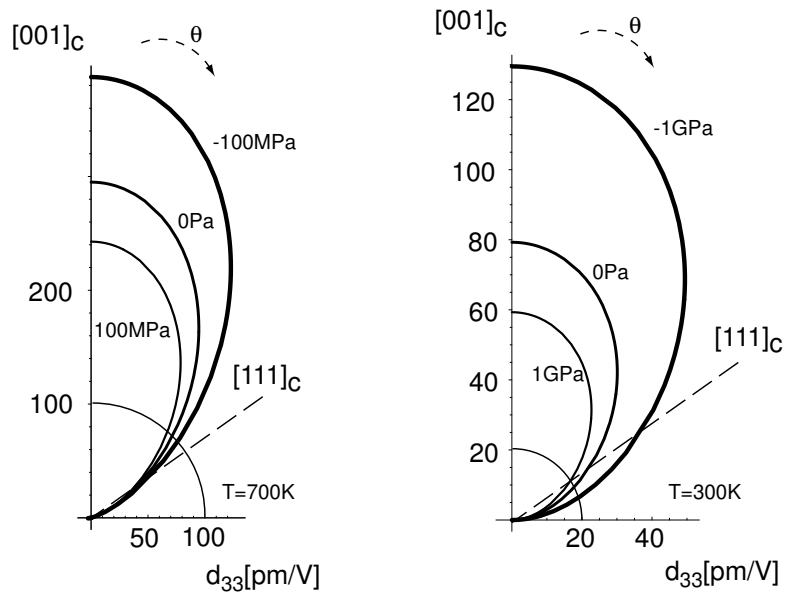


Figure 7.7: The orientation dependence of the longitudinal piezoelectric coefficient, $d_{33}^*(\theta)$, in PbTiO_3 at 700K and 300K for different values of bias stress X_3 . Note that from Eq. (6.1) $d_{33}^*(\theta) = d_{33}^*(-\theta)$.

and $T = 300K$.

Barium titanate shows a qualitative change in the behavior as the temperature changes from $T = 285K$ to $T = 365K$. At $285K$, the $d_{33}^*(\theta)$ in $BaTiO_3$ exhibits its maximum value along a direction ($\theta_{max} \approx 50^\circ$) that lies close to the $[111]_c$ axis. The value of $d_{33}^*(\theta_{max})$ has a strong dependence on the applied stress. At $T = 285K$, for $X_3 = 0$, $d_{33}^*(\theta_{max}) = 227pm/V$. If one applies a tensile bias stress, the calculations predict that $d_{33}^*(\theta_{max})$ will decrease. On the other hand, the compressive stress will *enhance* this piezoelectric coefficient. As shown in Fig. 7.6, at the compressive stress $X_3 = -100MPa$, $d_{33}^*(\theta_{max}) = 654pm/V$. This is a huge increase with respect to the zero stress value along the polar axis ($d_{33}^*(\theta = 0^\circ) = d_{33} = 89pm/V$), as well as with respect to the maximum value $d_{33}^*(\theta_{max}) = 227pm/V$ at $X_3 = 0$. It is clearly seen from Fig. 7.6a that both the enhancement effect by the compressive and reduction effect by the tensile stress are minimal along the polar axis and are the largest approximately along the $[111]_c$ axis.

Deeper in the tetragonal region of $BaTiO_3$, at $T = 365K$, one has again *an enhancement* of the piezoelectric response by the compressive stress and *reduction* by the tensile stress. However, the maximum response is now along the $[001]_c$ axis, Fig. 7.6b. At these temperatures the condition for having a maximum in $d_{33}^*(\theta)$ along a non-polar direction is not fulfilled, Eq. (6.7), so the piezoelectric response exhibits the maximum value along the polar axis. Similarly to what is predicted for lower temperatures, the tensile stress decreases the piezoelectric coefficient $d_{33}^*(\theta)$, while the compressive stress enhances it. At $X_3 = -75MPa$ and at $365K$, the maximum $d_{33}^*(\theta = 0^\circ)$ is $469pm/V$, compared to $268pm/V$ at $X_3 = 0$.

Qualitatively similar results can be shown for $PbTiO_3$, Fig. 7.7a and b. Analogous to the results for $BaTiO_3$ deep in the tetragonal phase, the maximum $d_{33}^*(\theta)$ and its maximum enhancement by the compressive stress in $PbTiO_3$ are observed along the polar axis. For example, at $T = 700K$, the compressive stress of $X_3 = -100MPa$ will give approximately the 150% increase of $d_{33}^*(\theta)$ along the $[001]_c$ axis, while at $T = 300K$, the compressive stress of $X_3 = -1000MPa$ increases $d_{33}^*(\theta = 0^\circ)$ by over 160% (Fig. 7.7). In contrast to $BaTiO_3$, however, this behavior does not qualitatively change as $PbTiO_3$ is cooled towards $T = 0K$ – this crystal stays strongly tetragonal and never exhibits a maximum of its longitudinal piezoelectric response along directions away from the polar axis $[102]$.

On the simple phenomenological level, one can understand the above results by considering the stress dependences of dielectric permittivities ε_{ij} and piezoelectric coefficients d_{im} , depicted for the tetragonal $BaTiO_3$ in Fig. 7.8 and for $PbTiO_3$ in Fig. 7.8. is sufficiently small under these conditions and can be neglected in the discussion; however,

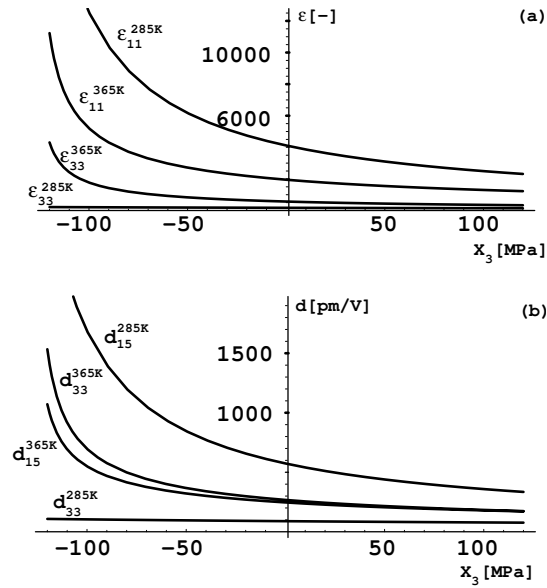


Figure 7.8: (a) Relative dielectric permittivities, ϵ_{11} and ϵ_{33} , and (b) piezoelectric coefficients, d_{33} and d_{15} , of BaTiO_3 as a function of the bias mechanical stress X_3 at 285K and 365K.

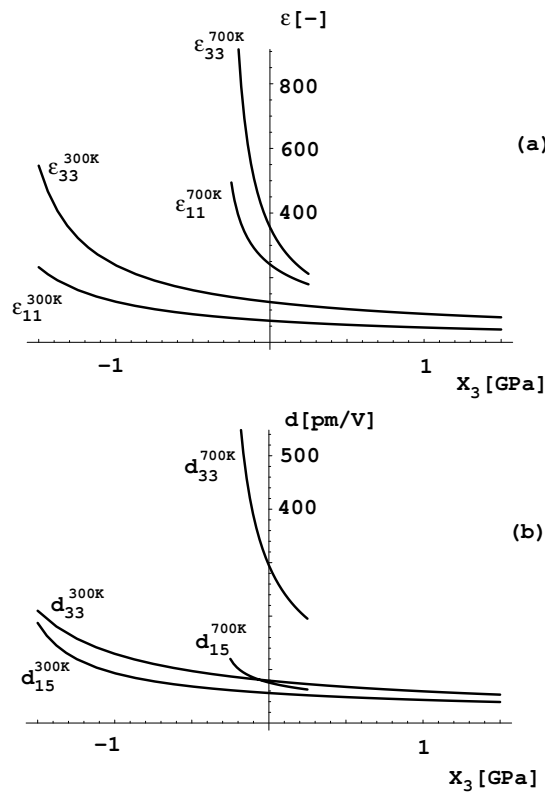


Figure 7.9: (a) Relative dielectric permittivities, ϵ_{11} and ϵ_{33} , and (b) piezoelectric coefficients, d_{33} and d_{15} , of PbTiO_3 as a function of the bias mechanical stress X_3 at $T = 300\text{K}$ and 700K .

this coefficient was taken into account to calculate $d_{33}^*(\theta)$ shown in Figs. 7.6 and 7.7. For the tetragonal BaTiO₃, at $T = 285K$, close to the tetragonal \leftrightarrow orthorhombic phase transition, the compressive bias stress increases ε_{11} while ε_{33} remains small, Fig. 7.8a. The large ε_{11} implies an easier polarization rotation in (100)_c or (010)_c plane, away from the polar axis [001]_c, and leads therefore to a high coefficient (Eq. (6.1) and Fig. 7.8b). Under conditions of a large dielectric anisotropy (large $\varepsilon_{11}/\varepsilon_{33}$ ratio), d_{15} dominates Eqs. (6.1) and the maximum of $d_{33}^*(\theta)$ appears approximately along the [111]_c axis. It is important to repeat here that the proximity of the tetragonal \leftrightarrow orthorhombic phase transition temperature leads by itself to the maximum of $d_{33}^*(\theta)$ along the [111]_c axis as discussed in *Chapter 6*. The effect is now considerably *enhanced* by the application of the compressive bias stress.

At higher temperatures the dielectric anisotropy $\varepsilon_{11}/\varepsilon_{33}$ in BaTiO₃ is reduced, Fig. 7.8a. A smaller ε_{11} leads to a smaller d_{15} (see Eq. (6.1) and Fig. 7.8) implying that the term containing d_{33} now dominates Eq. (6.1). Therefore, the maximum in $d_{33}^*(\theta)$ appears along the polar axis, Eq. (6.7), Fig. 7.7b. By applying the compressive stress, the maximum $d_{33}^*(\theta = 0^\circ)$ increases (Fig. 7.7b). The enhancement of the maximum $d_{33}^*(\theta = 0^\circ)$ by compressive stress X_3 is now primarily due to the dielectric softening of the crystal *along* the polar axis. Thus, at this temperature range, the compressive stress-assisted polarization rotation no longer plays the dominant role in the enhancement of the longitudinal piezoelectric coefficient.

Figure 7.7a shows that, throughout the tetragonal phase of BaTiO₃, the compressive stress causes softening of the dielectric properties both parallel and perpendicular to the polar axis. The tensile stress has the opposite effect. The direction along which the stress-assisted dielectric softening is dominant, and the direction of the maximal piezoelectric response, are determined by the temperature of the system. One should note that tensile stress increases the tetragonality (polarization) while the compressive stress reduces it. However, despite the reduced polarization, the compressive stress enhances the permittivity and consequently the piezoelectric coefficients. The enhancement of the material response by the compressive stress is due to the reduced stability of the polarization that is made more susceptible to a change by external fields. This point will be discussed further in the next section.

Exactly the same way of reasoning can be applied for the tetragonal PbTiO₃. The important difference is that, since there are no ferroelectric-ferroelectric phase transitions in this crystal, the maximal piezoelectric response lies *always* in the direction of the spontaneous polarization if the bias fields are not applied (see *Chapter 8*). In PbTiO₃, therefore, the stress causes the same effect as in the tetragonal BaTiO₃ at higher temperatures and can change the direction of the maximal longitudinal piezoelectric response

if the stress is high enough.

7.2.2 Flattening of the elastic Gibbs free energy profile by compressive stress

Now a profile of the Gibbs free energy for the tetragonal BaTiO₃ at $T = 285K$ and PbTiO₃ at $T = 300K$, as a function of the uniaxial mechanical stress bias, X_3 , applied along the polar axis is discussed. It will be shown that the dielectric softening of the crystal *perpendicular to* and *along* the polar axis, and the resulting enhancement of *the piezoelectric response*, are a consequence of the stress-assisted flattening of the Gibbs free energy profile.

In the ferroelectric BaTiO₃ and PbTiO₃ the spontaneous polarization is related to a temperature induced atom displacement with respect to their ideal positions in the cubic paraelectric phase [30]. External bias and measuring fields shift atoms and modify the polarization. The elastic Gibbs free energy thus reflects the free energy of the crystal as a function of atoms shifts by external fields or temperature variation. A flatter profile of $\Delta G(P_2, P_3)$ is a manifestation of the higher dielectric permittivity of the system to atom displacement, and signifies therefore enhanced piezoelectric coefficients. In the previous section we have shown that the enhancement of the dielectric and piezoelectric properties of the crystals by external stress is strongly anisotropic. In this section we demonstrate that the softening of the material response is a direct consequence of the anisotropic flattening of the Gibbs free energy profile by the external stress.

To support the following discussion, we first show in Fig. 7.10 a three-dimensional plot of $\Delta G(P_2, P_3)$ for BaTiO₃ ($T = 285K$, $X_3 = -100MPa$) and for PbTiO₃ ($T = 300K$, $X_3 = -1000MPa$). The thick solid lines represent $\Delta G(P_2)$ at the equilibrium spontaneous polarization P_3 for a given compressive stress X_3 ($P_3 = 0.257C/m^2$ in BaTiO₃ and $0.654C/m^2$ in PbTiO₃). The $\Delta G(P_2)$ profile reflects a polarization rotation away from the polar axis and in the $(100)_c$ plane, caused by a weak measuring field applied along the $[010]_c$ axis. The dashed lines represent $\Delta G(P_3)$ for $P_2 = 0$ and correspond to measurements along the polar axis. Black dots mark approximate positions of the stable and metastable tetragonal, orthorhombic and cubic phases. T_{0° indicates the tetragonal phase with the polarization along the $[001]_c$ axis ($P_3 \neq 0, P_2 = 0$), and T_{90° the tetragonal phase with the polarization switched by 90° , i.e. along the $[010]_c$ axis ($P_3 = 0, P_2 \neq 0$). The cross sections of $\Delta G(P_2, P_3)$ are shown in Figs. 7.11 for BaTiO₃ ($T = 285K$, for $X_3 = -100, 0, +100MPa$) and in Fig. 7.12 for PbTiO₃ ($T = 300K$, for $X_3 = -1000, 0, +1000MPa$). Note that, while Fig. 7.10 is calculated for compressive

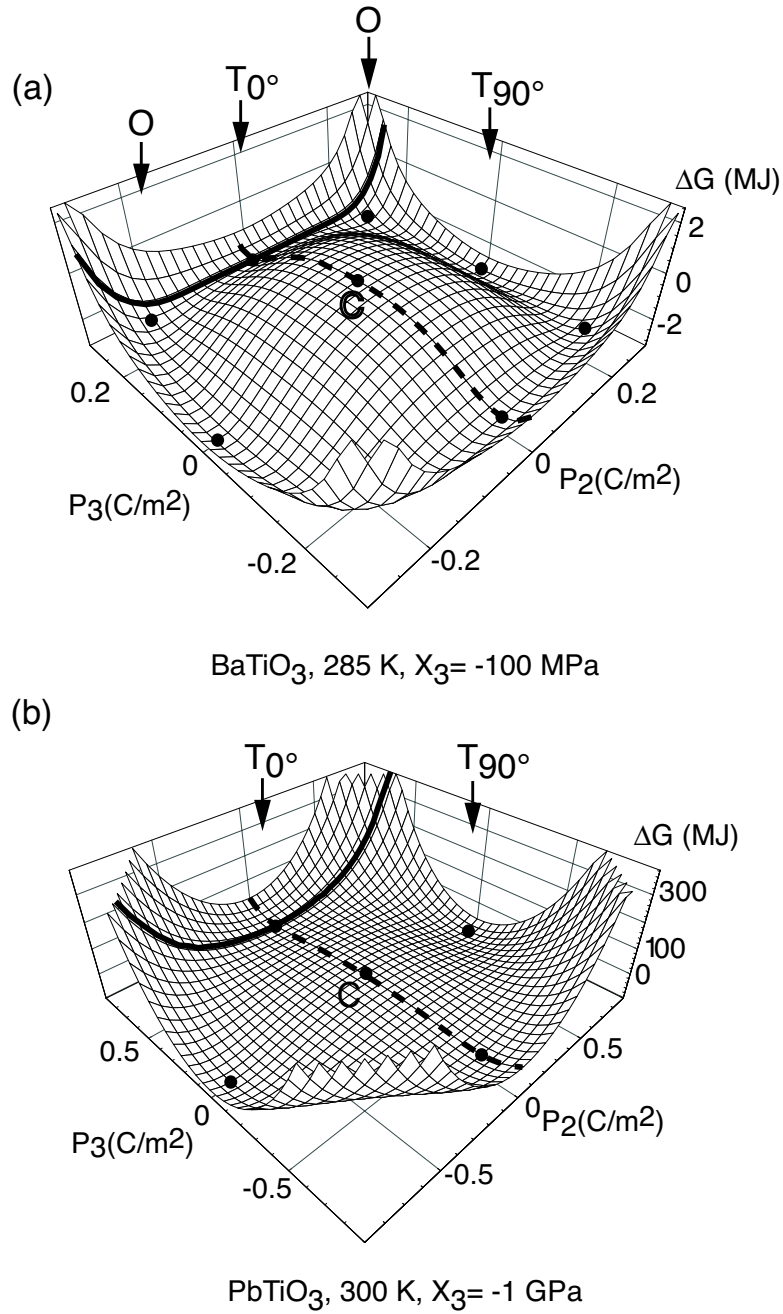


Figure 7.10: Gibbs free energy (7.7) at compressive stress for (a) BaTiO₃ ($T = 285\text{K}$, $X_3 = -1000\text{MPa}$) and (b) for PbTiO₃ ($T = 300\text{K}$, $X_3 = -1000\text{MPa}$). The thick solid lines represent $\Delta G(P_2)$ at equilibrium P_3 ($P_3 = 0.257\text{C/m}^2$ in BaTiO₃ and 0.654C/m^2 in PbTiO₃), reflecting the polarization rotation away from the polar axis in $(100)_c$ plane. The dashed lines represent $\Delta(P_3)$ for $P_2 = 0$. Black dots mark approximate positions of the stable and metastable tetragonal, orthorhombic and cubic phases. T_{0° indicates the tetragonal phase with polarization along the $[001]_c$ axis ($P_3 \neq 0$, $P_2 = 0$), and T_{90° the tetragonal phase with polarization switched by 90° , i.e. along the $[010]_c$ axis ($P_3 = 0$, $P_2 \neq 0$).

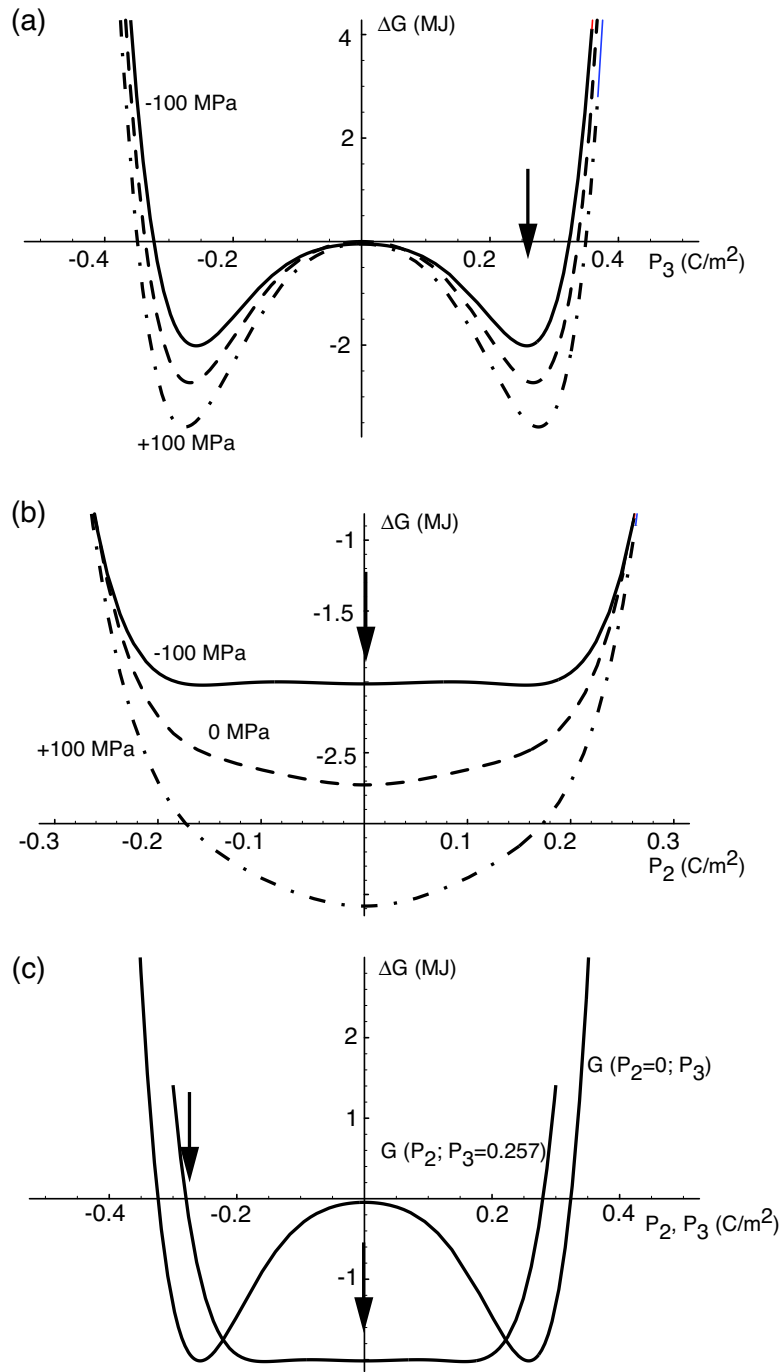


Figure 7.11: The profile of the Gibbs free energy at compressive (-100 MPa, solid lines), zero (dashed line), and tensile ($+100$ MPa, dashed-dotted line) stress for BaTiO₃ at $T = 285$ K. (a) $\Delta G(P_3)$ for $P_2 = 0$, (b) $\Delta G(P_2)$ at equilibrium P_3 ($P_3 = 0.257$ C/m²) and (c) comparison of the flatness of $\Delta G(P_2; P_3 = 0.257$ C/m²) and of $\Delta G(P_2 = 0; P_3)$. The former indicates the rotation of P_3 from $[001]_c$ towards $[010]_c$ in the $(100)_c$, and the latter indicates a dilatation or a reduction of the polarization along the $[001]_c$ axis. The arrows show a general position of the equilibrium tetragonal state. Compare with Fig. 7.10.

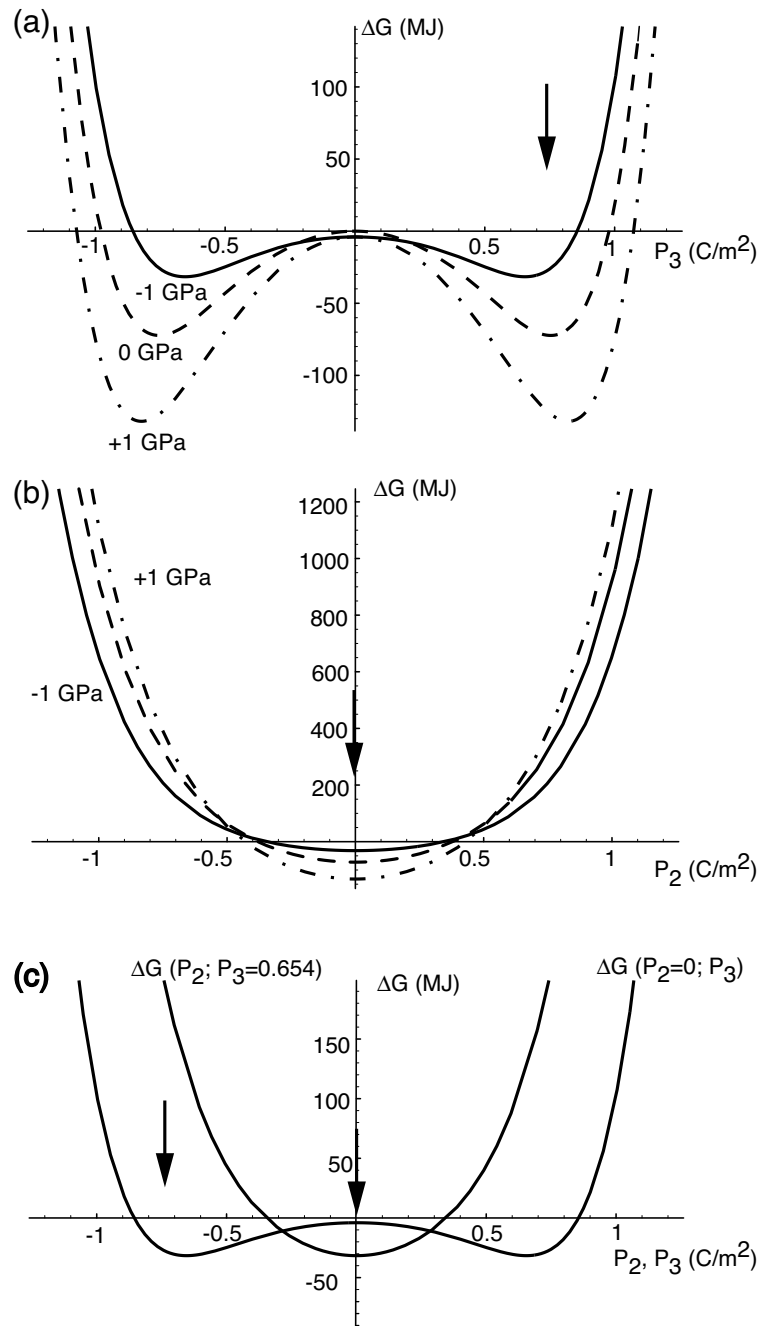


Figure 7.12: The profile of the Gibbs free energy at compressive ($-1000MPa$, solid lines), zero (dashed line), and tensile ($+1000MPa$, dashed-dotted line) stress for $BaTiO_3$ at $T = 300K$. (a) $\Delta G(P_3)$ for $P_2 = 0$, (b) $\Delta G(P_2)$ at equilibrium P_3 ($P_3 = 0.654C/m^2$) and (c) comparison of the flatness of $\Delta G(P_2; P_3 = 0.654C/m^2)$ and of $\Delta G(P_2 = 0; P_3)$. The former indicates the rotation of P_3 from $[001]_c$ towards $[010]_c$ in the $(100)_c$, and the latter indicates a dilatation or a reduction of the polarization along the $[001]_c$ axis. The arrows show a general position of the equilibrium tetragonal state. Compare with Fig. 7.10.

stress only, Figs. 7.11 and 7.12 include also data for stress free crystals and crystals under the tensile stress X_3 .

We first discuss the results for BaTiO_3 at $T = 285\text{K}$ shown in Fig. 7.11. The $\Delta G(P_2 = 0, P_3)$ given in Fig. 7.11a reflects the susceptibility of the crystal to dilatation and contraction of the polarization along the polar $[001]_c$ axis. Comparison of curves for the tensile (dashed-dotted line) and compressive stress (solid line) shows that, as the tetragonality decreases by the compressive stress, the $\Delta G(P_2, P_3)$ profile becomes somewhat flatter indicating an improved movement of atoms along the $[001]_c$ axis. However, the effect is modest, as it is shown in a small increase in the permittivity and the piezoelectric coefficient along the polar axis, Fig. 7.8. The effect is strikingly stronger for $\Delta G(P_2; P_3 = 0.257\text{C}/\text{m}^2)$, Fig. 7.11b, which reflects a change in the ΔG when the external measuring field has a component perpendicular to the polar axis $[001]_c$. For the dielectric response this situation corresponds to the polarization rotation in the $(100)_c$ plane, away from the $[001]_c$ and toward the $[010]_c$ axis; for the piezoelectric response the situation corresponds to the shear effect. The compressive stress strongly flattens the $\Delta G(P_2; P_3 = 0.257\text{C}/\text{m}^2)$ profile, Fig. 7.11b, leading to a considerable increase in ε_{11} and d_{15} , Fig. 7.8. The flattening of the ΔG profile along the polar axis (corresponding to the polarization dilatation and contraction) and within $(100)_c$ plane (corresponding to the polarization rotation) are compared in Fig. 7.11c. The flattening of the ΔG profile is clearly anisotropic - the effect of the flattening on the polarization rotation (and on ε_{11} and d_{15}) is much stronger than on the polarization contraction (and on ε_{33} and d_{33}). This ultimately leads to a much larger enhancement of d_{33}^* away from than along the polar axis, as shown in Fig. 7.6a.

Similar to its effect on the free energy of BaTiO_3 , the compressive stress has a tendency to flatten the $\Delta G(P_2, P_3)$ polarization dependence in PbTiO_3 , Fig. 7.12a and 7.12b, and thus to enhance its piezoelectric response. However, the anisotropy of the $\Delta G(P_2, P_3)$ profile flattening in PbTiO_3 is at all temperatures qualitatively different from that in BaTiO_3 at 285K . In PbTiO_3 , the flattening is more pronounced along the polar axis, Fig. 7.12c, than along the $[010]_c$ axis. Consequently, the contraction of the polarization along the $[001]_c$ axis is now at least as much important as the rotation in the $(010)_c$ plane. Using the same line of arguing as above, one sees that the longitudinal piezoelectric effect d_{33} and susceptibility ε_{33} now increase more by the compressive stress, Fig. 7.9, than d_{15} and ε_{11} . The shear effect no longer dominates in Eq. (6.1) and the maximum d_{33}^* and its maximum enhancement by the compressive stress appear along the polar axis.

At 365K BaTiO_3 behaves similarly to PbTiO_3 at low stresses (see *Chapter 8*), and will not be discussed in detail. The polarization rotation effects in BaTiO_3 in this temper-

ature range are stronger than in highly tetragonal PbTiO_3 , but still do not dominate the piezoelectric response. Therefore, the maximum d_{33}^* and its maximum enhancement appear along the polar axis, Fig. 7.6b. This is true for the tetragonal phase of BaTiO_3 above a certain critical temperature Eq. (6.7).

We next discuss the stability of the polarization along $[001]_c$ axis when a compressive stress is applied on the crystal. A compressive stress leads to a reduction of the polarization, which becomes zero at a certain coercive stress, Fig. 7.6. In terms of the Gibbs energy, the $\Delta G(P_3)$ develops, for sufficiently high compressive stress, a minimum at $P_3 = 0$, see Fig. 7.13. As mentioned before, this minimum does not correspond to

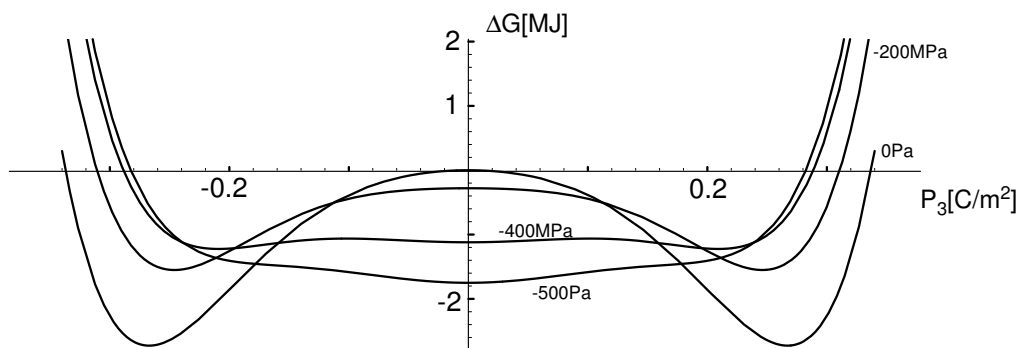


Figure 7.13: The Gibbs free energy of the tetragonal BaTiO_3 at $T = 285\text{K}$ as a function of the applied compressive stress. At coercive stress the free energy develops a minimum for P_3 corresponding to a saddle point in the two-dimensional graph, indicating the 90° switching into the $(P_2 \neq 0; P_3 = 0)$ state. Compare with Figs. 7.5 and 7.10.

the cubic phase, but to the switching by 90° into the tetragonal state characterized by $P_2 \neq 0; P_3 = 0$, indicated in Fig. 7.10 as T_{90° . That this state is not cubic but tetragonal, can be verified by analyzing $\Delta G(P_2, P_3)$. The analysis shows that the minimum in $\Delta G(P_3)$, seen in Fig. 7.13, corresponds to a saddle point in the two dimensional $\Delta G(P_2, P_3)$ plot; the system does not stay in the cubic state but moves into T_{90° state. In systems with the first order phase transitions, such as BaTiO_3 and PbTiO_3 , the phase transitions are hysteretic: the system can remain in a metastable state as long as this state represents a local minimum in ΔG . Thus, switching from the tetragonal T_{0° state ($P_2 = 0; P_3 \neq 0$) to the tetragonal T_{90° ($P_2 \neq 0; P_3 = 0$) state happens not when the minimum for T_{90° becomes an absolute minimum, but when the minimum for T_{0° transforms into an inflection point. In BaTiO_3 , at 285K , this happens at $X_3 < -400\text{MPa}$, while the calculations in Section 7.2.1 were made for $X_3 = -100\text{MPa}$. For all calculations, care was taken not to pass over the coercivity limit. Furthermore, an orthorhombic phase ($P_2 = P_3 \neq 0$) appears in BaTiO_3 at 273K . The stress applied along the $[001]_c$

can shift the tetragonal system into the T_{90° state, while only temperature can develop the orthorhombic state. Thus, in Fig. 7.11b, the curve for $X_3 = -100MPa$ has three minima: two for an incipient orthorhombic state (for P_2 between -0.2 and $-0.1C/m^2$ and between $+0.1$ and $+0.2C/m^2$) and one for T_{0° state for $P_2 = 0$. Even though T_{0° is not an absolute minimum, the system will stay in that state as long as it is a local minimum. Only when the temperature is sufficiently decreased and this minimum becomes an inflection point, the system will transform into the orthorhombic state.

We point out again that results presented refer to thermodynamically ideal systems. Real crystals will have lower coercive fields and the described effects will be weaker. However, these calculations demonstrate *general trends* that can be expected from tetragonal perovskite crystals under the influence of the uniaxial stress applied along the polar axis.

7.3 Extension of the dielectric tunability range in ferroelectric materials by electric bias field antiparallel to polarization

The results obtained in *Section 7.1* can directly and easily be applied for a discussion about another subject - the influence of *negative (anti-parallel) electric fields* on *dielectric tunability* in ferroelectrics.

The tunability of the dielectric permittivity by electric field is, in general, of interest for number of devices operating in the microwave region including dielectric resonators, filters, phase shifters and antennas [146, 47, 137, 93]. Ferroelectric materials are possible candidates for these applications because they exhibit high dielectric tunability, especially in the vicinity of the structural phase transitions. An additional advantage of ferroelectrics is a possibility of miniaturization and integration with other electronic components. In general, however, ferroelectrics exhibit *elevated dielectric loss*. Among different loss mechanisms [137, 53], important contributions to the dielectric loss in ferroelectric materials at microwave frequencies are related to presence of domain walls and quasi-Debye process [137]. The first mechanism is present only in the *polar phase* of ferroelectrics and in multidomain samples, whereas the second mechanism operates only in the *noncentrosymmetric phases*. Thus, most materials used for microwave applications are centrosymmetric; if ferroelectrics are employed, they are preferably used either as single domain crystals or in the temperature range where they are paraelectric. It should be mentioned, however, that application of the bias electric field breaks the symmetry of the material, inducing the quasi-Debye loss mechanism even in centrosymmetric materials [137].

In centrosymmetric materials the dielectric tunability is *symmetrical* with respect to the bias field direction [137]. Thus, only one field direction is usable. This is not the case for noncentrosymmetric materials, where the field dependence of the permittivity is *not the same* for positive and negative fields. This property of noncentrosymmetric materials, together with our results from *Section 7.1*, suggests an interesting possibility to broaden the dielectric tunability range and increase the tunability coefficient by applying both positive and negative bias fields, while keeping the absolute value of the bias field the same. Here, we try applying this idea to the tetragonal phases of BaTiO₃ and Pb(Zr,Ti)O₃ ferroelectric perovskites. By using the Landau-Ginzburg-Devonshire phenomenological thermodynamic theory, we show that the *theoretical tunability* in these materials and other ferroelectrics may, in principle, be *considerably increased* by applying an electric bias field antiparallel to polarization.

The thermodynamic dielectric tunability of the mentioned ferroelectrics is investigated here by studying their Gibbs free energy dependence on the electric bias field. The Gibbs free energy of tetragonal materials having polarization as the order parameter is shown in Eq. (7.1). The dielectric permittivity ε_{33} along the polar axis is then given by Eq. (5.10), where P_3 is a function of the bias field E_3 .

The dielectric tunability n is defined as the ratio between the dielectric permittivity of the material at zero electric bias field and its permittivity under a given electric field. In the present case the tunability coefficient is

$$n_{33} = \frac{\varepsilon_{33}(0)}{\varepsilon_{33}(E_3)}, \quad (7.13)$$

and can be calculated from Eq. (5.10). For BaTiO₃ the coefficients of the Gibbs free energy expansion can be found in Ref. [7] and for $Pb(Zr_{1-x}Ti_x)O_3$ from Ref. [63].

The results of the electric bias field dependence of the thermodynamic tunability in tetragonal ferroelectric BaTiO₃ at two temperatures ($T = 365K$ and $T = 300K$) and for two Pb(Zr_{1-x}Ti_x)O₃ compositions ($x = 0.6$ and 0.9) are shown in Figs 7.14 and 7.15, respectively. The thermodynamic tunability of BaTiO₃ at a temperature in the paraelectric phase is shown in Fig. 7.16 for comparison. In the centrosymmetric case (Fig. 7.16) the tunability is larger than $n_{33} = 1$ (the permittivity in general decreases with the field) for both negative and positive fields. Moreover, the tunability is symmetrical with respect to the field direction. This is the general case for centrosymmetric materials; hence, only one field direction is useful. In contrast, in the ferroelectric phase, Figs. 7.14 and 7.15, a field applied antiparallel to the polarization leads to an *increase* in the permittivity with increasing negative field, leading to $n_{33} < 1$. Moreover, the slope of the n_{33} is considerably steeper for negative fields and as the thermodynamic coercive field is approached. The reasons for such behavior are discussed in *Section 7.1*.

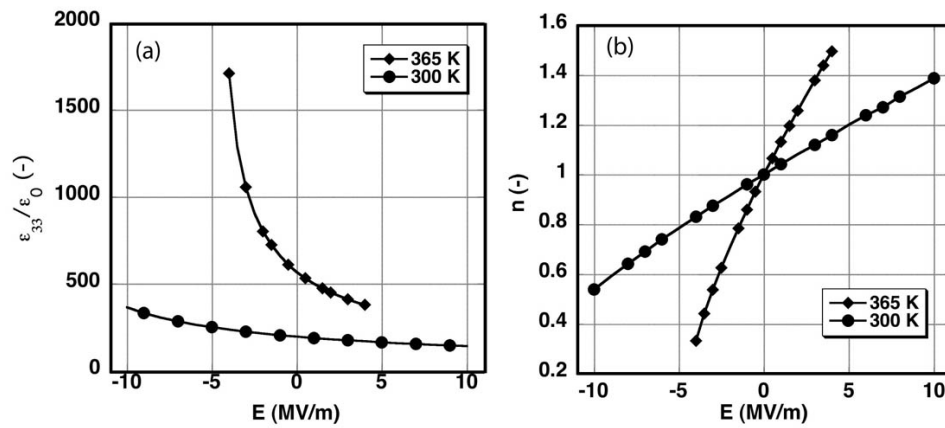


Figure 7.14: Calculated electric bias field dependence of (a) the dielectric permittivity along the polarization axis and (b) the dielectric tunability along same direction in tetragonal monodomain single crystal of $BaTiO_3$ at $T = 365K$ (diamonds) and $T = 300K$ (circles). Note: The tetragonal-orthorhombic phase transition temperature is $T = 278K$ upon cooling.

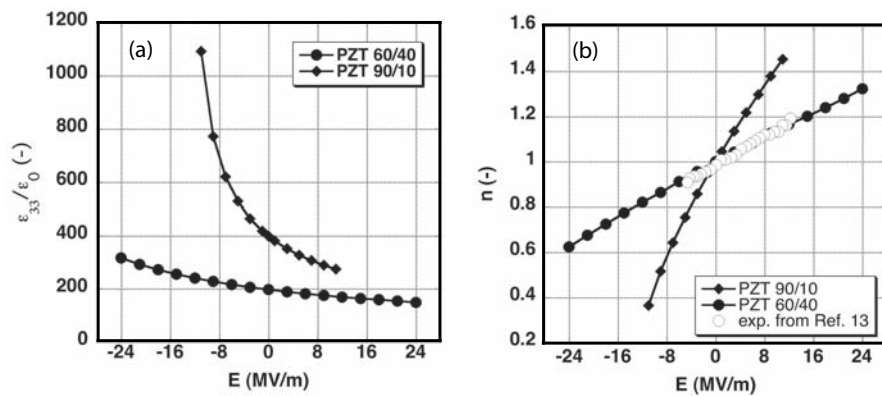


Figure 7.15: Calculated electric bias field dependence of (a) the dielectric permittivity along the polarization axis and (b) the electric tunability along the same direction in tetragonal $Pb(Zr_{1-x}Ti_x)O_3$ monodomain single crystal for two different compositions, $x = 0.6$ (PZT 60/40; closed circles) and $x = 0.9$ (PZT 90/10; diamonds) at $T = 298K$. Note: the tetragonal-rhombohedral morphotropic phase boundary is around $x = 0.48$ at room temperature. Open circles in (b) show the dielectric tunability coefficient for an epitaxial $\{100\}$ -oriented tetragonal $Pb(Zr,Ti)O_3$ thin film. (Experimental data are taken from Fig. 10(a) of Ref. [164]. The exact composition of the film in this reference is not specified and its permittivity is about twice as high as that calculated for the PZT 60/40 crystal.)

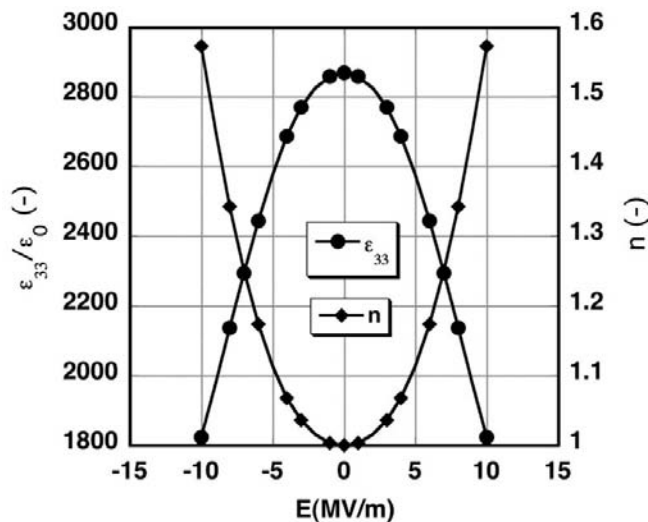


Figure 7.16: Calculated electric bias field dependence of the dielectric permittivity (circles) and the dielectric tunability (diamonds) along the polarization axis in cubic, paraelectric phase of BaTiO_3 at $T = 440\text{K}$. Note: The paraelectric-ferroelectric phase transition temperature is $T = 393\text{K}$ upon cooling.

Note that the enhancement of the tunability along the polar axis by antiparallel fields is *stronger* at temperatures and compositions that lie *further away* from the structural phase transitions where polarization changes direction. Thus, in BaTiO_3 , Fig. 7.14, the tunability changes faster at 365K , deeper in the tetragonal phase, than at 300K , which is only 22K above the tetragonal \leftrightarrow orthorhombic phase transition temperature. Similarly, the tunability along the polar axis is stronger in $\text{Pb}(\text{Zr}_{0.1}\text{Ti}_{0.9})\text{O}_3$, which lies further away from the morphotropic phase boundary, than in $\text{Pb}(\text{Zr}_{0.4}\text{Ti}_{0.6})\text{O}_3$. Interestingly, our calculations for BaTiO_3 show that this trend is opposite for tunability perpendicular to the polar direction, $n_{11} = \epsilon_{11}(0)/\epsilon_{11}(E_1)$. In that case the tunability becomes higher and changes faster in a vicinity of the tetragonal \leftrightarrow orthorhombic phase transition temperature where polarization changes its direction.

7.4 Conclusions

There are several important results obtained in this chapter.

Firstly, it is shown that, in the framework of the Landau-Ginzburg-Devonshire (LGD) theory, an application of a strong negative electric bias field (i.e. field applied along $[00\bar{1}]_c$ direction or anti-parallel to the spontaneous polarization) in the tetragonal barium titanate, leads, at low temperatures of this phase, to a *large enhancement* of the

piezoelectric properties along nonpolar $[111]_c$ axis. It is also shown that the negative bias field considerably enhances the piezoelectric response along the polar $[001]_c$ direction at high temperatures of this phase.

Furthermore, it is shown that the application of *uniaxial compressive bias stresses* along the polar axis of BaTiO_3 and PbTiO_3 can enhance the longitudinal piezoelectric response in these materials, and that this enhancement can be interpreted in terms of *the profile flattening of the Gibbs free energy*. This is true for the enhancement along the $[111]_c$ axis (in BaTiO_3 at 285K) as well as along the $[001]_c$ axis in PbTiO_3 (throughout the tetragonal phase) and in BaTiO_3 , at sufficiently high temperatures within the tetragonal phase. The Gibbs free energy profile flattening by the compressive stress can be directly related either to the facilitated polarization rotation in $(100)_c$ plane (BaTiO_3) or to the polarization contraction along the polar axis (BaTiO_3 , PbTiO_3).

Finally, it is demonstrated that the thermodynamic tunability in ferroelectric phase of perovskites behaves *differently and advantageously* comparing to their paraelectric phase: since the ferroelectric phase is not centrosymmetric, the tunability for the positive and negative fields is not the same and the tunability region is thus broader for the same absolute value of the field. In addition, the dielectric tunability changes quicker in the region of negative than for positive bias fields.

The results in this chapter may have broad implications:

- Calculations of the influence of the bias fields on the piezoelectric response and its anisotropy, followed by an attempt of tracing the thermodynamic origins of these effects by studying the flattening of the Gibbs free energy profile can be extended to give *a general explanation* of the improved piezoelectric response in perovskite ferroelectrics. This explanation might include the cases of complex solid solutions in the vicinity of the morphotropic phase boundary, and the temperature driven enhancement of piezoelectric properties near ferroelectric–ferroelectric phase transitions.
- In real (i.e., non-ideal) materials, the range in which the enhancement of the piezoelectric response could be obtained, and, consequently, the tunability range, at negative fields would be narrower than the thermodynamic range calculated here. The reason is that polarization switching occurs at fields that are much lower than the thermodynamic coercive fields. This is a general constraint for perovskite materials, and a problem from applications point of view. However, there are some indications that this may not be the case for very thin ferroelectric layers [36]; experiments on thin films could therefore directly confirm the results of the thermodynamic calculations. On the other hand, systems with dense domain structures could have charged domain walls creating strong enough electric fields

antiparallel to the spontaneous polarization within domains, and/or internal compressive stresses. This could be a possible origin of enhanced piezoelectric response in such systems [156]. In agreement with our phenomenological predictions, as an interesting note, one can speculate that composite materials may offer possibilities to design noncentrosymmetric materials with low losses [133], in which tunability region would be broadened by the asymmetry, even if none of the constituent phases is ferroelectric.

The last step towards a more general thermodynamic description is given in the next chapter. It relates the free energy instability and enhancements of the electromechanical properties induced by different variables (electric and mechanic bias fields, temperature, composition) and is applied to three different perovskites.

Different classic perovskites served as examples in a phenomenological study of the influence of different external field bias on their dielectric and piezoelectric properties. Some very interesting results were obtained - if an electric field is applied in the direction opposite to the spontaneous polarization direction, or an uniaxial compressive stress is applied along the polar axis, energetically metastable system states are obtained in which all dielectric permittivities and piezoelectric coefficients are increased. One of the most important results is that both the polarization rotation (piezoelectric enhancement along non-polar axes) and polarization contraction (piezoelectric enhancement along the polar axis) effects can be described by the common mechanism i.e. this metastability of the Gibbs free energy of the system.

Chapter 8

Piezoelectric response and free energy instability in classic perovskites

The question of the origin of the piezoelectric properties enhancement in perovskite ferroelectrics is approached by analyzing the Gibbs free energy of tetragonal BaTiO_3 , PbTiO_3 and $\text{Pb}(\text{Zr},\text{Ti})\text{O}_3$ in the framework of the Landau-Ginzburg-Devonshire theory. The generality of the approach is demonstrated by examining the free energy flattening and piezoelectric enhancement as a function of composition, temperature, electric field and mechanical stress.

The origins of the piezoelectric anisotropy and piezoelectric response enhancement were discussed in previous chapters of this work. It was demonstrated that the enhancement is dependent on *proximity of the phase transition temperatures (Chapter 6)*, *crystal instability induced by electric fields applied antiparallel to polarization*, or *compressive stresses applied along the polar axis (Chapter 7)*.

There are other studies of the enhancement origins - it has been demonstrated that these origins can be traced to *polarization rotation under external electric field* [44], *the density of domain walls in crystals with an engineered domain structure* [156, 3], *hierarchical domain structure* [80], and *composition/morphotropic phase boundary effects* [9, 52, 77, 78].

Considering the importance of this effect from both the fundamental and technological point of view, it is clearly of interest to see if there exists a *a common underlying process*

for piezoelectric enhancement in ferroelectric perovskites.

This problem will be addressed in the framework of the Landau-Ginzburg-Devonshire theory.

8.1 Calculations and discussion

As in previous two chapters, the Gibbs free energy and the longitudinal piezoelectric coefficient of the tetragonal phase of classic perovskites will be investigated and discussed - this time the suitable examples will be BaTiO₃ and (1-x)PbTiO₃-xPbZrO₃ (PZT) monodomain single crystals. In both materials the ferroelectric tetragonal phase exhibits $4mm$ and the paraelectric cubic phase $m\bar{3}m$ symmetry; the polar axis is oriented along the [001] direction of the cubic system. In the framework of the LGD theory [31, 32] the Gibbs free energy ΔG can be written as the series expansion of the polarization $P = (P_1, P_2, P_3)$. While all calculations in this article are concerned with the tetragonal phase ($P_1 = P_2 = 0; P_3 \neq 0$), the proximity of the orthorhombic phase ($P_1 = 0; P_2 = P_3 \neq 0$) is taken into account in BaTiO₃ near the tetragonal-orthorhombic phase transition temperature. Similarly, as shown in *Chapter 7*, variation of the ΔG with P_2 for equilibrium P_3 gives susceptibility of a tetragonal ferroelectric to polarization rotation and tendency towards a monoclinic distortion. In a more general case all three components of polarization may be included in the analysis [27], however, such generalization is beyond the scope of this discussion.

If external electric and elastic fields are applied along the P_3 , the Gibbs free energy can be written in the coordinate system of the cubic phase as

$$\begin{aligned} \Delta G = & \alpha_1(P_2^2 + P_3^2) + \alpha_{11}(P_2^4 + P_3^4) + \alpha_{12}P_2^2P_3^2 + \alpha_{111}(P_2^6 + P_3^6) \\ & + \alpha_{112}(P_2^4P_3^2 + P_3^4P_2^2) - s_{11}^D\sigma_3/2 - Q_{11}\sigma_3P_3^2 - Q_{12}\sigma_3P_2^2 - E_3P_3, \end{aligned} \quad (8.1)$$

where s_{11}^D is the elastic compliance at constant polarization. The values of the α and Q_{ij} coefficients are taken from Refs. [61, 62, 8]. At all examined temperatures s_{11}^D is taken as $9 \cdot 10^{-12}m^2/N$ for BaTiO₃ [130] and as $6.785 \cdot 10^{-12}m^2/N$ for Pb(Zr,Ti)O₃ [5]. The negative σ_3 and E_3 have the meaning of compressive stress and electric field applied antiparallel to polarization [4].

The dielectric susceptibilities are calculated by using Eq. (5.2) and the longitudinal, the transverse and the shear piezoelectric coefficients by using Eqs. (6.2)-(6.4). One should note that P_3 and ε_{ij} are functions of σ_3 , E_3 and T in those relations. The origin of the temperature dependence is in Curie-Weiss behavior of $1/\alpha_1$; in BaTiO₃ higher order dielectric stiffnesses are also temperature dependent [76, 8].

It is easily seen that the flattening of a simple polynomial such as ΔG in Eq. (8.1)

implies flattening and decrease of its first and second derivatives. Since $d \sim \varepsilon$ and $\varepsilon_{ij} = (\partial^2 \Delta G / \partial P_i \partial P_j)^{-1}$, the flattening of the free energy profile implies increase of the system's dielectric susceptibility, and thus the increase of its piezoelectric response.

To calculate effects away from the crystallographic axes, the orientation dependence of the longitudinal piezoelectric coefficient, d_{33}^* , of a tetragonal crystal may be expressed as in Eq. (6.1). As it can be seen there, $d_{33}^*(\theta)$ is a function of both the dielectric permittivity along the polar axis, ε_{33} , and the one perpendicular to it, ε_{11} . This dependence is the basis for $d_{33}^*(\theta)$ enhancement driven by either polarization rotation ($\sim \varepsilon_{11}$) [161, 9] or the polarization contraction ($\sim \varepsilon_{33}$), as discussed in previous chapters.

To illustrate the relation between the Gibbs free energy flattening and the enhancement of the d_{33}^* , ΔG and d_{33}^* of PZT are analyzed as a function of the Zr/Ti ratio, compressive stress and electric field applied along the polar axis. In BaTiO₃, ΔG and d_{33}^* are analyzed as functions of temperature and electric field applied along the polar axis.

One can first consider effects of Zr/Ti ratio on the Gibbs free energy and piezoelectric response in PZT at 298K. Two tetragonal compositions, one with Zr/Ti=0/100 (i.e., pure PbTiO₃) and the other with Zr/Ti=40/60 are considered. These two compositions are chosen to illustrate effects of the proximity of the morphotropic phase boundary (MPB) on the Gibbs free energy profile flattening and the piezoelectric enhancement. In PZT, the MPB appears at Zr/Ti=52/48 and PZT 40/60 is sufficiently far from it [113] that complications arising from possible presence of mixed phases or a monoclinic phase can be avoided. Two different free energy profiles were calculated - one along the polar direction with $P_2 = 0; P_3 \neq 0$ and the other with $P_2 \neq 0; P_3 = P_3(\sigma_3, E_3)$, where P_3 is fixed at its equilibrium value at 298 K. The former case (Fig. 8.1a) involves

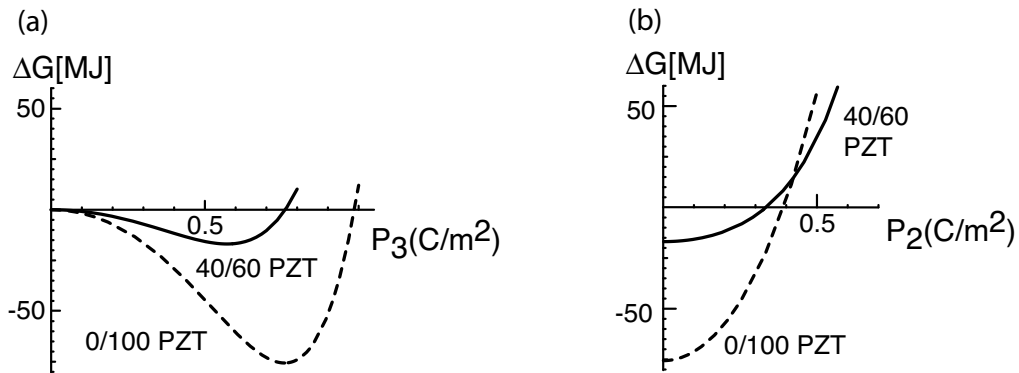


Figure 8.1: Effects of composition in PZT 0/100 (PbTiO₃) and PZT 40/60 at 298K on free energy flattening, (a) $\Delta G(P_2 = 0, P_3)$ profile related to polarization contraction, (b) $\Delta G(P_2, P_3 = 0.52c/m^2)$ profile indicating polarization rotation.

elongation ($E_3 > 0$) or contraction ($E_3 < 0$) of the polarization along the polar axis,

while the latter case (Fig. 8.1b) corresponds to the polarization rotation away from the polar direction, as described in detail in Ref. [27]. As expected [141], both profiles are flatter in PZT 40/60 lying closer to the MPB. As a consequence, ε_{33} and ε_{33} are larger in PZT 40/60 than in PZT 0/100 leading to enhancement of the corresponding piezoelectric coefficients, Fig. 8.2. This enhancement of the properties in compositions

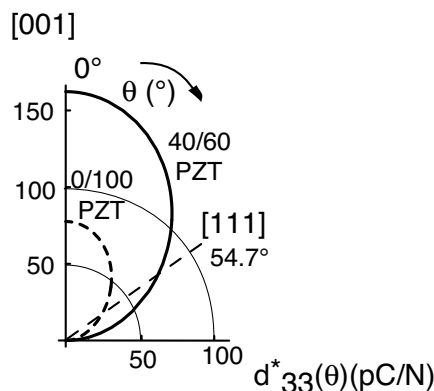


Figure 8.2: Effects of composition in PZT 0/100 (PbTiO_3) and PZT 40/60 at 298K on the longitudinal piezoelectric response in a general direction, $d_{33}^*(\theta)$.

close to the MPB is a well-known empirical and theoretical result [61], interpreted here in terms of the Gibbs free energy flattening. Significantly, the analysis shows that the flattening of the ΔG profile away from the polar axis and along the polar axis are comparable. In fact, the $d_{33}^*(\theta)$ surface is elongated along the polar axis, Fig. 8.2, indicating that the maximum enhancement is along the polar axis ($\theta = 0^\circ$). This is qualitatively different from the behavior of the rhombohedral phases of PZT [34, 9], BaTiO_3 [44], and relaxor ferroelectrics [118], where piezoelectric enhancement is strongest along nonpolar directions.

We next show that under external electric field and stress applied against polarization, the isotropy of the free energy profile is broken, leading to a large enhancement of the piezoelectricity by polarization rotation.

The effect of the electric field bias E_3 and the mechanical stress σ_3 on the ΔG and $d_{33}^*(\theta)$ in PZT 40/60 composition is shown in Figs. 8.3 - 8.6. Figures 8.3 and 8.4 compare the ΔG and $d_{33}^*(\theta)$ for the crystal at zero bias field and for $E_3 = -35, -43$ and -44 MV/m applied antiparallel to the polarization. Likewise, Figs. 8.5 and 8.6 show the ΔG and $d_{33}^*(\theta)$ for uncompressed crystal and for the crystal subjected to compressive stress of $\sigma_3 = -350$ and -500 MPa applied along the polar direction. In the limits of the phenomenological theory used, neither the electric field nor the stress are high enough to cause polarization switching by 180° or 90° ; thus, crystals remain in the tetragonal sin-

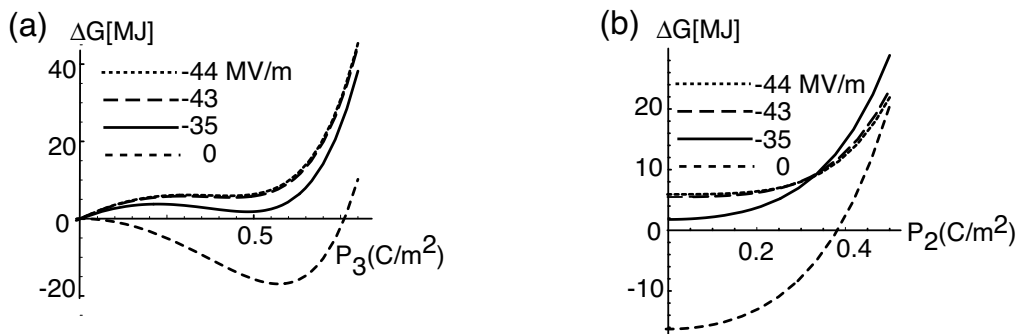


Figure 8.3: Effects of electric bias field ($E_3 = 0, -35, -43$ and -44 MV/m) on free energy profile and $d_{33}^*(\theta)$ in PZT 40/60 at 298 K: a) $\Delta G(P_2 = 0, P_3)$ profile indicating polarization contraction; (b) $\Delta G(P_2, P_3 = \cos t(E_3))$ profile indicating polarization rotation. Only $\Delta G(P_2 = 0, P_3 \geq 0)$ is of interest and is shown.

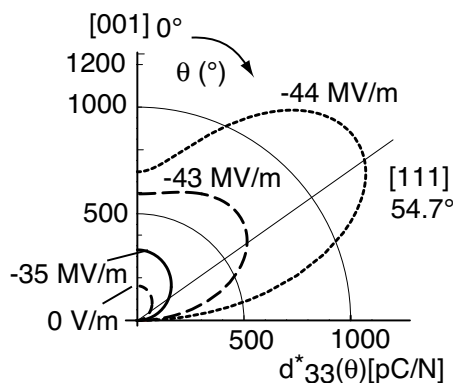


Figure 8.4: Effects of electric bias field ($E_3 = 0, -35, -43$ and -44 MV/m) on $d_{33}^*(\theta)$ in PZT 40/60 at 298 K. Coercive electric field for this composition is just above -44 MV/m. In highly unstable regions even small changes in the flatness of the ΔG (compare ΔG and $d_{33}^*(\theta)$ for $E_3 = -43$ and -44 MV/m) can have a huge impact on $d_{33}^*(\theta)$.

gle domain state, as stated in *Chapter 7*.

At low electric fields and compressive pressures the dominant enhancement of the $d_{33}^*(\theta)$ is along the polar direction, i.e. it is a consequence of colinear polarization contraction. This behavior changes dramatically at high antiparallel electric fields and compressive pressures approaching thermodynamic coercive fields, where instability of the ΔG and $d_{33}^*(\theta)$ enhancement become strongly anisotropic and polarization rotation effects dominate the piezoelectric response. At high fields (compare ΔG and $d_{33}^*(\theta)$ for $E_3 = -43$ and -44MV/m in Fig. 8.3 and 8.4) even a small increase in the flatness of the ΔG

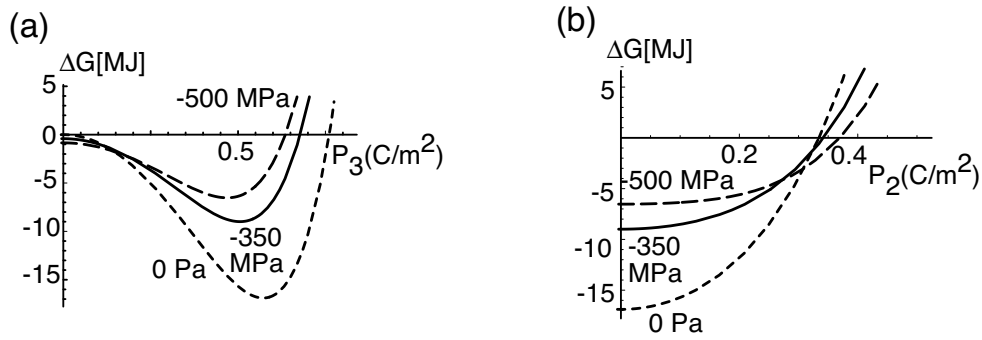


Figure 8.5: Effects of compressive stress ($\sigma_3 = 0, -350, -500\text{MPa}$) on free energy profile in PZT 40/60 at 298 K: a) $\Delta G(P_2 = 0, P_3)$ profile indicating polarization contraction; (b) $\Delta G(P_2, P_3 = \cos(E_3))$ profile indicating polarization rotation. Only $\Delta G(P_2 = 0, P_3 \geq 0)$ is of interest and is shown.

profile leads to a large enhancement of $d_{33}^*(\theta)$ along off-polar directions.

Remarkably, our calculations show that PbTiO_3 exhibits giant enhancement of the $d_{33}^*(\theta)$

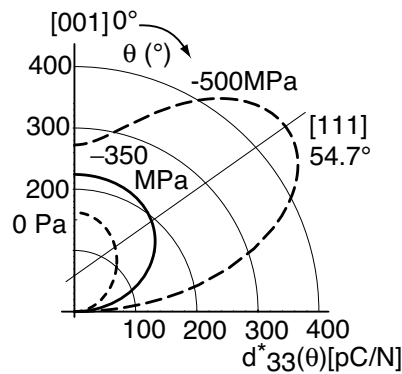


Figure 8.6: Effects of compressive stress ($\sigma_3 = 0, -350, -500\text{MPa}$) on $d_{33}^*(\theta)$ in PZT 40/60 at 298K.

along nonpolar directions once compressive stress is sufficiently large, Figs. 8.7 and 8.8.

At $300K$ and $\sigma_3 = 1.79GPa$, just below the thermodynamic coercive pressure, the value of the noncolinear $d_{33}^*(\theta)$ in $PbTiO_3$ is on the order of $10^3 - 10^4 pC/N$. This result is qualitatively similar to that obtained by *Wu* and *Cohen* using ab initio calculations for $PbTiO_3$ under hydrostatic pressure [161]. We emphasize, however, that in the two cases the origin of the free energy instability is different. In the report by *Wu* and *Cohen*, the instability is related to the presence of the morphotropic phase boundary that is induced by the hydrostatic pressure. At this boundary the polarization changes direction from pseudocubic [001] axis in the tetragonal phase to pseudocubic [111] axis in the rhombohedral phase. In our work, the instability is related to the multiple orien-

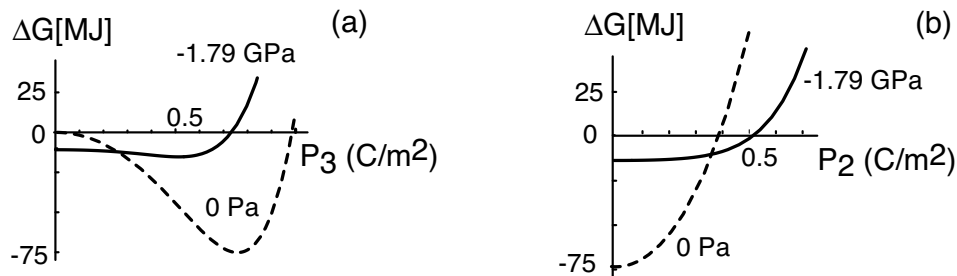


Figure 8.7: Effect of compressive stress ($\sigma_3 = 0$ and $-1.79GPa$) at $T=300 K$ on anisotropic free energy flattening in $PbTiO_3$: (a) $\Delta G(P_2 = 0, P_3)$ profile indicating polarization contraction; (b) $\Delta G(P_2, P_3 = const(\sigma_3))$ profile indicating polarization rotation.

tations of the ferroelectric polarization within the same crystal phase (i.e., switching by 90° in tetragonal materials from [001] to [010] axis). Once the thermodynamic coercive compressive pressure is approached *but not passed*, the crystal is destabilized, the free energy becomes shallow and the piezoelectricity is greatly enhanced.

Interestingly, the polarization rotation effects under antiparallel electric fields in $PbTiO_3$ are small. The reasons for this difference between effects of compressive pressure and antiparallel field on piezoelectric anisotropy will be discussed in one of our next publications.

Recent experimental studies of effects of hydrostatic pressure on 52/48 PZT MPB composition [126, 127] and studies of effects of tensile stress perpendicular to polarization in thin films of $PbTiO_3$, [17] indicate that polarization rotation indeed occurs in these material and that the symmetry becomes lower in both compositions under the effect of stress. Monoclinic or triclinic phases cannot be predicted in the framework of the 6th order LGD theory [145]; however, as indicated above and explained in more details in Ref. [27], our approach does indicate susceptibility of materials to monoclinic distortion, correctly predicting the relationship between the instability of the ΔG , susceptibility of the material to polarization rotation and ensuing enhancement of the $d_{33}^*(\theta)$.

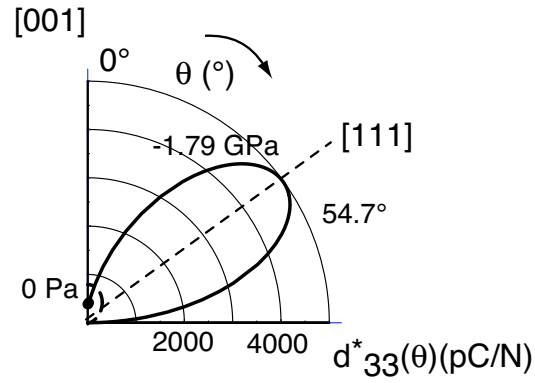


Figure 8.8: Effect of compressive stress ($\sigma_3 = 0$ and -1.79GPa) at $T = 300\text{K}$ on piezoelectric enhancement in PbTiO_3 . At $\sigma_3 = 0$ values for $d_{33}^*(\theta)$ (dashed line) is multiplied by 10. For σ_3 close to the coercive stress (approx. -1.9GPa) values of $d_{33}^*(\theta)$ are strongly sensitive to input parameters and vary between 10^3 and 10^4 pC/N.

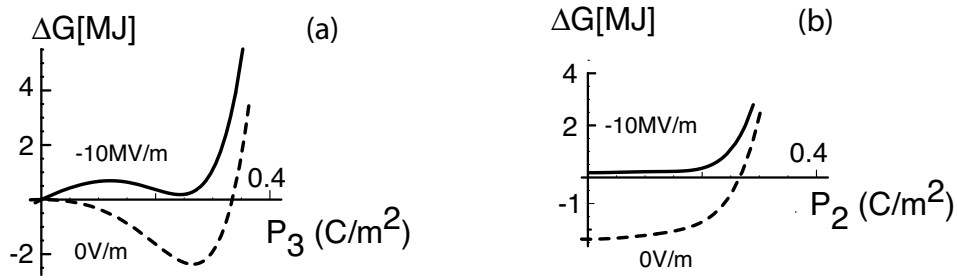


Figure 8.9: Effects of electric bias field ($E_3 = 0$, -10MV/m) at $T = 298\text{K}$ on anisotropic free energy flattening in BaTiO_3 : (a) $\Delta G(P_2 = 0, P_3)$ profile indicating polarization contraction; (b) $\Delta G(P_2, P_3 = \text{const}(\sigma_3))$ profile indicating polarization rotation.

We next show that the proposed approach is also applicable to processes involving temperature driven enhancement of the piezoelectric response. As an example, effects of electric field and temperature on the ΔG and $d_{33}^*(\theta)$ in the tetragonal phase of BaTiO_3 , in a vicinity of 298K , are analyzed. Figure 8.9 illustrates the flattening of the ΔG profile by application of a bias electric field antiparallel to polarization at 298K . The behavior

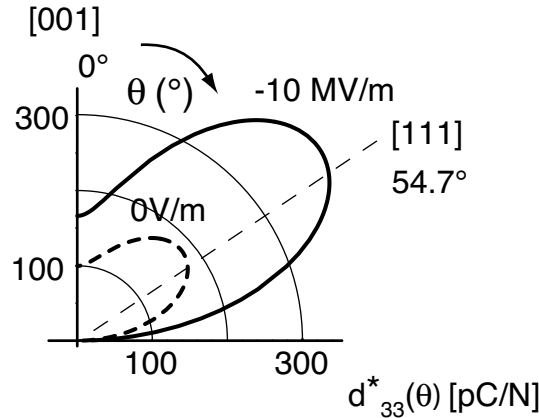


Figure 8.10: Effects of electric bias field ($E_3 = 0, -10\text{MV/m}$) at $T = 298\text{K}$ on piezoelectric enhancement in BaTiO_3 .

is similar to that predicted in BaTiO_3 at high compressive pressures (*Chapter 7*) and in PZT 40/60 and PbTiO_3 shown above: the flattening of the ΔG profile is anisotropic, being stronger away from the polar axis, Fig. 8.9b, than along the polar axis, Fig. 8.9a. This leads to the maximum $d_{33}^*(\theta)$ approximately along the $[111]$ axis, Fig. 8.10, while its enhancement along the polar axis $[001]$ is comparatively smaller. Finally, it

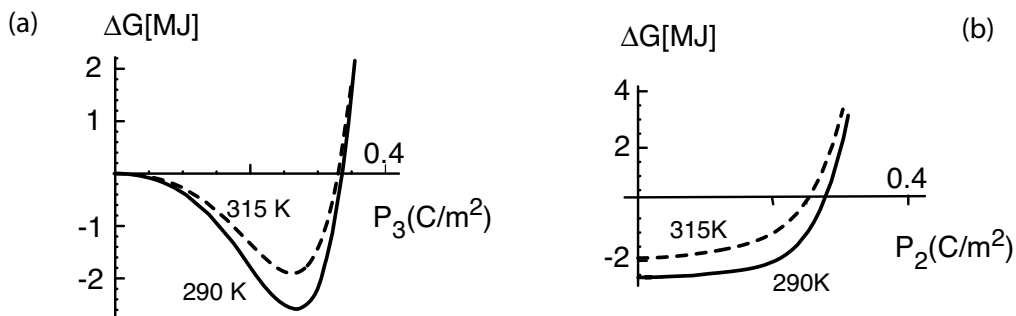


Figure 8.11: Effects of proximity of tetragonal-orthorhombic phase transition temperature ($T=283\text{K}$) at zero field on anisotropic free energy flattening in BaTiO_3 .

is interesting that the free energy anisotropy is strongly influenced by the proximity of the tetragonal-orthorhombic phase transition temperature that occurs at 283K . At this

phase transition temperature the polarization vector changes its direction from $[001]$ ($P_2 = 0, P_3 \neq 0$) to $[011]$ ($P_2 = P_3 \neq 0$) leading to the dielectric softening of the crystal in the plane perpendicular to the polar axis and to an increase in ε_{11} (*Chapter 6*). The dominant temperature effect is clearly seen in Figs. 8.11 and 8.12 which show that the anisotropic flattening of the ΔG profile and enhancement of the piezoelectric response at zero field become stronger as the tetragonal-orthorhombic phase transition temperature is approached on cooling. The antiparallel electric field in Figs. 8.9 and 8.10 has therefore an additional destabilizing effect on the crystal and enhances the temperature driven anisotropic flattening of the ΔG profile and enhancement of the $d_{33}^*(\theta)$ along a nonpolar axis.

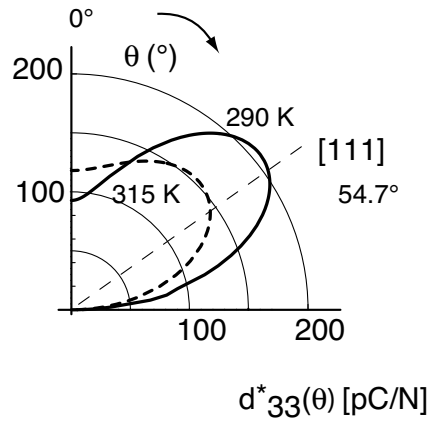


Figure 8.12: Effects of proximity of tetragonal-orthorhombic phase transition temperature ($T=283$ K) at zero field on piezoelectric enhancement in $BaTiO_3$.

8.2 Conclusions

Remarkably large piezoelectric responses along nonpolar crystallographic directions were reported in complex ferroelectrics [89, 118, 34] and qualitatively the same effects, but smaller in magnitude, were observed in simple perovskites [155, 110] - the idea that this behavior is a common characteristic of perovskite ferroelectrics has suggested itself naturally.

Numerous different studies by different groups revealed different mechanisms of the origins of this piezoelectric enhancement along non-polar axes [9, 52, 77, 78, 44, 156, 3, 80]. Here, we tried to find an universal thermodynamic background for these mechanisms. Several different classic perovskite systems under different system conditions (variation of different thermodynamic parameters) were used for this discussion. It is shown that

the flattening of the Gibbs free energy profile of each of these systems, regardless of whether it is caused by temperature or composition variation, or by applying compressive pressure or antiparallel electric field bias, leads to enhancements of the dielectric susceptibilities and of the piezoelectric response of examined materials.

The relationship between the enhancement of the piezoelectric response and a free energy profile flattening was introduced by *Fu* and *Cohen* using a first principles approach [44]. Recently, *Wu* and *Cohen* [161] made a link between the enthalpy difference between two pressure-induced crystal phases and enhanced piezoelectric response in PbTiO_3 . In both of these cases the large piezoelectric response is related to field (electrical or mechanical) induced phase transitions and polarization rotation. In contrast to the results of *Cohen* and co-workers, we show that phase transitions related free energy instabilities are not the only way to achieve large enhancement of the piezoelectric response. Huge enhancement of the piezoelectricity can be expected in the vicinity of and just below the thermodynamic coercive fields within the same ferroelectric phase (as in here presented case of PbTiO_3).

Furthermore, it is also shown here that the anisotropy of the free energy profile determines whether the enhancement of piezoelectricity will take place by polarization rotation or polarization contraction, and that, in contrast to rhombohedral perovskites, in the case of tetragonal $\text{Pb}(\text{Zr},\text{Ti})\text{O}_3$ materials lying in the vicinity of the morphotropic phase boundary, the composition related flattening of the free energy profile and piezoelectric enhancement are isotropic i.e. effects of polarization rotation and polarization contraction are comparable. This isotropy can be broken by external stresses and electric fields leading to large, polarization rotation related, enhancement of the piezoelectric effect.

The universality of the approach is further indicated by the fact that the anisotropic flattening of the free energy profile can explain both the enhancement of the piezoelectric response by polarization rotation away from the polar axis, and by polarization contraction along the polar axis. The huge enhancement of the piezoelectric response by compressive stress predicted in PbTiO_3 along off-polar directions suggests that compositional or structural disorder, such as present in complex relaxor-ferroelectrics, is not essential for the giant piezoelectric effect. Our results and those of ab initio calculations [161] hint that such disorder is probably responsible for the free energy instability, which, as shown here, leads to a large piezoelectric response.

It is shown that the flattening of the Gibbs free energy profile of each of examined perovskite systems here, regardless of whether it is caused by temperature or composition variation, or by applying compressive pressure or antiparallel electric field bias, leads to enhancements of their dielectric susceptibilities and piezoelectric response, and that the anisotropy of the free energy flattening is the origin of the anisotropic enhancement of the piezoelectric response, which can occur either by polarization rotation or by polarization contraction. Additionally, giant enhancement of the longitudinal piezoelectric response is predicted in PbTiO_3 under uniaxial compression.

Chapter 9

Conclusions and perspectives

The following questions were discussed during this thesis work:

How to measure the temperature dependence of single domain electromechanical properties of potassium niobate single crystal? This task is very difficult, especially for the high temperature tetragonal phase, where the electric conductivity of the material is elevated, and the low temperature rhombohedral phase, where obtaining the single domain state is extremely energetically unfavorable. There are other practical problems - KN samples are mechanically fragile¹; it is a nontrivial task to obtain and preserve the ferroelectrically single domain state of samples; the material surface layer can have a stoichiometry other than the bulk and this surface layer can have the dominant contribution in experimental results; during phase transitions samples can break because of large strains induced by instability at the transition temperature and the probability of the rupture is related to sample size; the material is a poor thermal conductor and changing the temperature of samples, while doing measurements of temperature dependence of its properties, can induce temperature gradients in them that can destroy the single domain state; the material shows elevated dielectric loss even at room temperature if the frequency of the electric measuring signal is low enough; the relatively small dielectric permittivity of the material makes measurements for some aspect ratios difficult (for example, measurements of the piezoelectric coefficient d_{33}), especially if the measurements are not performed at room temperature (stray capacitances of temperature dependence resonance measurements setups are comparable to the capacities of the samples); and, it is difficult to obtain hysteresis loops that can clearly give values of the spontaneous polarization and coercive fields.

Up to our best knowledge, there are few experimental results obtained on the KN sam-

¹There is a crystal growth company that warns that shaking and stressing of their KN crystals can induce domains in them (<http://www.u-oplaz.com/crystals/crystals05.htm>).

ples in the tetragonal phase, none of those are single domain values, and there are no results obtained from the rhombohedral phase, apart the measurements of the phase transition temperature and multidomain state dielectric permittivity. The measurements performed in this thesis work were thus confined to the orthorhombic ferroelectric, room temperature, phase.

How to obtain the LGD coefficients for potassium niobate? When describing electromechanical properties of barium titanate in the framework of the phenomenological Landau-Ginzburg-Devonshire theory, it has been necessary to extend the description proposed by *Devonshire* in 1949 and 1951 to a more complex one, having more higher order terms (including the order parameters coupling) in the Taylor series expansion of the Gibbs free energy, if one wanted to describe this perovskite system behavior with high accuracy. At present, the phenomenological description of barium titanate electromechanical properties generally contains in its series expansion all terms up to the 6th power of order parameters, and there is even a recently published work by *Li et al.* in which the authors used a series expansion up to the 8th power of the polarization as order parameter.

On the other hand, for all perovskites for which accurate phenomenological descriptions already exist, there are reported single domain measurements of electromechanical properties in the ferroelectric phase that occurs immediately below the Curie temperature. Using such experimental results, it is possible to do a fit to the phenomenological expressions, because they are simple enough, and it is possible to analytically compare the neighboring phases energies at the phase transition temperatures, and obtain additional phenomenological coefficients. Fitting procedures in the low temperature phases are generally used to obtain only the higher order coefficients.

If one wants to obtain qualitatively the same phenomenological description of electromechanical properties behavior for potassium niobate as it has been done for barium titanate, one can see the following obstacles. For potassium niobate single crystal there is not enough of experimental results in the ferroelectric phase that occurs immediately below the Curie temperature (the tetragonal phase) to perform fitting procedures that will easily give lower order coefficients.

The idea in this thesis work was to combine the experimental results that could be found in the literature with the results obtained in our experiments, and to perform a fitting using only the measured single domain properties in the orthorhombic ferroelectric phase of KNbO_3 . It was probable that the coefficients obtained would be relatively inaccurate, because the fitting was done in a lower temperature phase of potassium niobate and because the experimental data used were obtained on samples from different

sources. Gathering data from different authors has already been done before for this material, by *Wiesendanger*. However, up to our best knowledge, the estimate of a set of the ferroelectric dielectric stiffness coefficients at constant stress, α , was done in this work for the first time, up to the 6th order in polarization.

What are the intrinsic origins of the piezoelectric anisotropy in perovskites?

The origins are free energy instabilities caused either by an anticipation of a structural phase transition in materials with well defined phases, either by mesoscopic disorder in the complex relaxor ferroelectric solid solutions or destabilization of the structure by temperature. When approaching the structural changes, these materials will dielectrically soften in directions in which new components of the order parameter will appear. In the case when the order parameter is the spontaneous polarization, phase changes are represented by appearing or disappearing of the polarization components in certain crystallographic directions - dielectric permittivity will increase or decrease in corresponding directions, according to the phase changes. The increase of the dielectric permittivity along the direction perpendicular to the spontaneous polarization direction implies an increase of the corresponding shear piezoelectric coefficient - these large shear coefficients can be the dominant contributors to the piezoelectric response of a domain engineered crystal in some perovskites.

How can external bias fields influence the piezoelectric response in perovskites?

In the literature, one can find studies about the influence of the hydrostatic pressure on the electromechanical properties, as well as studies of the influence of the electric bias fields on the piezoelectric properties of certain classic perovskites. However, studies of the influence of the special bias configurations such as the uniaxial compressive stress or the electric bias field applied antiparallel to the spontaneous polarization have never been published. The reason for that may be an intuitive feeling that decreasing the ferroelectricity of a material by application of "unfavorable" strong electric and mechanical bias fields will decrease the electromechanical constants, or not taking into account a fact that ferroelectric switching does not occur immediately after changing the sign of the applied electric field.

In spite of this, a phenomenological study of the influence of "negative" electric fields and compressive mechanical stresses on electromechanical properties of classic perovskites was done in this work, and some very interesting results were obtained, possibly with broad implications. The fields that decrease the value of the spontaneous polarization, and do not cause the polarization switching at the same time, lead to a significant enhancement of the dielectric properties in all crystallographic directions, and, analo-

gously, to the enhancement of the piezoelectric response. By approaching the values of coercive electric and mechanical fields, the dielectric (and piezoelectric) properties may increase up to giant values. Thus, qualitatively, the anticipation of the spontaneous polarization switching induced by biases and the anticipation of the polarization rotation in the vicinity of a phase transition have the same influence on the dielectric and piezoelectric properties of classic perovskites.

Is there a general thermodynamic description of the piezoelectric response enhancement and its anisotropy for classic perovskites? Yes. It is shown in this thesis that this enhancement is related to the free energy flattening, regardless of variable (temperature, stress, electric field and composition) that induces it. It is furthermore demonstrated that the anisotropy of the enhancement (either along or away from the polarization direction) is directly related to the anisotropic flattening of the free energy. Thus, the enhancement can take place by polarization rotation and by polarization contraction. This approach additionally predicts that huge enhancement of the longitudinal piezoelectric response may be expected along nonpolar directions in PbTiO_3 . This material exhibits only one, tetragonal, ferroelectric phase, and never fulfills the condition (a high shear piezoelectric coefficient) necessary for having an enhancement of piezoelectric response along a non-polar axis only by changing the temperature, without bias fields applied.

This result suggests that a large piezoelectric effect is not limited to relaxor-ferroelectrics or disordered systems. In fact, our results hint that the large piezoelectric response in relaxor-ferroelectrics is due to the flattening of the free energy profile, the flatness probably being a consequence of the disorder or of the internal fields.

The only explicit link between the free energy and enhanced piezoelectric response that can be found in the literature was made by *Cohen* and his coworkers in two papers. In the first, ab initio calculations were used for BaTiO_3 under external electric field and concept of polarization rotation was introduced, and in the second the same link in PbTiO_3 under hydrostatic pressure was shown. Our calculations, based on Landau thermodynamic theory, which is advantageously much less consuming in time and computer power than ab initio calculations, expand this idea to $\text{Pb}(\text{Zr},\text{Ti})\text{O}_3$ (PZT), PbTiO_3 and BaTiO_3 , and stress, composition and temperature as variables.

The origins of the piezoelectric enhancement are different in this discussion, compared to the work of *Cohen* and his coworkers. In their case the enhancement is due to proximity of the electric field/stress induced phase transformations, and in our case the instability of the free energy under electric field/stress is due to the proximity of applied field/stress to the thermodynamic coercive field/stress.

What to do next? There are always many unanswered questions at the end of a thesis work, that might encourage future work. Here we point out some important unsolved problems and suggestions: a) a method that will measure single domain dielectric properties of KN single crystals in the tetragonal ferroelectric phase should be mastered; b) if one takes a closer look at the graphic comparison among the phenomenologically calculated and experimentally obtained results for transverse piezoelectric coefficients in the orthorhombic phase of potassium niobate, d_{31} and d_{32} , and the room temperature values of piezoelectric coefficients in *Chapter 5*, it can be seen that the results are generally discrepant, and that the measurements of the dielectric properties done by *Fukuda* and the spontaneous polarization by *Günter* yield our phenomenological estimate that agrees with the piezoelectric coefficients measured by *Zgonik* and *Günter*, and not with our results and the recent values obtained by *Wada*; our suggestion is, thus, that measurements of the piezoelectric coefficients and spontaneous polarization should be redone; c) it is not clear what is the origin of the very large thickness mode coupling coefficient, k_t , in potassium niobate - one can speculate that the opposite signs of the transverse piezoelectric coefficients in this material might decrease the planar coupling coefficient value, k_p , and thus increase the thickness mode coefficient; d) it can be noted in our discussion about the influence of bias fields on the piezoelectric response in perovskites that there is a qualitative difference in the influence of electric bias field and mechanic bias compressive stress (for example, very high mechanical stresses can induce a non polar piezoelectric maximum in PbTiO_3 , but electric bias fields cannot)- this difference will be discussed in one of our next publications.

Appendix A

Transformations of coordinate systems. Diagonalization of matrices and eigenvalues

Transforming from one coordinate system to another was an important issue in this thesis report, so it is useful to describe these transformations in more detail.

When a perovskite system undergoes a phase transition from the cubic paraelectric phase to the tetragonal ferroelectric one, with the spontaneous polarization along the x_3 axis, one keeps the same reference frame for description of the properties in both phases. For example, in the cubic phase the dielectric permittivity tensor is

$$\mathcal{E}^c = \begin{pmatrix} \varepsilon_{33}^c & 0 & 0 \\ 0 & \varepsilon_{33}^c & 0 \\ 0 & 0 & \varepsilon_{33}^c \end{pmatrix}, \quad (\text{A.1})$$

while in the tetragonal phase it is

$$\mathcal{E}^t = \begin{pmatrix} \varepsilon_{11}^t & 0 & 0 \\ 0 & \varepsilon_{11}^t & 0 \\ 0 & 0 & \varepsilon_{33}^t \end{pmatrix}. \quad (\text{A.2})$$

The tetragonal phase has more of independent coefficients, and one can keep the same reference frame, because in both phases one has a diagonal matrix.

If one now wants to calculate, for example, what is the value of a dielectric permittivity in some general directions, one has to take a new coordinate system, rotate it with respect to the old one and calculate coefficients in this new system. Two coordinate systems relation is uniquely determined by Euler angles (see *Chapter 6*). Changing the direction in which one wants to consider permittivity coefficients, one also changes Euler

angles.

The matrix of transformations from one coordinate system to another by using Euler angles is given by

$$T = \begin{pmatrix} \cos\psi\cos\phi - \cos\theta\sin\psi\sin\phi & \cos\psi\sin\phi + \cos\theta\sin\psi\cos\phi & \sin\theta\sin\psi \\ -\sin\psi\cos\phi + \cos\theta\cos\psi\sin\phi & -\sin\psi\sin\phi + \cos\theta\cos\psi\cos\phi & \cos\psi\sin\theta \\ \sin\theta\sin\phi & -\sin\theta\cos\phi & \cos\theta \end{pmatrix}, \quad (\text{A.3})$$

where θ , ψ and ϕ are Euler angles.

Now, to transform a vector (tensor of order 1) from an old system, $X = (x_1, x_2, x_3)$, to a new one, $X' = (x'_1, x'_2, x'_3)$, one has that its components change as

$$x'_i = \sum_{j=1}^3 T_{ij}x_j, \quad (\text{A.4})$$

or

$$X' = TX. \quad (\text{A.5})$$

For a tensor of order 2 (permittivity, for example), one has

$$\varepsilon'_{ij} = \sum_{k=1}^3 \sum_{l=1}^3 T_{ik}T_{jl}\varepsilon_{kl}, \quad (\text{A.6})$$

or

$$\mathcal{E}' = T^2\mathcal{E}, \quad (\text{A.7})$$

and for a tensor of order 3 (piezoelectric coefficients tensor), one has

$$d'_{ijk} = \sum_{m=1}^3 \sum_{n=1}^3 \sum_{p=1}^3 T_{im}T_{jn}T_{kp}d_{mnp}, \quad (\text{A.8})$$

or

$$\mathcal{D}' = T^3\mathcal{D}. \quad (\text{A.9})$$

In the tetragonal phase, one thus has expressions for a longitudinal piezoelectric coefficient,

$$d_{33}^{t*}(\theta, \psi, \phi) = d_{33}^{t*}(\theta) = \cos\theta(d_{15}^t\sin^2\theta - d_{31}^t\sin^2\theta + d_{33}^t\cos^2\theta), \quad (\text{A.10})$$

a transversal piezoelectric coefficient

$$\begin{aligned} d_{31}^{t*}(\theta, \psi, \phi) &= d_{31}^{t*}(\theta, \psi) = \cos\theta(-d_{15}^t\sin^2\theta \sin^2\psi - \\ &\frac{d_{31}^t}{8}(-6 - 2\cos 2\theta + \cos 2(\theta - \psi) - 2\cos 2\psi + \cos 2(\theta + \psi)) + \\ &d_{33}^t\sin^2\theta \sin^2\psi), \end{aligned} \quad (\text{A.11})$$

or a shear piezoelectric coefficient

$$d_{15}^{t*}(\theta, \psi, \phi) = d_{15}^{t*}(\theta, \psi) = \cos\theta \left(-\frac{d_{15}^t}{4} (-2 - 2\cos 2\theta + \cos 2(\theta - \psi) - 2\cos 2\psi + \cos 2(\theta + \psi)) + 2\sin^2\theta \sin^2\psi (-d_{31}^t + d_{33}^t) \right). \quad (\text{A.12})$$

These coefficients are obtained by using the matrix of tetragonal $4mm$ symmetry piezoelectric coefficients in the short notation [116]

$$\begin{pmatrix} 0 & 0 & 0 & 0 & d_{15}^t & 0 \\ 0 & 0 & 0 & d_{15}^t & 0 & 0 \\ d_{31}^t & d_{31}^t & d_{33}^t & 0 & 0 & 0 \end{pmatrix}. \quad (\text{A.13})$$

In the orthorhombic phase this matrix has the form

$$\begin{pmatrix} 0 & 0 & 0 & 0 & d_{15}^o & 0 \\ 0 & 0 & 0 & d_{24}^o & 0 & 0 \\ d_{31}^o & d_{32}^o & d_{33}^o & 0 & 0 & 0 \end{pmatrix}, \quad (\text{A.14})$$

where one can calculate that, for example, a transverse piezoelectric coefficient in a general direction, d_{32}^{o*} , has the analytic form

$$\begin{aligned} d_{32}^{o*}(\theta, \psi) = & -d_{15}\cos\psi\sin^2\theta\sin\phi(\cos\theta\cos\psi\sin\phi + \cos\phi\sin\psi) \\ & -d_{24}\cos\phi\cos\psi\sin^2\theta(\cos\theta\cos\phi\cos\psi - \sin\phi\sin\psi) \\ & +d_{31}\cos\theta(\cos\theta\cos\phi\cos\psi + \cos\phi\sin\psi)^2 \\ & +d_{32}\cos\theta(\cos\theta\cos\phi\cos\psi - \sin\phi\sin\psi)^2 \\ & +d_{33}\cos\theta\cos^2\psi\sin^2\theta \end{aligned} \quad (\text{A.15})$$

while in the rhombohedral phase, the form of the piezoelectric matrix is

$$\begin{pmatrix} 0 & 0 & 0 & 0 & d_{15}^r & -2d_{22}^r \\ -d_{22}^r & d_{22}^r & 0 & d_{15}^r & 0 & 0 \\ d_{31}^r & d_{31}^r & d_{33}^r & 0 & 0 & 0 \end{pmatrix}. \quad (\text{A.16})$$

The piezoelectric coefficients in these matrices are all presented in the crystallographic phase axes systems. In these systems, the property tensors have the simplest form. One can illustrate that by considering the permittivity in the orthorhombic phase. In this phase, in the paraelectric cubic axes system, permittivity tensor can be calculated to give

$$\mathcal{E}^o = \begin{pmatrix} \varepsilon_{11}^c & 0 & 0 \\ 0 & \varepsilon_{22}^c & \varepsilon_{23}^c \\ 0 & \varepsilon_{23}^c & \varepsilon_{33}^c \end{pmatrix}. \quad (\text{A.17})$$

If one looks for *eigenvalues* of this matrix, one has the equation

$$\mathcal{E}^o - \lambda \mathcal{I} = 0, \quad (\text{A.18})$$

where \mathcal{I} is the identity matrix, and solutions $\lambda_{1,2,3}$ of this polynomial equation of the 3rd order will give the *eigenvalues*. The eigenvalues will give us *eigenvectors* x by solving the next equation

$$\mathcal{E}^o x = \lambda_{1,2,3} x. \quad (\text{A.19})$$

Eigenvectors obtained for the orthorhombic phase are the base vectors for constructing the orthorhombic crystallographic coordinate system. In the coordinate system of the orthorhombic eigenvectors, the permittivity matrix has the form

$$\mathcal{E}^o = \begin{pmatrix} \varepsilon_{11}^o & 0 & 0 \\ 0 & \varepsilon_{22}^o & 0 \\ 0 & 0 & \varepsilon_{33}^o \end{pmatrix}. \quad (\text{A.20})$$

It is now in the simplest possible form and thus generally the most appropriate for studying the permittivity in the orthorhombic phase.

Appendix B

Direction dependence of transverse and shear coefficients of barium titanate

Transverse and shear coefficients in general directions, as it can be seen in *Appendix A*, have analytical forms that are nontrivially more complex for discussions than the ones for the longitudinal piezoelectric response, used often in this thesis work. Nevertheless, we performed calculations of all coefficients in general directions, and here we present some results, for the sake of completeness. All coefficients are calculated for single domain barium titanate, and all axes labels are [pC/N].

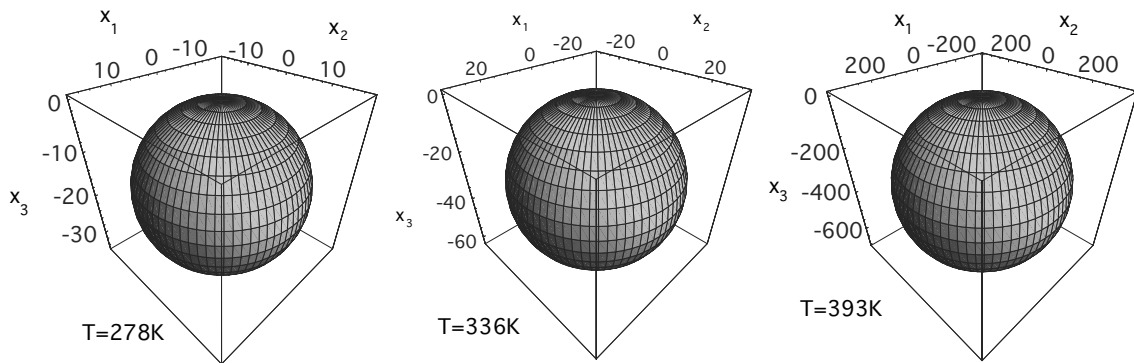


Figure B.1: Transverse coefficient d_{31}^* - tetragonal phase.

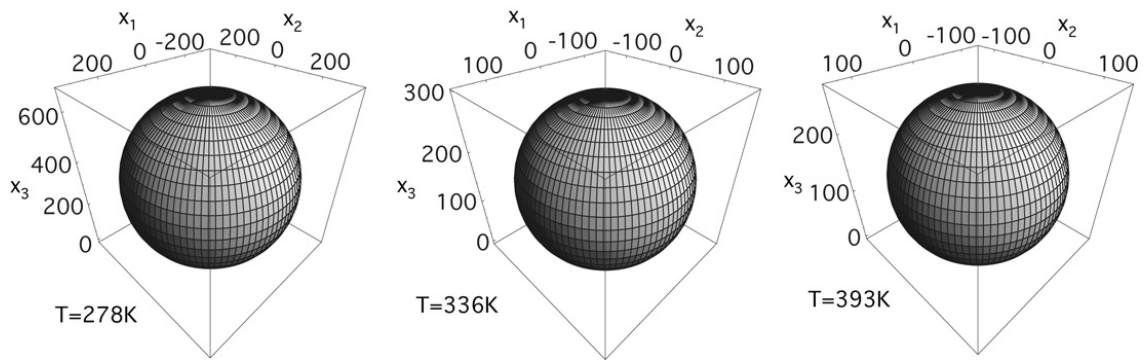


Figure B.2: Shear coefficient d_{15}^{t*} - tetragonal phase.

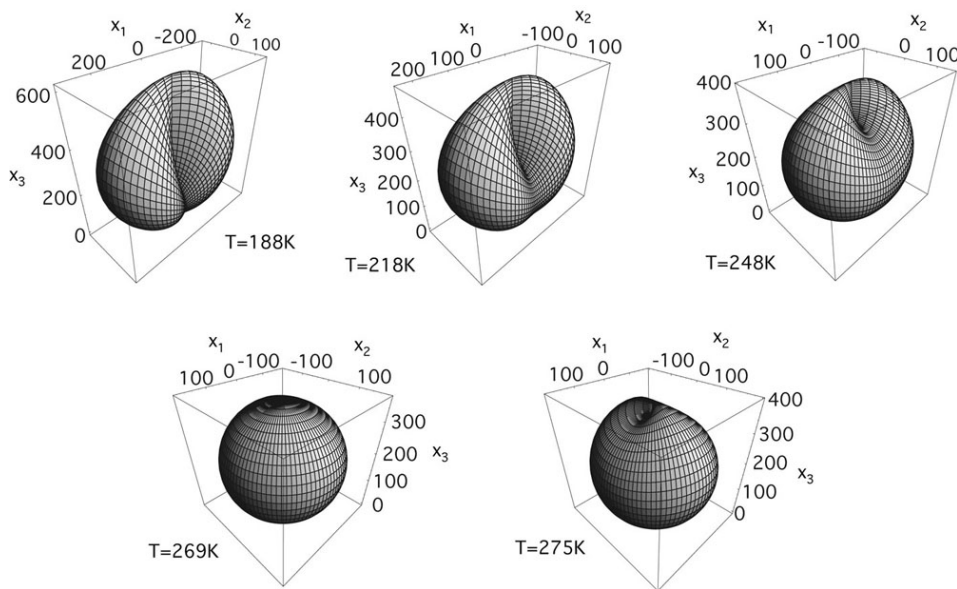


Figure B.3: Shear coefficient d_{15}^{o*} - orthorhombic phase.

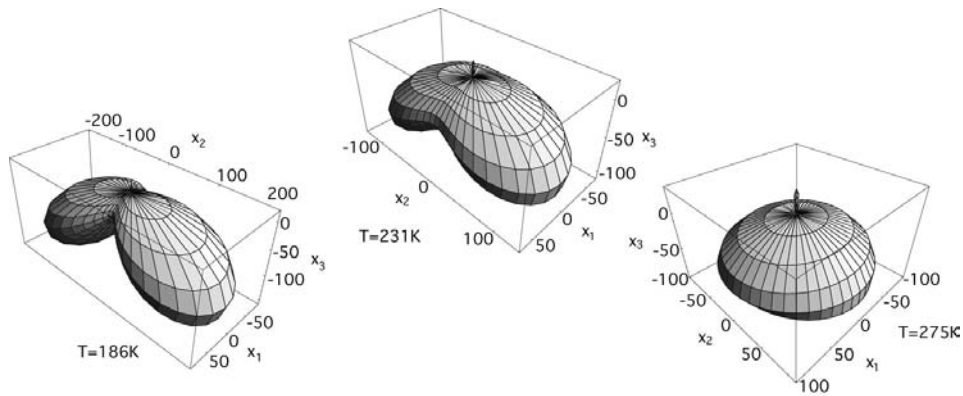


Figure B.4: Transverse coefficient d_{32}^{o*} - orthorhombic phase.

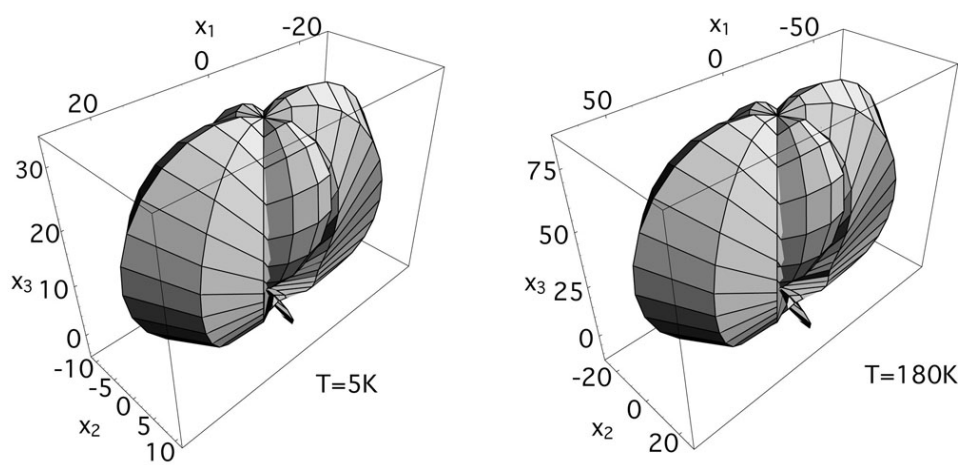


Figure B.5: Shear coefficient d_{15}^{r*} - rhombohedral phase.

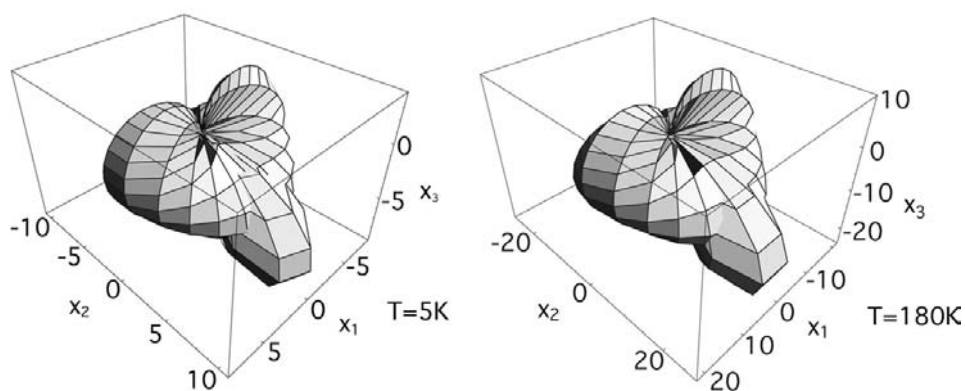


Figure B.6: Transverse coefficient d_{31}^{r*} - rhombohedral phase.

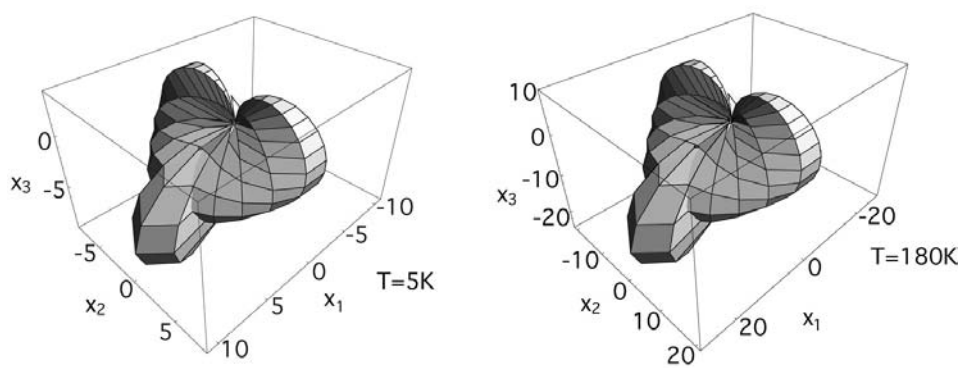


Figure B.7: Transverse coefficient d_{32}^{r*} - rhombohedral phase.

Bibliography

- [1] *IEEE Standard on Piezoelectricity*. The Institute of Electrical and Electronics Engineers, New York, 1988.
- [2] Standard definitions and methods of measurements for piezoelectric vibrators. In *IEEE Trans. UFFC*, volume 40, page 1, 1993.
- [3] R. Ahluwalia, T. Lookman, A. Saxena, and W. Cao. Domain-size dependence of piezoelectric properties of ferroelectrics. *Phys. Rev. B*, 72:014112, 2005.
- [4] A. Amin, L. E. Cross, and R. E. Newnham. Sign notation in ferroelectric free energy functions. *Ferroelectrics*, 99:145, 1989.
- [5] A. Amin, R. E. Newnham, and L. E. Cross. Effect of elastic boundary conditions on morphotropic $\text{Pb}(\text{Zr},\text{Ti})\text{O}_3$ piezoelectrics. *Phys. Rev. B*, 34(3):1595, 1986.
- [6] L. E. Balyunis, V. Y. Topolov, I. S. Bah, and A. V. Turik. The S-type domain and twin boundaries in plate-like PbZrO_3 crystals having complicated twinned structures. *J. Phys.: Condens. Matter*, 5:1419, 1993.
- [7] A. J. Bell. Phenomenologically derived electric field-temperature phase diagrams and piezoelectric coefficients for single crystal barium titanate under fields along different axes. *J. Appl. Phys.*, 89(7):3907, 2001.
- [8] A. J. Bell and L. E. Cross. A Phenomenological Gibbs Function for BaTiO_3 Giving Correct E Field Dependence of all Ferroelectric Phase Changes. *Ferroelectrics*, 59:197, 1984.
- [9] L. Bellaiche, A. Garcia, and D. Vanderbilt. Finite-Temperature Properties of $\text{Pb}(\text{Zr}_{1-x}\text{Ti}_x)\text{O}_3$ Alloys from First Principles. *Phys. Rev. Lett.*, 84:5427, 2000.
- [10] L. Bellaiche, A. Garcia, and D. Vanderbilt. Electric-field induced polarization paths in $\text{Pb}(\text{Zr}_{1-x}\text{Ti}_x)\text{O}_3$ alloys. *Phys. Rev. B*, 64:060103, 2001.

- [11] H. Bilz, G. Benedek, and A. Bussman-Holder. Theory of ferroelectricity: The polarizability model. *Phys. Rev. B*, 35(10):4840, 1987.
- [12] E. I. Bondarenko, V. Y. Topolov, and A. V. Turik. The role of 90° domain wall displacements in forming physical properties of perovskite ferroelectric ceramics. *Ferroelectrics Letters*, 13:13, 1991.
- [13] I. N. Bronštejn and K. A. Semendjajev. *Matematički priručnik za inženjere i studente (in Croatian)*. TEHNIČKA KNJIGA, ZAGREB, 1991.
- [14] W. R. Buessem, L. E. Cross, and A. K. Goswami. Phenomenological theory of high permittivity in fine-grained barium titanate. *J. Am. Ceram. Soc.*, 49(1):33, 1966.
- [15] J. C. Burfoot and G. W. Taylor. *Polar Dielectrics and Their Applications*. Macmillan, London, 1979.
- [16] I. Camlibel. Spontaneous polarization measurements in several ferroelectric oxides using a pulsed-field method. *J. Appl. Phys.*, 40(4):1690, 1969.
- [17] G. Catalan, A. Janssens, G. Rispens, S. Csiszar, O. Seeck, G. Rijnders, D. H. A. Blank, and B. Noheda. *arXiv:cond-mat*, (0512632 v1), 2005.
- [18] G. L. Catchen, S. J. Wukitch, D. M. Spaar, and M. Blaszkievicz. Temperature dependence of the nuclear quadrupole interactions at Ti sites in ferroelectric PbTiO₃ and in ilmenite and perovskite CdTiO₃: Evidence for order-disorder phenomena. *Phys. Rev. B*, 42(4):1885, 1990.
- [19] R. E. Cohen and H. Krakauer. Electronic structure studies of the differences in ferroelectric behavior of BaTiO₃ and PbTiO₃. *Ferroelectrics*, 136:65, 1992.
- [20] R. Comes, M. Lambert, and A. Guinier. The chain structure of BaTiO₃ and KNbO₃. *Sol. State Comm.*, 6:715, 1968.
- [21] D. E. Cox, B. Noheda, G. Shirane, Y. Uesu, K. Fujishiro, and Y. Yamada. Universal phase diagram for high-piezoelectric perovskite systems. *Appl. Phys. Lett.*, 79(3):400, 2001.
- [22] L. E. Cross. Ferroelectric ceramics: tailoring properties for specific applications. In N. Setter and E. L. Colla, editors, *Ferroelectric Ceramics*, page 1. Birkhäuser, Basel, 1993.

- [23] L. E. Cross and Jr. G. A. Rosetti. Origin of the first - order change at the Curie temperature in KNbO_3 . *J. Appl. Phys.*, 69(2):896, 1991.
- [24] M. Daglish. A dynamic method for determining the pyroelectric response of thin films. *Integrated Ferroelectrics*, 22(1-4):993, 1998.
- [25] D. Damjanovic. Stress and frequency dependence of the direct piezoelectric effect in ferroelectric ceramics. *J. Appl. Phys.*, 82(4):1788, 1997.
- [26] D. Damjanovic. Ferroelectric, dielectric and piezoelectric properties of ferroelectric thin films and ceramics. *Rep. Prog. Phys.*, 61:1267, 1998.
- [27] D. Damjanovic. Contributions to the Piezoelectric Effect in Ferroelectric Single Crystals and Ceramics. *J. Am. Ceram. Soc.*, 88(10):2663, 2005.
- [28] D. Damjanovic, F. Brem, and N. Setter. Crystal orientation dependence of the piezoelectric d_{33} coefficient in tetragonal BaTiO_3 as a function of temperature. *Appl. Phys. Lett.*, 80(4):652–654, 2002.
- [29] D. Damjanovic and M. Demartin. Contribution of the irreversible displacement of domain walls to the piezoelectric effect in barium titanate and lead zirconate titanate ceramics. *J. Phys.: Condens. Matter*, 9:4943, 1997.
- [30] M. Davis, D. Damjanovic, and N. Setter. Direct piezoelectric effect in relaxor-ferroelectric single crystals. *J. Appl. Phys.*, 95(10):5679, 2004.
- [31] A. F. Devonshire. Theory of Barium Titanate PART I. *Philosophical Magazine*, 40:1040, 1949.
- [32] A. F. Devonshire. Theory of Barium Titanate PART II. *Philosophical Magazine*, 42:1065, 1951.
- [33] T. P. Dougherty, G. P. Wiederrecht, K. A. Nelson, M. H. Garret, H. P. Jensen, and C. Warde. Femtosecond Resolution of Soft Mode Dynamics in Structural Phase Transitions. *Science*, 258:770, 1992.
- [34] X. Du, U. Belegundu, and K. Uchino. Crystal Orientation Dependence of Piezoelectric Properties in Lead Zirconate Titanate: Theoretical Expectation for Thin Films. *Jpn. J. Appl. Phys.*, 36(9A):5580, 1997.
- [35] X. Du, J. Zheng, U. Belegundu, and K. Uchino. Crystal orientation dependence of piezoelectric properties of lead zirconate titanate near the morphotropic phase boundary. *Appl. Phys. Lett.*, 72(19):2421, 1998.

- [36] S. Ducharme, V. M. Fridkin, A. V. Bune, S. P. Palto, L. M. Blinov, N. N. Petukhova, and S. G. Yudin. Intrinsic ferroelectric coercive field. *Phys. Rev. Lett.*, 84(1):175, 2000.
- [37] P. J. Edwardson. Corridors-between-Adjacent-Sites of the Four Phases of KNbO_3 . *Phys. Rev. Lett.*, 63(1):55, 1989.
- [38] O. E. Fesenko and V. S. Popov. Phase T,E - diagram of barium titanate. *Ferroelectrics*, 37:729, 1981.
- [39] D. Fluck, B. Binder, M. Küpfer, H. Looser, Ch. Buchal, and P. Günter. Phase-matched second harmonic blue light generation in ion implanted KNbO_3 planar waveguides with 29% conversion efficiency. *Opt. Comm.*, 90:304, 1992.
- [40] M. D. Fontana, G. Métrat, J. L. Servoin, and F. Gervais. Infrared spectroscopy in KNbO_3 through the successive ferroelectric phase transitions. *J. Phys. C: Solid State Phys.*, 16:483, 1984.
- [41] M. D. Fontana, A. Ridah, G. E. Kugel, and C. Carabatos Nedelec. The intrinsic central peak at the structural phase transitions in KNbO_3 . *J. Phys. C: Solid State Phys.*, 21:5853, 1988.
- [42] Jr. Forsbergh, P. W. Domain structures and phase transitions in barium titanate. *Phys. Rev.*, 76(8):1187, 1949.
- [43] J. Fousek and V. Janovec. The orientation of domain walls in twinned ferroelectric crystals. *J. Appl. Phys.*, 40(1):135–142, 1969.
- [44] H. Fu and R.E. Cohen. Polarization rotation mechanism for ultrahigh electromechanical response in single-crystal piezoelectrics. *Nature*, 403:281–283, 2000.
- [45] T. Fukuda, H. Hirano, Y. Uematsu, and T. Ito. Dielectric Constant of Orthorhombic KNbO_3 Single Domain Crystal. *Jap. J. Appl. Phys.*, 13(6):1021, 1974.
- [46] A. Garcia and D. Vanderbilt. Electromechanical behavior of BaTiO_3 from first principles. *Appl. Phys. Lett.*, 72(23):2981–2983, 1998.
- [47] S. Gevorgian, E. Carlsson, E. Wikborg, and E. Kollberg. Tunable microwave devices based on bulk and thin film ferroelectrics. *Integrated Ferroelectrics*, 22:245, 1998.
- [48] H. Goldstein. *Classical Mechanics*. Addison-Wesley, Reading, MA, 1978.

- [49] A. K. Goswami. Theory on the effect of hydrostatic pressure on the permittivity and curie point of single crystal barium titanate. *J. Phys. Soc. Jpn.*, 21(6):1037, 1966.
- [50] A. K. Goswami and L. E. Cross. Pressure and temperature dependence of the dielectric properties of the perovskite barium titanate. *Phys. Rev.*, 171(2):549, 1968.
- [51] L. Grigorjeva, D. Millers, A. I. Popov, E. A. Kotomin, and E. S. Polzik. Luminescence properties of KNbO₃ crystals. *J. Lumin.*, 72-74:672, 1997.
- [52] R. Guo, L. E. Cross, S-E. Park, B. Noheda, D. E. Cox, and G. Shirane. Origin of the High Piezoelectric Response in PbZr_{1-x}Ti_xO₃. *Phys. Rev. Lett.*, 84(23):5423, 2000.
- [53] V. L. Gurevich and A. K. Tagantsev. Intrinsic dielectric loss in crystals. *Adv. Phys.*, 40(6):719, 1991.
- [54] P. Günter. Piezoelectric Tensor of KNbO₃. *Jpn. J. Appl. Phys.*, 16(9):1727, 1977.
- [55] P. Günter. Spontaneous polarization and pyroelectric effect in KNbO₃. *J. Appl. Phys.*, 48(8):3475, 1977.
- [56] H. J. Hagemann. Loss mechanisms and domain stabilization in doped BaTiO₃. *J. Phys. C: Solid State Phys.*, 11:3333, 1978.
- [57] J. Harada, J. D. Axe, and G. Shirane. Neutron-Scattering Study of Soft Modes in Cubic BaTiO₃. *Phys. Rev. B*, 4(1):155, 1971.
- [58] M. J. Haun. Thermodynamic Theory of PbZrO₃. *J. Appl. Phys.*, 65(8):3173, 1989.
- [59] M. J. Haun. Thermodynamic Theory of the Lead Zirconate-Titanate Solid Solution System, Part I: Phenomenology. *Ferroelectrics*, 99:13, 1989.
- [60] M. J. Haun, E. Furman, S. J. Jang, and L. E. Cross. Modelling of the Electrostrictive, Dielectric and Piezoelectric Properties of Ceramic PbTiO₃. *IEEE Transactions on Ultrasonics, Ferroelectrics, and Frequency Control*, 36(4):393, 1989.
- [61] M. J. Haun, E. Furman, S. J. Jang, and L. E. Cross. Thermodynamic Theory of the Lead Zirconate-Titanate Solid-Solution System, 5. Theoretical Calculations. *Ferroelectrics*, 99:63, 1989.
- [62] M. J. Haun, E. Furman, S. J. Jang, H. A. McKinstry, and L. E. Cross. Thermodynamic theory of PbTiO₃. *J. Appl. Phys.*, 62(8):3331, 1987.

- [63] M. J. Haun, Z. Q. Zhuang, E. Furman, S. J. Jang, and L. E. Cross. Thermodynamic Theory of the Lead Zirconate-Titanate Solid-Solution System, .3. Curie Constant and 6-th Order Polarization Interaction Dielectric Stiffness Coefficients. *Ferroelectrics*, 99:45, 1989.
- [64] A. W. Hewat. Cubic-tetragonal-orthorhombic-rhombohedral ferroelectric transitions in perovskite potassium niobate: neutron powder profile refinement of the structures. *J. Phys. C: Solid State Phys.*, 6:2559, 1973.
- [65] A. W. Hewat. Soft modes and the structure, spontaneous polarization and Curie constants of perovskite ferroelectrics: tetragonal potassium niobate. *J. Phys. C: Solid State Phys.*, 6:1074, 1973.
- [66] J. Hirohashi, K. Yamada, H. Kamio, and S. Shichijyo. Fabrication of 90° Domain Structures in KNbO₃ Single Crystals. *Ferroelectrics*, 282:29, 2003.
- [67] J. Hirohashi, K. Yamada, H. Kamio, M. Uchida, and S. Shichijyo. Control of specific domain structure in KNbO₃ single crystals by differential vector poling method. *J. Appl. Phys.*, 98:034107, 2005.
- [68] R. Holland and E. EerNisse. Accurate Measurement of Coefficients in a Ferroelectric Ceramic. In *IEEE Transactions on Sonics and Ultrasonics SU-16*, page 173, 1969.
- [69] T. Ikeda. *Fundamentals of piezoelectricity*. Oxford University Press, Oxford, 1990.
- [70] S. G. Ingle and J. G. Dupare. Determination of the Type of Ferroelectric Domain Nucleated around the Dislocation by the Mechanism of Domain Wall Nucleation. *Jpn. J. Appl. Phys.*, 30(3):522, 1991.
- [71] S. G. Ingle and J. G. Dupare. Switching in KNbO₃ single crystals containing cooperatively ordered impurity dipoles. *Phys. Rev. B*, 45(6):2638, 1992.
- [72] S. G. Ingle, H. S. Dutta, and A. P. David. Domain wall nucleation by impurity ions in KNbO₃ single crystals. *J. Appl. Phys.*, 64(9):4640, 1988.
- [73] S. G. Ingle and S. C. Joshi. A dislocation for nucleation of domain walls in KNbO₃ single crystals. *J. Phys. D: Appl. Phys.*, 17:2065, 1984.
- [74] S. G. Ingle and S. C. Joshi. Unstable point domains in ferroelectrics. *Phys. Rev. B*, 34(7):4480, 1986.

- [75] S. G. Ingle and R. N. Kakde. Unusual electric response of the dislocations and the impurity dipoles in KNbO_3 single crystals. *J. Appl. Phys.*, 78(1):104, 1995.
- [76] J. Iniguez, S. Ivantchev, J. M. Perez-Mato, and A. Garcia. Devonshire-Landau free energy of BaTiO_3 from first principles. *Phys. Rev. B*, 63:144103, 2001.
- [77] Y. Ishibashi and M. Iwata. Morphotropic Phase Boundary in Solid Solution Systems of Perovskite-Type Oxide Ferroelectrics. *Jpn. J. Appl. Phys.*, 37(Part 2, No. 8B):L985, 1998.
- [78] M. Iwata, H. Orihara, and Y. Ishibashi. Anisotropy of Piezoelectricity near Morphotropic Phase Boundary in Perovskite-Type Oxide Ferroelectrics. *Ferroelectrics*, 226:57, 2002.
- [79] B. Jaffe, W. R. Cook, and H. Jaffe. *Piezoelectric Ceramics*. Academic, New York, 1971.
- [80] Y. M. Jin, Y. U. Wang, A. G. Khachatryan, J. F. Li, and D. Viehland. Conformal Miniaturization of Domains with Low Domain-Wall Energy: Monoclinic Ferroelectric States near the Morphotropic Phase Boundaries. *Phys. Rev. Lett.*, 91(19):197601, 2003.
- [81] F. Jona and G. Shirane. *Ferroelectric Crystals*. Pergamon, New York, 1962.
- [82] M. Kahn, R. P. Ingel, and D. III Lewis. On the Determination of the Piezoelectric Shear Coefficient, d_{15} , in a PZT Ceramic. *Ferroelectrics*, 102:225, 1990.
- [83] A.G. Kalinichev, J.D. Bass, C.S. Zha, P.D. Han, and D.A. Payne. Elastic properties of orthorombic KNbO_3 single crystals by Brillouin scattering. *J. Appl. Phys.*, 74(11):6603–6608, 1993.
- [84] K.-S. Kam and J. H. Henkel. Band structure and spontaneous polarization in tetragonal KNbO_3 . *Ferroelectrics*, 34:143, 1981.
- [85] N. M. Kari, T. A. Ritter, S-E. Park, T. R. Shrout, and K. K. Shung. Investigation of potassium niobate as an ultrasonic transducer material. In *IEEE Ultrason. Symp.*, page 1065, 2000.
- [86] J.H. Kim and C.S. Yoon. Domain switching characteristics and fabrication of periodically poled potassium niobate for second-harmonic generation. *Appl. Phys. Lett.*, 81(18):3332, 2002.

- [87] W. Kleemann, F. J. Schäfer, and M. D. Fontana. Crystal optical studies of spontaneous and precursor polarization in KNbO_3 . *Phys. Rev. B*, 30(3):1148, 1984.
- [88] J. Kobayashi, Y. Uesu, and Y. Sakemi. X-ray and optical studies on phase transition of PbTiO_3 at low temperatures. *Phys. Rev. B*, 28(7):3866, 1983.
- [89] J. Kuwata, K. Uchino, and S. Nomura. Dielectric and piezoelectric properties of $0.91\text{Pb}(\text{Zn}_{1/3}\text{Nb}_{2/3})\text{O}_3$ - 0.09PbTiO_3 single crystals. *Jap. J. Appl. Phys.*, 21(9):1298, 1982.
- [90] D. La-Orauttapong, B. Noheda, Z.-G. Ye, P. M. Gehring, J. Toulouse, D. E. Cox, and G. Shirane. Phase diagram of the relaxor ferroelectric $(1-x)\text{Pb}(\text{Zn}_{1/3}\text{Nb}_{2/3})\text{O}_3$ - $x\text{PbTiO}_3$. *Phys. Rev. B*, 65:144101, 2002.
- [91] D. La-Orauttapong, J. Toulouse, Z.-G. Ye, W. Chen, R. Erwin, and J. L. Robertson. Neutron scattering study of the relaxor ferroelectric $(1-x)\text{Pb}(\text{Zn}_{1/3}\text{Nb}_{2/3})\text{O}_3$ - $x\text{PbTiO}_3$. *Phys. Rev. B*, 67:134110, 2003.
- [92] M. Lambert and R. Comes. The chain structure and phase transition of BaTiO_3 and KNbO_3 . *Sol. State Comm.*, 7:305, 1969.
- [93] M. J. Lancaster, J. Powell, and A. Porch. Thin-film ferroelectric microwave devices. *Supercond. Sci. Technol.*, 11:1323, 1998.
- [94] L. D. Landau and E. M. Lifshitz. *Statistical Physics, Part 1*, volume 5 of *Course of Theoretical Physics*. Elsevier Science Ltd., 1980.
- [95] Y. L. Li, L. E. Cross, and L. Q. Chen. A phenomenological thermodynamic potential for BaTiO_3 single crystals. *J. Appl. Phys.*, 98:064101, 2005.
- [96] L. Lian, T. C. Chong, H. Kumagai, M. Hirano, L. Taijing, and S. C. Ng. Temperature evolution of domains in potassium niobate single crystals. *J. Appl. Phys.*, 80(1):376, 1996.
- [97] M. E. Lines and A. M. Glass. *Principles and Applications of Ferroelectrics and Related Materials*. Clarendon, Oxford, 1979.
- [98] G. R. Lockwood, D. H. Turnbull, D. A. Christopher, and F. S. Foster. Beyond 30 MHz. *IEEE Eng. Med. Biol. Mag.*, 15:60, 1996.
- [99] Y. Lu, D.-Y. Jeong, Z.-Y. Cheng, and Q.M. Zhang. Phase transitional behavior and piezoelectric properties of the orthorhombic phase of $\text{Pb}(\text{Mg}_{1/3}\text{Nb}_{2/3})\text{O}_3$ - PbTiO_3 single crystals. *Appl. Phys. Lett.*, 78(20):3109, 2001.

- [100] B. T. Matthias and J. P. Remeika. Dielectric properties of sodium and potassium niobates. *Phys. Rev.*, 82(5):727, 1951.
- [101] W. J. Merz. Switching Time in Ferroelectric BaTiO₃ and Its Dependence on Crystal Thickness. *J. Appl. Phys.*, 27(8):938, 1956.
- [102] H. Mestric, R. A. Eichel, T. Kloss, K. P. Dinse, So. Laubach, St. Laubach, P. C. Schmidt, K. A. Schönau, M. Knapp, and H. Ehrenberg. Iron-oxygen vacancy defect centers in PbTiO₃: Newman superposition model analysis and density functional calculations. *Phys. Rev. B*, 71:134109, 2005.
- [103] J.-P. Meyn, M. E. Klein, D. Woll, R. Wallenstein, and D. Rytz. Periodically poled potassium niobate for second-harmonic generation at 463 nm. *Opt. Lett.*, 24(16):1154, 1999.
- [104] M. B. Mishra and S. G. Ingle. Domain-impurities interaction in KNbO₃ single crystals. *J. Appl. Phys.*, 45(12):5152, 1974.
- [105] T. Mitsui and J. Furuichi. Domain Structure of Rochelle Salt and KH₂PO₄. *Phys. Rev.*, 90(2):193, 1953.
- [106] T. Mitsui, I. Tatsuzaki, and E. Nakamura. *An Introduction to the Physics of Ferroelectrics*. Gordon and Breach, London, 1976.
- [107] K. A. Müller, Y. Lushin, J. L. Servoin, and F. Gervais. Displacive-order-disorder crossover at the ferroelectric-paraelectric phase transitions of BaTiO₃ and LiTaO₃. *J. Physique Lett.*, 43(15):L537, 1982.
- [108] K. Nakamura. Potassium niobate (KNbO₃) Crystals and Their Piezoelectric Applications. In S. Trolier McKinstry, L. E. Cross, and Y. Yamashita, editors, *Piezoelectric Single Crystals and Their Application*, page 377. 2004.
- [109] K. Nakamura, T. Tokiwa, and Y. Kawamura. Piezoelectric Properties of KNbO₃ Crystals for Extensional Modes. In *12th IEEE International Symposium on the Applications of Ferroelectrics*, 2000.
- [110] K. Nakamura, T. Tokiwa, and Y. Kawamura. Domain structures in KNbO₃ crystals and their piezoelectric properties. *J. Appl. Phys.*, 91(11):9272, 2002.
- [111] Kiyoshi Nakamura. Orientation Dependence of Electromechanical Coupling Factors in KNbO₃. *IEEE Transactions on Ultrasonics, Ferroelectrics, and Frequency Control*, 47(3):750, 2000.

- [112] B. Noheda. Structure and high-piezoelectricity in lead oxide solutions. *Curr. Opinion Solid State Mat. Sci.*, 6:27, 2002.
- [113] B. Noheda, D. E. Cox, G. Shirane, J. A. Gonzalo, L. E. Cross, and S-E. Park. A monoclinic ferroelectric phase in the $\text{Pb}(\text{Zr}_{1-x}\text{Ti}_x)\text{O}_3$ solid solution. *Appl. Phys. Lett.*, 74(14):2059, 1999.
- [114] B. Noheda, D. E. Cox, G. Shirane, S-E. Park, L. E. Cross, and Z. Zhong. Polarization Rotation via a Monoclinic Phase in the Piezoelectric $92\%\text{PbZn}_{1/3}\text{Nb}_{2/3}\text{O}_3$ - $8\%\text{PbTiO}_3$. *Phys. Rev. Lett.*, 86(17):3891, 2001.
- [115] B. Noheda, J. A. Gonzalo, L. E. Cross, R. Guo, S.-E. Park, D. E. Cox, and G. Shirane. Tetragonal-to-monoclinic phase transition in a ferroelectric perovskite: The structure of $\text{PbZr}_{0.52}\text{Ti}_{0.48}\text{O}_3$. *Phys. Rev. B*, 61(13):8667, 2001.
- [116] J. F. Nye. *Physical Properties of Crystals*. Oxford University Press Inc., New York, 1985.
- [117] K. Okada and T. Sekino. *Agilent Technologies Impedance Measurement Handbook*. Agilent Technologies Co. Ltd, 2003.
- [118] S.-E. Park and T. R. Shrout. Ultrahigh strain and piezoelectric behavior in relaxor based ferroelectric single crystals. *J. Appl. Phys.*, 82(4):1804, 1997.
- [119] S.-E. Park, S. Wada, L. E. Cross, and T. R. Shrout. Crystallographically engineered BaTiO_3 single crystals for high-performance piezoelectrics. *J. Appl. Phys.*, 86(5):2746, 1999.
- [120] S. D. Phatak, R. C. Srivastava, and E. C. Subbarao. Elastic Constants of Orthorhombic KNbO_3 by X-ray Diffuse Scattering. *Acta Cryst.*, A28:227, 1972.
- [121] L. E. Reichl. *A Modern Course in Statistical Physics*. EDWARD ARNOLD (PUBLISHER) LTD, 1980.
- [122] A. E. Renault. PhD thesis, Ecole Central de Paris, 2002.
- [123] A.-E. Renault, H. Dammak, G. Calvarin, M. Pham Thi, and P. Gaucher. Domain Structures in Monoclinic $\text{Pb}[(\text{Zn}_{1/3}\text{Nb}_{2/3})_{0.91}\text{Ti}_{0.09}]\text{O}_3$ Poled Single Crystals. *Jpn. J. Appl. Phys.*, 41:3846, 2002.
- [124] R. Resta, M. Posternak, and A. Baldereschi. Towards a Quantum Theory of Polarization in Ferroelectrics: The Case of KNbO_3 . *Phys. Rev. Lett.*, 70(7):1010, 1993.

- [125] T. Ritter, K. K. Shung, W. Cao, and T. R. ShROUT. Electromechanical properties of thin strip piezoelectric vibrators at high frequency. *J. Appl. Phys.*, 88(1):394, 2000.
- [126] J. Rouquette, J. Haines, V. Bornand, M. Pintard, and Ph. Papet. Pressure-induced rotation of spontaneous polarization in monoclinic and triclinic $\text{PbZr}_{0.52}\text{Ti}_{0.48}\text{O}_3$. *Phys. Rev. B*, 71:024112, 2005. PZT - rotacija i redukcija polarizacije pod tlakom.
- [127] J. Rouquette, J. Haines, V. Bornand, M. Pintard, Ph. Papet, C. Bousquet, L. Konczewicz, F. A. Gorelli, and S. Hull. Pressure tuning of the morphotropic phase boundary in piezoelectric lead zirconate titanate. *Phys. Rev. B*, 70:014108, 2004.
- [128] Yu. B. Rumer and M. Sh. RYVKIN. *Thermodynamics, Statistical Physics, and Kinetics*. Mir Publishers, Moscow, 1980.
- [129] C. B. Sawyer and C. H. Tower. Rochelle salt as a dielectric. *Phys. Rev.*, 35:269, 1930.
- [130] A. Schaefer, H. Schmitt, and A. Dörr. Elastic and Piezoelectric Coefficients of TSSG Barium Titanate Single Crystals. *Ferroelectrics*, 69:253, 1986.
- [131] I. A. Sergienko, Y. M. Gufan, and S. Urazhdin. Phenomenological theory of phase transitions in highly piezoelectric perovskites. *Phys. Rev. B*, 65(14):144104, 2002.
- [132] G. Shirane, H. Danner, A. Pavlovic, and R. Pepinsky. Phase Transitions in Ferroelectric KNbO_3 . *Phys. Rev.*, 93(4):672, 1954.
- [133] Y. Somiya, A. S. Bhalla, and L. E. Cross. Dielectric Properties of $(\text{Sr}_{1-x}\text{Pb}_x)\text{TiO}_3$, SPT ceramics ($x=0.05, 0.1$ and 0.15) and phase transition of SPT ($x=0.05, 0.1, 0.15, 0.2, 0.25$ and 0.3). *Ferroelectr., Lett. Sect.*, 30:81, 2003.
- [134] S. Stemmer, S. K. Streiffer, F Ernst, and M. Rühle. Atomistic structure of 90° domain walls in ferroelectric PbTiO_3 thin films. *Philosophical Magazine A*, 71(3):713, 1995.
- [135] K. Szot, F.U. Hillebrecht, D.D. Sarma, and M. Campagna. Surface defect segregation in the perovskite-type ferroelectric KNbO_3 . *Appl. Phys. Lett.*, 48(7):490, 1986.
- [136] K. Szot, W. Speier, S. Cramm, J. Herion, Ch. Freiburg, R. Waser, M. Pawelczyk, and W. Eberhardt. Surface layer on KNbO_3 and the hysteresis loop anomaly. *J. Phys. Chem Solids*, 57(11):1765–1775, 1996.

- [137] A. K. Tagantsev, V. Sherman, K. Astafiev, J. Venkatesh, and N. Setter. Ferroelectric materials for microwave tunable applications. *J. Electroceramics*, 11:5, 2003.
- [138] T. Takagi, T. Fujii, and Y. Sakabe. Growth and characterization of KNbO_3 by vertical Bridgman method. *J. Crystal Growth*, 259:296, 2003.
- [139] H. Takahasi. A note on the theory of barium titanate. *J. Phys. Soc. Jpn.*, 16(9):1685, 1961.
- [140] D. V. Taylor and D. Damjanovic. Piezoelectric properties of rhombohedral $\text{Pb}(\text{Zr,Ti})\text{O}_3$ thin films with (100), (111) and "random" crystallographic orientation. *Appl. Phys. Lett.*, 76:1615, 2000.
- [141] J.-C. Toledano and P. Toledano. *The Landau Theory of Phase Transitions*. World Scientific, Singapore, 1987.
- [142] A.Y. Topolov. Domain wall displacements and piezoelectric activity of KNbO_3 single crystals. *J. Phys.: Condens. Matter*, 15:561–565, 2003.
- [143] S. Triebwasser. Behavior of Ferroelectric KNbO_3 in the Vicinity of the Cubic-Tetragonal Transition. *Phys. Rev.*, 101(3):993, 1956.
- [144] S. Triebwasser and J. Halpern. Curie Constant, Spontaneous Polarization, and Latent Heat in the Ferroelectric Transition in KNbO_3 . *Phys. Rev.*, 98(5):1562, 1955.
- [145] D. Vanderbilt and M.H. Cohen. Monoclinic and triclinic phases in higher-order Devonshire theory. *Phys. Rev. B*, 63:094108, 2001.
- [146] O. G. Vendik, E. K. Hollmann, A. B. Kozyrev, and A. M. Prudan. Ferroelectric tuning of planar and bulk microwave devices. *J. Supercond.*, 12(2), 1999.
- [147] D. Viehland, A. Amin, and J. F. Li. Piezoelectric instability in $\langle 011 \rangle$ -oriented $\text{Pb}(\text{B}_{1/3}^I\text{B}_{2/3}^{II})\text{O}_3$ - PbTiO_3 crystals. *Appl. Phys. Lett.*, 79(7):1006, 2001.
- [148] D. Viehland, J. Powers, L. E. Cross, and J. F. Li. Importance of random fields on the properties and ferroelectric phase stability of $\langle 001 \rangle$ oriented $0.7\text{Pb}(\text{Mg}_{1/3}\text{Nb}_{2/3})\text{O}_3$ - 0.3PbTiO_3 crystals. *Appl. Phys. Lett.*, 78(22):3508, 2001.
- [149] S. Wada. personal communication.

- [150] S. Wada, H. Kakemoto, and T. Tsurumi. Enhanced piezoelectric properties of piezoelectric single crystals by domain engineering. *Materials Transactions*, 45(2):178, 2004.
- [151] S. Wada, K. Muraoka, H. Kakemoto, H. Kumagai, and T. Tsurumi. Potassium niobate single - domain crystals as piezoelectrics with low dielectric constants and high electromechanical coupling properties. In G. White and T. Tsurumi, editors, *2002 13th IEEE International Symposium on Applications of Ferroelectrics*, Nara, Japan, 2002.
- [152] S. Wada, K. Muraoka, H. Kakemoto, T. Tsurumi, and H. Kumagai. Preparation of Potassium Niobate Single-Domain Crystals and Their Piezoelectric Properties. *Ferroelectrics*, 292:127, 2003.
- [153] S. Wada, K. Muraoka, H. Kakemoto, T. Tsurumi, and H. Kumagai. Enhanced Piezoelectric Properties of Potassium Niobate Single Crystals by Domain Engineering. *Jpn. J. Appl. Phys.*, 43(9B):6692, 2004.
- [154] S. Wada, A. Seike, and Tsurumi T. Poling treatment and piezoelectric properties of potassium niobate ferroelectric single crystals. *Jpn. J. Appl. Phys.*, 40(9B):5690, 2001.
- [155] S. Wada, S. Suzuki, T. Noma, T. Suzuki, M. Osada, M. Kakihana, S-E. Park, L. E. Cross, and T. R. ShROUT. Enhanced piezoelectric property of barium titanate single crystals with engineered domain configuration. *Jpn. J. Appl. Phys.*, 38:5505, 1999.
- [156] S. Wada, K. Yako, H. Kakemoto, T. Tsurumi, and T. Kiguchi. Enhanced piezoelectric properties of barium titanate single crystals with different engineered-domain sizes. *J. Appl. Phys.*, 98:014109, 2005.
- [157] H. Wang, W. Jiang, and W. Cao. Characterization of lead zirconate titanate piezoceramic using high frequency ultrasonic spectroscopy. *J. Appl. Phys.*, 85(10):8083, 1999.
- [158] E. Wiesendanger. *Dielectric, Mechanical and Optical Properties of Orthorhombic KNbO₃*. PhD thesis, Eidgenössischen Technischen Hochschule Zürich, 1973.
- [159] E. Wiesendanger. Domain structures in Orthorhombic KNbO₃ and characterisation of single domain crystals. *Czech. J. Phys. B*, 23:91, 1973.
- [160] E. Wiesendanger. Dielectric, Mechanical and Optical Properties of Orthorhombic KNbO₃. *Ferroelectrics*, 6:263, 1974.

- [161] Z. Wu and R. E. Cohen. Pressure-Induced Anomalous Phase Transition and Colossal Enhancement of Piezoelectricity in PbTiO_3 . *Phys. Rev. Lett.*, 95:037601, 2005.
- [162] B. Yang, P. D. Townsend, and M. Maghrabi. Optical detection of phase transitions in potassium niobate. *J. Mod. Opt.*, 48(2):319, 2001.
- [163] V. K. Yanovskii. Electrical conductivity and dielectric properties of KNbO_3 crystals with impurities. *Sov. Phys. Solid State*, 22(7):1284, 1981.
- [164] S. Yokoyama, Y. Honda, H. Morioka, S. Okamoto, H. Funakubo, T. Ijima, H. Matsuda, K. Saito, T. Yamamoto, H. Okino, O. Sakata, and S. Kimura. Dependence of electrical properties of epitaxial $\text{Pb}(\text{Zr},\text{Ti})\text{O}_3$ thick films on crystal orientation and $\text{Zr}/(\text{Zr}+\text{Ti})$ ratio. *J. Appl. Phys.*, 98:094106, 2005.
- [165] Z. Yu, R. Guo, and A. S. Bhalla. Orientation dependence of the ferroelectric and piezoelectric behavior of $\text{Ba}(\text{Ti}_{1-x}\text{Zr}_x)\text{O}_3$ single crystals. *Appl. Phys. Lett.*, 77(10):1535, 2000.
- [166] M. Zgonik, R. Schlessler, I. Biaggio, E. Voit, J. Tscherry, and P. Günter. Materials constants of KNbO_3 relevant for electro- and acousto-optics. *J. Appl. Phys.*, 74(2):1287, 1993.
- [167] Q. M. Zhang, W. Y. Pan, S. J. Jang, and L. E. Cross. Domain wall excitations and their contributions to the weak-signal response of doped lead zirconate titanate ceramics. *J. Appl. Phys.*, 64(11):6445, 1988.
- [168] Q. M. Zhang, H. Wang, N. Kim, and L. E. Cross. Direct evaluation of domain-wall and intrinsic contributions to the dielectric and piezoelectric response and their temperature dependence on lead zirconate-titanate ceramics. *J. Appl. Phys.*, 75(1):454, 1994.
- [169] R. Zhang, B. Jiang, and W. Cao. Elastic piezoelectric, and dielectric properties of multidomain $0.67\text{Pb}(\text{Mg}_{1/3}\text{Nb}_{2/3})\text{O}_3$ - 0.33PbTiO_3 single crystals. *J. Appl. Phys.*, 90(7):3471–3475, 2001.
- [170] R. Zhang, B. Jiang, and W. Cao. Single-domain properties of $0.67\text{Pb}(\text{Mg}_{1/3}\text{Nb}_{2/3})\text{O}_3$ - 0.33PbTiO_3 single crystals under electric field bias. *Appl. Phys. Lett.*, 82(5):787, 2003.

CURRICULUM VITAE

Marko Budimir

born 1st of September 1973 in Sinj, Croatia, single, Croatian nationality.

Education:

2002-present: Ph. D. student at Ceramics Laboratory, Institute of Materials, School of Engineering, EPF Lausanne, Switzerland

1992-2000: Diploma student at Physics Department, Faculty of Science, University of Zagreb, Croatia

Awards:

2000: Rector's Prize for the best student work in physics, University of Zagreb, Croatia

1990: 3rd Prize at the Croatian national competition in mathematics

Other:

2004-present: Player of basketball club Morges Basket (champion of the Swiss 4^{ème} Ligue in the season 2005/2006)

2000-2001: Military service

1995-1997: Responsible for Children Computer Workshop, "Medveščak" Library, Zagreb

1990-1996: Member of City Orchestra Sinj

PUBLICATIONS

Regular papers:

1. M. Budimir, D. Damjanovic and N. Setter, *Piezoelectric response and free energy instability in the perovskite crystals $BaTiO_3$, $PbTiO_3$ and $Pb(Zr,Ti)O_3$* , accepted for publishing in PHYSICAL REVIEW B
2. M. Budimir, D. Damjanovic and N. Setter, *Extension of the dielectric tunability range in ferroelectric materials by electric bias field antiparallel to polarization*, APPLIED PHYSICS LETTERS 88: Art. No. 082903 FEB 2006
3. D. Damjanovic, M. Budimir, M. Davis and N. Setter, *Piezoelectric anisotropy: Enhanced piezoelectric response along nonpolar directions in perovskite crystals*, JOURNAL OF MATERIALS SCIENCE 4: 65-76 JAN 2006
4. M. Budimir, D. Damjanovic and N. Setter, *Enhancement of the piezoelectric response of tetragonal perovskite single crystals by uniaxial stress applied along the*

- polar axis: A free-energy approach*, PHYSICAL REVIEW B 72 (6): Art. No. 064107 AUG 2005
5. M. Budimir, D. Damjanovic and N. Setter, *Large enhancement of the piezoelectric response in perovskite crystals by electric bias field antiparallel to polarization*, APPLIED PHYSICS LETTERS 85 (14): 2890-2892 OCT 2004
 6. M. Budimir, D. Damjanovic, N. Setter, *Piezoelectric anisotropy-phase transition relations in perovskite single crystals*, JOURNAL OF APPLIED PHYSICS 94 (10): 6753-6761 NOV 2003
 7. D. Damjanovic, M. Budimir, M. Davis and N. Setter, *Monodomain versus polydomain piezoelectric response of $0.67\text{Pb}(\text{Mg}_{1/3}\text{Nb}_{2/3})\text{O}_3$ - 0.33PbTiO_3 single crystals along nonpolar directions*, APPLIED PHYSICS LETTERS 83 (3): 527-529 JUL 2003
 8. A. Smontara, I. Tkalcec, A. Bilusic, M. Budimir and H. Berger, *Anisotropy of the thermal conductivity in $(\text{TaSe}_4)_2\text{I}$* , PHYSICA B 316: 279-282 MAY 2002

Book section: .

D. Damjanovic, M. Budimir and N. Setter, *Phase Transitions, Piezoelectric Shear Effects and Anisotropy of d_{33} in BaTiO_3 and PbTiO_3 Monodomain Single Crystals*, In S. Trolier-McKinstry, L. E. Cross, and Y. Yamashita, editors, *Piezoelectric Single Crystals and Their Application*, page 207, 2004.